Fossett

1999 Pacific Cell Friends of the Pleistocene Field Trip
September 24-26, 1999

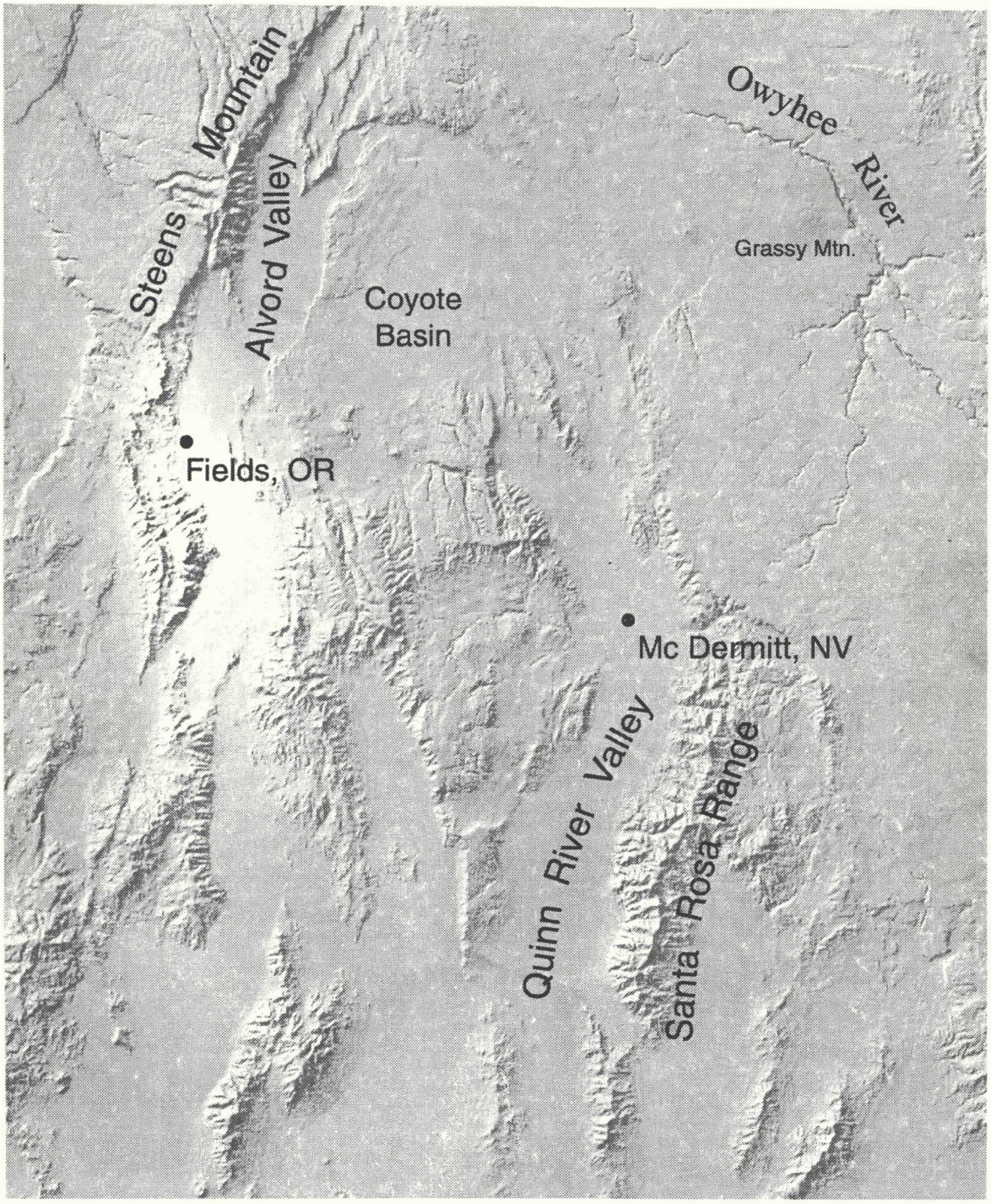

Quaternary Geology of the Northern Quinn River and Alvord Valleys, Southeastern Oregon

Quaternary Geology of the Northern Quinn River and Alvord Valleys, Southeastern Oregon

1999 Friends of the Pliestocene Field Trip
Pacific cell

September 24-26, 1999

Field Trip Guide

Organized by:
Charlie Narwold

Trip leaders:
Charlie Narwold
David Lindberg
Mark Hemphill-Haley
Marith Reheis
Silvio Pezzopane
Tom Sawyer
Ken Adams

Sponsored by:
Geology Department
Humboldt State University
Arcata, California

Table of Contents

List of contributed articles in the Appendices

Appendix 1. Narwold, C. F., 1999, Late Quaternary faulting along the Quinn River fault zone; a soils investigation.

Appendix 2. Hemphill-Haley, M. A., Lindberg, D. N, and Reheis, M. C., 1999, Lake Alvord and Lake Coyote; a hypothesized flood.

Appendix 3. Lindberg, David N., 1999, A synopsis of late Pleistocene shorelines and faulting, Tule Springs Rims to Mickey Basin, Alvord Desert, Harney County, Oregon.

Appendix 4. Hemphill-Haley, M. A., and Humphreys, Gene, 1999, Contemporary Deformation of the Pacific Northwest: Regional Kinematics.

Appendix 5. Hemphill-Haley, Mark A., Carver, Gary A., and Burke, Bud, 1999, Late Quaternary Stratigraphy and Holocene Faulting Along the eastern margin of Steens Mountain, Southeastern Oregon.

Appendix 6. Pezzopane, Silvio, 1999, Regional tectonic setting and fault studies in Quinn River Valley and surrounding regions, Oregon and Nevada.

Appendix 7. Sawyer, Thomas L., and Adams, Kenneth D., 1999, Temporal and spatial patterns of quaternary fault activity in northwestern Nevada.

Appendix 8. Smith, S. C., 1999, The Rush Peak fault zone, Cuddy Mountains, western Idaho: Evidence for sinistral-oblique Late-Quaternary movement and analysis of longitudinal stream profiles crossing an active range front.

Appendix 9. Wood, S. H., 1999, Quaternary faulting in southwest Idaho and adjacent Oregon.

Appendix 10. Bevis, Kenneth A., 1999, A brief history of glaciation at Steens Mountain, southest Oregon.

Appendix 11. Craven, Gilbert, 1999, Holocene deformation of shorelines in Warner Valley correlated with 1968 earthquake swarm epicenters and Miocene structural control.

Appendix 12. Simpson, Gary A., and Davis, Jonathan O., 1989, Compressional deformation of late Pleistocene pluvial sediments in the northwestern Summer Lake basin, south-central Oregon.

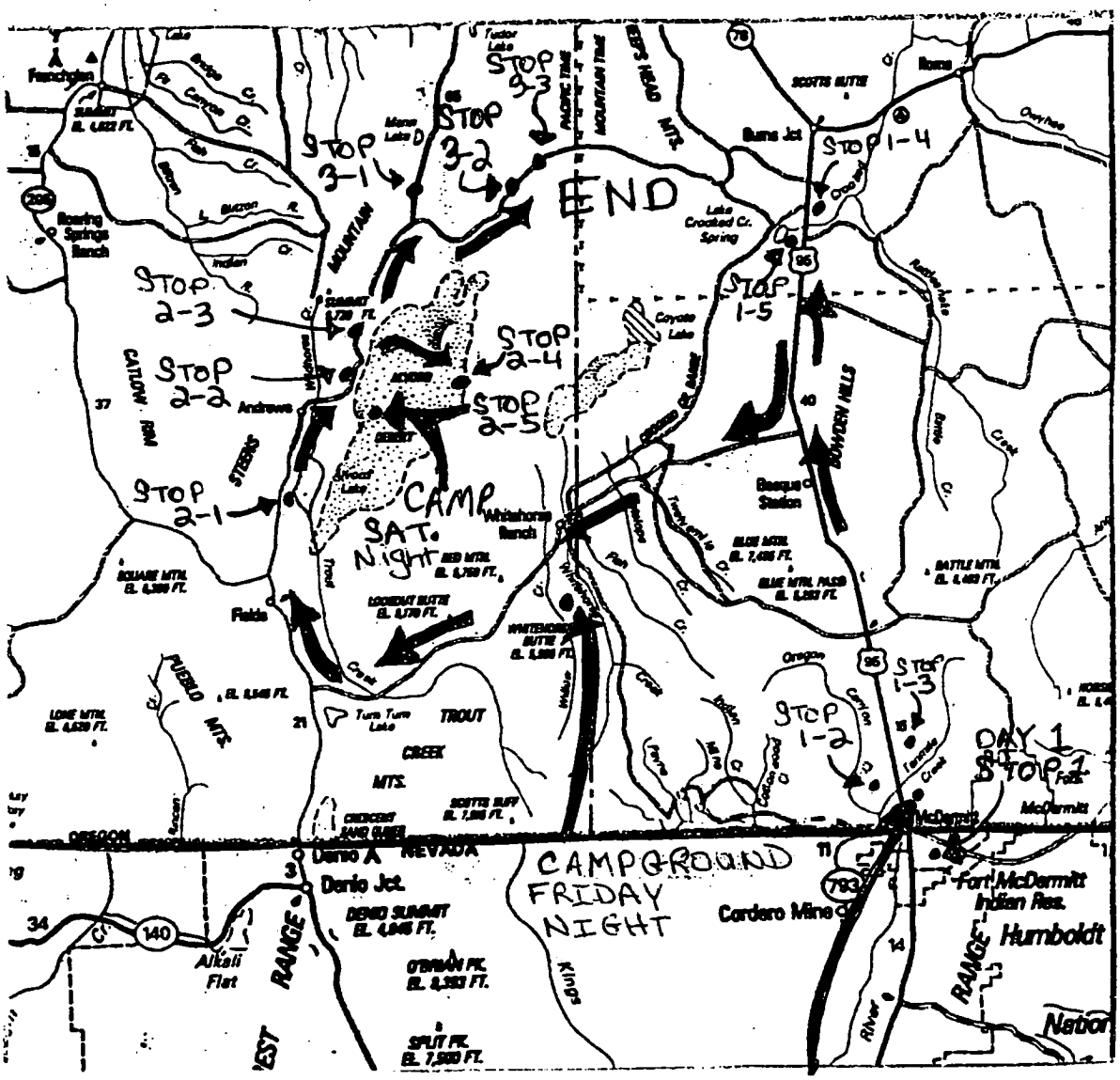

FUNKY FOP ROUTE MAP

SEPTEMBER 24 – 26, 1999

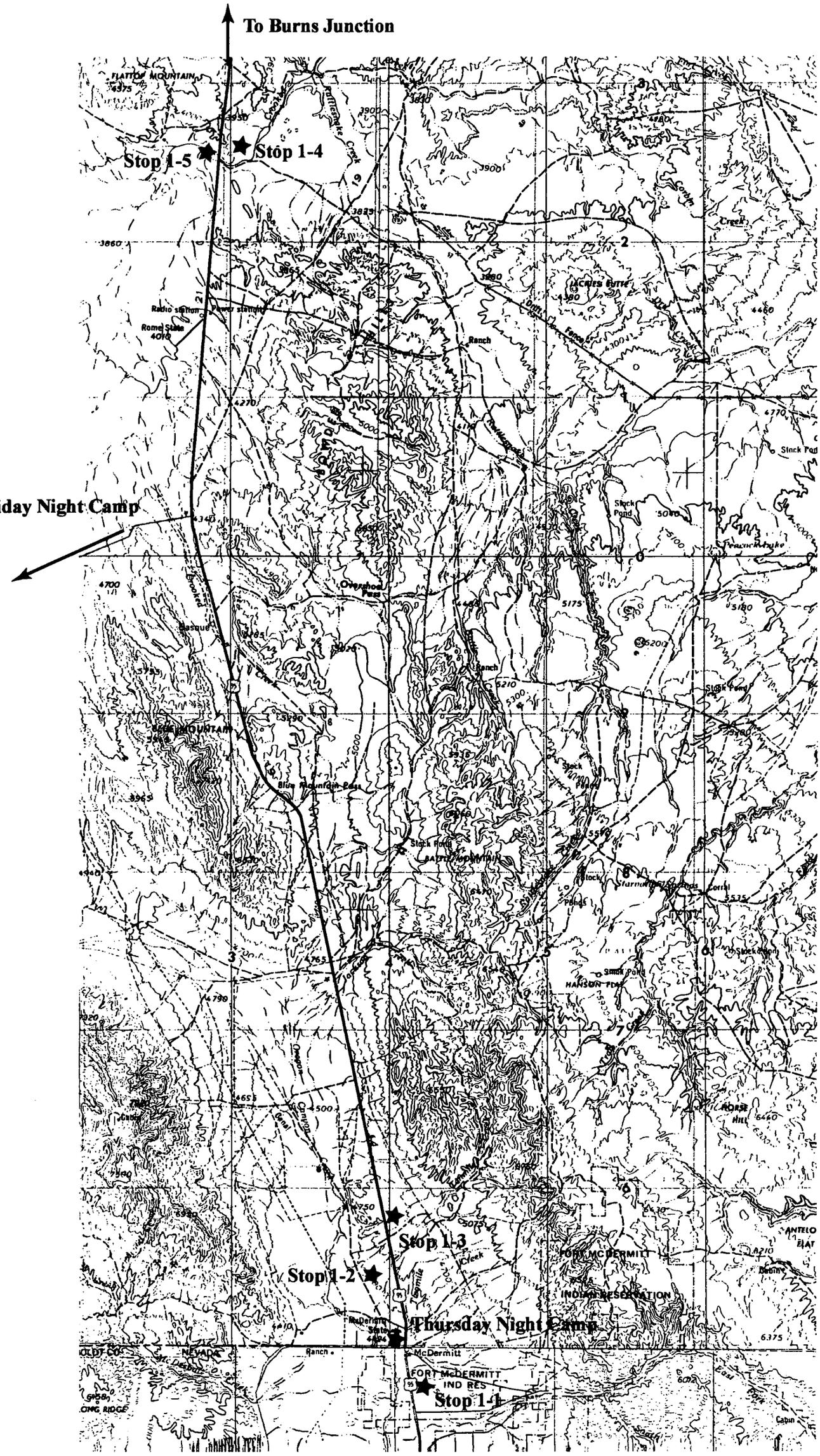

1:125,000 McDermitt and Jordan Valley Sheets, Nevada and Oregon, Day 1

Introduction

Welcome to this year's Pacific Cell Friends of the Pleistocene field trip. I would like to begin by thanking Bud Burke and the folks at Humboldt State University for their invaluable help in producing this guidebook. I want to thank David Lindberg and Mark Hemphill-Haley for their generous contributions and willingness to participate in this year's trip. I would also like to thank all the people whose cooperation made this year's trip logistically possible. Lastly, I would like to thank Jenny Curtis who was a good listener and offered sound advice throughout the preparation process.

Since my first FOP field trip in 1995, I have often wondered how the Friends of the Pleistocene got started. Seeing as how this year's trip is the last FOP of this century, I thought it fitting to include a summary of how FOP began.

Charlie Narwold
September, 1999

Who are the "Friends" ?

An enthusiastic bunch of scientists and other folks that meet once a year in the field at locations across the United States. The Friends gather to discuss diverse geological topics, see old friends, meet new friends, sing songs about the way things were and talk about the way things are.

But how did this all get started? In the winter of 1934, Dick Flint (Yale) the father of the idea, wrote Walter Goldthwait (Dartmouth) stating he would like to see whether a late Wisconsin lake in the Merrimac Valley of New Hampshire was similar to a well-studied one in the Connecticut Valley (or did the glacial ice front melt southward?). So Walter Goldthwait, George White (UNH), and Don Chapman (UNH), who had been mapping in New Hampshire, asked Flint to come early on Friday May 25, 1934. Flint, Goldthwait, White, and Chapman spent the next three days traversing the state thinking out loud and arguing the whole way. And there you have it, the first FOP field trip. However, the name of the unorganized organization was not coined until the following year. In 1935 Dick Flint wrote Walter Goldthwait a letter that said, "Isn't it about time that the Friends of the Pleistocene meet again?" By 1938 Flint had copyrighted the name and the word "Friends" began appearing in field literature by 1939.

The annual Friends of the Pleistocene trip has been called a "Conference", a "Celebration", a "Reunion", and even an "Invasion". From the very start, arguing has been an integral part of FOP field trips. Attendance at the early FOP trips was limited to typically 100 folks, however interest has grown enormously over the years with some trips having in excess of 200 Friends. Even as numbers grew the organization remained decidedly unorganized. There is no chairman, no secretary, no treasurer, and no dues. Trip leaders simply pass along the active mailing list from year to year. As to where to have the trips, any place is fair game that a herd of ardent geological types will go for a weekend.

As old "Friends" migrated west the desire to get together for the annual ritual continued and regional groups sprang up. The Midwest Group was founded in 1950, the Rocky Mountain Group in 1952, the South Central Group and Southeast Groups in 1963, and the Pacific Cell in 1966. With Dick Flint at the helm of the Eastern Group it's not surprising that the early trips focused on glacial geology. However, as FOP spread across the country, topics became more diversified, ranging from faulting, landslides, volcanism, river terraces, and soil development to list a few.

In 1966, Don Easterbrook (U of W) led the first Pacific Cell trip, which was entitled "Pleistocene geology of Puget and Fraser Lowlands, WA". This year's FOP trip is the 32nd annual reunion of the Pacific Cell (no field trips in 1968, 1974, and 1977). This year's trip also marks the 20th anniversary of the memorable 1979 Pacific Cell trip to the central Sierra Nevada lead by Bud Burke, Pete Birkeland, and Jim Yount. As we approach the next millennium we look forward to many more annual reunions and the great times ahead!

Information in this brief summary was taken from Friends of the Pleistocene; Recollections of Fifty Annual Reunions 1934-1988 by Richard P. Goldthwait (Ohio State) son of co-founder Walter Goldthwait and a devoted Friend.

jac

ROAD LOG

DAY 1

FOP ROAD LOG

DAY 1

Day 1 - Introduction

An overview of the regional tectonics and evidence for late Quaternary faulting along the Hot Spring Hills fault, a segment of the Quinn River fault zone, will be presented at STOP 1. At STOPS 2 and 3 we will examine the end members of a carbonate soil chronosequence that were used to constrain the time of faulting along the Hot Spring Hills fault. We will then switch gears and head north to examine evidence for a catastrophic flood eastward from the Coyote basin at stops 4 and 5; a topic we will revisit and expand upon on Day 2 of the trip.

The road log for Day 1 of the fieldtrip starts at the rodeo grounds on the west side of Hwy 95, 0.4 miles north of the Nevada-Oregon border in the town of Mc Dermitt, NV.

Approximate mileage — Driving directions are underlined.

For those of you driving vehicles with low clearance, we recommend you leave your vehicles at the rodeo grounds and ride with someone else to get to STOP 1-1. The dirt road on which we will travel is in good condition but there is sagebrush growing between the tracks. We will pass the rodeo grounds on our way back north en route to STOP 1-2, at which time you can retrieve your vehicles.

0.0 Reset odometer upon exiting rodeo grounds at intersection with Hwy 95. Turn right and proceed south on Hwy 95.

0.4 Entering state of Nevada and town of Mc Dermitt, elev. ~4430 ft (1350 m).

2.0 To your left (east) is an 18 meter high, compound fault scarp of the Hot Spring Hills fault. Note the vegetation lineament on the lower part of the scarp, it denotes a latest Pleistocene-early Holocene surface rupture. STOP 1-1 is atop the compound scarp.

2.5 Good view of Santa Rosa Range to south. The three prominent peaks from north to south are Buckskin Mtn, Granite Peak, elev. 9728 ft (2965 m), and Santa Rosa Peak.

3.0 Turn left onto North Road and continue east. There is a BLM fire station on your left.

3.6 Turn left onto dirt road before North Road curves to south. The East Fork of the Quinn River exits the mountains in front of you through a notch at approx. 11:00.

3.7 At four-way dirt intersection turn left and proceed north.

4.5 **STOP 1-1. (8:00-9:30 am) Compound Fault Scarp of Hot Spring Hills Fault.** Park vehicles in main tracks of the road and walk approximately a half mile to your right (northeast) and assemble atop of the compound fault scarp. We will be gone from the vehicles for approximately and hour and a half.

We are standing atop a compound fault scarp of the Hot Spring Hills fault (Figure 1-1) which is approximately 46 km in length and extends from Canyon Creek to Oregon Canyon Creek (Figure 1-2). The Hot Spring Hills fault is part of the Quinn River fault zone (QRfz); the northern segment of the Santa Rosa Range fault system.

The measured vertical separation of the ground surface at this location is 15.9 m which is a minimum value due to burial of the original ground surface on the footwall block. A recent surface faulting event is recorded on the face of the compound scarp, with a measured vertical separation of 0.7 m (Figure 1-3). Estimates of the amount of dip-slip displacement on the fault were calculated for the compound scarp as well as the young surface rupture. Using nomograms for estimating components of fault displacement from Caskey (1995), the amount of dip-slip displacement was calculated for 3 different fault dip angles.

	Vertical Separation of ground surface (m)	Estimate of dip-slip displacement (m) for specified fault dip		
		50°	70°	90°
Compound Scarp	15.9	20.7	19.1	15.9
Young Surface Rupture	0.7	1.1	0.8	0.7

The amount of lateral slip on the fault is unknown, but the estimated dip-slip displacements are useful in that they serve as minimum values of the amount of net slip. It is important to note that these are minimum estimated values and are only approximations due to uncertainties in the actual vertical separation of the original ground surface, and recognition of the fact that fault planes often steepen near the ground surface.

Age of faulting

The surface on which you are standing is estimated to be between 750 ka and 1.5 ma years old based on carbonate soil development and correlation to alluvial units of Hawley and Wilson (1965). The age of the surface serves as a maximum limiting age for the time faulting initiated along the Hot Spring Hills fault.

Soil MS1 (Figure 1-3) is developed in what is interpreted to be mainly aeolian and some colluvial material that was deposited at the base of the scarp after the most recent surface faulting event at this site. The secondary (pedogenic) carbonate index of Machette (1985) was used to estimate an age of 8.5 ka for the soil. For a complete soil profile description of soil MS1 and an explanation of how an age for the soil was determined, see Appendix 1. The age of soil MS1 is a minimum age for the timing of the most recent surface faulting event. Based on the degree of preservation of the fault scarp on a relatively steep slope, the scarp is probably latest Pleistocene-early Holocene in age which is consistent with the estimated age of soil MS1.

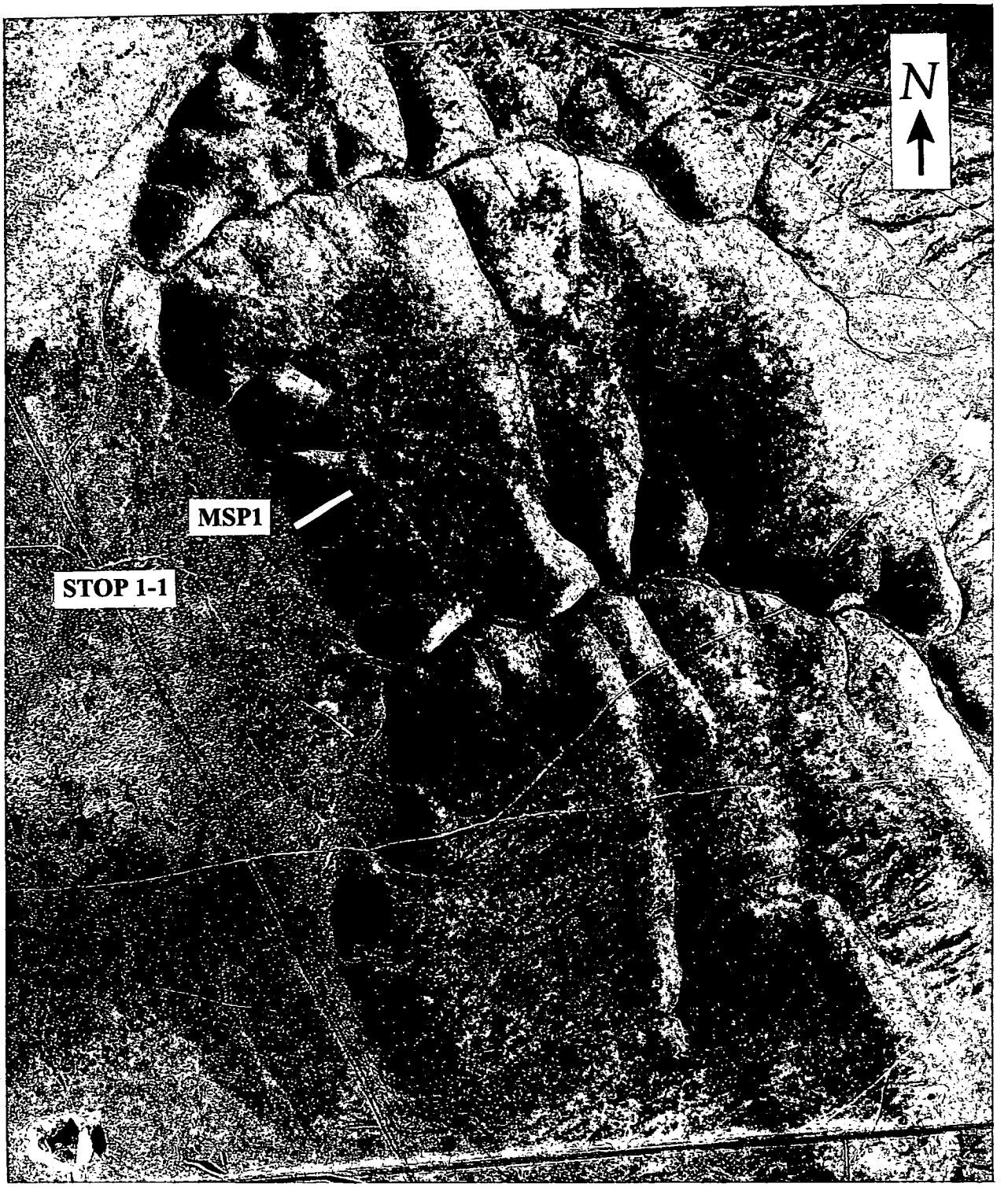

Figure 1-1. Aerial photo of compound fault scarp of Hot Spring Hills fault showing location of STOP 1-1 and topographic profile MSP1. The slope of the shadowed southwest-facing scarp records evidence of latest Pleistocene/early Holocene faulting event.

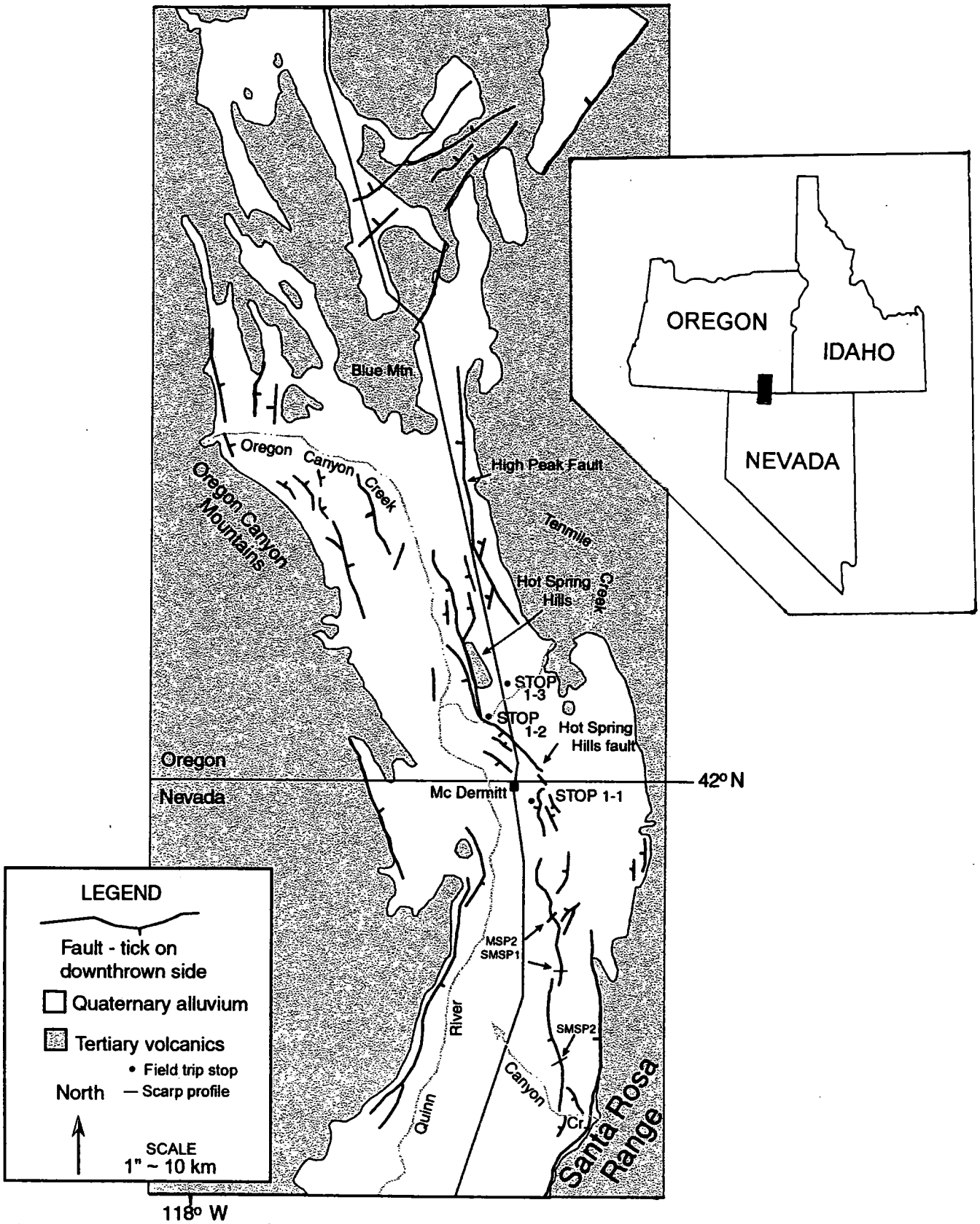

Figure 1-2. Generalized fault map of the northern Quinn River Valley showing location of STOPS 1-1, 1-2, 1-3, and scarp profiles MSP2, SMSP1, and SMSP5.

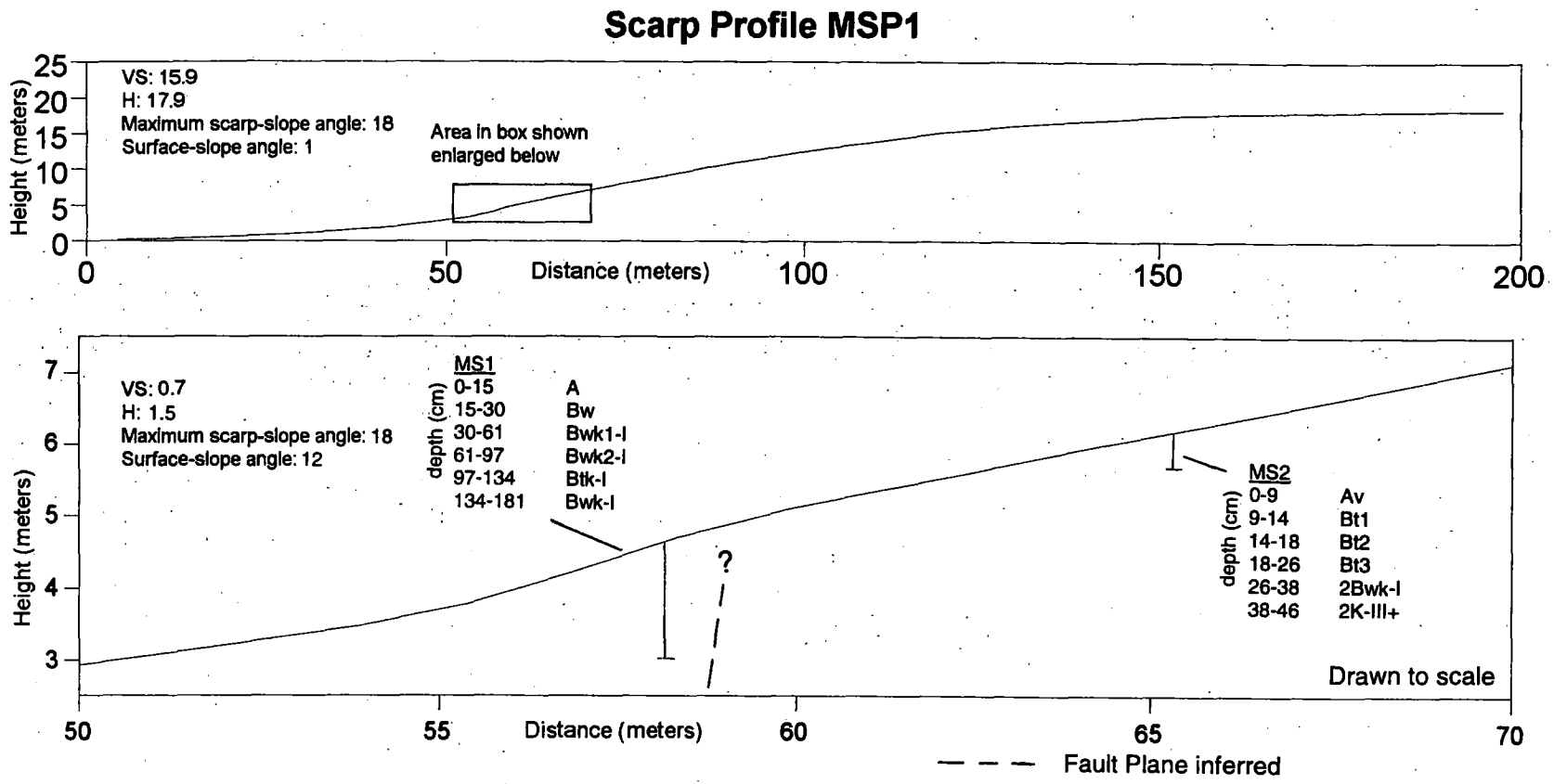

Figure 1-3. Surveyed topographic profile of compound fault scarp at STOP 1-1 showing location of soils MS1 and MS2. Break in slope shown enlarged is interpreted to be a fault scarp generated by a latest Pleistocene/early Holocene faulting event. Note the discordance between soils MS1 and MS2. VS – vertical separation of the ground surface, H – scarp height.

Estimate of Paleoearthquake Magnitude

Evidence of a young rupture exists along the Hot Spring Hills fault over most of it's length; inflections preserved on faces of compound scarps (Figures 1-3 and 1-4) and the presence of small (~0.5-1.5 m high) scarps displacing all but the youngest (late Holocene and modern) alluvial surfaces (Figures 1.5 and 1.6). Whether the observed ruptures are the result of a single paleoearthquake or multiple smaller earthquakes closely spaced in time is unknown. Based on the continuity of the ruptures, the consistent offset of geomorphic features, and lack of obvious segment boundaries, it is plausible that the ruptures are the result of a single paleoearthquake. Assuming the observed breaks in slope on compound scarps, and small single event(?) scarps, are the result of a single earthquake, the rupture(s?) would have extended from Canyon Creek to Oregon Canyon Creek (Figure 2), a length of approximately 45± 5 km (measured as a straight-line distance between the rupture endpoints). The ± 5 km reflects the uncertainty in identifying the ends of the rupture where displacements were likely small and could easily have been obscured by subsequent erosion. The measured vertical displacement of 13 scarps interpreted to be the result of a the most recent earthquake over the length of the Hot Spring Hills fault, were averaged to estimate a mean displacement of 0.6 m for the rupture(s?). It is possible that 0. 6m is a minimum value for the average displacement because scarps larger than ~1.5-2 m that could be the result of the most recent event were not measured; based on morphology alone, it was not obvious that these larger scarps were the result of a single event. By comparing the inferred paleoearthquake rupture length and estimated average displacement to corresponding measurements from historic earthquakes of known magnitude, the magnitude of the paleoearthquake can be estimated. Wells and Coppersmith (1994) developed the following equations for determining the moment magnitude (M) of an earthquake as a function of the surface rupture length (SRL) and average displacement (AD):

(1) $$M = 5.08 + 1.16*\log(SRL)$$

(2) $$M = 6.93 + 0.82*\log(AD).$$

The equations are derived from regressions of moment magnitude (M) on (SRL) and (AD) for 77 and 56 historic earthquakes with magnitudes of 5.8 to 8.1, respectively. Using equation one and an inferred rupture length of 45 km, the calculated paleoearthquake magnitude is 7.0. The calculated paleoearthquake magnitude using an estimated average displacement of 0.6 m and equation two, is 6.7. Preference is given to the estimate based on rupture length due to the small number of measurements used to estimate average displacement, and the possible bias in the data explained above. It is important to note that these are estimates based on the assumption that the Hot Spring Hills fault broke over it's entire length in a single event. It is possible that the observed ruptures are the result of multiple earthquakes of lesser magnitude.

Slip Rates

The most commonly used method for calculating slip rates is dividing the cumulative displacement of a landform or deposit by it's age. Slip rates can also be calculated by dividing the measured displacement per event by recurrence interval (McCalpin, 1996),

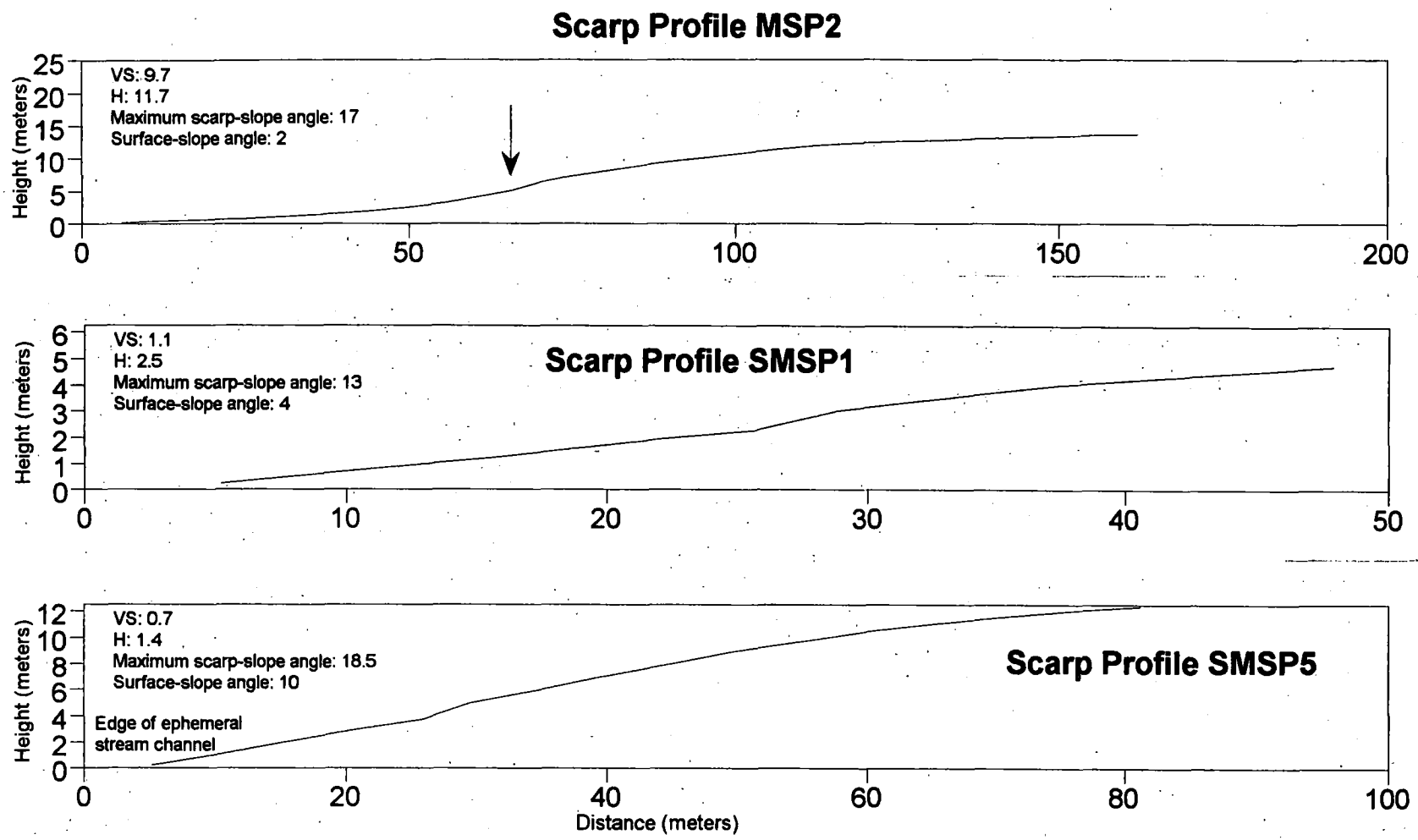

Figure 1-4. Surveyed topographic profiles of Hot Spring Hills fault scarp. Profile locations are shown in figure 1-2. Breaks in slope present in all profiles are interpreted to be fault scarps generated by a latest Pleistocene/early Holocene faulting event.

however, only the first method is used here. Given the large uncertainty in the age of the bajada surface and not knowing when faulting initiated relative to the estimated age of the surface, the slip rates presented here are considered rough estimates. Not knowing the actual amount of displacement due to burial of the original ground surface on the hanging wall also adds uncertainty in calculating a slip rates. Assuming a fault dip of 70°, the estimated dip-slip displacement at this site is 19.1 m. Using a range of 750 ka to 1.5 ma for the age of the bajada surface, the minimum slip rate is 0.03 and 0.01 mm/yr, respectively (19.1m/750 ka and /1.5 ma).

Return to vehicles and continue north on dirt road.

5.1 Turn left (west), go through gate and proceed on dirt road. PLEASE MAKE SURE THE GATE IS CLOSED behind you if you are the last vehicle through. If you are not certain if there are others behind you please be on the safe side and close the gate. Thanks - THE MANAGEMENT.

5.5 Dirt road enters from right, stay left.

5.6 Go through gate and continue on dirt road. The same goes for this gate, PLEASE MAKE SURE THE GATE IS CLOSED behind you if you are or might be the last vehicle through.

5.7 Intersection with Hwy 95. Turn right and proceed north on Hwy 95. Follow the compound fault scarp of the Hot Spring Hills fault on your right (east) as you drive north on Hwy 95.

7.1 Entering state of Oregon.

7.5 Entrance to rodeo grounds on left. If you left your vehicle here you should now pick it up.

8.3 The fault that we examined at STOP 1 crosses Hwy 95 about 0.2 miles in front of you. The fault scarp at this location has a height of 3.1 m and a measured vertical separation of the ground surface of 2.3 m. You can follow our route to Stop 2 on Figure 5.

9.0 The surface you are currently driving on is a cut terrace inset into the bajada surface and has an estimated soil age of 45 ka (see soil TRS5 Appendix 1). The surface is vertically offset a minimum of 2.3 m, (measured from scarp profile TRSP1, Figure 4). Assuming a fault dip of 70°, and an estimated dip-slip displacement of 3.5 m, the minimum slip rate at this site is 0.08 mm/yr (3.5 m/45 ka).

9.4 You are currently driving on the oldest bajada surface which is locally dissected and has an estimated age of 750 ka to 1.5 ma. This is the same surface from STOP 1-1.

10.4 Note the well developed carbonate soil of the bajada exposed in the road cut on both sides the of the highway **but** don't miss the turn at 10.5 miles!

10.5 Turn left (west) onto dirt road before Hwy 95 descends into the arroyo of Tenmile Creek. Again for those of you with vehicles that have low clearance we recommend you leave your car at the open grassy area at the base of the hill. We will be returning the same way so you can retrieve your vehicle en route to STOP 1-3.

11.3 Dirt road enters from right, stay left.

11.6 Road forks, stay right.

11.7 Good view of the large compound scarp of the Hot Spring Hills fault to your right (north).

12.0 Intersection with another dirt road. Turn left and continue southeast.

12.3 Vague dirt road enters on your left at an acute angle from the northeast; turn onto this road. Don't miss the turn!

12.5 **STOP 1-2. (10:30-11:00 am) Recent Surface Faulting of Tenmile Creek Fan.** Park vehicles in main tracks of road and assemble near flagged markers. People arriving first should park beyond the designated stop so people carrying up the rear don't end up having to walk a half mile to get to the stop.

We are standing on the Tenmile Creek fan which is offset by a recent surface rupture (Figure 5). The rupture is difficult to detect on the ground but can be easily seen on air photos and in surveyed scarp profiles (Figure 6). There are compound scarps on either side of Tenmile Creek fan. Tenmile Creek has apparently been competent enough at times during the Quaternary to destroy all evidence of any prior faulting events except the most recent surface rupture. The fan is interpreted to be latest Pleistocene or early Holocene in age based on the Stage 1 carbonate horizon (see Appendix 1, Tables 1 and 2) developed in soil TRS3 (Appendix 1). It was not possible to calculate an age for soil TRS3 using the secondary (pedogenic) carbonate index (cS) index of Machette (1985) because there was no secondary pedogenic carbonate present in the <2 mm fraction of the soil and the amount of $CaCO_3$ in the >2 mm fraction, mainly carbonate coatings on gravel clasts, was determined to be negligible. Therefore, this soil/surface is thought to be at least no older than the MS1 soil at STOP 1-1. The estimated age of the soil and the deposit in which it is developed (latest Pleistocene or early Holocene) serves as a maximum limiting age for the surface faulting event that generated the scarp at this site.

Return to vehicles and proceed on dirt road.

12.6 Intersection with the road we drove in on. Turn right (east) and return to Hwy 95. For people who left their vehicles near the highway, you are going to want to retrieve

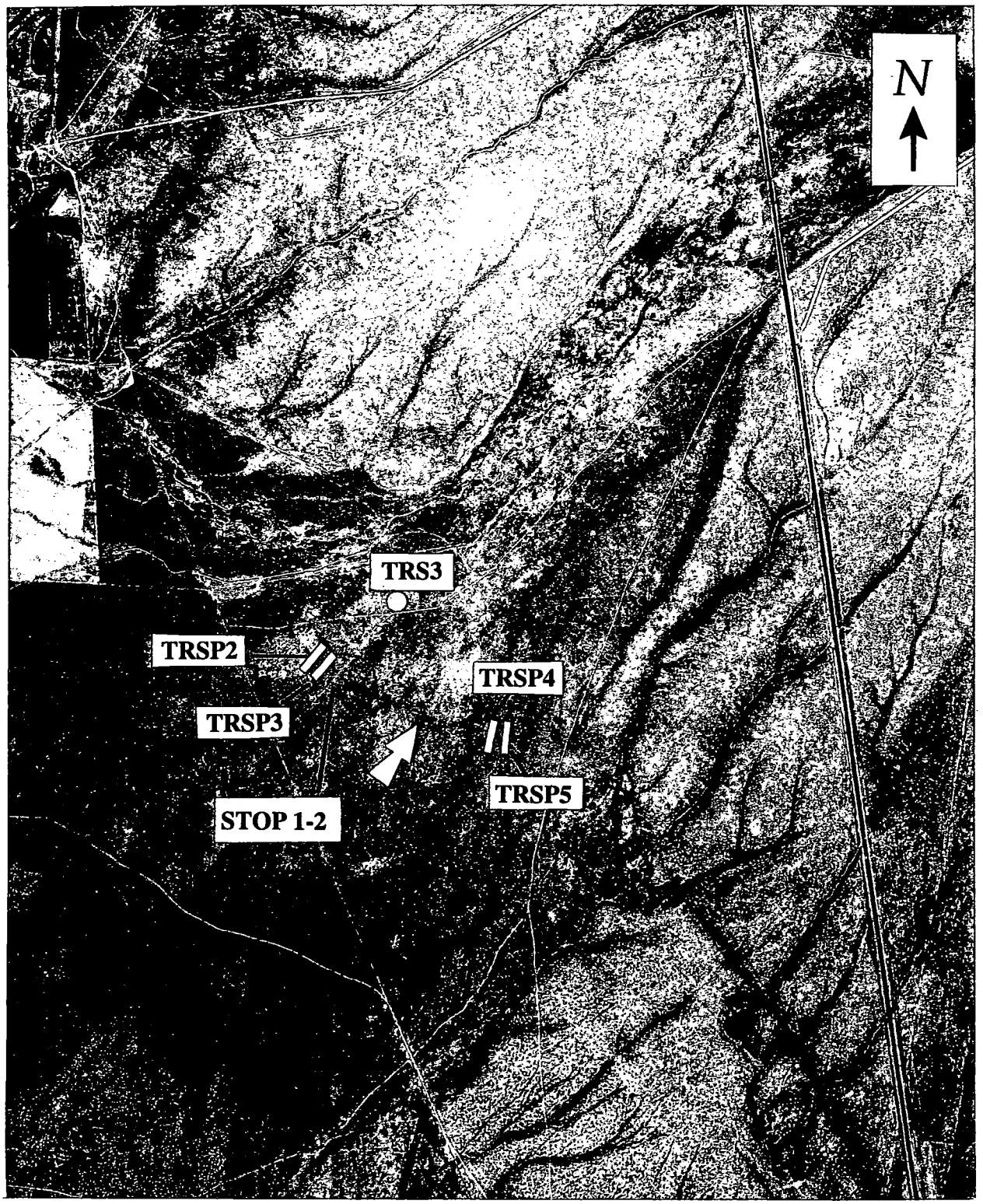

Figure 1-5. Aerial photo of Tenmile Creek fan showing location of STOP 1-2, scarp profiles TRSP2 through 5 and soil TRS3. Arrow points to trace of a latest Pleistocene/early Holocene surface rupture.

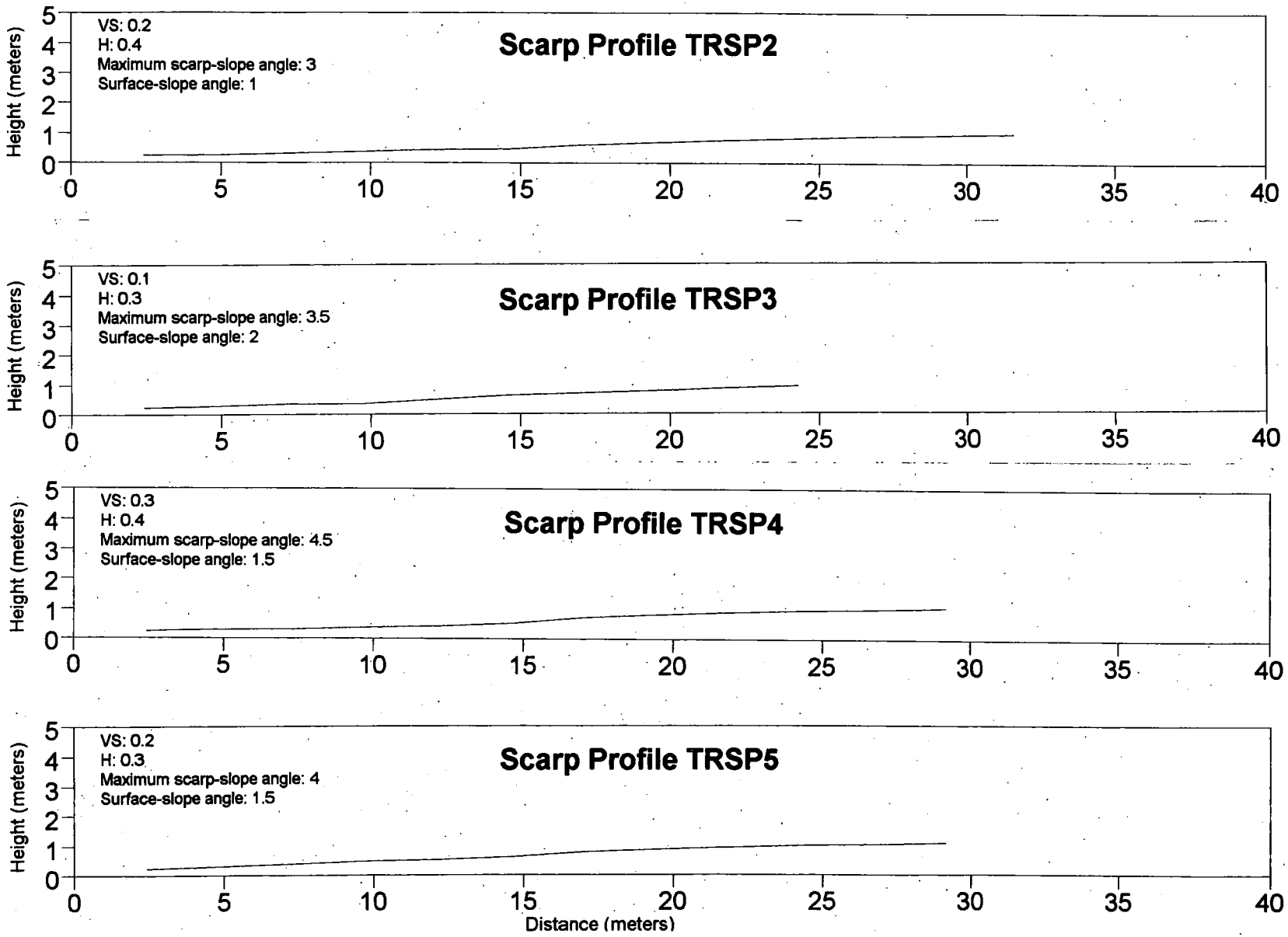

Figure 1-6. Surveyed topographic profiles of fault scarps displacing Tenmile Creek fan. Profile locations are shown on figure 1-5. VS – vertical separation of the ground surface; H – scarp height.

your vehicles before returning to Hwy 95. You can follow our route to STOP 1-3 on Figure 1-7.

13.7 Back at intersection with Hwy 95. Turn left and proceed north on Hwy 95.

14.1 Note the well developed carbonate soil of the bajada surface exposed in the road cut on both sides of the highway.

15.4 **STOP 1-3. (12:00-1:00 pm) Borrow Pit Exposure of Bajada Soil.**
Turn right (east) and enter borrow pit. You can either park in the borrow pit or turn left before you descend into the pit and you can park around the periphery.
12-12:30 Presentation.
12:30-1:00 Lunch and geologic perusal.

The greatest amount of displacement observed along the Hot Spring Hills fault, is near Hot Spring Hills. Here, the bajada has been uplifted and backtilted so that it now dips to the east towards the rangefront from which it was derived (Figure 7). The borrow pit exposes the soil developed in the bajada surface. In the southern portion of the borrow pit a west-facing cut exposes about a meter of matrix supported, sub angular to rounded, poorly sorted, coarse alluvial gravels that are capped by a 60 cm thick calcic horizon. The upper 25 cm of the gravel beneath the calcic horizon is also plugged with carbonate. The calcic horizon displays Stage IV morphology (see Appendix 1, Tables 1 and 2). It is not known how much is missing from the top of the calcic horizon. In soil TRS2, 150 m east of the borrow pit, the top of a well developed carbonate horizon was encountered at a depth of 39 cm. Based on carbonate soil development, topographic position, degree of dissection, surface morphology, and the amount of offset by the Hot Spring Hills fault, the bajada is considered early Pleistocene (~750 ka -1.5ma) in age. The bajada is comparable to the Thomas Creek Surface of Hawley and Wilson (1965) which is also considered to be early Pleistocene in age. The age of the bajada surface potentially serves as a maximum limiting age on the time faulting initiated along the Hot spring Hills fault; older surfaces which could provide earlier fault data don't exist today. Soil TRS4, which is developed in the east-sloping backtilted bajada surface is comparable to Soil TRS2 and is interpreted to represent the same soil as and is developed in the same geomorphic surface.

The crest of Hot Spring Hills is nearly 100 m above the valley floor. Dividing the apparent vertical displacement of 100 m by the estimated age of the bajada surface (750 ka-1.5 ma) yeilds vertcal displacement rates of 0.1 to 0.07 mm/yr.

Return to vehicles and exit borrow pit.

*ATTENTION FRIENDS, it is about a 45 minute drive to the next stop and we encourage passengers, not drivers, to peruse the article in Appendix 2, as an introduction to the topics we will discuss at stops 1-4 and 1-5 and which we will revisit and expand upon during Day 2 of the trip.

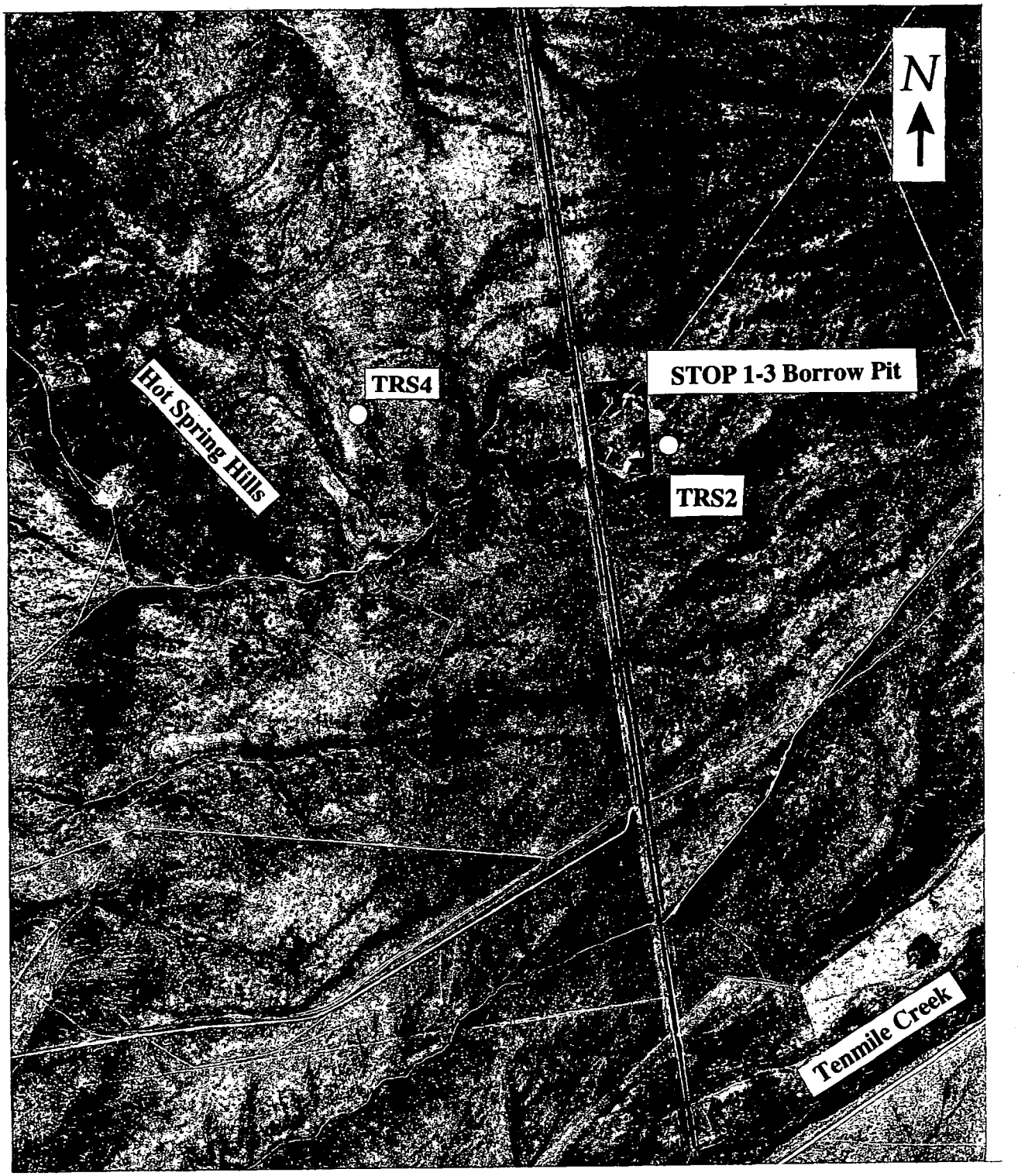

Figure 1-7. Aerial photo of dissected bajada in vicinity of Hot Spring Hills showing location of STOP 1-3 and soils TRS2 and TRS4.

15.5 <u>At intersection with Hwy 95, turn right and continue north on Hwy 95</u>.

19.3 Observe the compound fault scarp of the High Peak fault to your right (east). The High Peak fault is approximately 14 km long and extends roughly from Little Louse Canyon to Jackson Creek. Compound fault scarps of the High Peak fault record evidence of a latest Pleistocene-early Holocene faulting event near its southern end where recent faulting appears to have been restricted to two relatively short northeast trending segments of the fault, and an intervening northwest trending segment. It is possible that this portion of the High Peak fault ruptured simultaneously with or in response to movement on the Hot Spring Hills fault. There appears to be a young surface rupture at the northern end of the High Peak fault as well.

20.3 The Oregon Canyon Mountains to your left (west) attain an elevation of 7697 ft (2346 m) and are composed of mid-Miocene basalt and andesite that are petrographically and stratigraphically equivalent to the Steens Basalt and Steens Mtn. Volcanic Series of Fuller (1931).

22.6 Observe the fault scarp to your right (east) at the base of the slope denoted by the strong vegetation lineament; this is the northern end of the High Peak fault.

25.6 To your left (west) is the northernmost extent of faulting observed in the central axis of the valley. Faults which are middle to late Pleistocene in age (based on the estimated age of the deposits they offset) at the base of the Oregon Canyon Mountains (to your left) continue to the northwest into Blue Mountain Draw.

26.9 You are about to drive up a cutbank of Horse Corral Creek which may be fault controlled.

28.3 To your right (east) is a good view of the western edge of the Owyhee-Humboldt Volcanic Field, a plateau comprised of Miocene and Pliocene(?) volcanics.

32.8 Summit of Blue Mountain Pass. Peak to left is Blue Mountain, elev. 6843 ft (2085 m)

35.7 The Mendi Gore Hills come into view to the northeast at about 2:00. There are several faults that trend from the small valley in the foreground through the prominent saddles in the Mendi Gore hills and continue to the northeast in the valley beyond. The faults appear temporally similar to faulting in the northern Quinn River Valley, but their relation to the Quinn River fault zone is not known.

38.3 Note the compound fault scarp to your right (east).

39.3 Passing Basque highway maintenance station on your left. Shortly thereafter, beautiful views of Steens Mountain at 10:00.

43.8 Intersection with Whitehorse Road on left. We will return to this road at the end of the day and travel west to the Willow Creek campground and ultimately to Fields, OR where we will fuel up and resupply tomorrow (Saturday) morning en route to Day 2, STOP 2-1. Rise in ground between this point and Steens Mountain is Twelvemile Ridge. Coyote basin (Lake Coyote) is west of this ridge, and overflow from Lake Coyote was through the saddle at the north end of the basin.

53.0 Passing Mountain Standard Time boundary. Do NOT set your watches forward!

58.0 Crossing Crooked Creek; prepare to turn right. Much of the overflow from Lake Coyote was confined to these narrows, but if the flood hypothesis is correct, water also flowed over the valley walls.

58.5 **STOP 1-4. (2:00-3:00 pm) Overlook of Crooked Creek, Introduction to Pluvial Lakes and Overflow.**
Turn right (east) into hardrock gravel quarry and park. Short overview stop. From here we can see the area between Crooked Creek, the possible flood-scoured channels, the east rim of the Coyote basin, and Steens Mountain in the far distance.

In this hard-rock pit, ledgy rhyolite is mined and crushed for aggregate. To the south and east is Crooked Creek, which flows northeast about 35 km to join the Owyhee River (fig. 2, Appendix 2). The valley here is narrow and bedrock-confined, but opens into a broad plain 2 km to the east. Crooked Creek heads less than 5 km to the west at Crooked Creek Spring and Pothole Springs (not visible). This stop sets the stage for discussions over the remainder of the field trip (especially STOPS 1-5 and 2-4, fig. 2, Appendix 2) regarding the pluvial history of Lakes Alvord and Coyote, the overflow connection between them, and a hypothesized catastrophic flood eastward from Lake Coyote down Crooked Creek; read Appendix 2 for background to these discussions.

In the far distance to the southwest is Steens Mountain; pluvial Lake Alvord filled Alvord and Pueblo Valleys east and south of Steens Mountain (fig. 1, Appendix 2). The low ridge visible in the middle ground is the eastern rim of the Coyote basin; Lake Coyote lay east of this rim and was at times separated from Lake Alvord by the Tule Springs rim. A spillway (not discernible from here) at the lowest point on the eastern rim of the Coyote basin lies at 1278 m, coincident with the most obvious shorelines of Lake Coyote (fig. 2, Appendix 2), and water clearly drained through this spillway and down a now-dry channel toward Crooked Creek and Potholes Springs. The low hills nearby, also to the southwest, are cored by rhyolite and cut by vertical-walled channels interpreted to have formed by overflow from Lake Coyote, either fed by or conjoined with Lake Alvord. The low hills bear a thin cover of rounded gravel and sand, possibly deposited when a flood emanating from Lake Coyote overtopped the hills (Stop 1-5 is on the southernmost hill looking down into a channel; fig. 2, Appendix 2). The hypothesized flood would have been confined by the narrow valley of

Crooked Creek below us, then spread out over many kilometers of the broad valley to the east before becoming confined to the narrow gorge of Crooked Creek canyon about 10 km east of Burns Junction.

Return to vehicles. Leaving this stop, turn back left (south) on Hwy 95.

61.1 Turn right (west) at wire gate, between mileposts 75 and 76. As you approach, watch for traffic behind you, slow down and prepare for some milling around. Cars with low clearance must be left here; the road we will drive is not rutted or bouldery, but does have sagebrush grown up between the tracks. The gate MUST be closed behind us; keep in mind we are on private land (owner, Harry Stoddard). Proceed west on dirt track.

62.1 Turn sharp right (north), road comes in at an acute angle, don't miss the turn.

63.6 **Stop 1-5. (3:30-5:00 pm) Possible flood deposits and channel scour along a tributary of Crooked Cr.**
Intersection with another dirt track heading west. Park however you can in this area amongst the sage. However, be extremely aware of and avoid starting a range fire. We will be gone from the vehicles for approximately an hour and a half.

Walk northwest from the parking area at the intersection of dirt roads to cliffs above a spring-fed wet meadow. As you walk, observe the clasts on the ground. At the parking area, the ground surface is mostly weathered bedrock with small scattered pebbles and sand covering the surface. Beginning about 500 m northwest, rounded gravel clasts litter the bedrock surface and become larger (up to small boulders) and increasingly abundant toward the cliffs. At the cliff edge, the exposed bedrock surfaces are angular with many vertical faces; they appear to have been plucked by vigorous water flow. The hill to the northwest across the wet meadow (interpreted as the bottom of a flood channel) is cut by a similar channel on its west side (fig. 2, Appendix 2; not in view). Not apparent from here is that this middle hill has a teardrop shape in map view. The hill is only 150 m wide (between the channels) and low at its southwest end; it broadens rapidly to 550 m wide and increases in height to the northeast. This shape is characteristic of flood-molded topography in the Channeled Scablands of Washington.

A nearby gully eroded into the west side of the hill on which we stand exposes a patch of indurated, poorly sorted pebbly sand. Superficially it appears inset with respect to the bedrock, but the degree of induration suggests that it may underlie the rhyolite flow rather than representing a flood deposit.

Return to vehicles. Retrace route back to highway.

66.1 Turn right (south) on Hwy 95 and retrace route to Whitehorse Road.

78.2 **Leave Hwy 95 and turn right (west) on Whitehorse Road. Please be very cautious and pay attention while driving on this road!**

85.9 Crest of Twelvemile Ridge. Visible due north is the east rim of the Coyote basin, and sill through which overflow went east into Crooked Creek. The playa of Lake Coyote is to the northwest.

87.9 Cresting a hill. Lake Coyote is to the north. At 11:00 is Big Sand Gap, the sill between the Alvord and Coyote basins, identified by Mark Hemphill-Haley and studied by David Lindberg, which carried overflow from Lake Alvord eastward into Lake Coyote.

99.1 Whitehorse Ranch on the right.

101.8 Look for FOP sign and turn left (south) on the otherwise unmarked Willow Creek road.

104.2 Turn left and follow signs to designated FOP camping area.

We are camping in a very beautiful area and ask all of you to be conscious of your impact on the fragile landscape. Please **DO NOT** drive over any sage brush, please stay away from the spring deposits, and please **DO NOT** modify the ground for a better camping spot. We ask that people keep vehicles on or very close to the roads and stay in the area designated for FOP. There is private land and BLM Wilderness Study Area in close proximity to where we are camping so if people stray from the area designated for FOP, it could potentially compromise our agreements with private land owners and BLM.

FIRES ARE NOT ALLOWED AT INDIVIDUAL CAMPSITES! We hope to have one centrally located campfire (which we can monitor closely) for everyone to enjoy. **Thousands of acres have burned in the area recently** and we cannot afford any accidents from people insisting that they have their own fires. So **PLEASE DO NOT have individual fires at your campsite.**

Hot springs: as all of you probably know by now, there is a hot spring just to the west of where we are camping. Our agreement with BLM (which we ask you to honor) is that nobody camp near the hot spring and that we use our portable toilets, not the toilet at the hot springs.

Thank you for your cooperation and enjoy the beautiful views and full moon!

END OF ROAD LOG FOR DAY 1

References

Caskey, S. J., 1995, Geometric relations of dip slip to a faulted ground surface: new nomograms for estimating components of fault displacement, Journal of Structural Geology, v. 17, n. 8, p. 1197-1202.

Hawley, J. W., and Wilson, W. E., 1965, Quaternary geology of the Winnemucca area, Nevada, Tehnical Report No. 5, Desert Research Institute, University of Nevada, Reno, NV, 92 p.

Machette, M. N., 1985, Calcic soils of the southwestern United States, in Weide, D. L., ed., Soils and Quaternary geology of the southwestern United States, Geol. Soc. Am. Special Paper, 203, p. 1-21.

McCalpin, J. P., 1996, Paleoseismology, Academic Press Inc., San Diego, CA, 588 p.

Fuller, R. E., 1931, The geomorphology and volcanic sequence of Steens Mountain in southeastern Oregon: Washington Univ. Pub. Geology, v. 3, p. 1-130.

Wells, D. L., and Coppersmith, K. J., 1994, New empirical relationships among magnitude, rupture length, rupture width, rupture area, and surface displacement, Bulletin of the Seismological Society of America, v. 84, n. 4, p. 974-1002.

ROAD LOG

DAYS 2 & 3

DAY TWO

Miles	Description
Start	Turn right at the intersection of Trout Creek Road and the Harney County, Fields - Denio Road. Travel north toward Fields. The range front escarpment of the northern Pueblo Mountains lies to the west. Southern Steens Mountain is to the north (Figure 2-1 and Figure 2-4).
1.5	Driving north, the fan surfaces west of the county road are faulted. The offset is down-to-the-east, normal with no strike-slip component. Fuller first reported youthful-appearing fault scarps in this area in 1931.
3.5	Additional faulted fan surfaces can be observed to the west of the county road. Low-sun-angle air photos also show similar scarps to the east of the road.
5.0	Shorelines of pluvial Lake Alvord are visible east of the county road on the far side of the northern Pueblo Valley. The base of the range front is notched by a prominent shoreline at or below 1280 m (4200 ft), based on the topographic maps.
6.8	A prominent scarp is visible to the west near the bend in the county road.
7.0	The scorched hills in the distance were burned in early August. The town of Fields was prepared to evacuate by the time the fire was controlled.
8.2	Fields is to the left. Stay on the main county road at the V intersection and it brings you to the Fields parking lot. The general store has a limited supply of sundries and groceries, a café and a gas pump. There will be no more chances to buy cold drinks, eat at a restaurant (they can seat about a dozen, maybe), or to gas up on the remainder of the trip.
	Depart Fields and continue north on the county road.
9.7	Continue north along the west side of the northern Pueblo Valley. Keep right (leave the pavement for the gravel-surfaced road) at the V Junction with the county road that heads west to Catlow Valley and Frenchglen. To the north, "the High Steens" portion of Steens Mountain forms the highest promontory. The road to Catlow Valley (that you are not traveling on) continues west through Long Hollow, a pass that divides the Pueblo Mountains to the south from southern Steens to the north. The trip route stays on the gravel county road for now and will follow the base of the Steens escarpment to the north. A well preserved remnant of a convex-to-the-east, deltaic bar of pluvial Lake Alvord makes up much of the "fan" surface east of the road.

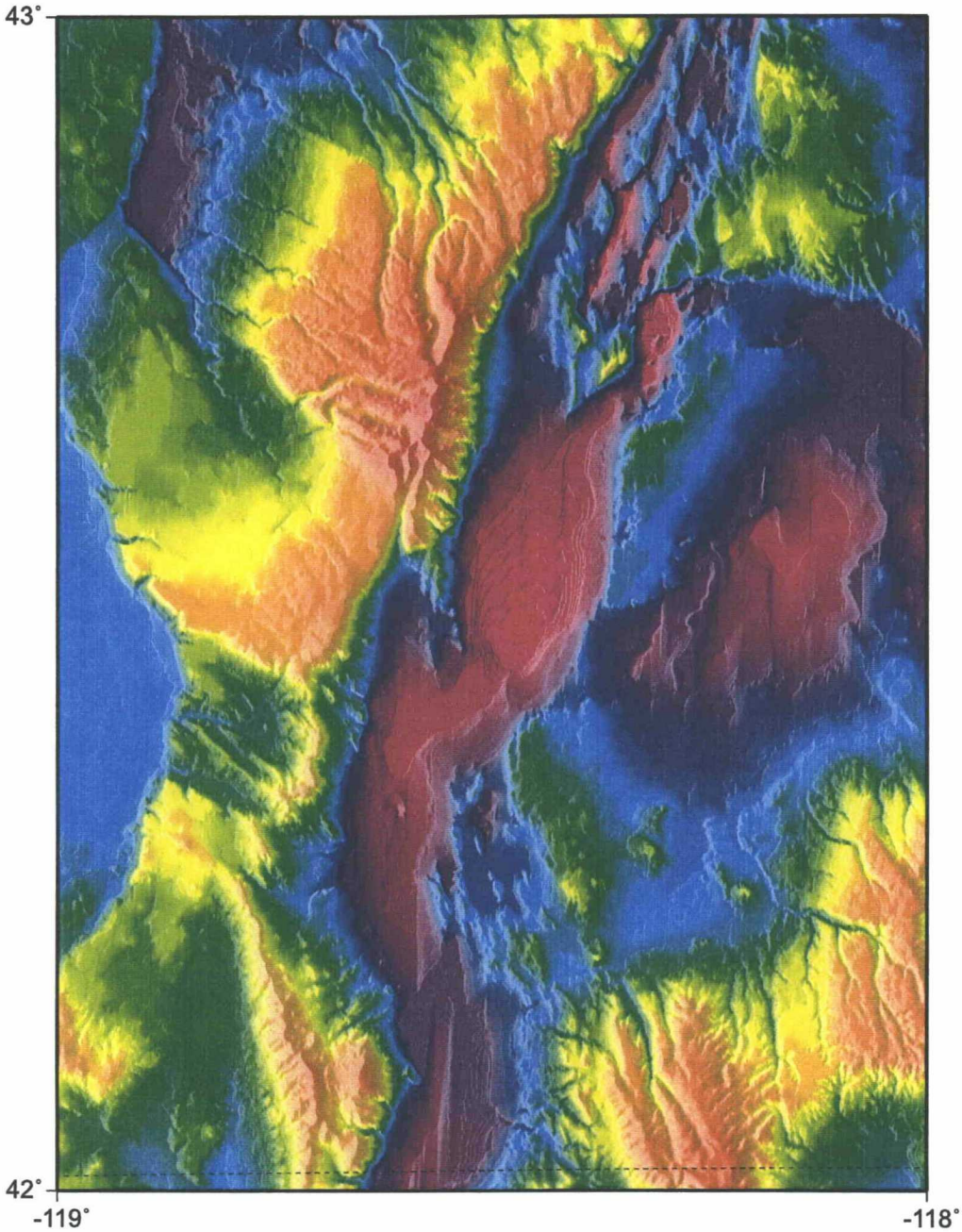

Figure 2-1 - Color shaded-relief map centered on the Alvord Valley. The northern Pueblo Valley is located in the bottom of the image. Coyote Lake Valley is located in the eastern part of the image. The large high elevation to the west of the Alvord Valley is the High Steens. Note the large glaciated valleys that radiate from the crest of the mountain.

10.4 The delta bar intersects the road from the southeast, north of the power transformers, about where the road starts down hill after passing the gravel quarry on the left.

12.1 Alvord Peak (elevation 2156 m 7075 ft) is the prominent peak in the southern Steens Mountains to the west of the highway.

14.8 The south end of Alvord Lake is visible east of the highway. Borax Lake is slightly south of Alvord Lake, but cannot be seen from this perspective. The hot springs at Borax Lake have been the subject of geothermal studies for a potential power plant project.

15.9 The route crests over the top of an alluvial fan – pluvial delta complex at the head of Scoubes Creek. A prominent shoreline (elevation 1280 m, 4200 ft) can be observed at the base of the escarpment. The trip now leaves the Fields quad and enters the V Lake quad.

17.5 The road turns northeast and crosses the Bone Creek fan. To the west, a large pluvial delta complex is offset by multiple, down-to-the-east normal faults. To date, we have only done some preliminary aerial photo reconnaissance on the Steens fault zone from Denio to the Alvord Desert. The faults offset what are likely ~12ka shoreline deposits.

18.0 **Stop 2-1**. Gravel bar (T36S, R33E sec 21, V Lake quad). Park on the right near the borrow pit in the pluvial bar (Figure 2-2). At this stop we will describe stratigraphic and tectonic features that are representative of features that will be seen often on the rest of the trip.

The bar that we have parked by is a remnant of a pluvial shoreline at elevation about 1244 m (4080 ft). As a pluvial deposit well below the Lake Alvord sill elevation (1280 m, 4200 ft), this bar formed reasonably late in the history of the lake and may be related to an early Holocene pluviation or may represent a short period of stabilization of lake level during the ca. 12 ka recession of the lake. The cross-bedded nature of the deposit is exposed in the working face.

West of the stop, the range front in the foreground is generally Miocene basalt, with crests at about 1525 m (5000 ft) (see Appendix 5 for descriptions of Steens Mountain Tertiary stratigraphy). To the southwest, the pluvial paleoshore, at an elevation of about 1280 m (4200 ft), is formed in a delta deposit at the mouth of Bone Creek. A down-to-the-east normal fault crosses the pluvial delta near the mouth of the canyon. Near the north side of the Bone Creek delta the fault scarp is visible where it crosses between the two large boulders. A series of recessional shorelines are formed along the east side of the delta bar (Figure 2-2). The top of the delta bar appears to have been significantly eroded, probably due to the proximity of nearby Bone Creek. The southern edge of the delta bar has been truncated by post-pluvial alluvial fans.

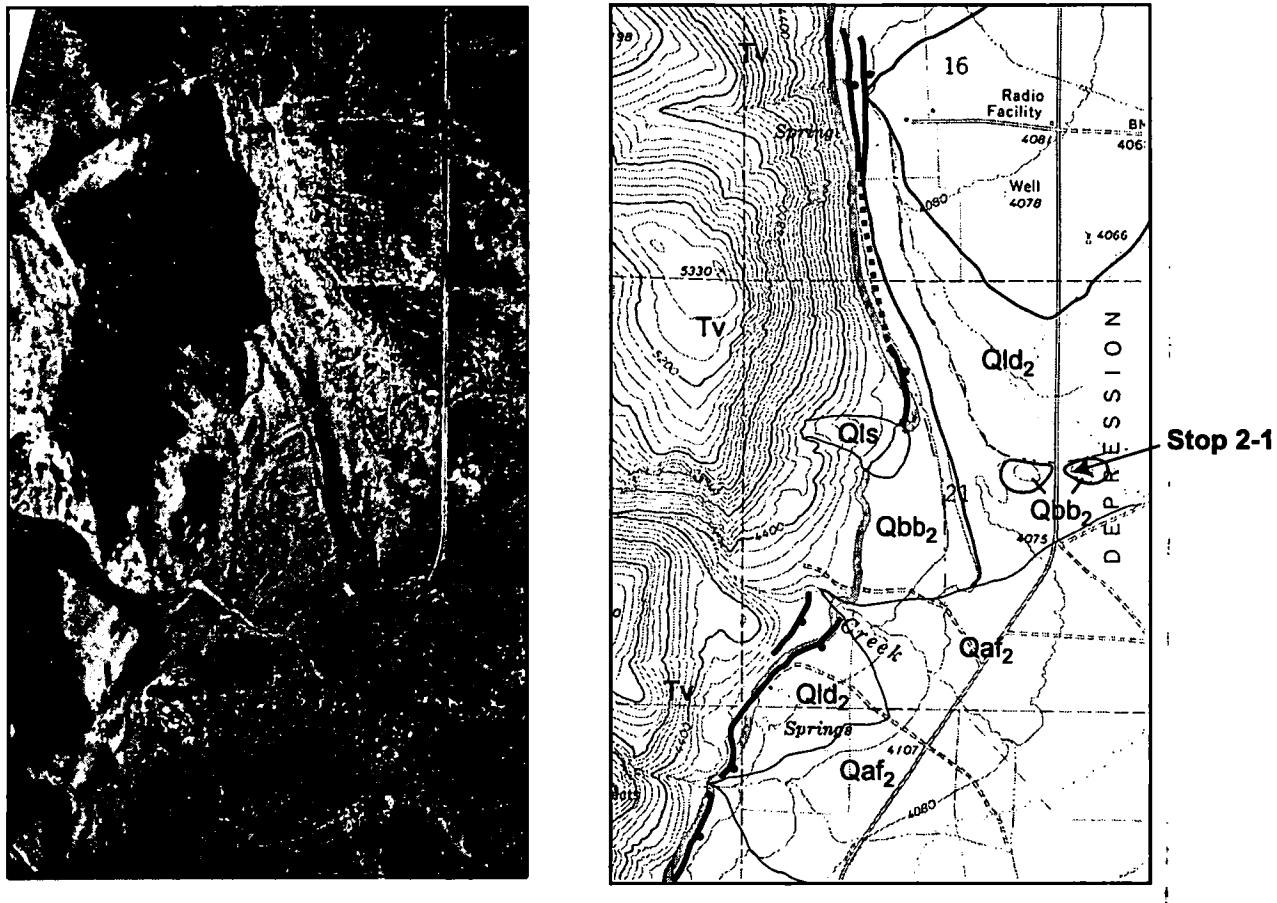

Figure 2-2 **Stop 2-1**. Low-sun-angle air photo and preliminary geologic map. Youthful (Holocene?) faulting (bold dark line) along the range front nearly coincides with the 1280 m (4200 ft) shoreline (bold gray line). A large gravel bar (Qbb_2) is preserved along the north side of Bone Creek. Several of a series of recessional shorelines formed along the eastern edge of the gravel bar are shown (thin dashed and dotted line). Our first stop is in a quarry within a remnant of the gravel bar.

North of the Bone Creek delta, the fault scarp becomes lost in the talus slope. Prominent stone stripes are highlighted where they are truncated by shorelines in the face of the escarpment. Stone stripes truncated by a pluvial shoreline may indicate that periglacial conditions prevailed in this part of the valley during pluvial maxima. The highest, and presumably the oldest, shorelines are therefore probably younger than or contemporaneous with the stone stripes.

Figure 2-2 b. Cut face of the pluvial gravel bar at Stop 2-1. The bar at 1244 m (4080 ft) is a deposit from a very late Pleistocene or Holocene lake, well below the elevation of the 1280 m (4200 ft) constraining sill.

The view to the north at this stop is of Steens Mountain summit at 2947 m (9670 ft). On the Alvord Desert north of here, the valley floor is 1728 m (5670 ft) below the summit at about 1219 m (4000 ft) in elevation. Wildhorse Canyon is visible below and west of the summit. Wildhorse Canyon attests to occupation by late Pleistocene glaciers.

North-northeast of Stop 2-1, the spur ridge which forms the east wall of Wildhorse Canyon extends down to the valley floor at Serrano Point.

Tule Springs Rims is east across the valley, with Howluk Butte (elevation 1417 m, 4648 ft) east of the Rims.

18.0 West of the road is a pluvial delta remnant at the mouth of Carlson Creek. A single tree marks the head of the Holocene post-pluvial fan. Youthful fault scarps cross the mouth of this canyon and offset the pluvial deposits.

20.7 Soon after the road bends northeast, the route crosses Miranda Creek at elevation 1254 m (4115 ft) with the Kueny Ranch to the east. A series of large Holocene alluvial fans blanket all pluvial shoreline features along the range front from this point for several miles. Here the route leaves the V Lake quad and enters the Andrews quad.

Directly east across the valley, the low point in the escarpment is Little Sand Gap, where an interesting suite of shorelines is preserved. Five prominent shorelines at elevations of 1269, 1278, 1287, 1294 and 1302 m (4162, 4193, 4222, 4245 & 4272 ft) were surveyed with an engineering level (an altimeter was used to measure the 1302 m shoreline) at this locality. Based on topographic maps of the Little Sand Gap, the elevation of the lowest point of the divide between the Pueblo Valley and the Coyote Lake Valley to the east is at an elevation of just over 1329 m (4360 ft). A lower sill occurs about four miles to the north at Big Sand Gap suggesting the Little Sand Gap was probably not an overfill outlet to Coyote Lake.

The road curves to the north on the alluvial fan complex near Juniper Creek. Serrano Point (elevation 1380 m, 4531 ft) is on the right, about two miles away, across Wildhorse Valley. The large Cottonwood trees mark the site of the former Serrano Point Ranch. An exploratory trench (Dust Bowl Trench of Hemphill-Haley et al. (1989) was excavated in faulted latest Pleistocene (<12 ka) lacustrine and eolian sediments along the southernmost Alvord fault (Appendix 5). The trench, located about 1.5 miles east of the ranch site, was aptly named. Although it provided excellent exposures of faulted lake beds and tephra, the crew looked like they had spent the day in a flour factory. Figure 2-3 now shows much of the area that will be covered before we head east across the playa.

22.6 Slow down to limit the dust in the town of Andrews (no services).

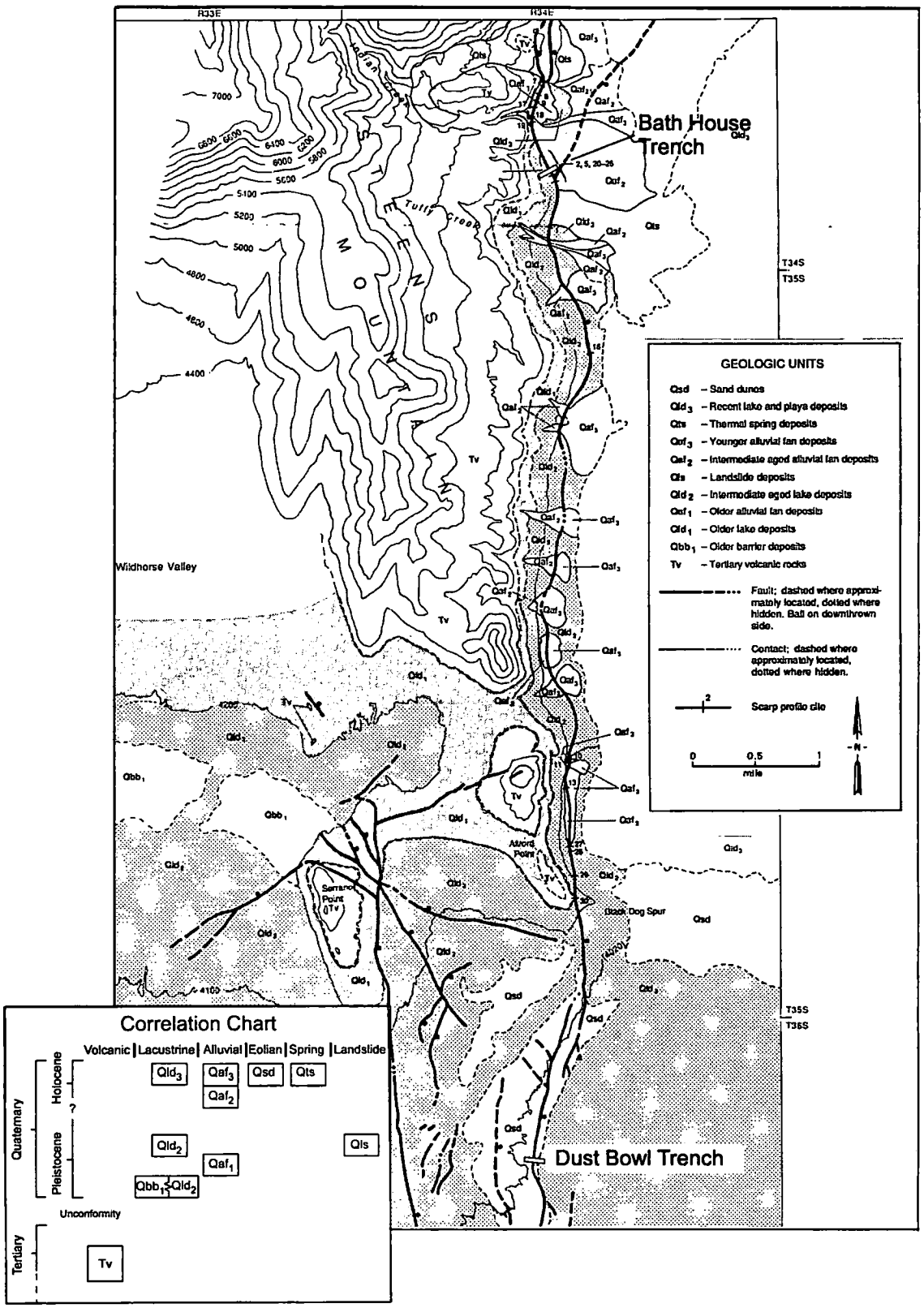

Figure 2-3 Geologic map of the southern Alvord fault.

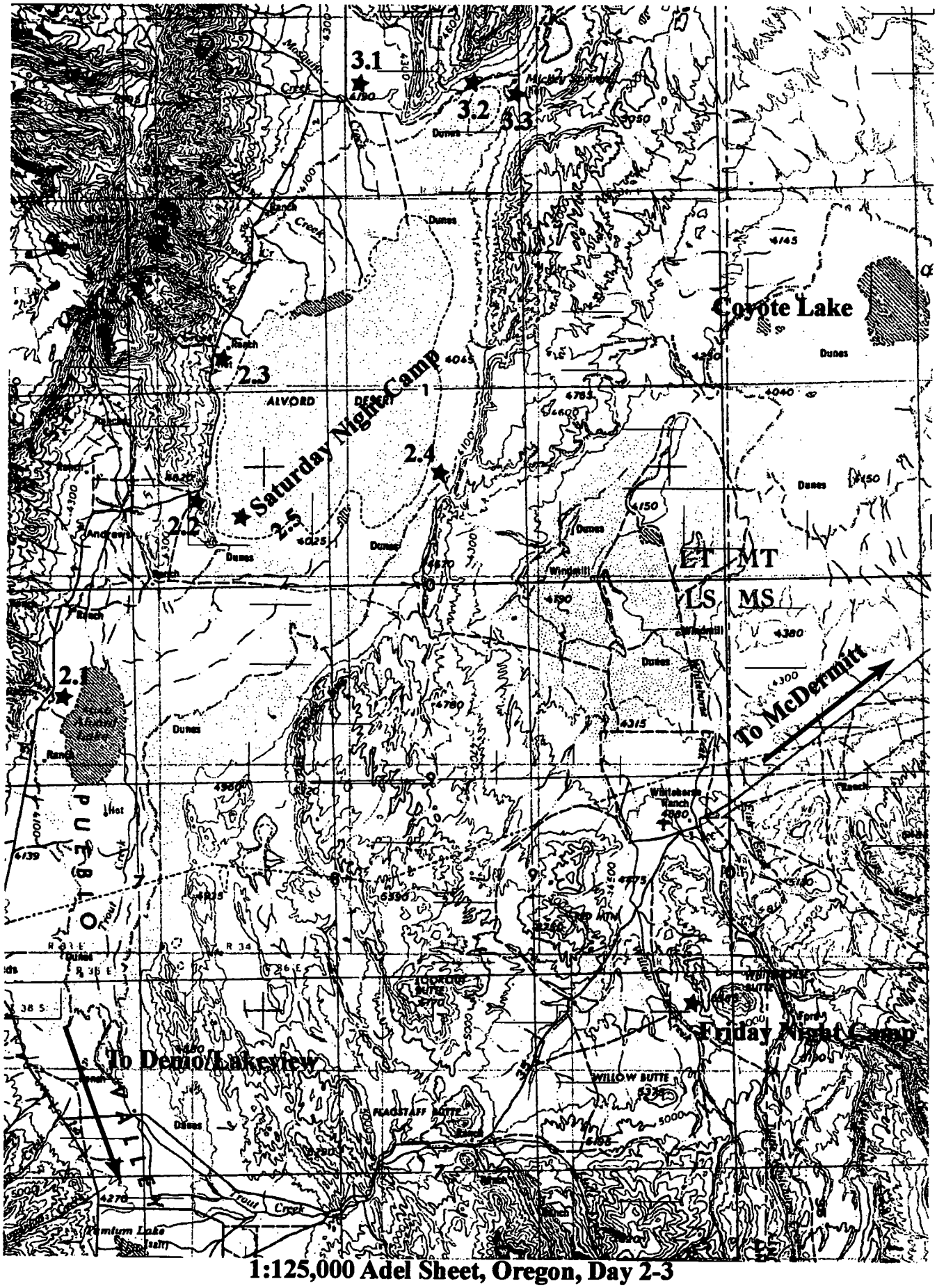

1:125,000 Adel Sheet, Oregon, Day 2-3

22.7 Andrews School, on the left. Until recently it was the one room schoolhouse for the valley children for many years. Elementary School is now held in Fields for all the children from the Pueblo Valley and the ranches to the north. High school children leave the valley for classes at a high school in Crane, near Burns, where they live on campus during the school year, coming home on weekends and in the summer. The Crane School is one of the last public boarding schools in the nation.

23.7 Slow down for the sharp right hand turn. After the road turns east and crosses Wildhorse Valley, a pluvial shoreline bar is visible to the left at an elevation of about 1281 m (4205 ft).

25.4 Road turns toward the northeast. Alvord Point (1401 m, 4598 ft) is due east.

26.9 Road crosses a subtle shoreline at elevation 1295 m (4250 ft).

27.1 **Stop 2-2**. Alvord Point Saddle (T35S, R34E, Sec. 20, Andrews quad). Park on right side of the road (Figure 2-5). At this stop we will look at deposits associated with the highest late Pleistocene lake stand. These deposits, at an elevation of ~1304 m (4280 ft) are associated with the highest shoreline (~1310 m, 4300 ft) recognized in this part of the basin. At present, the basin is closed at about 1283 m (4210 ft) at Big Sand Gap, so the gravel deposits here must predate the establishment of that sill. Age of this highest-standing gravel bar is not known. Its elevation is consistent with faint shorelines at locations along the west side (Hemphill-Haley, 1987) and east side (Lindberg, 1999) of the valley. Hemphill-Haley (1987, Figure 2-6) speculates that the ~1310 m shoreline represents the rising limb of the most recent significant pluviation in the basin (Appendix 5). The faint representation of the shoreline is likely related to the fact that the lake was stable at that elevation for only a brief time before down-cutting at Big Sand Gap occurred.

The 1295 m (4250 ft) shoreline, a few hundred meters to the west, is possibly related to establishment of some interim sill at Big Sand Gap or Coyote basin. This shoreline is about 15 m (49 ft) above the prominent 1280 m (4200 ft) shoreline. It may represent the second oldest and second highest lake stand to persist for a time in the valley. It is not clear how this shoreline relates to the down-cutting event at Big Sand Gap except that it is lower than the highest lake occupation and higher than the established sill. Nor are we sure how other shorelines around both Alvord and Coyote at 1290 to 1295 m may relate to each other.

As the trip proceeds, we will discuss scenarios that consider various pluvial and tectonic explanations for the various shoreline elevations and their potential ages in the valley.

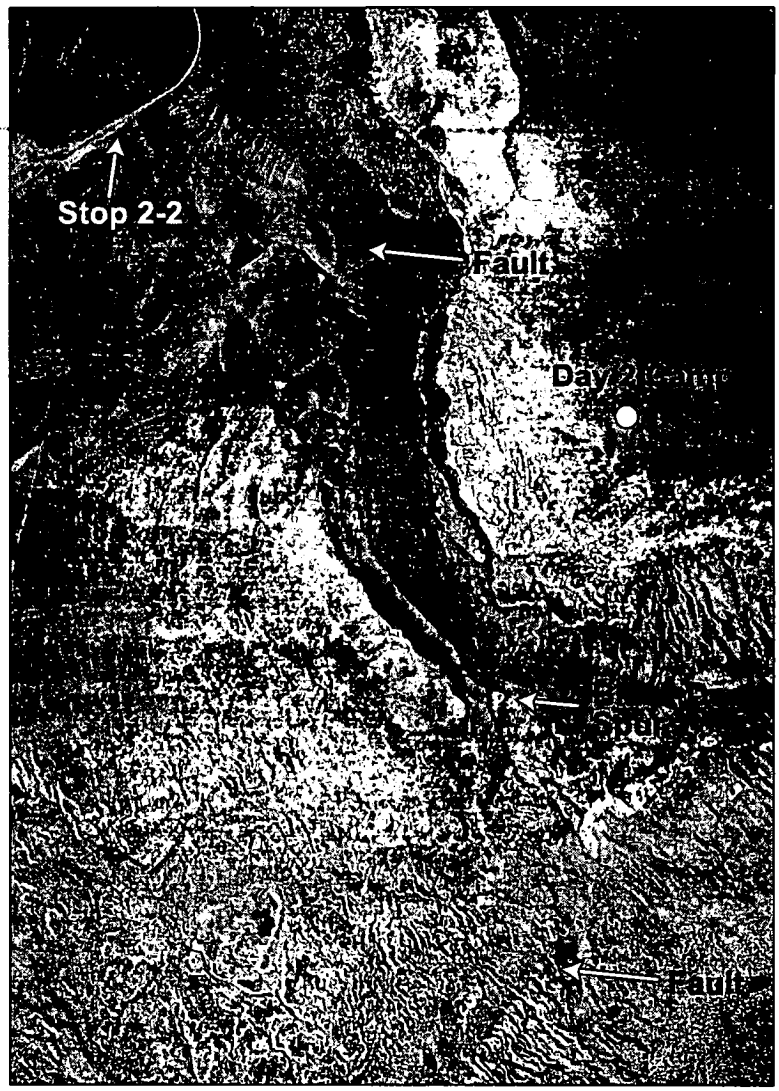

Figure 2-5 - Low-sun-angle aerial photograph of the southern Alvord fault. Stop 2-2 is along the Alvord Saddle. The Alvord fault traverses dune and playa deposits to the south. It then displaces late Pleistocene shorelines and intermediate-age lacustrine sediments at Black Dog Spur. The camp for Day 2 is located in the southwestern corner of the Alvord playa.

If you look behind you (that is, toward the west) you will see that we have traversed a large (>13 km, 8 mi) right-step in the Steens Mountain range-front. The right-step coincides with the transition from the Southern (low) to Central (high) Steens. At the base of the northernmost Southern Steens, the "Fields" structural segment of the Steens fault zone terminates in the Wildhorse Canyon (Appendix 5, Figure 7). The Alvord segment of the fault is located less than 800 m (0.5 mi) to the east of our location, along the eastern base of Alvord Point (the low hills immediately to our east). There is an overlap of several km between the two segments. Interestingly, based on very preliminary observations of low-sun-angle aerial photos, the portion of the Fields segment encompassed by the overlap appears to have scarps that are significantly older than the Alvord segment or southern Fields segment scarps. Additionally, the Alvord segment is associated with both the highest part of the Steens escarpment and the lowly basalts at Alvord Point. Displacements along the Holocene scarp are about the same at Alvord Point as at the base of the Central Steens. Does this suggest a relatively recent evolutionary stage of the Steens fault zone where the Central Steens range front is expanding southward at the expense of the southern Steens? Clearly the Alvord fault at its southern end has not had similar displacements along its length for a significant period of time or Alvord Point would be much higher.

The right-step also coincides with the approximate eastward termination of the Brothers fault zone, one of several diffuse, northwest-trending regional deformation zones. Lawrence (1976) speculates that these zones have minor dextral shear and mark the northward decrease in Basin and Range extension. He also speculates that the Brothers fault zone terminates against the Steens fault zone. We have not been able to confirm or refute the presence of the Brothers fault zone at this location. But, this significant transition in the Steens fault zone approximately coincides with the projection of the Brothers fault zone. Within the step in the range front is a complex zone of faults (Figure 2-7A) with diverse orientations. Some faults displace post-12 ka shorelines while others appear truncated by older shoreline features.

From this point we will travel north and our next stop will be near Alvord Hot Springs (but no soaking until this evening).

28.0 Cross north through the Alvord Point saddle and start down the hill. Slow down for the sharp left-hand bend in the road. Steens Mountain crest is in view to the north, straight ahead. Beyond the High Steens, the Northern Steens begin to come into view. East of the Northern Steens is the northwest branch or fork of the Alvord Valley at Miranda Flat. Beyond the horizon in the Miranda Flat area, the county road continues north past Mann Lake, Juniper Lake and over the valley summit (1347m, 4420 ft), finally reaching the pavement across Folly Farm Flat near Baker Pass (Highway 78). The lowest modern wind gap in the northern end of the valley is at about 1340 meters (4395 ft) at Neals Hill north of Five Cent Lake.

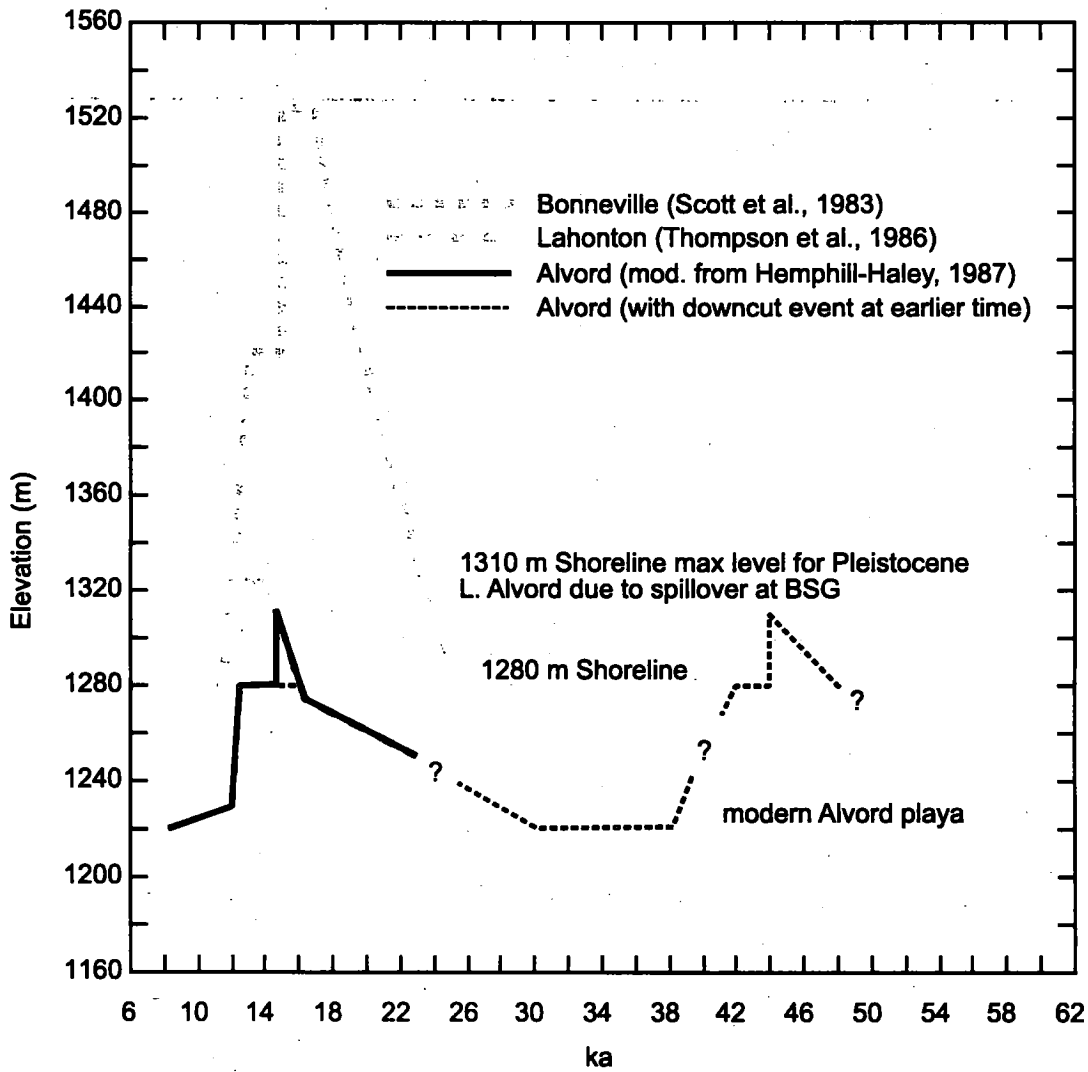

Figure 2-6 Latest Pleistocene (Pinedale?) pluvial chronology for Lakes Bonneville, Lahonton and Alvord. The solid gray lines depict shoreline elevations in the Alvord basin, the faint shoreline at 1310 m, prominent shoreline at 1280 m, and modern playa at 1220 m. Solid black line is the Alvord chronology proposed by Hemphill-Haley (1987) suggesting that down-cutting at BSG occurred in the last high-stand of the lake. An alternative chronology (black dotted line) would have the down-cutting occur at an earlier high-stand. The downcutting event forces the elevation of subsequent high-stands in the Alvord Valley to no more than 1280 m.

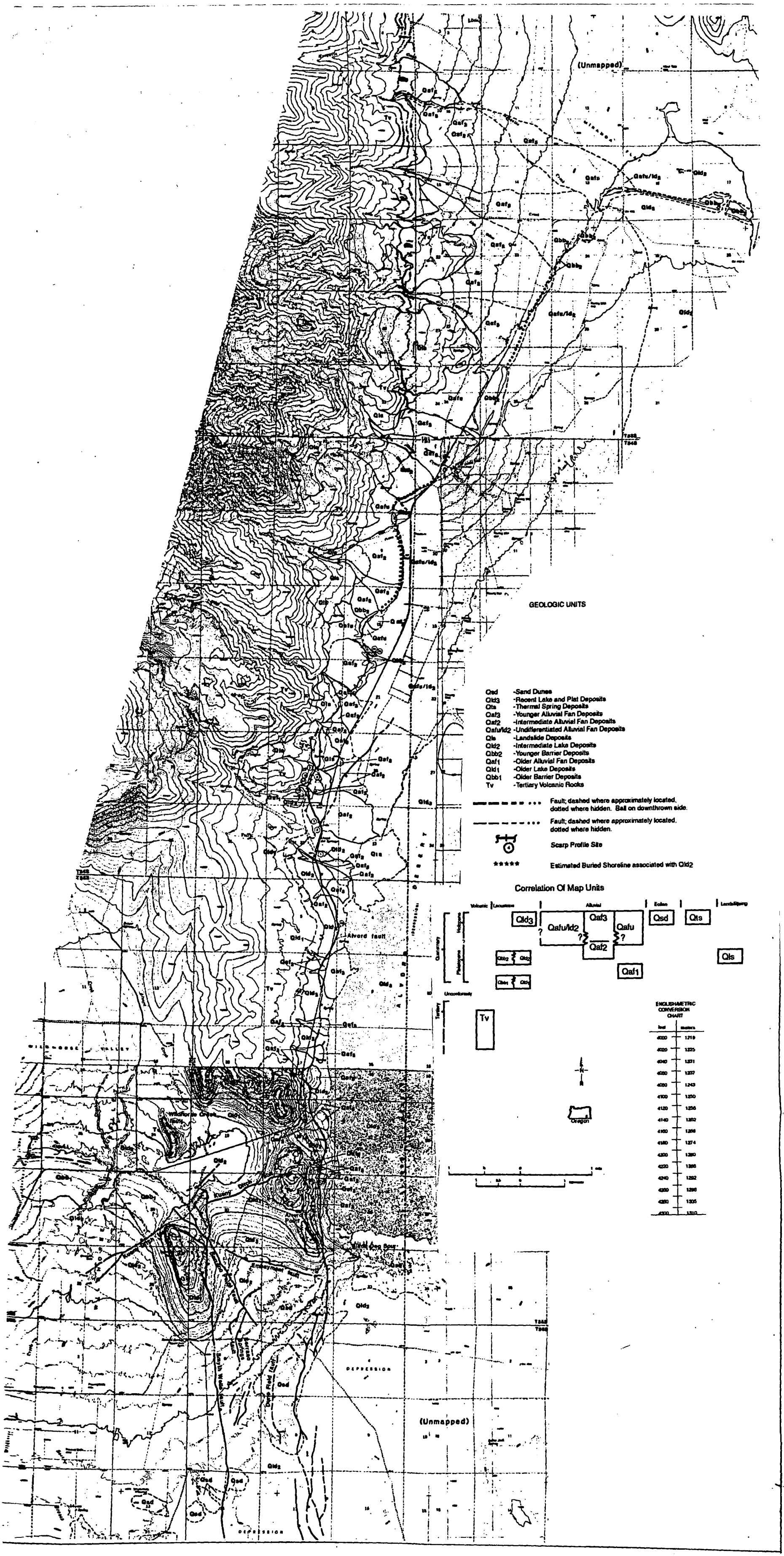

Figure 2-7A. GEOLOGIC MAP OF THE BASE OF THE EASTERN ESCARPMENT OF STEENS MOUNTAIN, HARNEY COUNTY, OREGON

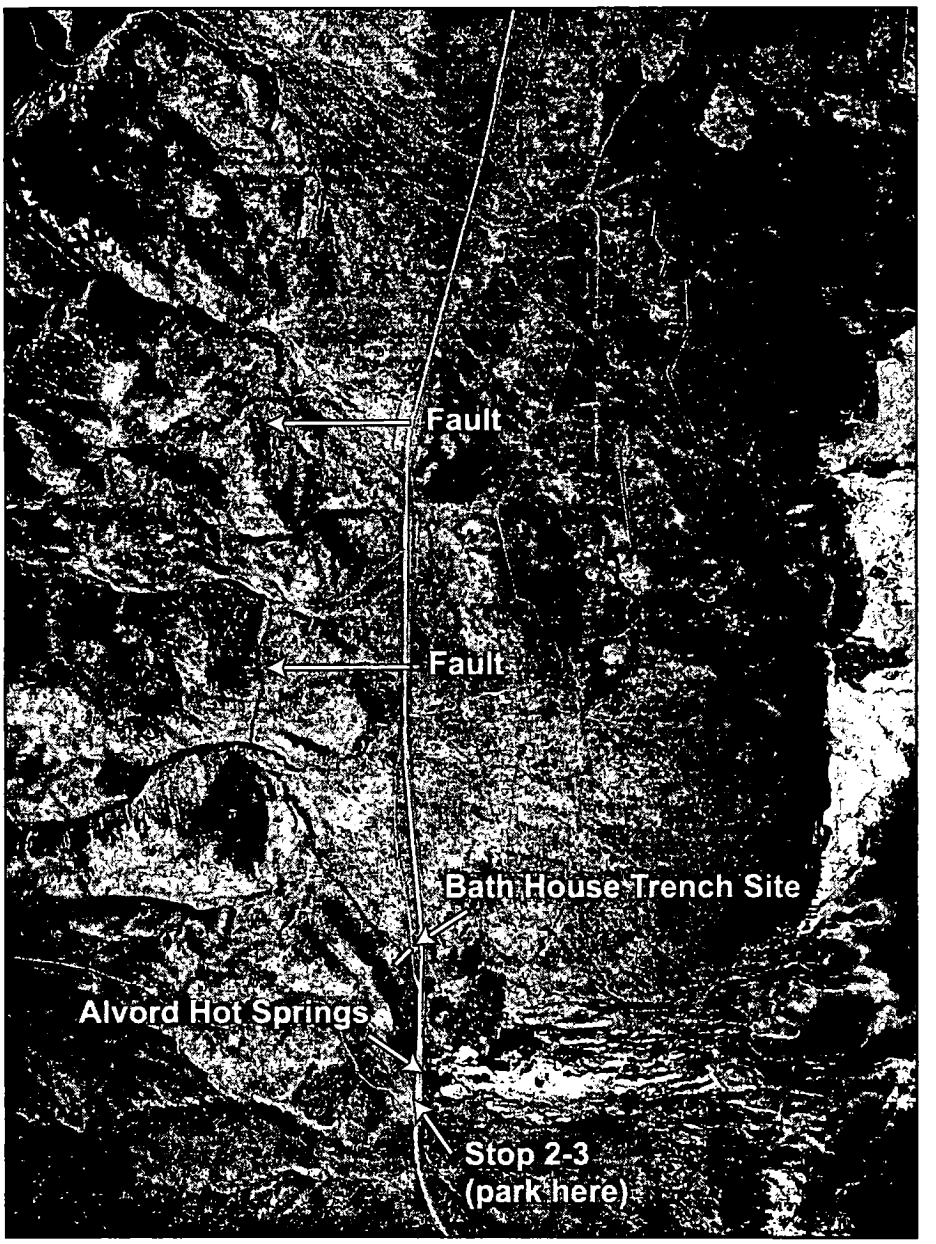

Figure 2-7B Low-sun-angle aerial photograph of the Alvord fault in the vicinity of Stop 2-3. The Alvord Hot Springs originate in the fault at the road. Please park to the south of the cattle guard.

East of Miranda Flat is Mickey Butte (elevation 1904 m, 6294 ft), bounded to the east by Mickey Basin, the northeast branch of the northern Alvord Valley. The trip will officially end tomorrow at Mickey Springs in Mickey Basin. Mickey Basin is truncated in the north by the Sheepshead Mountains and Coffin Butte (the highest peak almost north of Mickey Butte). The summit elevation of the lowest divide northeast of Mickey Basin is east of White Sage Flat at about 1371 m (4500 ft) at the upper (northwestern) end of the Wildcat Creek drainage.

South from White Sage Flat is the continuation of Tule Springs Rims. Tule Springs Rims provides the eastern topographic closure to Alvord Valley. To the east, Big Sand Gap (1280 m, 4200 ft) is the ultimate sill for a lake constrained by the modern topography. Note the large drifts of sand forming eolian ramps cresting the range front south of Big Sand Gap.

40.0 We have been driving on the footwall of the Alvord fault since we made the sharp northward turn. Its well-defined scarp, below the road to the east, is marked by numerous cold springs. Scarp height along this portion of the fault is about 2.5 m. Look for the scarp of the Alvord fault west if the playa edge as we approach our campsite later this afternoon.

41.0 **Stop 2-3**. Alvord fault (T34S, R34E, sec. 32, Alvord Hot Springs quad). Park SOUTH of the approaching cattle guard. (Figure 2-7 B). At the conclusion of this stop we will turn our cars around and travel south. **Please do not try to get turned around now because it will only delay our lunch. There will be ample time after the stop.**

The purpose of this stop is to show you the Alvord segment of the Steens fault zone. At this location we will head to an exploratory trench site (now back-filled) that is a couple hundred meters from our parking site. We will discuss evidence for Holocene activity of the Alvord fault (see Appendix 5). **We will eat lunch at this stop**. Following lunch we will take a hike of about 30 minutes duration (< 800 m) toward the range-front to view a preserved graben in older fan deposits along the fault.

After the hike to the graben, return to the vehicles and drive 0.9 miles south along the county road. Turn left at the flagged turn-off and proceed down onto the Alvord Desert, the playa. Drive southeast, directly toward Big Sand Gap. We pass from the Alvord Hot Springs quad to the Miranda Flat SW quad, and reach stop 2-4 on the Tule Springs quad.

The far edge of the playa, where brush is first encountered again, is about 6 miles from the western edge. Park vehicles that may become stuck in the sand and buddy-up with a sand worthy vehicle. **This is a loose sand site and street vehicles may get stuck.** The route, as reconnoitered, was readily traversable by two-wheel-drive vehicles with good ground clearance and tires. Follow the flagged route through the greasewood toward the gap. The route winds through vegetated dunes on lake sediments (Figure 2-8).

Figure 2-8. Big Sand Gap in the Tule Springs Rims east of Alvord Desert, Stop 2-4 is in the distance. The view is southeast from the east edge of the Alvord Desert playa.

50.0 **Stop 2-4.** Big Sand Gap. (T35E, R35E Sec. 22, Tule Springs quad, Figures 2-8 through 2-11). Park on the last relatively solid ground (well-marked) and hike up the north side of the gap to the shoreline terrace at the mouth of the gap (Figure 2-9). As you proceed, look for evidence for shorelines preserved at elevations documented in other parts of the Alvord Valley. To summarize, four miles south, at Little Sand Gap, there are shorelines at about 1302 m (4272 ft), at 1294 m (4245 ft), and 1287 m (4222 ft). The lake or lakes which formed these shorelines at Little Sand Gap could be contained by the modern sill of pluvial Lake Alvord.

About 17 miles north, at Mickey Springs, shorelines are found at 1291 m (4236 ft) and 1287 m (4222 ft), neither of these lake elevations could be contained within the basin at the present sill elevation.

Twenty miles north of Big Sand Gap, in White Sage Flat, shorelines are preserved at about 1290 m (4233 ft) and at 1283 m (4210 ft), a lake occupying this shoreline would fill the basin just to the sill and replicate late Pleistocene pluvial Lake Alvord.

Almost 14 miles north of Big Sand Gap, Miranda Flat bar is at elevation 1283 m (4209 ft), equal in elevation to the second-highest well-preserved shoreline at

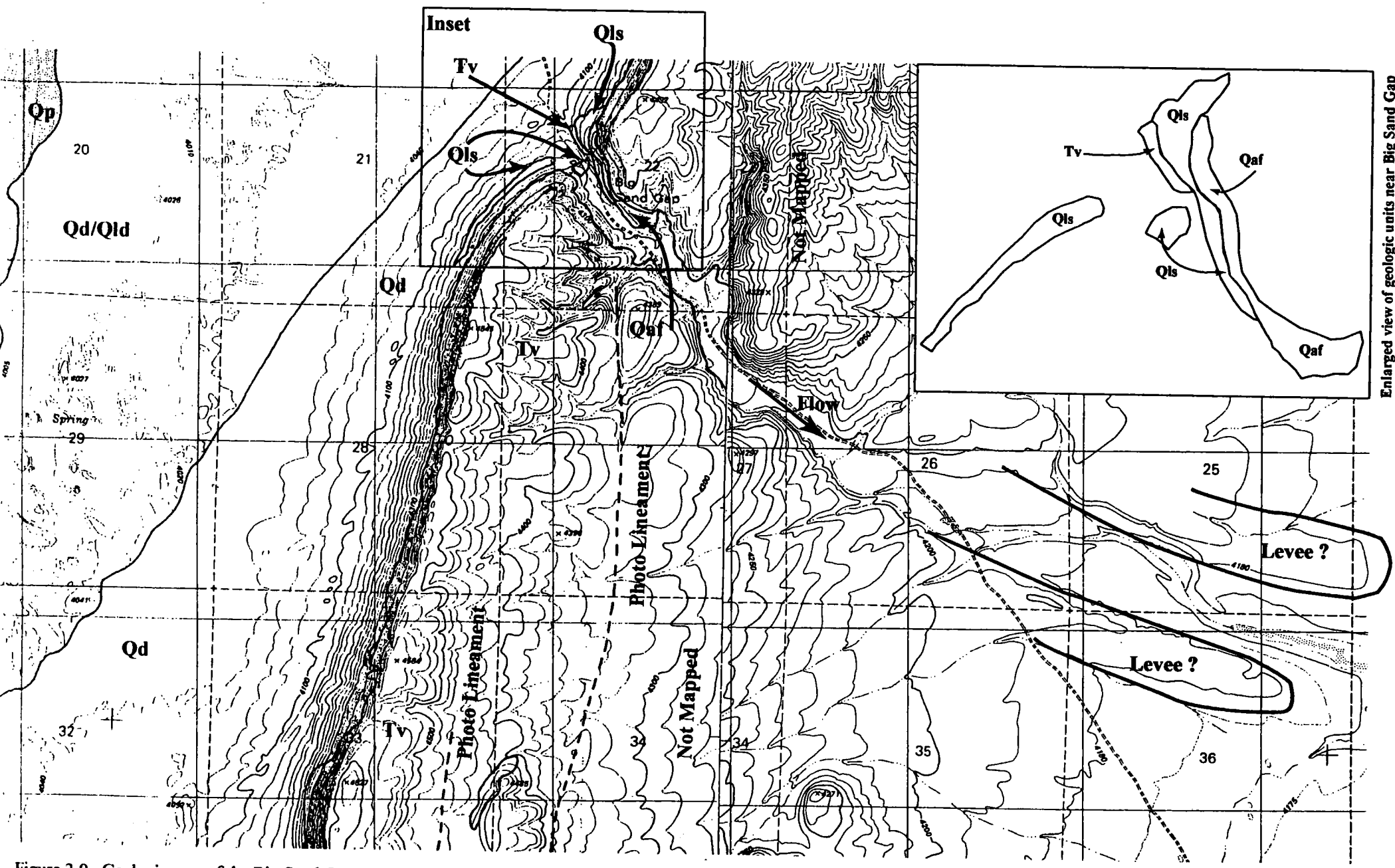

Figure 2-9. Geologic map of the Big Sand Gap. Alvord Valley is closed in Big Sand Gap at elevation 1280 m by the 4200 ft contour line. Big Sand Gap is incised into the Tertiary volcanic rocks of the Tule Springs Rims range front, and provided an outlet for late Pleistocene pluvial Lake Alvord to drain east into Coyote lake basin. Note the prominent leves that appear to have formed at or below 1280 m where the overflow would be expected to reach Lake Coyote if its shoreline was at about theat elevation. Shallow lake (shoreline bar) gravel deposits are observable on volcanic bedrock at about elevation 1259 m (4130 m) in the gulch near the west end of the gulley. Holocene fans and eolian deposits blanket much of the surface within and to the east of the gap. Contour interval is 10 feet (with some 5 ft) on the east half of the figure (Tule Springs NE quad). Contour interval is 20 feet on the west half of the figure (Tule Springs quad, T35S, R35E, sec. 22).

White Sage Flat. This 1283 m (4209 ft) shoreline is also about equal to the elevatio ·: which Big Sand Gap now closes Alvord Valley.

Finally, across the valley, the 1304 and 1295 m-high gravel bars at the Alvord Saddle (Stop 2-2) are at elevations that could not be contained by the present sill.

Despite the existence of several shorelines at elevations up to 24 m (~80 feet), or so higher than the Big Sand Gap, there remain no obvious shorelines higher than 1280 m (4200 ft) in the gap or around the nearby range front. However, minor local vegetation differences and sporadic, local bench-like features along the upper slopes north and south of the gap may be noteworthy.

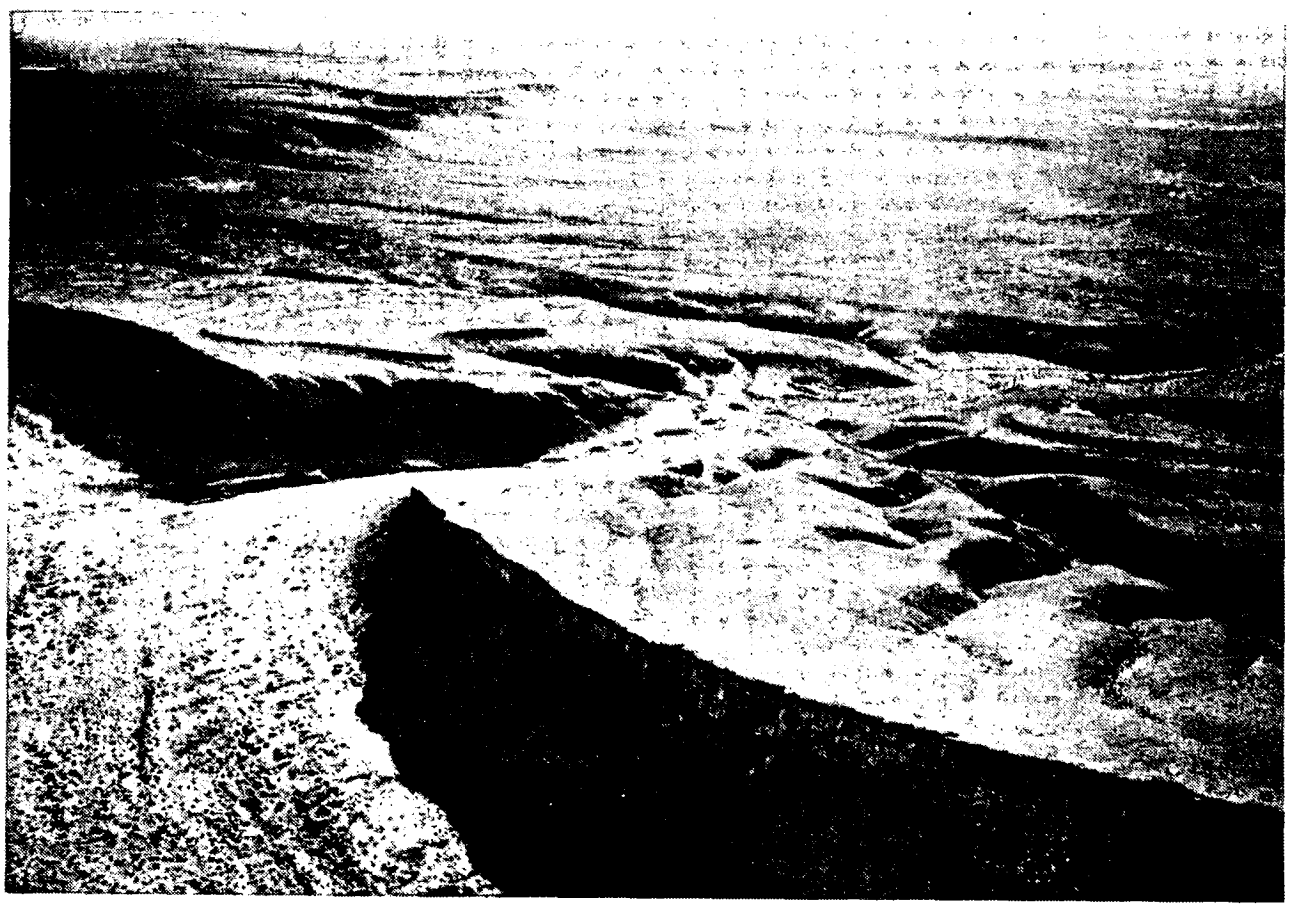

Figure 2-1c Site of spillover of pluvial Lake Alvord at Big Sand Gap in the Tale Springs Rim along the eastern Alvord Valley.

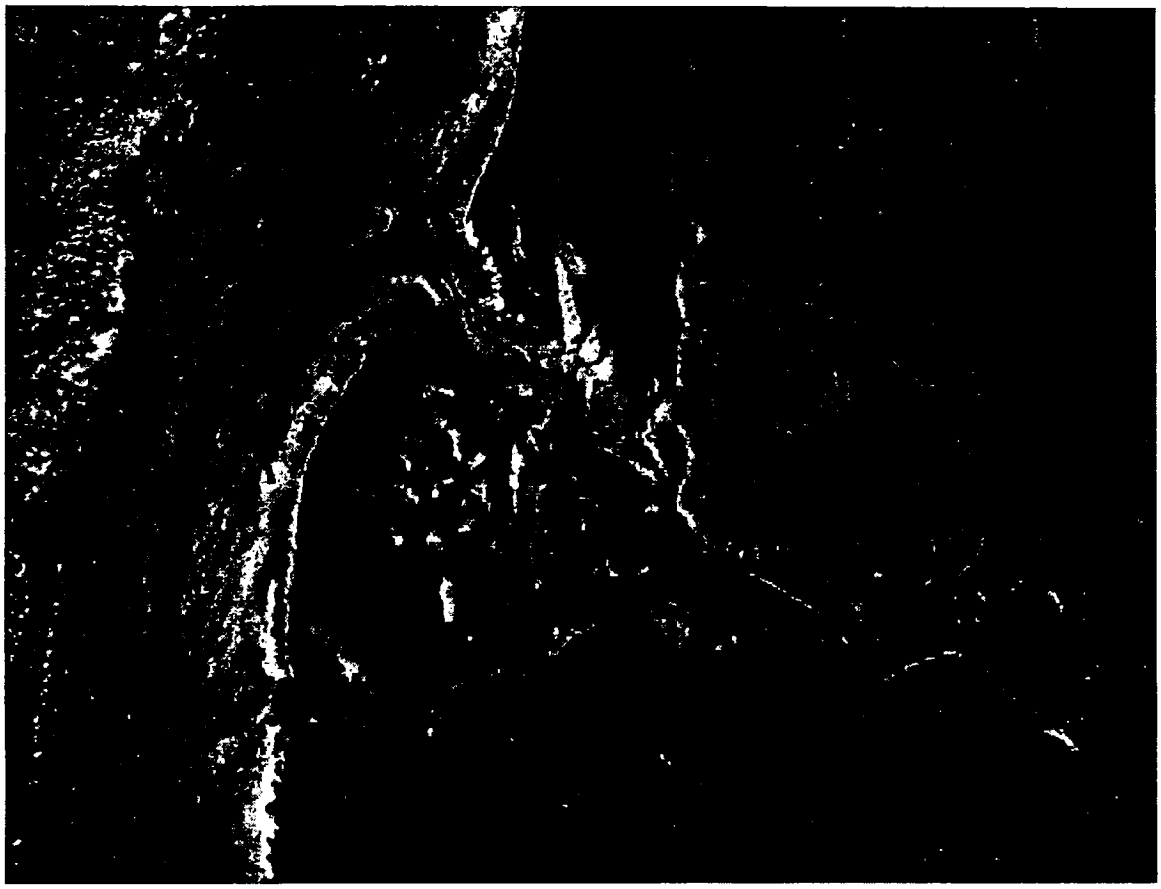

Figure 2-11. Low sun angle air photo of the Big Sand Gap. Note the wide, almost meandering channel cut into the volcanic tableland east of the Gap.

We will walk east through the gap and climb the low ridge of volcanic rock. The view is into Coyote Lake basin to the east. To the southeast is a portion of yesterdays route where the road crossed to the north of the Trout Creek Mountains. Lake Alvord overflowed into Coyote Lake basin.

Coyote Lake basin has a floor elevation of 1241 m (4075 ft). The basin has two potential sills, 1276 m (4185 ft) near Grassy Ridge Well north of Lake Coyote and 1278 m (4192 ft) near the east of Lake Coyote, where the route came west from 95. A catastrophic flood, or a series of floods, such as may have been released from Lake Alvord in a down-cutting event, would have rapidly filled the smaller Coyote basin to beyond its capacity. It is possible that water levels stabilized at nearly the same elevation, perhaps once between 1290 to 1295 m, in both lakes, when such a gap-down-cutting or flood event occurred. A graphic representation of the distribution of preserved shorelines and sills is included in (Figure 1, Appendix 3).

Water flowed east-southeast into the valley to the east, and then turned northeast to the deepest part of the Coyote Lake basin. About two miles to the east-southeast, well-developed levees, believed formed by outpourings from Lake Alvord, can be seen on 1:24k-scale topography (Figure 2-9).

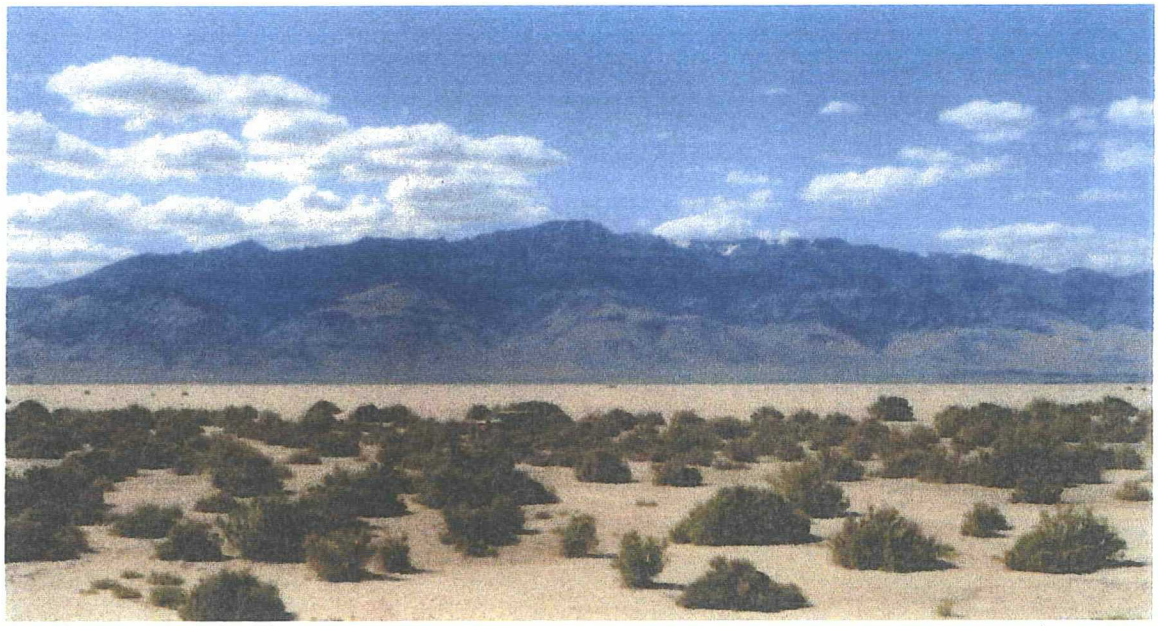

Figure 2-12. View to the west of Steens Mountain across the Alvord Desert playa. The vertical relief between the summit and the playa is 1728 m (5670 ft).

Walk back through the gap on the south side and look for any shorelines around 1310, 1304, 1302, 1295, 1290 or 1286 m (4300, 4280, 4270, 4250, 4235, or 4220 ft). Only the last sill at about 1280 m (4200 ft) clearly preserved a shoreline in the gap. Significant hydraulic forces generated with down-cutting may be sufficiently great to erode earlier, higher shorelines near the gap.

The gully cut exposes the gap stratigraphy beneath a surface mantle of alluvium and eolian silt. The sedimentary sequence is interpreted to record the rise and fall of pluvial Lake Alvord. At the eastern end of the gully, fine-grained, quiet water sediments are exposed. A short distance to the west, gravel underlies the fine-grained deposit. The gravel rises and pinches-out the fine-grained lake deposits. Farther west, where the gully empties into the basin, the gravel is underlain by the igneous bedrock of the range front.

It is interesting to speculate upon how, after flow through the gap ceased, the shoreline gravel terrace could have been constructed across the west end of the gap. The sediments exposed in the gully may have been deposited in a pond or lagoon behind the barrier of a gravel shoreline bar, which gradually filled with sand and silt. Some snail shells and small (fish?) bones have been observed in parts of the fine grained "lagoon" deposit.

We have also speculated if the lake might have fluctuated seasonally. If as late Pleistocene winters froze the surrounding ranges, greatly reducing inflow to Lake Alvord, the lake may have filled and spilled east with each spring thaw. Perhaps there are varve-like deposits in the Coyote basin sediments. If the surrounding countryside froze, then could the lake have also frozen over?

A frozen pluvial Lake Alvord would be subject to a spring thaw break up of some kind. Spring thaws may have clogged the gap with ice dams, perhaps trapping spring surges of melt water runoff and releasing jökulhlaups through the gap with more regularity than is suggested by the few shorelines now preserved in scattered parts of the Lake Alvord basin. Seasonal outpourings, or even occasional floods from Lake Alvord could be the process driving the down cutting through the resistant bedrock of the Tule Springs Rims. Prominent shorelines may be preserved in the Alvord basin where the lake outflow spent multiple seasons working through more resistant strata. Where there are no prominent shorelines evident between well-expressed shorelines, we conclude no stable sill existed and the lake did not persist for long at any intermediate elevation between the prominent shorelines.

Enjoy the view of Steens Mountain as we walk back to the cars and drive back out to the playa on the trail taken in. **Please do not attempt to cross-country back to the playa. Not only do we want to minimize the impact to the desert here (yes, we do see all of the %*#^*$% ATV tracks everywhere) but people who travel on their own, risk getting boxed in at places and possibly stuck. We don't want to spend the rest of the afternoon looking for you in the desert.**

51.8 Once on the playa again (elevation 1219 m, 4000 ft), drive west toward where we entered the playa by taking a bearing toward the point where the ridge of the Southern Steens disappears behind the ridge of Alvord Point (Figure 2-13).

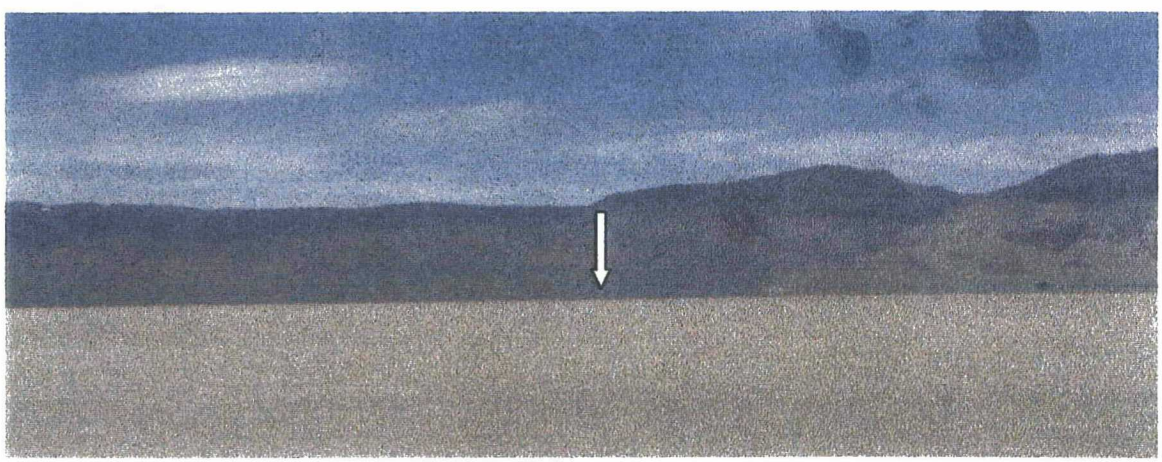

Figure 2-13. After reaching the playa, drive about five miles west toward the point where the ridgeline of the Southern Steens disappears behind the ridge of the Alvord Point spur.

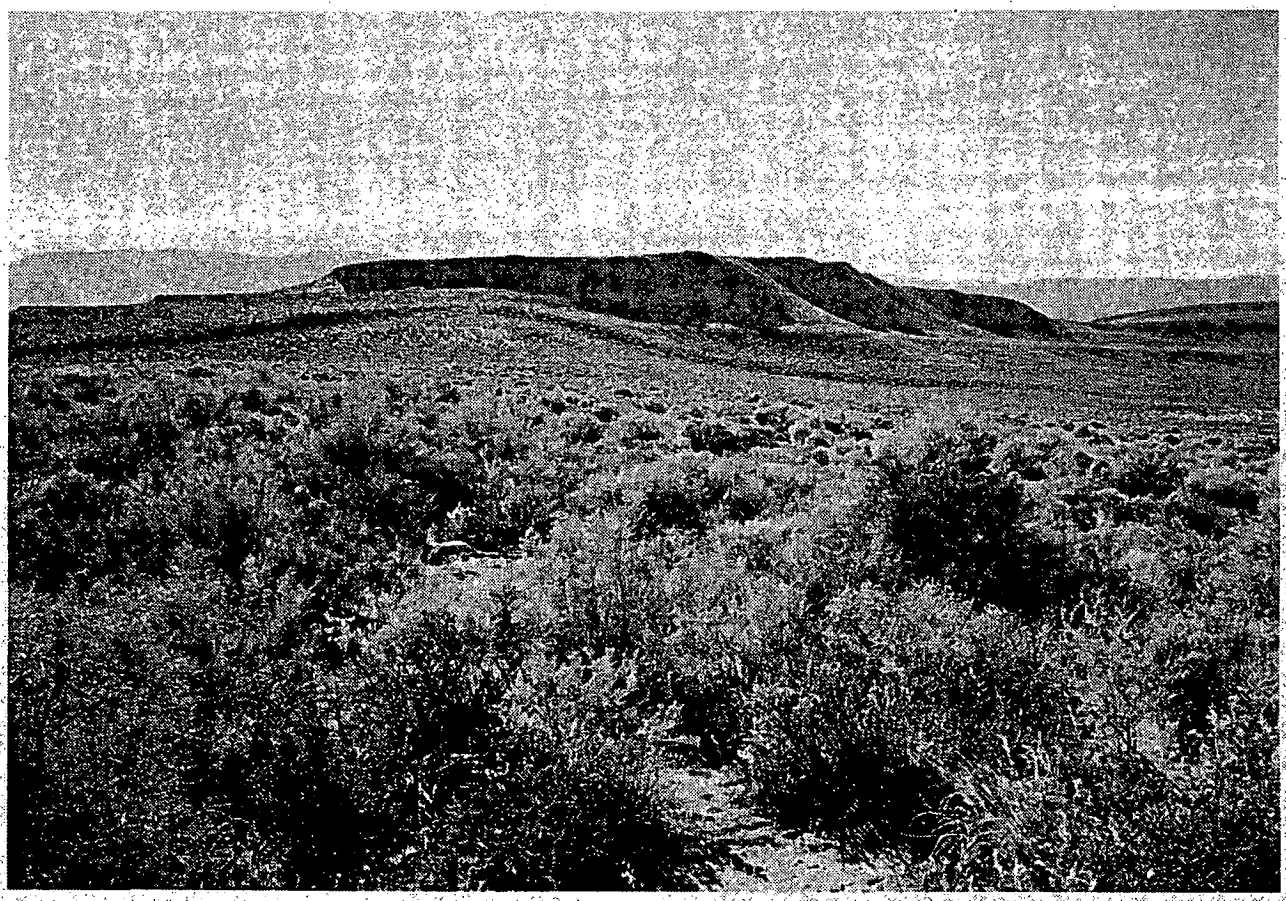

Figure 2-14 View to the east of the Alvord fault as it crosses Black Dog Spur and displaces shorelines at 4200 ft (1280 m).

57.0 After about five miles, or within a country mile of the west edge of the playa, turn south toward the southwest corner of the playa and drive toward the lower end of the Alvord Point spur, also called Black Dog Spur.

Watch for rocks and park near the southwest edge of the playa. The grasses along the edge of the playa are fragile so we ask that you limit your camping and parking to the nonvegetated playa. Once again, anyone seeking quieter camping has numerous options. The playa is over 19 km (12 mi) long and 9.6 km (6 mi) wide.

65.0 <u>Stop 2-5.</u> Camp at The Playascene. (T35S, R34E, sec. 28, Andrews quad). At this stop, as the sun hangs low in the western sky we will take a short walk to the south into the dune field to observe the Holocene Alvord fault in low-sun where it displaces the 1280 m shoreline at Black Dog Spur (Figure 2-14).

A SIGNIFICANT WORD OF WARNING – Consider this fact when choosing your campsite, late at night there are bound to be people (from FOP or elsewhere) driving across the playa. Those folks may be in various stages of altered awareness, driving at various speeds with lights on or off. We suggest that a light of some sort be displayed for the evening at your camp. **Do not camp out in the playa away from vehicles or tents!** Also, we will be marking a lighted route from the camp to the county road. Please consider the fact that obstacles such as rocks, cars and sleeping backs (with human occupants) may be scattered about the playa. **DO NOT DRIVE FAST!**

The annual business meeting will begin at about 8:30 or 9:00 p.m.

DAY THREE

Drive north on the playa and return to the county road near the Alvord Hot Springs.

Reset the odometer at the county road and drive north (turn right). The trip route proceeds north for about 12 miles over the fans at the base of the High Steens. In about 1 mile cross the cattle guard and pass the Hot Springs on the right, and Stop 2-3 from yesterday.

2.7 The Alvord fault is to the west and is marked by springs. Note the fault and shoreline (Stop 2-3) on the Indian Creek fan. Faults and shorelines continue north to the Pike Creek fan. The most prominent shoreline is at about 1280 m (4200 ft).

Pike Creek has developed a large bouldery fan surface which is dissimilar to the other nearby large fans along the High Steens. It is fun to speculate about the cause of this grain-size difference for this fan. Some suggestions include: a) rock type differences in the Pike Creek drainage promoted movement of larger clasts, b) a landslide (coseismic?) in the drainage provided larger clasts to the fan, c) an

ice dam in the narrow throat of the drainage failed and a jökulhlaup event occurred.

Faulting and shorelines continue to be visible as we drive north along the range front. Mickey Butte lies to the north and the Tule Springs Rims are across the Alvord Desert playa to the east.

2.8 Intersection with the Pike Creek road on the left. A small undeveloped camp is at the mouth of the canyon of Pike Creek.

3.2 West of the road are shoreline bars where the 1280 m (4200 ft) shoreline crosses the Pike Creek fan (Figure 3-1). A section of about 1524 m (5000 ft) of Miocene basalt is exposed in the range front.

4.1 Faults in the base of the range-front are highlighted by springs.

4.2 Little Alvord Creek fan.

5.9 The road climbs the fans of Big Alvord Creek. Youthful scarps cross the margin of the fan at the range-front.

6.3 Note the large landslide in the mouth of Big Alvord canyon.

6.4 Please drive slowly past the Alvord Ranch on the right after crossing Big Alvord Creek to reduce the dust. We are crossing the private property of our good friends who have been kind enough to let us work and bring large groups of people on their property.

7.0 Pluvial shoreline east of the road at an elevation of about 1280 m (4200 ft). There are good views to the west of small cirques and moraines on the High Steens.

7.2 To the west is a large landslide in the range front at Cottonwood Creek. East of the road the 1280 m (4200 ft) shoreline parallels the route.

8.3 Cottonwood Creek cuts the lakeshore bar deposits at a good exposure on the right. Please do not stop to inspect this site on private land.

8.4 Cottonwood Creek fan on the left. There are more landslide deposits at the range-front. North of Cottonwood creek along the range-front are Little Willow Creek and Willow Creek.

10.2 Slow for sharp turn to the right. Miranda Flat lies between this part of the route and Mickey Butte, now to the northeast.

11.2 Slow for sharp turn to the left at Mosquito Creek. Cross the cattleguard in ¼ mile.

Figure 3-1. Low-sun-angle photograph of the Pike Creek fan. Delta bar deposits (Qbb_2) mark the sustained lake level at 1280 m (4200 ft). The Alvord fault parallels Pike Creek for a short distance (between the arrow at "Fault" and arrow at "Pike Cr".

11.7 **Stop 3-1**. Turn right into the borrow pit in Miranda Flat bar (T33S, R35S, sec. 18, Miranda Flat quad). Note the weathering of the gravel deposits with a geochemical gradient of carbonate(?) down to manganese down to iron. Compare this outcrop with those examined at stops 2-1 and 2-2.

This stop is close to the transition between the High Steens and the lower Northern Steens. The range-front continues north for more than 40 km (25 mi) to Folly Farm and highway 78 (30 miles). Recognized Holocene faulting does not continue northward along the base of the Northern Steens.

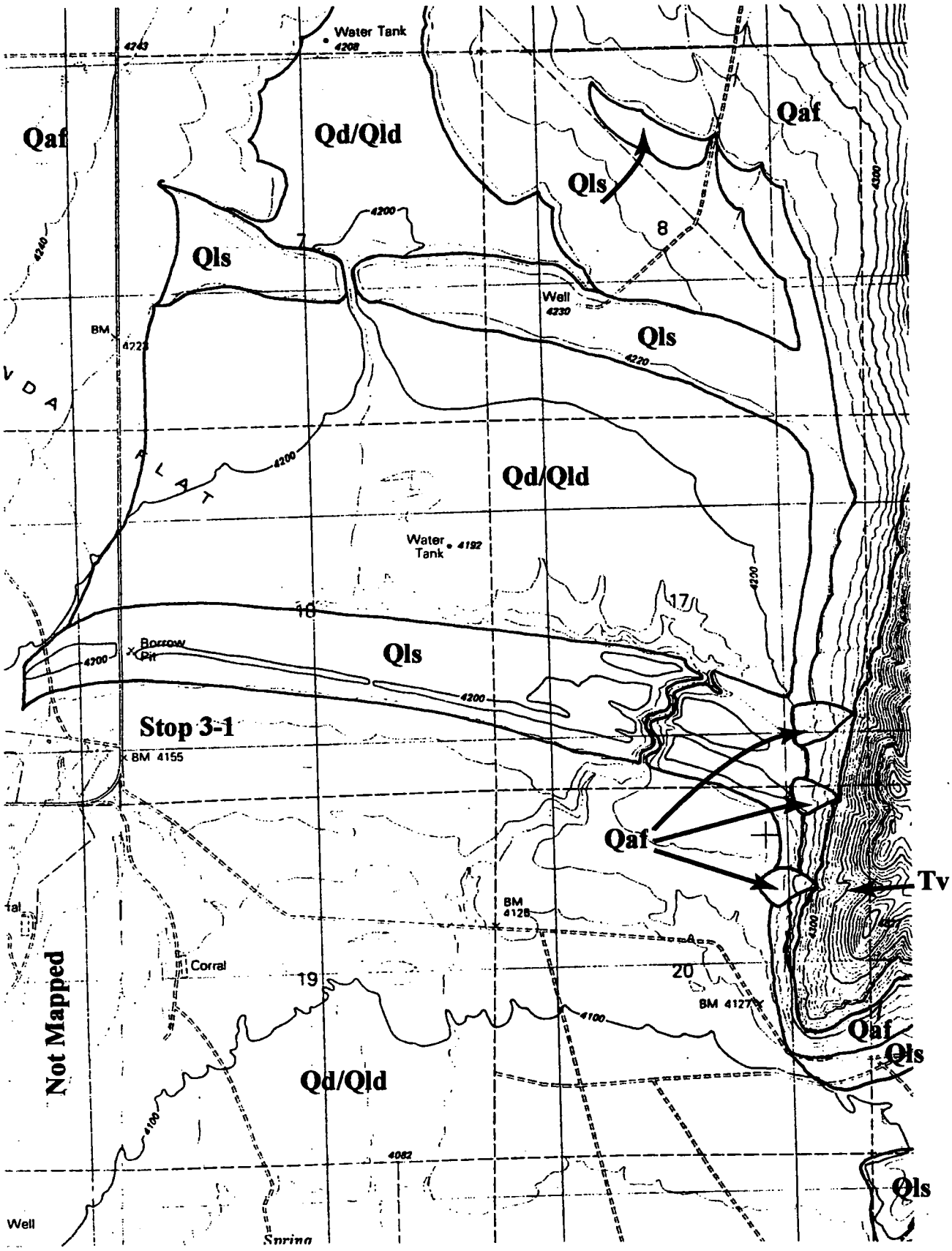

Figure 3-2. Geologic map of Miranda Flat bar, stop 3-1. Miranda Flat bar, with an average elevation of about 1283 m is the more southerly of the two prominent shoreline bars in Miranda Flat. North of Miranda Flat bar, the shoreline is at an elevation of about 1288 m. Contour interval is 20 feet, with supplemental contours at 10 feet (Miranda Flat quad, T33S, R35E, sec 18).

Miranda Flat bar (Figure 3-2) is another shoreline at an average elevation of about 1283 m (4209 ft), as measured by engineering level from the 1266 m (4155-ft) USGS benchmark to the south. These preliminary level data, from a traverse west to east along the crest of the bar, suggest it may be about 1282 m at the west, slightly higher in the middle at about 1283 m and about 1282 m near the base of Mickey Butte. This may be the result of differences in loess deposition or erosion as the bar crosses the axis of the valley. Alternately, the valley floor and the bar may be tilted. A plane fitted to the data strikes about N80W and is inclined slightly toward the south (3.5 m/km). The strike is parallel to the crest of the bar and about perpendicular to the axis of the valley.

About 1.6 km (1 mi) to the north is another shoreline at elevation 1288 meters (~4226 ft). Beyond, the crest of the divide to Mann Lake is approximately at elevation 1291 m (4235 ft), based on the 10-foot contours on the topographic map. As noted previously, in the Mickey Basin east of Mickey Butte there are well-defined shorelines at 1290 to 1291 m (4233 - 4236 ft) near White Sage Flat and Mickey Springs; these elevations represent the highest recognized lake elevations (shorelines) in each of these areas. At stop 2-2 a shoreline lies at 1295 m. There is also a shoreline at 1287 m (4222 ft) near Mickey Springs (stop 3-3).

This stop is as far north as we will explore in the Alvord Valley. Our route now proceeds east, around the south end of Mickey Butte to the north east branch of the valley. Proceed south on the county road 0.3 miles.

12.1 Turn left before the cattle guard. Follow the graded road across Miranda Flat toward Mickey Butte. Miranda Flat bar continues to the east, north of the route. Around mile 13 the bar is breached by a south-flowing drainage.

13.2 Sharp right turn through a cattle guard. The view to the south is of the Alvord Desert and the Tule Springs Rims.

13.6 Slow down for a sharp left turn at the "Wilderness Study Area" sign. Do not continue straight ahead unless you enjoy exploring dune fields solo, go left.

14.5 Round the south end of Mickey Butte, the Alvord Desert is to the south and the northern Tule Springs Rims is to the east.

14.6 Bear left at the "Y". The low hill of gravelly lake deposits to the east mantles a horst of volcanic bedrock barely emerging through the valley fill. Beyond the hill is a low sill at elevation 1237 m (4058 ft) which separates the Alvord Desert from the small playa to the north. When filled to this elevation, Lake Alvord would spill north into the small playa on the south side of Mickey Springs, and flood it, then flow through a constricting gap near Mickey Springs (Figure 3-3) and would continue flowing north into the Mickey Basin.

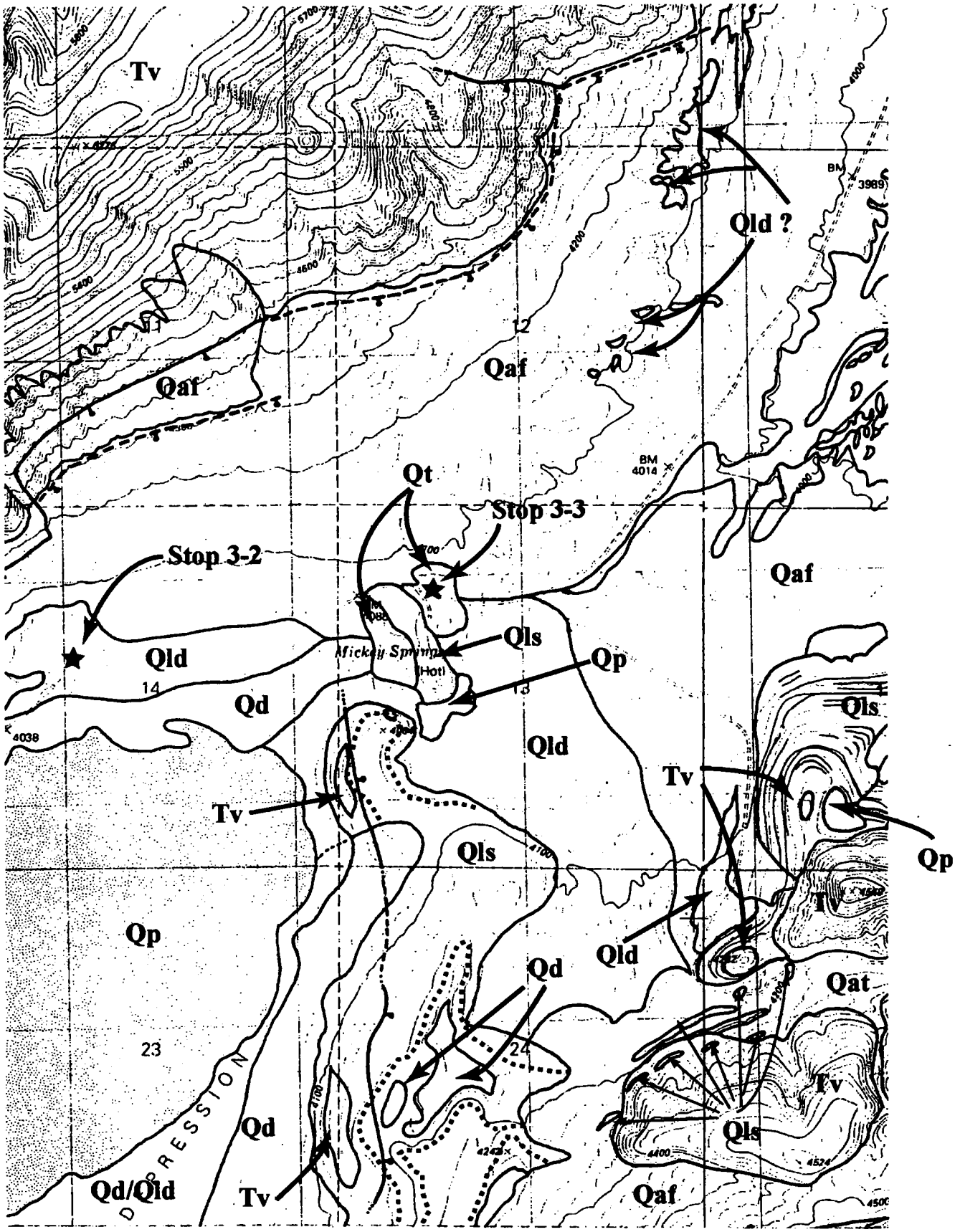

Figure 3-3. Geologic map of Mickey Springs, stops 3-2 and 3-3. Stop 3-3 is in the amphitheater to view tephra in lake sediments and the exposure of the Mickey Springs fault. Stop 3-3 is at Mickey Springs to examine a suite of shoreline bars (dotted lines) on the southern side of the valley from Mickey springs. Contour interval is 20 feet (Mickey Springs quad, T33S, R35E, sec 13 and 14).

15.1 At the crest in the road is a good view of the small playa between Alvord Desert and Mickey Springs. The floor of this playa is at elevation 1229 m (4033 ft).

15.5 The scarp of the Mickey fault is visible to the left crossing the fan surfaces. The shoreline at about 1280 m (4200 ft) is above, closer to the range-front. Leave the Miranda Flat quad and begin on the Mickey Springs quad.

15.9 Two or three shorelines are above and behind the fault scarp. The highest shoreline appears to truncate at the talus slope near elevation 1295 m (4249 ft).

17.5 **Stop 3-2.** The amphitheater (T33S, R35 E, sec. 14, Mickey Springs quad). Park along the road and proceed into the amphitheater on the left. The Holocene scarp of the Mickey fault is particularly well-preserved on the fan slope above the stop. The fault was profiled on the slope above for degradation modeling (Slopeage, Nash, 1987). Five profiles of the scarp (Appendix 3, Figure 2) yielded a mean offset of 1.9 m, and a mean scarp-face angle of 22.5 degrees. Inferred ages of the scarp ranged from 864 to 2100 years; so we conclude that the scarp is close to 2000 years old. To the north, the scarp is lost in the range-front, south it disappears in the dunes south of the butte.

A tephra of unknown origin is exposed in the lake sediments in the west wall of the amphitheater. Below the tephra in the section is reworked tephra mixed with silty lake sediments.

Proceed north along the road to Mickey Springs.

18.5 **Stop 3-3**. Mickey Hot Springs (T33S, R35 E, sec. 13, Mickey Springs quad). Note the BLM warning signs. There is hot water in these deep pools, and boiling mud and steam vents, which are said to occasionally erupt and spew material several feet into the air. There are some former thermal vents north and east of the modern springs that appear to have been active until rather recently.

On the west side of Mickey Springs, the small rise is a shoreline bar, at about 1247 m (4091 ft), composed of sand and gravel cemented by siliceous sinter (Figure 3-3). This shoreline bar is at about the same elevation as the bar we examined at stop 2-1 and explained that we presumed it was late Pleistocene or Holocene. Looking north along the fan surface below the east face of Mickey Butte it appears that the lake at the 1279/1276 m shoreline elevation constructed extensive, prominent shorelines. This shoreline raises the interesting question of how a lake could have been stable long enough to construct such prominent shoreline features at an elevation so much lower than the controlling sill at Big Sand Gap.

This cemented gravel bar has a continuation to the south across the eroded cut or former channel between the Mickey Basin to the northeast and the Alvord to the

southwest. The Holocene scarp of a north-south trending, down-to-the-east, normal fault crosses the west face of this bar to the south, across the channel. The bar and the fault mark the divide between the small playa toward the Alvord side and the broad wash that eventually drains to the Mickey Basin. To overflow into the Mickey Basin, the water surface would have to reach an elevation of about 1230 m (4036 ft), or just about one meter of water would fill the small playa (Figure 3-4).

Across the channel, south of Mickey Springs, are several cuspate shoreline bars at increasingly higher elevations. Above the cemented bar is a shoreline that has been offset by faulting and now lies at a *split* elevation of 1276 m (4188 ft) and 1279 m (4195 ft). The scarp of the fault appears quite youthful on the 1279/1276 m shoreline, but on the 1247 m shoreline the scarp is indistinct, suggesting that the rupture occurred after the abandonment of the 1279/1276 m shoreline and during the occupation of the 1247 m shoreline. Post-pluvial eolian deposition may also be responsible for obscuring the scarp on the 1247 m shoreline, but in the air photo (Figure 3-4) the trace of the fault appears distinctly. On the ground, however, this is not the case. This is the longest and best expressed of the shorelines here at Mickey Springs and probably correlates with the Big Sand Gap sill. Above the faulted shoreline are two, smaller cuspate bars, at 1287 and 1291 m (4222 ft and 4236 ft).

These prominent shorelines continue to the north and, along with several less distinct shorelines, may be continuously traceable along the east side of the valley into the Mickey Basin and White Sage Flat. In White Sage Flat, there are distinct shorelines at 1290 and 1283 m (4233 ft and 4210 ft), a faulted shoreline at 1274 and 1272 m (4180 ft and 4174 ft), and the low shoreline at 1260 m (4132 ft). The shoreline at 1260 m is roughly equivalent to the estimated elevation of the bedrock outcrop at the west end of the Big Sand Gap gully (Stop 2-4). The fault offsetting the 1274/1272 m shoreline was not visible on the ground, but was readily apparent when the total station theodolite line crossed it.

Shoreline suites, like these at Mickey Springs, imply that at least three persistent stands of Pluvial Lake Alvord occupied the Alvord basin in late Pleistocene time. At an elevation of 1302 to 1310 m the oldest of these lakes (the "1310 m" lake) is proposed to have initiated the down cutting at Big Sand Gap. Coyote basin then filling to an elevation above 1290 m, and a persistent lake cut shorelines in both basins at some elevation between 1290 and 1295 m (the "1295 m" lake. A lake above 1290 m would fill the Mann Lake basin north of Miranda Flat; falling below that elevation would have isolated the Mann Lake basin.

Another persistent stand of the lake cut shorelines at 1287 to 1288 m ("1288 m" lake) before Lake Alvord stabilized yet again at or near 1280 m and constructed most of the most-prominent shorelines preserved today ("1280 m" lake). This lake-level drop, from the 1228 m lake to the 1280 m lake, might have isolated

trout in Mann Lake from their Alvord basin and Owyhee River relatives. Pluvial Lake Alvord at 1280 m was the most persistent late Pleistocene lake in the basin and was in equilibrium with the sill at Big Sand Gap. When Lake Alvord receded from its 1280 m highstand, Coyote basin appears to have been constrained at an elevation several meters lower. When Lake Alvord fell below 1280 m, the fish population would have been isolated from their Owyhee River antecedents.

Shorelines below the 1280 m lake are all inferred to have been constructed since the last late Pleistocene pluvial maximum. At least one late Pleistocene or Holocene lake below the elevation of Big Sand Gap sill persisted long enough to construct the relatively prominent shorelines at Bone Creek and Mickey Springs.

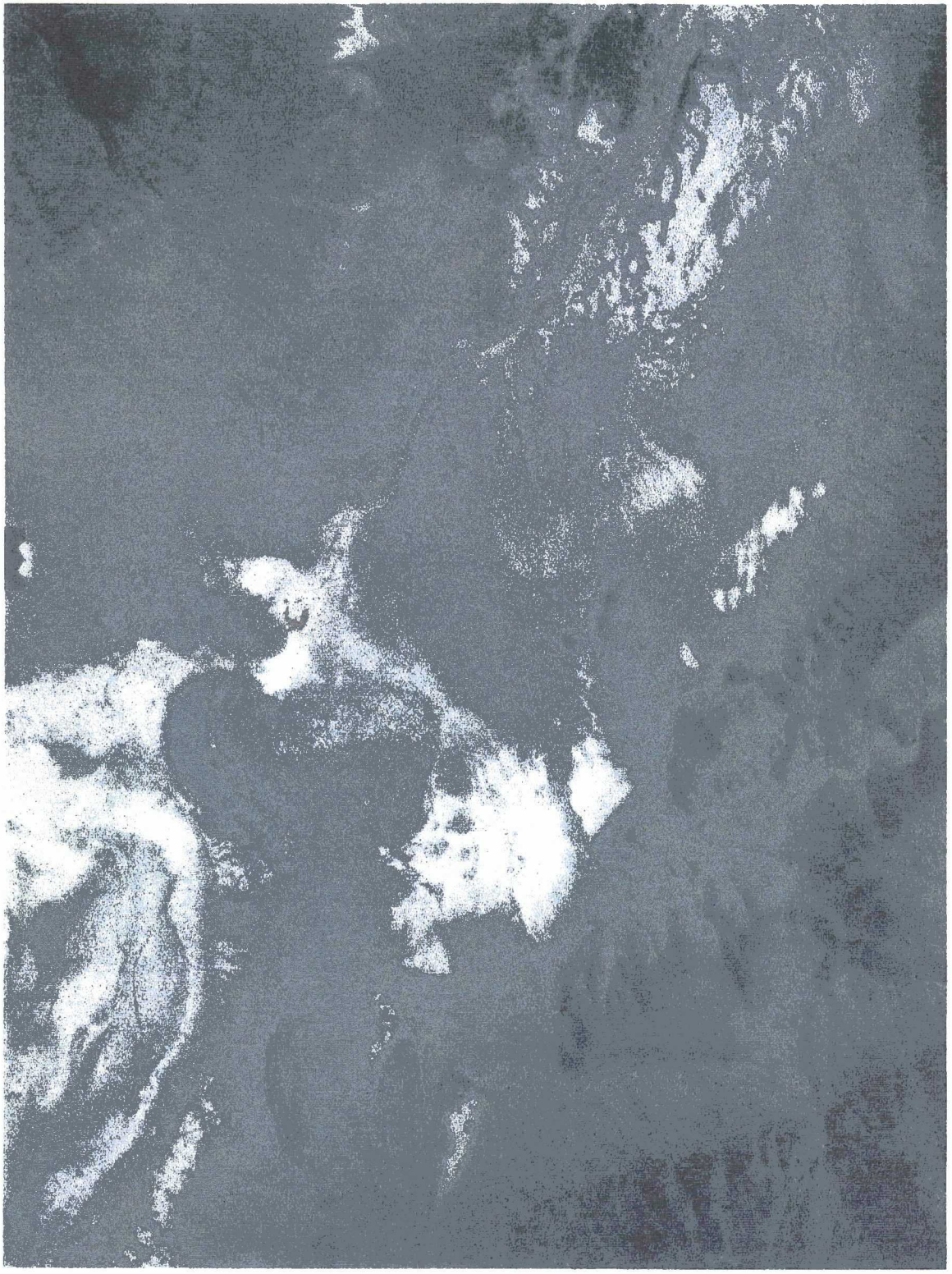

Figure 3-4. Color IR air photo of Mickey Springs and vicinity. Mickey Springs is visible as a red vegetated area west of the center of the figure. Intersecting normal faults provide hot water an outlet at the surface. Multiple shorelines are preserved south of the springs and on the east side of the valley. Photo courtesy of JPL.

APPENDICES

Page numbers are self contained within each appendix.
(e,g, pg. A1-1 is first page of appendix 1, and page A6-7 is seventh page of appendix 6)

Late Quaternary Faulting Along the Quinn River Fault Zone (QRfz); A Soils Investigation

Charlie Narwold, MS thesis in progress, Humboldt State University, Arcata, CA

Introduction

The northern segment of the Santa Rosa Range fault system, herein referred to as the Quinn River fault zone (QRfz), is a 50 km zone of en echelon faults of middle to late Pleistocene and Holocene (?) age that continue northward from the western flank of the Santa Rosa Range, Nevada into Oregon (Figure 1). The fault zone is defined by late Pleistocene fault scarps on the order of 1-2 meters high and older escarpments with as much as 100 m of apparent vertical displacement. The QRfz trends northward from Canyon Creek through the Quinn River Valley to near Oregon Canyon Creek. Northeast of Blue Mountain, several faults trend through prominent saddles in the Mendi Gore hills and continue to the northeast. The faults appear temporally similar to faulting in the northern Quinn River Valley, but their relation to the QRfz is not known. The QRfz is aligned with historically active fault zones in central Nevada and it has been proposed that the QRfz is possibly a northern continuation of the Central Nevada Seismic Belt (Michetti and Wesnousky, 1993; Pezzopane and Weldon, 1993).

Late Quaternary faulting along the QRfz has mainly occurred on two fault segments, the Hot Spring Hills fault and the High Peak fault (Figure 1). The Hot Spring Hills fault is approximately 46 km in length and extends from Canyon Creek to Oregon Canyon Creek. The High Peak fault is approximately 14 km long and extends roughly from Little Louse Canyon to Jackson Creek. Faulting along the Hot Spring Hills fault has occurred since the early and middle Pleistocene, with the most recent event being latest Pleistocene-early Holocene in age (see Stop 1-1, this volume). Compound fault scarps of the High Peak fault also record evidence of a latest Pleistocene-early Holocene faulting event (see road log, Day 1, mile 19.3, this volume).

Determination of ages of Quaternary deposits in the northern Quinn River Valley based on soil development

The purpose of the soils investigation is to establish age estimates for different deposits along the QRfz in order to provide limiting ages on the time of faulting. The degree of soil development has been widely used to estimate the age of relict soils and deposits in which they are developed. Relict soils are defined as those that have remained at the ground surface since the time of initial formation (Birkeland, 1984). The age of a relict soil should approximate the time that has elapsed since the parent material was deposited, provided there has been no significant modification of the original ground surface. This relation is based on the assumption that that the soil began to form soon after the parent material was deposited.

Relict soils developed in Quaternary deposits in the study area are calcic soils, that is they contain a significant amount of secondary carbonate in the form of carbonate horizons. Secondary carbonate refers to the carbonate that has accumulated in a soil since the deposition of the parent material (Machette, 1985). The continual translocation of dissolved

Ca^{2+} and solid $CaCO_3$ through the upper horizons of the soil, and subsequent precipitation and accumulation at depth, is responsible for the carbonate ($CaCO_3$) horizons present in the soils. Because pedogenic processes are responsible for the carbonate accumulations, the secondary carbonate present in the soils is also referred to as pedogenic carbonate. The primary sources of pedogenic carbonate are eolian inputs of solid $CaCO_3$ (dust, silts, and sand) and Ca^{2+} dissolved in rainwater. One must be aware of any parent material (primary) carbonate when determining the amount of pedogenic carbonate in a soil.

Gile and others (1966) described four stages (I-IV) of carbonate horizon morphology developed in soils of increasing age with gravelly and non-gravelly parent materials, in southern New Mexico. Machette (1985), modified the classification scheme of Gile and proposed two additional stages (V and VI) of carbonate horizon morphology for older calcic horizons with more advanced morphology than the four previously described. A complete description of the individual stages developed in soils with gravelly and non-gravelly parent materials is listed in Table 1. The morphology of a carbonate horizon is in part a function of the age of the soil. Factors which affect the rate of morphologic change in a carbonate soil include soil texture, the amount, seasonal distribution, and concentration of Ca^{2+} in rain-water, and the $CaCO_3$ content and net influx of airborne particles (Machette, 1985). The rate at which individual stages of carbonate morphology develop can vary significantly between different geographic locations. Machette (1985) compared the carbonate soils of eight chronosequences in the southwest in an attempt to understand the regional variations in the amount of time required to developed various stages of carbonate morphology (Table 2).

Ages of calcic soils can be estimated based on the morphologic stage of carbonate horizons, but determining the maximum stage of carbonate morphology in the field can be difficult and subjective. Furthermore, stages of carbonate morphology can develop faster in soils with gravelly parent materials than in soils with non-gravelly parent materials. The whole-profile soil-development index of Machette (1985) can be used to quantitatively estimate the age of calcic soils and therefore is a better method of estimating ages than one based on carbonate morphology alone. Knowing the amount of secondary (pedogenic) carbonate in a soil profile, and estimating the rate at which it has accumulated, allows the age of the soil and the deposit in which it is formed to be estimated.

Methods

Detailed soil profile descriptions were made for nine hand dug excavations following criteria listed in (Soil Survey Staff, 1975), and Birkeland (1984). Inspection of additional hand dug pits, borrow pits, and natural exposures augmented these detailed analyses. Soil properties described in the field include horizon thickness, color, structure, percent gravel, consistence, texture, nature of horizon boundaries, estimated clay content (%), and carbonate morphology (see soil profile descriptions, this article). The particle size distribution, carbonate content, and bulk density, of each soil horizon was determined in the laboratory. Samples were pretreated to remove $CaCO_3$ and the weight % sand, silt, and clay, of the <2 mm fraction of the soil was determined by pipette analysis (Janitzky, 1986). The amount of calcium carbonate in the <2 mm fraction of the soil was determined using a Chittick apparatus and methods outlined by Machettte (1986). The amount of $CaCO_3$ in the >2 mm fraction, mainly carbonate coatings on gravel clasts, was determined to be negligible. The paraffin-clod

method (Singer, 1986) was used to determine the bulk density of soil peds developed in fine grained (<2 mm) horizons and for cemented K (petrocalcic) horizons. For horizons with little to no soil structure (e.g. a noncemented sandy horizon), published bulk density values (Carmichael, 1984) for materials with similar textures were used.

The amount of secondary (pedogenic) $CaCO_3$ in gm/cm^2 of soil column was determined for each soil profile except one for reasons discussed in the results below. The secondary $CaCO_3$ value is calculated for a soil profile from the thickness, the carbonate content, and the bulk density of the <2 mm fraction of each horizon. For a complete description of how to make this calculation see Machette and others (1997).

Dividing the secondary $CaCO_3$ value of a soil by the estimated rate at which $CaCO_3$ accumulates in the soil yields an age for the soil and the deposit in which it is formed. In lieu of an independently dated soil in the study area for which the accumulation rate is accurately known, a rate of $CaCO_3$ accumulation for soils in the northern Quinn River Valley was estimated by comparing the climatic parameters of the area to areas where the rates of $CaCO_3$ accumulation in soils are well constrained (Table 2). Local geologic and geomorphic controls on the rate of solid $CaCO_3$ influx were also considered in determining a rate of $CaCO_3$ accumulation for soils in the Quinn River Valley. Of the areas listed in Table 2 for which a long term rate of $CaCO_3$ accumulation exists, the mean annual precipitation and temperature of the study area, 23 cm and 9°C respectively, most closely resemble the climatic means of Albuquerque, New Mexico. An estimated long term rate of $CaCO_3$ accumulation of 0.22 $g/cm^2/10^3$ yr has been calculated for the Albuquerque area (Machette, 1985). Machette (1985) observed that latest Pleistocene and Holocene age soils in southern New Mexico that have formed mainly under interpluvial climatic conditions, have accumulated carbonate at nearly twice the long term rate estimated for the region. Chadwick and Davis (1990) observed a similar trend in soils in the Carson Sink, attributing the increase in carbonate accumulation during interpluvial conditions to rapid loess influx, which not only drives carbonate accumulation, but the accumulation of silt, clay, and soluble salts. It is reasonable to assume that soils of latest Pleistocene and Holocene age in the northern Quinn River Valley have experienced a similar increased rate of carbonate accumulation relative to older soils that have developed under one or more pluvial-interpluvial climatic cycles. The Quinn River Valley was recently occupied by Lake Lahontan during the Sehoo highstand (~12,700 yr BP) which attained elevation of ~1322 m in the northern part of the valley (Adams, 1996). The lake level dropped approximately 100 m in 630 years shortly after the highstand (Adams, 1996) which means Lake Lahontan would have completely withdrawn from the Quinn River Valley by 12 ka. Prevailing wind directions during Sehoo time were to the north (up valley) as evidenced by spits developed on the west side of the valley which indicate longshore drift directions to the north based on morphology. As the level of Lake Lahontan lowered, exposing playa surfaces, soils in the northern Quinn River Valley likely experienced high rates of $CaCO_3$ accumulation as the influx of eolian material increased.

The secondary carbonate values in gm/cm^2 for seven of the soils in the study were divided by the estimated long term rate of 0.22 $g/cm^2/10^3$ yr to calculate an age for each deposit. The secondary carbonate values for one soil interpreted to be latest Pleistocene-Holocene in age (soil MS1), was divided by a carbonate accumulation rate of 0.44 $g/cm^2/10^3$ yr, for reasons discussed above. Final age estimates were made for each soil

based upon the consideration of the soils secondary carbonate content and stage of carbonate morphology, as well as the topographic position, surface morphology, and degree of dissection of the deposit in which it is developed. The age estimates are also based on comparison of soil development to other alluvial units from a nearby study (Hawley, 1965).

Results

The amount of secondary (pedogenic) $CaCO_3$ (cS) in gm/cm^2 of soil column was determined for eight soil profiles (MS1, MS2, TRS1 through 5, and BSS1). The results of the analyses are presented in Table 3. The amount of secondary $CaCO_3$ present in soil profile HPS1 was not determined because the soil is developed in beach gravels and the amount of primary (initial) $CaCO_3$ present in the gravels is not known. Soils MS2, TRS2, and TRS4 did not extend down into noncalcareous material so their secondary carbonate values are considered minimum values. See Figure 1 for the location of the soil profiles. The estimated ages of soils TRS3 and MS1 provide maximum and minimum limiting ages respectively, for the most recent faulting event on the Hot Spring Hills fault (see Stop 1-1 and 1-2, this volume). Soils TRS2 and TRS4 are interpreted to be the same soil and their estimated age potentially serves as a maximum limiting age on the time faulting initiated along the Hot spring Hills fault (see Stop 1-3, this volume). Soil TRS5 is also developed in a deposit offset by faulting (see roadlog, Day 1, mile 9, this volume). The estimated age of Soil BSS1 provides a maximum limiting age on the time of faulting on a splay of the Hot Spring Hills fault that displaces the Hot Spring Hills fan. The stream terrace in which soil TRS1 is developed, appears to be offset by only the most recent surface faulting event on the Hot Spring Hills fault. The estimated age of Soil TRS1 and the deposit in which it is developed (40 ka), does not closely constrain the age of the faulting which is estimated to be latest Pleistocene-Holocene in age based on work elsewhere along the Hot Spring Hills fault (see Stops 1-1 and 1-2, this volume). For more information on these soils and their relevance to your lives see Chuck's thesis which is due out in early next century.

References

Adams, K. D., 1996, Quaternary history, isostatic rebound and active faulting in the Lake Lahontan Basin, Nevada and California, Friends of the Pleistocene Pacific Cell Field Trip Guidebook, 57 p.

Birkeland, P. W., 1984, Soils and Geomorphology, Oxford University Press, Inc., New York, New York, 372 p. Carmichael, R. S., 1984, CRC handbook of physical properties of rocks, volume III, CRC Press, Inc., Boca Raton, Florida, p. 22-23.

Chadwick, O. A., and Davis, J. O., 1990, Soil-forming intervals caused by eolian sediment pulses in the Lahontan basin, northwestern Nevada, Geology, 18, p. 243-246.

Gile, L. H., Peterson, F. F., and Grossman, R. B., 1966, Morphological and genetic sequences of carbonate accumulation in desert soils, Soil Science, v. 101, n. 5, p. 347-360.

Hawley, J. W., and Wilson, W. E., 1965, Quaternary geology of the Winnemucca area, Nevada, Tehnical Report No. 5, Desert Research Institute, University of Nevada, Reno, NV, 92 p.

Janitzky, P., 1986, Particle-size analysis, *in* Singer, M. J. and Janitzky, P., eds., Field and laboratory procedures used in a chronosequence study, U.S. Geological Survey Bulletin 1648, Washington, D.C., U.S. Government Printing Office, p. 11-16.

Machette, M. N., Long, T., Bachman, G. O., and Timbel, N. R., 1997, Laboratory data for calcic soils in central New Mexico: Background information for mapping Quaternary deposits in the Albuquerque Basin, Circular 205, New Mexico Bureau of Mines and Mineral Resources, Socorro, NM, 63 p.

Machette, M. N., 1985, Calcic soils of the southwestern United States, *in* Weide, D. L., ed., Soils and Quaternary geology of the southwestern United States, Geol. Soc. Am. Special Paper, 203, p. 1-21.

Machette, M. N., 1986, Calcium and Magnesium Carbonates, 1986, *in* Singer, M. J. and Janitzky, P., eds., Field and laboratory procedures used in a chronosequence study, U.S. Geological Survey Bulletin 1648, Washington, D.C., U.S. Government Printing Office, p. 33.

Michetti, A. M., and Wesnousky, S. G., 1993, Holocene surface faulting along the west flank of the Santa Rosa Range (Nevada-Oregon) and the possible northern extension of the central Nevada seismic belt, Geol. Soc. Am. Abstr. Programs, v. 25, p. 120-121.

Pezzopane, S. K., and Weldon, R. J., 1993, Central Oregon fault activity. Tectonics, v. 12, p. 1140-1169.

Singer, M. J., 1986, Bulk density-paraffin clod method, *in* Singer, M. J. and Janitzky, P., eds., Field and laboratory procedures used in a chronosequence study, U.S. Geological Survey Bulletin 1648, Washington, D.C., U.S. Government Printing Office, p. 18-19.

Soil Survey Staff, 1975, Soil taxonomy: A basic system of soil classification for making and interpreting soil surveys: U.S. Dept. of Agriculture, Soil Conservation Service, Agricultural Handbook No. 436, U.S. Government Printing Office, 754 p.

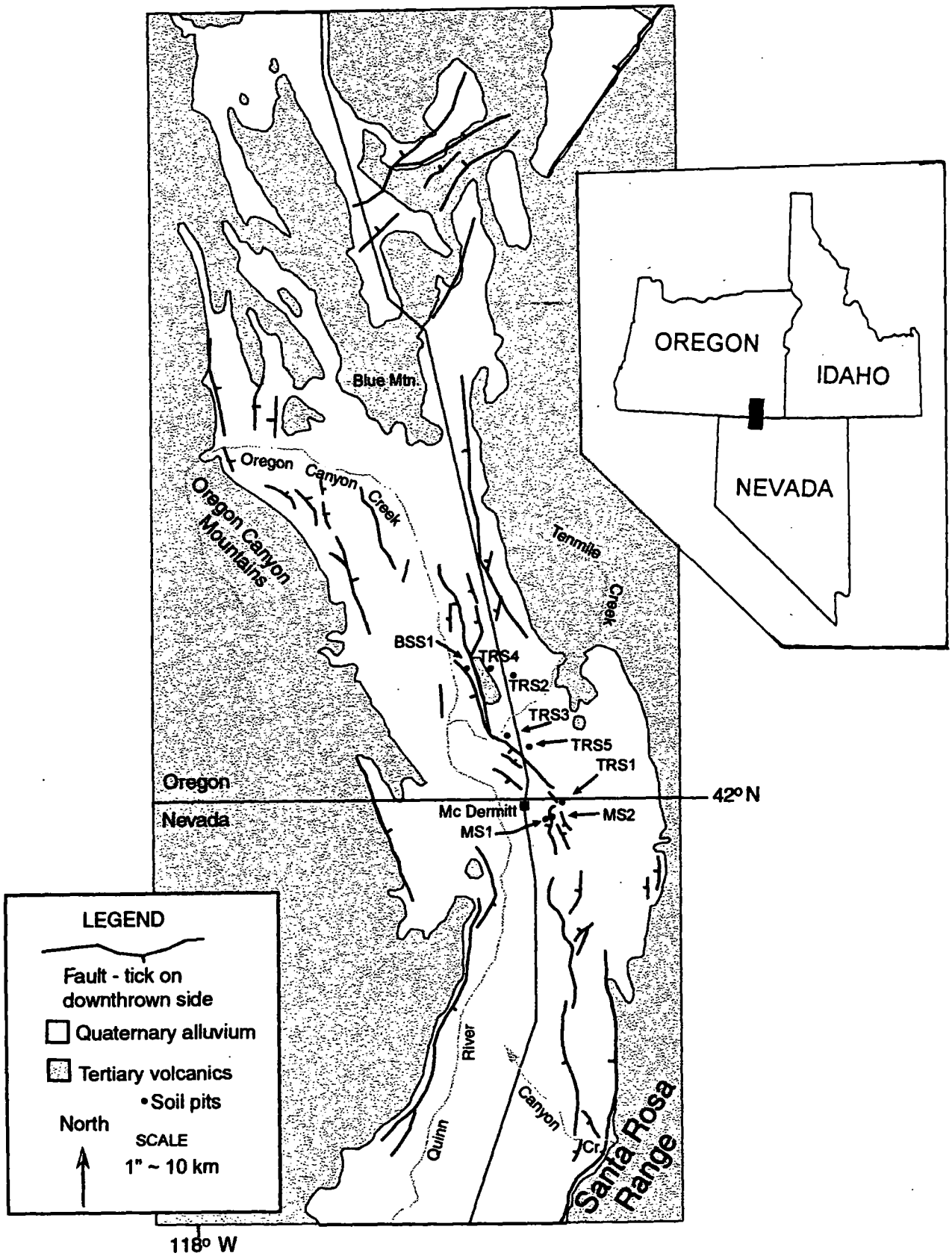

Figure 1. Generalized fault map of the northern Quinn River Valley showing location of soil profiles.

Table 1. Stages of carbonate morphology in gravelly and nongravelly parent materials (from Birkeland and others, 1991).

STAGE	GRAVELLY PARENT MATERIAL	NONGRAVELLY PARENT MATERIAL
I	Thin discontinuous clast coatings; some filaments; matrix can be calcareous next to stones; about 4% $CaCO_3$.	Few filaments or coatings on sand grains; <10% $CaCO_3$.
I+	Many or all clast coatings are thin and continuous.	Filaments are common.
II	Continuous clast coatings; local cementation of few to several clasts; matrix is loose and calcareous enough to give somewhat whitened appearance.	Few to common nodules; matrix between nodules is slightly whitened by carbonate (15-50% by area), and the latter occurs in veinlets and as filaments; some matrix can be noncalcareous; about 10-15% $CaCO_3$.
II+	Same as stage II, except carbonate in matrix is more pervasive.	Common nodules; 50-90% of matrix is whitened; about 15% $CaCO_3$.
Continuity of fabric high in carbonate		
III	Horizon has 50-90% of grains coated with carbonate, forming an essentially continuous medium; color mostly white; carbonate-rich layers more common in upper part; about 20-25% $CaCO_3$.	Many nodules, and carbonate coats so many grains that over 90% of horizon is white; carbonate-rich layers more common in upper part; about 20% $CaCO_3$.
III+	Most clasts have thick carbonate coats; matrix particles continuously coated with carbonate or pores plugged by carbonate; cementation more or less continuous; > 40% $CaCO_3$.	Most grains coated with carbonate; most pores plugged; >40% $CaCO_3$.
Partly or entirely cemented (irrespective of parent material)		
IV	Upper part to K horizon is nearly pure cemented carbonate (75-90% $CaCO_3$) and has a weak platy structure due to the weakly expressed laminar depositional layers of carbonate; the rest of the horizon is plugged with carbonate (50-75% $CaCO_3$).	
V	Laminar layer and platy structure are strongly expressed; incipient brecciation and pisolith (thin, multiple layers of carbonate surrounding particles) formation.	
VI	Brecciation and recementation (multiple generations), as well as pisoliths, are common.	

Table 2. Maximum stages of carbonate morphology in relict soils formed in gravelly alluvium in the southwestern United States (modified from Machette, 1985).

[Soils that have the same stages of $CaCO_3$ morphology are shown by tie lines. Alluvial units designated by letters and those shown with "alluvium" lowercased are informally named; all other names of alluvial units are formal. Names of geomorphic surfaces shown in italics. Ages are shown on a nonlinear scale. Climatic data from U.S. National Oceanic and Atmospheric Administration (1978).]

	(1)	(2)	(3)	(4)	(5)	(6)	(7)	(8)
Geographic area	Upper valley of Arkansas River, Colo.	Colorado Piedmont, Colo.	Albuquerque, N. Mex.	San Acacia, N. Mex.	Las Cruces, N. Mex.	Roswell-Carlsbad, N. Mex.	Vidal Junction, Calif. and Overton, Nev.	Beaver, Utah
Annual climatic means:								
Precipitation (cm)	24.6	37.6-47.2	20.5	21.2	20.4	35.5-32.8	11.5	30.0
Temperature (°C)	6.6	9.7-11.0	13.1	14.7	15.5	15.3-17.2	22.1	8.4
Weather station (s)	Buena Vista	Denver-Boulder	Albuquerque	Socorro	NM State Univ.	Roswell-Carlsbad	Parker, Ariz.	Beaver
Climate type	Cool arid	Temperate semiarid	Warm semiarid	Warm semiarid	Warm semiarid	Warm semiarid	Hot arid	Temperate semiarid

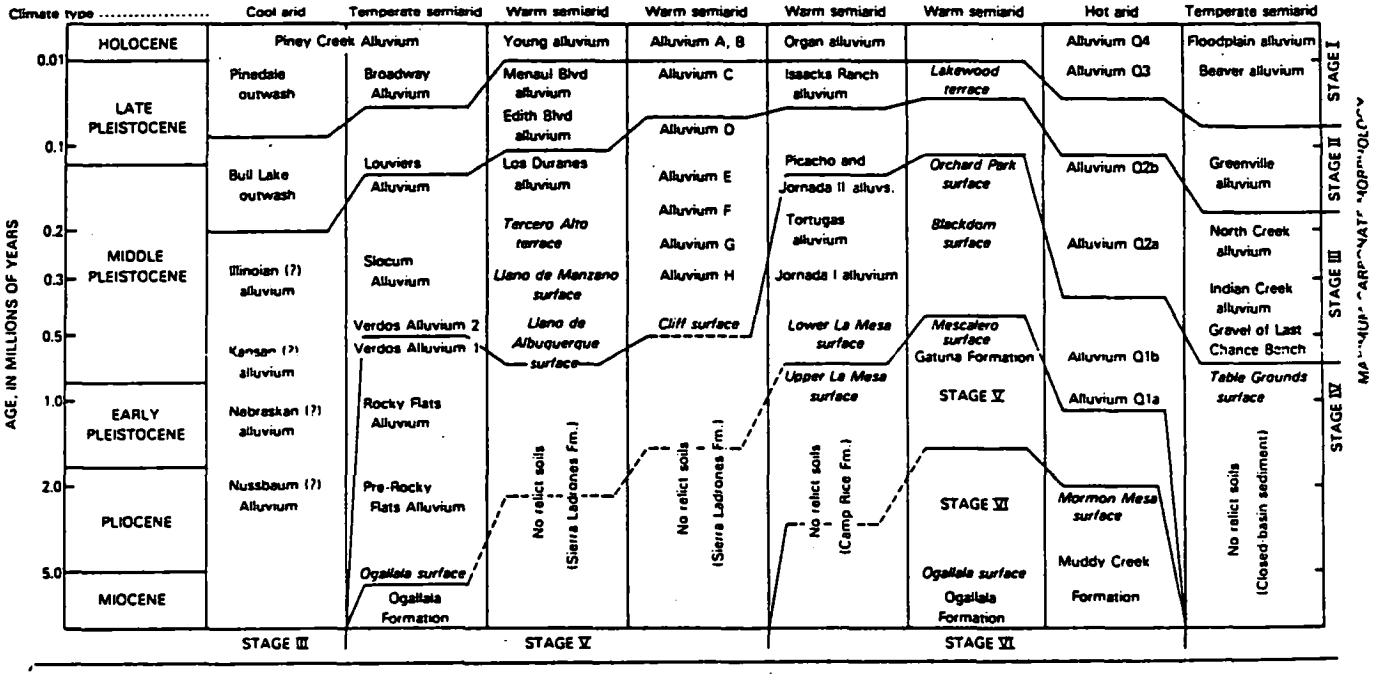

Pedogenic carbonate accumulation rate:	——	~0.09	0.22	~0.22	0.26	0.51	~0.10-0.15	0.14

References for geologic and soils data used in the above columns: (1) Scott (1975); G.R. Scott and R.R. Shroba, written commun., 1977; (2) Modified from Scott (1963) and Machette and others (1976); (3) Modified from Lambert (1968), Bachman and Machette (1977). All alluvial units are informally named. (4) Bachman and Machette (1977), modified from Machette (1978a); (5) Modified from Gile and others (1979 and 1981), Machette, unpubl. data. All alluvial units are informally named. (6) Modified from Bachman (1976) and Hawley and others (1976); (7) Modified from Gardner (1972), Bull (1974), and Ku and others (1979); Machette, unpubl. data; and (8) Machette (1982); Machette, unpubl. data. All alluvial units are informally named.

TABLE 3. Accumulation of secondary carbonate in soils developed in Quaternary deposits in the northern Quinn River Valley

Soil Profile*	Maximum stage of carbonate morphology ◊	(cT) Total $CaCO_3$ in <2mm fraction (gm/cm^3)†	(cP) Primary (initial) concentration of $CaCO_3$ in <2mm fraction (gm/cm^3)**	(cS) Estimated total secondary $CaCO_3$ in <2mm fraction (gm/cm^2)◊◊	Estimated soil age ††
MS1	I	0.187	0.087	3.75	8.5 ka§
MS2	III+	0.393	0.089	2.08^	300 ± 150 ka
TRS1	II+	0.336	0.088	8.37	40 ka§§
TRS2	IV	0.730	0.073	9.42^	1.5 ma
TRS3	I	0.0ϛ	0.59	0.0	10 ka
TRS4	IV	0.898	0.001	21.55^	1.5 ma
TRS5	II+	0.649	0.001	9.31	45 ka§§
HPS1	I+	0.229	???	???	12 ka
BSS1	III+	1.223	0.102	21.22^	300 ± 150 ka

*For map location of soil profiles see Figure 1.

◊Based on classification scheme of Gile and others (1966), and Machette (1985).

†Total amount of $CaCO_3$ present in <2 mm fraction of the soil.

**Estimated or measured $CaCO_3$ content of the parent material in which the soil is developed. Approx. 1% for all soils except HPS1.

◊◊Total secondary $CaCO_3$ content of the soil. Calculation: (cS) = the sum of (cT) - (cP) x (horizon thickness) for each horizon within the profile. For a complete description on how (cS) is calculated, see Machette (1997).

††Based on the consideration of the soils (cS) value and stage of carbonate morphology, as well as the topographic position, surface morphology, and degree of dissection of the deposit in which it is developed. Also based on correlation of soil development to other alluvial units from a nearby study (Hawley, 1965).

^Soil profile did not extend down into noncalcareous material so (cS) is considered a minimum value.

ϛThe <2 mm fraction of the soil has been leached of carbonate. The stage I carbonate morphology is based on carbonate coating on gravel clasts.

??? – The intial concentration of $CaCO_3$ is not known, so the total secondary $CaCO_3$ content of the soil was not determined.

§Based on estimated carbonate accumulation rate of 0.44 $g/cm^2/10^3$ yr. Age = ~(cS)/(0.44 $g/cm^2/10^3$ yr).

§§Based on estimated carbonate accumulation rate of 0.22 $g/cm^2/10^3$ yr. Age = ~(cS)/(0.22 $g/cm^2/10^3$ yr).

Soil Profile: MS1
Date described and sampled: December 3, 1997
Location: Lat. 41°58'32" N, Long. 117°41'51" W
Elevation: 1353 m (4440 ft)
Slope/Aspect: 18°/250°
Geomorphic surface: fault scarp
Parent material: Loess and colluvium
Vegetation: Wyoming big sagebrush and grasses
Annual climatic means: Precipitation (cm) 23
Temperature (°C) 9

Described by: C. Narwold

Horizon[ς]	Depth (cm)	Color (dry)	Structure	Gravel % (field)	Consistence Wet	Consistence Dry	Texture (lab)	Lower Boundary	$CaCO_3$ (%)[†]	Grain Size (% wt) Sand	Silt	Clay
A	0-15	2.5Y5/3	1msbk[◊]	10	ss ps	so	SiL	c s	1	34	52	14
Bw	15-30	2.5Y6/3	2 c sbk	10	ss ps	sh	SiL	c s	1	28	56	16
Bwk1-I	30-61	2.5Y6/3	2 c sbk	25	ss ps	sh	SiL	c s	3	30	54	16
Bwk2-I	61-97	10YR6/3	2 c sbk	5	ss ps	sh	SiL	c s	4	30	54	16
Btk-I	97-134	10YR6/3	2 c sbk	5	ss ps	sh	SiL	c s	3	29	52	19
Bwk-I	134-180+	10YR6/3	2 c sbk	5	ss ps	sh	SiL	*	2	28	57	15

Notes:
Descriptions and abbreviations follow criteria in (Soil Survey Staff, 1975), and Machette (1985).
[ς]Roman numerals denote morphologic stage of carbonate.
[◊]Secondary structure: 1msbk breaking to 1fpl.
[†]Based on measurement of the <2mm fraction of the soil using a Chittick apparatus (Machette, 1986).
*Not determined.

Soil profile: MS2
Date described and sampled: December 3, 1997
Location: Lat. 41°58'32" N, Long. 117°41'50" W
Elevation: 1355 m (4445 ft)
Slope/Aspect: 11°/250°
Geomorphic surface: fault scarp
Parent material: Alluvial gravels of predominantly basaltic and andesitic composition mantled by loess
Vegetation: Wyoming big sagebrush and grasses
Annual climatic means: Precipitation (cm) 23
Temperature (°C) 9

Described by: C. Narwold

Horizon[c]	Depth (cm)	Color (dry)	Structure	Gravel % (field)	Consistence Wet	Consistence Dry	Texture (lab)	Lower Boundary	$CaCO_3$ (%)†	Grain Size (% wt) Sand	Silt	Clay
Av	0-9	2.5Y6/3	2 vc sbk	10	ss ps	sh	SiL	a s	1	30	59	11
Bt1	9-14	2.5Y6/3	2 f pl	10	ss ps	so	SiL	a s	1	26	57	17
Bt2	14-18	10YR6/3	2 vf sbk	10	ms p	sh	C	g s	1	15	39	46
Bt3	18-26	10YR5/4	2 vf sbk	10	ms ps	sh	CL	a s	0	23	39	38
2Bwk-I	26-38	10YR6/4	1 m sbk	50-75	ss ps	sh	L	c s	2	51	32	17
2K-III+	38-45+	10YR7/3	*	50-75	*	*	*	*	54	*	*	*

Notes:
Descriptions and abbreviations follow criteria in (Soil Survey Staff, 1975), and Machette (1985), except: Av - vesicular A horizon.
[c]Roman numerals denote morphologic stage of carbonate.
†Based on measurement of the <2mm fraction of the soil using a Chittick apparatus (Machette, 1986).
*Not determined.

Soil profile: TRS1
Date described and sampled: November 10, 1997
Location: Lat. 42° 0' 9" N, Long. 117° 42' 8" W
Elevation: 1366 m (4480 ft)
Slope/Aspect: Nearly level
Geomorphic surface: Stream terrace
Parent material: Alluvial gravels of predominantly basaltic and andesitic composition mantled by loess
Vegetation: Wyoming big sagebrush and grasses
Annual climatic means: Precipitation (cm) 23
Temperature (°C) 9

Described by: C. Narwold

Horizon[ς]	Depth (cm)	Color (dry)	Structure	Gravel % (field)	Consistence Wet	Consistence Dry	Texture (lab)	Lower Boundary	$CaCO_3$ (%)†	Grain Size (% wt) Sand	Silt	Clay
A	0-10	2.5Y5/3	m	5	ss ps	lo	SiL	a s	0	32	50	18
Bwk1-I	10-28	2.5Y6/3	2 c sbk	5	ss ps	sh	SiL	c w	3	31	54	15
Bwk2-II+	28-63	2.5Y7/3	2 c sbk	5	ss ps	sh	SiL	c w	19	34	49	17
Bwk3-I+	63-86	2.5Y6/3	2 c sbk	10	ss ps	sh	SiL	c w	5	*	*	*
Bt	86-110	2.5Y6/2	2 c sbk	10	ss ps	h-vh	CL	c s	1	22	47	31
2Bwb	110-130+	10YR6/3	gr	75	*	*	SL	*	1	65	20	15

Notes:
Descriptions and abbreviations follow criteria in (Soil Survey Staff, 1975), and Machette (1985).
[ς]Roman numerals denote morphologic stage of carbonate.
†Based on measurement of the <2mm fraction of the soil using a Chittick apparatus (Machette, 1986).
*Not determined.

Soil profile: TRS2
Date described and sampled: November 12, 1997
Location: Lat. 42° 4'30" N, Long. 117° 43' 6" W
Elevation: 1420 m (4660 ft)
Slope/Aspect: Nearly level
Geomorphic surface: Distal bajada
Parent material: Alluvial gravels of predominantly basaltic and andesitic composition mantled by loess
Vegetation: Wyoming big sagebrush and grasses
Annual climatic means: Precipitation (cm) 23
Temperature (°C) 9

Horizon[ς]	Depth (cm)	Color (dry)	Structure	Gravel % (field)	Consistence Wet	Consistence Dry	Texture (lab)	Lower Boundary	$CaCO_3$ (%)†	Grain Size (% wt) Sand	Grain Size (% wt) Silt	Grain Size (% wt) Clay
Av	0-6	2.5Y6/2	2 c sbk[◊]	5	ss ps	sh	SiL	a s	0	21	61	18
Bt	6-16	2.5Y7/2	2-3 f pl	5	ss ps	sh	SiL	a s	0	19	56	25
Bw	16-29	10YR6/3	3 f abk	5	s ps	h	CL	a s	1	26	45	29
Bwk-II+	29-39	10YR7/3	2 f sbk	5	ss ps	sh	SiL	c w	18	32	63	5
2K-IV	39-55+	10YR8/2	*	20	*	*	*	*	40	*	*	*

Notes:
Descriptions and abbreviations follow criteria in (Soil Survey Staff, 1975), and Machette (1985), except: Av - vesicular A horizon.
[ς]Roman numerals denote morphologic stage of carbonate.
[◊]Secondary structure: 2 c sbk breaking to 2 vf-f pl.
†Based on measurement of the <2mm fraction of the soil using a Chittick apparatus (Machette, 1986).
*Not determined.

Soil profile: TRS3
Date described and sampled: December 4, 1997
Location: Lat. 42°44'25" N, Long. 117°44'24" W
Elevation: 1373 m (4505 ft)
Slope/Aspect: Nearly level
Geomorphic surface: Alluvial fan
Parent material: Alluvial gravels of predominantly basaltic and andesitic composition mantled by loess
Vegetation: Wyoming big sagebrush and grasses
Annual climatic means: Precipitation (cm) 23
Temperature (°C) 9

Described by: C. Narwold

Horizon[ς]	Depth (cm)	Color (dry)	Structure	Gravel % (field)	Consistence Wet	Consistence Dry	Texture (lab)	Lower Boundary	$CaCO_3$ (%)†	Grain Size (% wt) Sand	Silt	Clay
A	0-10	2.5Y5/3	1 m sbk[◊]	20	ss ps	so	L	a s	0	46	42	12
Bw1	10-29	2.5Y5/3	1f sbk	25	ss ps	so	L	g s	0	42	44	14
Bw2	29-62	2.5Y6/3	1 m sbk	30	ss ps	sh	L	a s	0	48	39	13
2Bwk-I	62-110+	10YR5/3	sg	50	so po	lo	S	*	0	92	6	2

Notes:
Descriptions and abbreviations follow criteria in (Soil Survey Staff, 1975), and Machette (1985).
[ς]Roman numerals denote morphologic stage of carbonate.
[◊]Secondary structure: 1 m sbk breaking to 1 f pl.
†Based on measurement of the <2mm fraction of the soil using a Chittick apparatus (Machette, 1986).
*Not determined.

Soil profile: TRS4
Date described and sampled: December 5, 1997
Location: Lat. 42° 4' 39" N, Long. 117° 44' 25" W
Elevation: 1425m (4675 ft)
Slope/Aspect: 15°/75°
Geomorphic surface: Backtilted distal bajada
Parent material: Alluvial gravels of predominantly basaltic and andesitic composition mantled by loess
Vegetation: Wyoming big sagebrush and grasses
Annual climatic means: Precipitation (cm) 23
Temperature (°C) 9

Horizon[ς]	Depth (cm)	Color (dry)	Structure	Gravel % (field)	Consistence Wet	Consistence Dry	Texture (lab)	Lower Boundary	$CaCO_3$ (%)†	Grain Size (% wt) Sand	Grain Size (% wt) Silt	Grain Size (% wt) Clay
A	0-8	2.5Y 5/3	3 vc sbk[◊]	5	ss ps	vh	SiL	a s	1	24	56	20
Bw	8-26	2.5Y 6/3	2 vc sbk	5	ss ps	sh	SiL	c s	0	28	50	22
Bwk-II+	26-36	10YR6/3	2 m sbk	15	ss ps	sh	L	c s	12	44	43	13
K-IV	36-63+	10YR8/2	*	10	*	*	*	*	61	*	*	*

Notes:
Descriptions and abbreviations follow criteria in (Soil Survey Staff, 1975), and Machette (1985).
[ς]Roman numerals denote morphologic stage of carbonate.
[◊]Secondary structure: 3 vc sbk breaking to 3 vf pl.
†Based on measurement of the <2mm fraction of the soil using a Chittick apparatus (Machette, 1986).
*Not determined.

Soil profile: TRS5
Date described and sampled: December 5, 1997
Location: Lat. 42° 1' 40" N, Long. 117° 42' 56" W
Elevation: 1384m (4540 ft)
Slope/Aspect: Nearly level
Geomorphic surface: Stream terrace cut into bajada
Parent material: Alluvial gravels of predominantly basaltic and andesitic composition mantled by loess
Vegetation: Wyoming big sagebrush and grasses
Annual climatic means: Precipitation (cm) 23
Temperature (°C) 9

Horizon[ς]	Depth (cm)	Color (dry)	Structure	Gravel % (field)	Consistence Wet	Consistence Dry	Texture (lab)	Lower Boundary	$CaCO_3$ (%)[†]	Grain Size (% wt) Sand	Silt	Clay
A	0-20	2.5Y6/3	2 vc sbk[◊]	5	ss ps	sh	SiL	a s	0	17	63	20
Bt	20-54	10YR5/4	2 f abk	5	ss ps	sh	C	g s	0	19	38	43
Bwk-I+	54-79	10YR6/3	2 f sbk	10	ss ps	sh	L	c s	5	47	34	19
Bwk-II+	79-94	10YR7/3	2 vf sbk	20	ss ps	h	L[§]	a s	18	*	*	10[§]
Btk-I+	94-101	10YR6/3	2 f abk	25	ss ps	h	L	a s	7	51	34	15
Bwk1'-II+	101-114	10YR7/3	*	5	*	*	*	c w	19	*	*	*
Bwk2'-I+	114-130+	10YR6/3	2 m sbk	25	ss ps	sh	SL	*	5	59	30	11

Notes:
Descriptions and abbreviations follow criteria in (Soil Survey Staff (1975), and Machette (1985).
[ς]Roman numerals denote morphologic stage of carbonate.
*Not determined.
[◊]Secondary structure: 2 vc sbk breaking to 2 f pl.
[†]Based on measurement of the <2mm fraction of the soil using a Chittick apparatus (Machette, 1986).
[§]Field estimate.

Soil profile: BSS1
Date described and sampled: November 13, 1997
Location: Lat. 42° 4' 14" N, Long. 117° 45' 32" W
Elevation: 1363m (4470 ft)
Slope/Aspect: Nearly level
Geomorphic surface: Alluvial fan derived from Hot Spring Hills
Parent material: Alluvial gravels of predominantly andesitic composition mantled by loess
Vegetation: Wyoming big sagebrush and grasses
Annual climatic means: Precipitation (cm) 23
Temperature (°C) 9

Horizon[ς]	Depth (cm)	Color (dry)	Structure	Gravel % (field)	Consistence Wet	Consistence Dry	Texture[§]	Lower Boundary	$CaCO_3$ (%)[†]	Grain Size (% wt) Sand*	Silt*	Clay[§]
Av	0-6	10YR6/3	2 c sbk	5	ss ps	sh	SiL	a s	0	*	*	8
Bw1	6-14	10YR6/3	1-2 f pl	5	ss ps	sh	SiL	a s	0	*	*	8
Bw2	14-23	10YR6/3	2 c sbk	5	ss ps	sh-h	SiL	a s	0	*	*	10
Bt	23-40	10YR5/3	2 m sbk	10	ss ps	sh	SiCL	c s	1	*	*	20
Btk-I+	40-60	10YR6/4	2 m sbk	10	ss ps	h	SL-SCL	c s	8	*	*	18
2Bwk-II+	60-93	10YR7/3	m	25	so ps	lo	SL	a s	32	*	*	10
2K-III+	93-105+	10YR8/3	*	25	*	vh-eh	*	*	67	*	*	*

Notes:
Descriptions and abbreviations follow criteria in (Soil Survey Staff, 1975), and Machette (1985), except: Av - vesicular A horizon.
[ς]Roman numerals denote morphologic stage of carbonate.
[§]Field estimate.
[†]Based on measurement of the <2mm fraction of the soil using a Chittick apparatus (Machette, 1986).
*Not determined.

Soil profile: HPS1
Date described and sampled: October 14, 1998
Location: Lat. 41° 47' 28" N, Long. 117° 48' 21" W
Elevation: 1317 m (4320 ft)
Slope/Aspect: Nearly level
Geomorphic surface: Pocket barrier bar that formed ~12,500 yr BP during regression of Sehoo highstand of pluvial Lake Lahontan, based on work of Adams (1996) and this study.
Parent material: Beach gravels of predominantly basaltic and andesitic composition mantled by loess
Vegetation: Grasses
Annual climatic means: Precipitation (cm) 23
Temperature (°C) 9

Horizon[ς]	Depth (cm)	Color (dry)	Structure	Gravel % (field)	Consistence Wet	Consistence Moist	Texture (lab)	Lower Boundary	$CaCO_3$ (%)[†]	Grain Size (% wt) Sand	Silt	Clay
A	0-9	2.5Y6/2	2 c sbk[◊]	5	so ps	fr	SiL	c s	0	2	88	10
Bw	9-21	2.5Y7/2	2 c sbk	10	ss ps	fr	SiL	c s	0	21	62	17
2Bw1	21-35	2.5Y6/2	1 vf sbk	50	ss ps	fr	SiL	c s	0	22	61	17
2Bw2	35-51	2.5Y6/2	1 vf sbk	50	so ps	vf	L	c s	1	40	48	12
2Bwk1-I	51-88	2.5Y7/2	1 vf sbk	80	so ps	vf	SL	c s	7	63	28	9
2Bwk2-I+	88-107	2.5Y5/2	sg	60	so po	lo	S	c s	11	87	7	6
Ck-I+	107-130+	2.5Y6/2	sg	40	so po	lo	S	*	14	96	2	2

Notes:
Descriptions and abbreviations follow criteria in (Soil Survey Staff, 1975), and Machette (1985).
[ς]Roman numerals denote morphologic stage of carbonate.
[◊]Secondary structure: 2 c sbk breaking to 1 f pl.
[†]Based on measurement of the <2mm fraction of the soil using a Chittick apparatus (Machette, 1986).
*Not determined.

LAKE ALVORD and LAKE COYOTE; A HYPOTHESIZED FLOOD

Mark Hemphill-Haley, David Lindberg, and Marith Reheis

Lake Alvord has been recognized as one of the largest pluvial lakes in the Great Basin (fig. 1) for over a hundred years. Russell (1884) first described the abundant, well-preserved shoreline features around the margins of the valley. The most conspicuous shorelines lie at and below an altitude of 1280 m (4200 ft), representing a lake with an area of about 1,150 km2 (fig. 2). The Coyote Lake basin east of Lake Alvord was not known to have held a pluvial lake until recently. As recognized by Hemphill-Haley in 1987, the well-developed shorelines of Lake Alvord lie at and below the same altitude as a gap in the Tule Springs Rim on the east side of Alvord Valley. Hemphill-Haley (1987) also recognized that an indistinct shoreline and lacustrine deposits in Alvord Valley represented a higher stand of Lake Alvord at 1310 m (4300 ft). He inferred that the higher shoreline formed in the late Pleistocene when Lake Alvord filled, then spilled eastward through Big Sand Gap (Field Trip Stop 2-4) into the Coyote basin, and suggested that the higher shoreline was indistinct because the lake did not remain long at that level before spilling. Big Sand Gap contains a fluvial channel incised in bedrock and partly filled by Holocene fan and eolian deposits overlying older lacustrine deposits. Big Sand Gap presently closes the basin at an elevation of about 1283 m (Lindberg, in prep 1999). In a later abstract, Lindberg and Hemphill-Haley (1988) noted that a pluvial lake in the Coyote basin apparently formed as a result of overflow from Lake Alvord (fig. 2). They found Lake Coyote to have a shoreline altitude of 1278 m, only 2 m lower than the strongest shoreline of Lake Alvord, and suggested that the difference in shoreline altitudes could be due to faulting and sedimentation in Big Sand Gap rather than being a real difference in lake levels. If this is true, then Lakes Alvord and Coyote formed one contiguous water body during part of the last pluvial maximum.

In detailed field work, Lindberg (in prep, 1999) found shorelines at three or four distinct (more or less) elevations. The shoreline preserved at about 1280 m is commonly the most obvious and best developed of the shorelines at a given site. Four miles south of Big Sand Gap on the east side of the Alvord Desert at Little Sand Gap, there are shorelines at about 1302 m, at 1294 m, and 1287 m. None of the lakes that formed these shorelines at Little Sand Gap could be contained by the modern sill (1283 m) of pluvial Lake Alvord. Almost 14 miles north of Big Sand Gap, Miranda Flat Bar in White Sage Flat lies at elevation 1283 m. About 17 miles north, at Mickey Springs, shorelines lie at 1291 m and 1287 m; neither of these lake elevations could be contained within the basin at the present sill elevation. Twenty miles north of Big Sand Gap, in White Sage Flat, shorelines are preserved at about 1290 m and at 1283 m, the lower of which would fill the basin just to the sill. Despite the existence of several shorelines at elevations as much as 21 m higher than the Big Sand Gap, there remain no clear shorelines from any lakes higher than 1283 m in the gap or along the nearby range front.

New evidence obtained during a brief field reconnaissance in 1997 indicates that Lake Coyote, like Lake Alvord, also rose to a higher shoreline sometime prior to the formation

of its 1278-m shoreline, and identified a spillway at 1278 m (Sec. 21, R.38E., T.34S.) on the east side of Lake Coyote (fig. 2). A lake reoccupying the Alvord basin today would fill to about 1283 m and then presumably cut down rapidly through the Holocene fans and dune deposits in Big Sand Gap. Downcutting of five meters seems possible and could result in both lakes being at the same elevation (1278 m) if no cutting occurs through the Coyote sill. In addition, several lines of evidence suggest that water may have spilled eastward as a very large flood at least once in the late Pleistocene. Overflow from Lake Coyote would travel down Crooked Creek (Field Trip Stop 1-4) to join the Owyhee River northeast of Burns Junction, Oregon (fig. 2), thus connecting the Alvord basin with the Snake-Columbia drainage at least temporarily. There's nothing new under the sun; this scenario was suggested by Smith and Young (1926) but was discounted by Hubbs and Miller (1948), who relied on Russell's (1884) report that the mountains around Coyote basin were too high to allow eastward drainage.

Localities representing higher shorelines of Lake Coyote (fig. 2) include (two are shown on a recently published map of pluvial lakes; Reheis, 1999): (1) a shoreline and beach pebbles at and below 1295 m on the west side; (2) beach pebbles and a small playette at 1283 m north of the spillway; (3) beach pebbles and two abandoned spillways extending up to 1292 m on the north side of the present spillway; and (4) possible slack-water deposits extending up to 1290 m in a narrow valley south of the spillway. These deposits together suggest that Lake Coyote reached an altitude of about 1295 m some time before establishing the 1278-m shoreline controlled by the sill on the east side. Note that 1295 m corresponds to shorelines observed on the east side of Lake Alvord (see above; Lindberg, in prep. 1999) and on the west side at Alvord Point Saddle (Field Trip Stop 2-2). The strongly developed berms and shoreline notches at and below 1278 m suggest that Lake Coyote remained at this level for a lengthy period, possibly with continuing eastward overflow. Evidence that supports a large flood emanating from the eastern rim of the Coyote basin includes scoured bedrock, irregular blankets of fluvial sand and gravel on drainage divides and hillslopes (Field Trip Stop 1-5), and tear-drop-shaped hills that widen in a down-flow direction. Northeast of Burns Junction, the inferred flood apparently became confined to the incised canyon of Crooked Creek and may have left little record of its passing.

We emphasize that the inferred flood and the suggested 1295-m highstand of Lake Coyote represent extremely preliminary results from three days of field reconnaissance (in contrast to information on Lake Alvord shorelines from theses of Hemphill-Haley, 1987, and Lindberg, in prep. 1999). We would be quite unhappy if these suggestions were to be cited in any rigorous way, and might call for excommunication from FOP membership if that were to happen! However, we do strongly believe that this is an exciting research opportunity that would make an excellent M.S. or Ph.D. thesis, tying together pluvial-lake history with paleoflood reconstructions. In that spirit, we list the following interesting ideas, possibilities and mysteries that emanate from the data thus far.

Ideas and Mysteries; The Lake Alvord-Lake Coyote-Owyhee River Connection

1. What are the ages of the multiple higher shorelines that lie above the prominent, last-overflow shorelines tied to modern sill altitudes in the Alvord and Coyote basins (fig. 2)? We will visit shorelines at 1304 m and 1295 m at the Alvord Point Saddle, Field Trip Stop 2-2. Lacustrine gravel at 1304 m is associated with the highest shoreline (~1310 m) recognized in this part of the basin; a 1295-shoreline is cut into this gravel. Both clearly predate the establishment of the 1283-m sill at Big Sand Gap. Bud Burke is exploring the carbonate development between these two shorelines, and the 1283-m shoreline at Miranda Flat Bar, Field Trip Stop 3-1, to determine relative age. There are two possibilities: (A) The higher shorelines are only a little older than the overflow shorelines, and all of these features essentially formed during one pluvial period as a result of overflow and rapid downcutting of sills. (B) One or more of the higher shorelines are significantly older than the overflow shorelines, suggesting that overflow and downcutting may have occurred during more than one pluvial period.

2. Following possibility A above, if the 1295-m shoreline of Lake Coyote is late Pleistocene in age, was it formed by very rapid inflow through Big Sand Gap as Lake Alvord fell from 1310 m and incised its sill? Shorelines are preserved at several locations in the Alvord basin at about 1290-1295 m, 1287 m, and 1280-1283 m (Lindberg, in prep., 1999). Given a couple meters of documented Holocene faulting, one could argue that these altitudinal clusters of shorelines in widely separated parts of Alvord Valley (and Coyote, too) are too close to be coincidental. Lindberg (in prep., 1999) thinks the 1300-1310-m cluster of Alvord shorelines represent the highest oldest lake, from which the lake spilled, after which the lake (or a succeeding lake) cut a new shoreline represented by the cluster of shoreline elevations between about 1290-1295 m. Then successive downcuts could have brought the lake(s) to 1287, and then to 1280-83 m by the time pluvial conditions waned at the end of the Pleistocene.

3. Were Lakes Alvord and Coyote a continuous body of water? If so, at what altitude? Could they have formed one lake at the 1295-m shoreline, and then jointly lowered to about 1280 m (the overflow level of Lake Alvord) by incision of both sills? Lake Coyote would then at times be a great bay of Lake Alvord. This would require that Lake Coyote continue to lower its eastern sill to about 1278 m after the lakes separated; presumably overflow from Lake Alvord would have to persist to accomplish this.

4. There are TWO outlets through the Coyote basin rim at both 1295 m and 1278 m: the eastern spillway, which has clearly been eroded and scoured by overflow, and a valley about 7 km to the north-northwest (Sec. 31, T.33S., R.38E. which shows no channel or obvious signs of erosion by water, yet according to the topographic map (Grassy Ridge Well 7.5' quadrangle) is actually about 2 m lower than the obvious spillway (? on fig. 2). How is this possible? A minor error in contour lines could explain the apparent northern sill at 1276 m (there are no obvious fault scarps in this area), but not the higher gap. A linear valley leads north from this divide to drain into Wildcat Creek, an ephemeral drainage that ends at Crooked Creek Spring within the inferred flood path.

5. Following possibility B in question 1 above, could there have been more than one pluvial episode that resulted in spill from Lake Alvord into Lake Coyote and subsequent overflow eastward, possibly through different outlets? This could help to explain the lack of obvious erosion in the possible northern sill—it served as the outlet in a pluvial period older than latest Pleistocene, during which time the northern sill was lowered from 1295 m to about 1278 m (assuming the topographic map is in error, see #4 above. According to Lindberg, that's real arm waving stuff (as if any of this is very solid).

6. Was there a catastrophic flood eastward from Lake Coyote down Crooked Creek to the Owyhee River? What were the boundaries (possible limits are shown in fig. 2)? What was the discharge rate? Possibly the rate could be defined by measurements at constrictions along the course of Crooked Creek if the flood level can estimated. Similar measurements at Big Sand Gap might yield the flow rate out of Lake Alvord into Lake Coyote, but could not determine the size of a flood east from the Coyote basin if the two lakes merged.

7. Lake Coyote is a small shallow pan that can hold relatively little water (depth ~ 56 m at the 1295 m shoreline). Could such a flood be generated only from Lake Coyote? A large flood may require Lakes Alvord and Coyote to be one body of water. If Lake Alvord spilled and downcut as much as 15 m quickly, the volume of discharge could have been as much as 18 km3 (1200 km2 x 15 m deep). However, the rate of flow into Lake Coyote would have been constricted by the narrows in Big Sand Gap. The amount of water in Lake Coyote before influx from Lake Alvord is unknown. The area of Lake Coyote at the 1295-m shoreline is about 452 km2, and at 1280 m is about 317 km2; if the lake were to spill and downcut 15 m rapidly, Lake Coyote alone could generate a total discharge of about 6 km3. The east Coyote sill is much wider (more cross-sectional area) than Big Sand Gap and could drain faster.

8. Did channelized overflow from Lake Coyote to the Owyhee River persist after the flood when one or both lake basins achieved stable shoreline levels—or during previous pluvial periods? Did such flow persist at Big Sand Gap at the same time?

9. If it did, could this help to explain the presence of Columbia River-type fish the Alvord and Whitehorse cutthroat trouts in the Alvord and Coyote basins (Lindberg, in prep. 1999)? Previously, the presence of these fish has been attributed to (1) drainage-switching between the Lahontan and Alvord basins via Summit Lake (Mifflin and Wheat, 1979), or (2) descent from a Miocene or Pliocene ancestral stock common to the Lahontan-Alvord-Whitehorse basins, complicated by stream captures (Behnke, 1992; Smith, in press). The average modern stream gradient from the Lake Coyote sill to the Owyhee River is 4.5 m/km (24 ft/mi), which should not provide an obstacle to trout migration.

10. More wild ideas: Would Lake Alvord-Coyote rise and fall seasonally at Big Sand Gap? Big spring snowmelt from the Alvord drainage basin may have flooded out with each thaw. Did the lakes freeze? Could there be ice dams? Or how about a spring—

each thaw. Did the lakes freeze? Could there be ice dams? Or how about a spring—summer run of Alvord salmon up from the Snake and into the now so arid country of southeast Oregon and northern Nevada?

With apologies to Sendak (1988): "And now, let the wild rumpus start!"

References Cited

Behnke, R. J., 1992, Native trout of western North America: American Fisheries Society, Monograph 6, 275 p.

Fuller, R. E., 1931, The geomorphology and volcanic sequence of Steens Mountain in southeastern Oregon: Washington Univ. Pub. Geology, v. 3, p.1-130.

Hemphill-Haley, M. A., 1987, Quaternary stratigraphy and late Holocene faulting along the base of the eastern escarpment of Steens Mountain, southeastern Oregon: M.S. thesis, Humboldt State University, Arcata, 84 p.

Hubbs, C. L., and Miller, R. R., 1948, The Great Basin. II. The zoological evidence: University of Utah Bulletin 38, p. 16-166.

Lindberg, D. N, and Hemphill-Haley, M. A., 1988, Late Pleistocene Pluvial History of the Alvord Basin, Harney County, Oregon. Northwest Science, v. 62, no. 2, p. 81.

Lindberg, D. N., 1999 (in prep.) Quaternary stratigraphy and tectonics of the eastern Alvord Desert; Harney County Oregon: M.S. Thesis, Humboldt State University, Arcata, CA, 95521.

Mifflin, M. D., and Wheat, M. M., 1979, Pluvial lakes and estimated pluvial climates of Nevada: Nevada Bureau of Mines and Geology, Bulletin 94, 57 p.

Reheis, M. C., 1999, Extent of Pleistocene lakes in the western Great Basin: U.S. Geological Survey Miscellaneous Investigations Map MF-2323 (digital; can be downloaded from web site http://greenwood.cr.usgs.gov/pub/mf-maps/mf-2323/).

Reheis, in press 1999 (?), Highest pluvial-lake shorelines and Pleistocene climate of the western Great Basin: Quaternary Research.

Russell, I. C., 1884, A geologic reconnaissance in southern Oregon. U. S. Geological Survey Annual Report 4, p. 431-464.

Sendak, Maurice, 1988 (originally published in 1963), Where the Wild Things Are: Harpercollins Juvenile Books, 37 p.

Smith, G. R., in press, Historical biogeography of Great Basin fishes, in Currey, D., Hershler, R., and Madsen, D., eds., Great Basin Aquatic Systems History: Smithsonian Institution, Washington, D.C.

Smith, W. D., and Young, F. G., 1926, Physical and economic geology of Oregon. Chapter XI, The southeastern lake district: Commonwealth Review, University of Oregon, v. 8, p. 195-253.

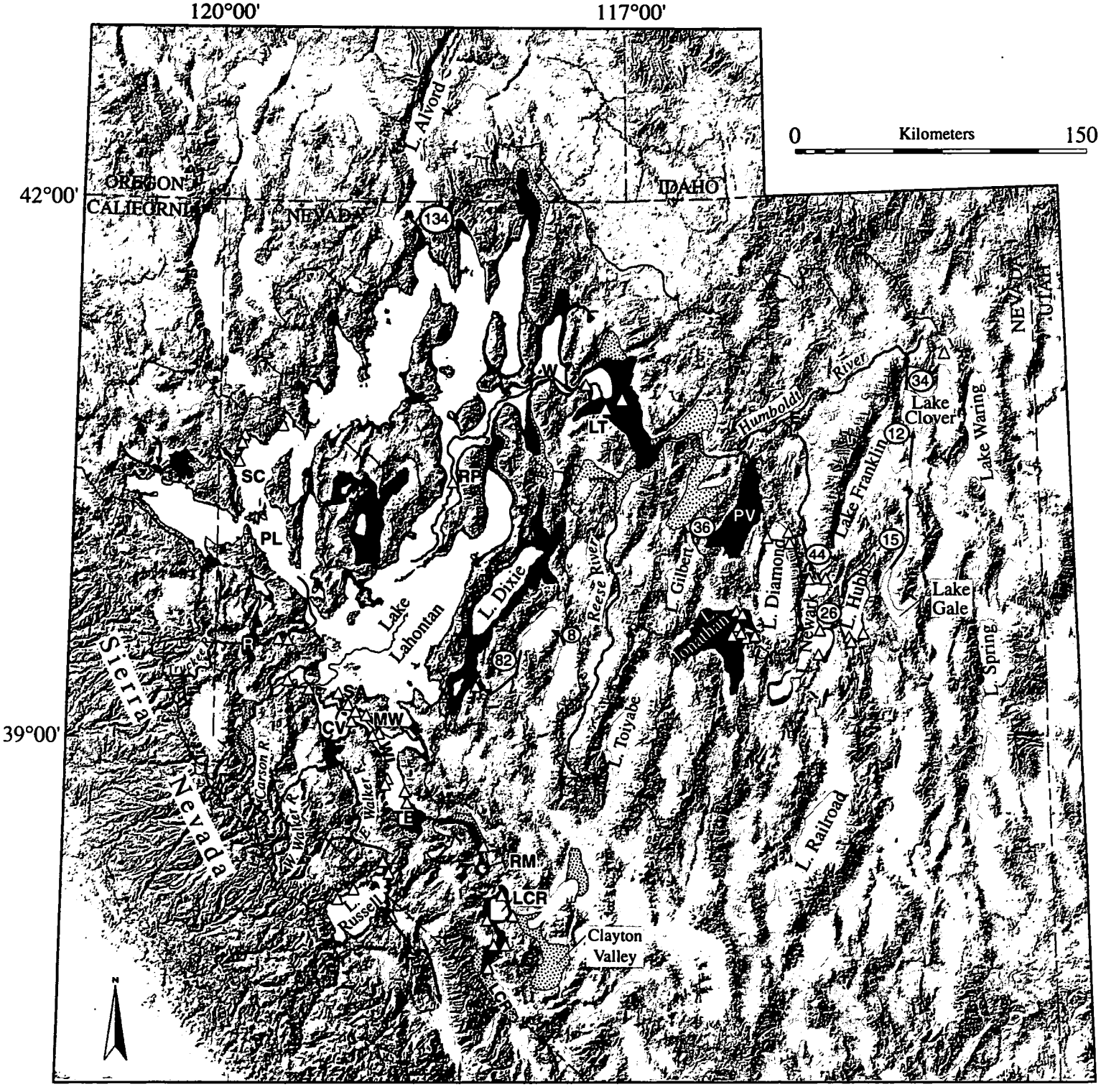

Area of late Pleistocene lakes (not all are shown)

Maximum known area of middle Pleistocene lakes

Possible additional area of middle Pleistocene lakes

Pre-late Pleistocene lake deposit locality

Late Pleistocene overflow

Inferred earlier overflow and modern sill height (m) above late Pleistocene shoreline

Late Pleistocene boundary of Lahontan basin

Possible additional area of basin in middle Pleistocene

Figure 1 . Regional map showing pluvial lakes of northern Nevada and vicinity, taken from Reheis (1999, in press). CV—Campbell Valley, E—Elko, LCR—Lake Columbus-Rennie, LM—Lone Mountain, LT—Lone Tree Hill, MW—McGee Wash, PV—Pine Valley, R—Reno, RM—Rhodes Salt Marsh, SA—Sunshine Amphitheater, SC—Smoke Creek Desert, TB—Thorne bar, W—Winnemucca, WL—Walker Lake.

Possible Alvord → Coyote → Owyhee Flood

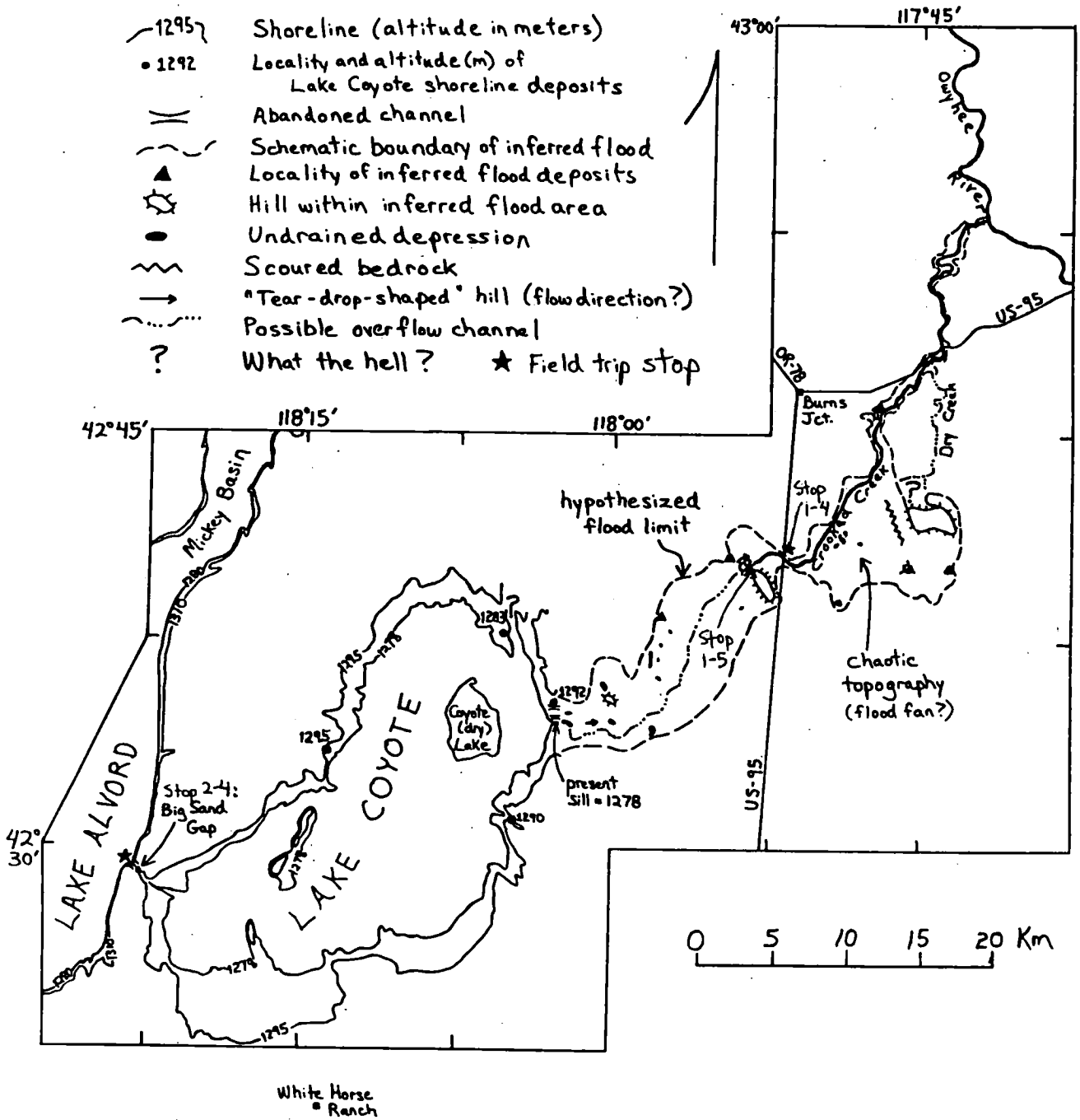

Figure 2. Sketch geomorphic map of region northeast of Alvord basin showing some shorelines of pluvial Lakes Alvord and Coyote and outline of inferred flood deposits between Lake Coyote and the Owyhee River in southeast Oregon. See top of figure for location.

A SYNOPSIS OF LATE PLEISTOCENE SHORELINES AND FAULTING, TULE SPRINGS RIMS TO MICKEY BASIN, ALVORD DESERT, HARNEY COUNTY, OREGON

David N. Lindberg*

Alvord Desert, the playa of late Pleistocene pluvial Lake Alvord, is a prominent feature of the Alvord Valley. Alvord Valley is the north end of the Pueblo Valley in Harney County, Oregon and drains a large area in southeastern Oregon and northern Nevada. Abundant shoreline features and youthful scarps were noted by early workers in the area, notably Russell (1884) and Fuller (1931). Based on these early reports, it was generally thought that pluvial Lake Alvord had no outlet. More recently, Hemphill-Haley (1987) noted shorelines at differing elevations (1310 m and 1280 m) at the base of Steens Mountain escarpment, and the prominent wind gap (Big Sand Gap) in the range front north of the Tule Springs Rims. Hemphill-Haley (1987) surmised that pluvial Lake Alvord had overtopped a low point in the range front rim and downcut (~30 m) to the present sill elevation in the gap. Downcutting of such magnitude at Big Sand Gap appears to have the potential to have flooded the Coyote basin to the east beyond its capacity and resulted in Coyote in turn spilling east into Owyhee River tributaries (Lindberg and Hemphill-Haley, 1988). Inspection of topographic maps, at contour intervals of 10 feet, suggest that Lake Coyote was constrained by a sill at elevation about 1278 meters (Map 1) and 1276 meters (Map 2).

Holocene fan deposition in the Big Sand Gap, and regional tectonic adjustments since pluvial time, were suggested as possible explanations for the two meter difference in elevation between the Coyote sills and the estimated pluvial closure in Big Sand Gap (Lindberg and Hemphill-Haley, 1988). Multiple shoreline deposits at elevations of about 1292 meters and 1280 meters, and additional potential spillover points in Coyote basin at elevations of about 1292 meters (Reheis, 1999), and at 1276 meters and 1278 meters (Lindberg and Hemphill-Haley, 1988) imply a more complex drainage history. Multiple shorelines preserved in the range front east of Alvord Valley are interpreted to record periods of persistent lake stability between downcutting events at Big Sand Gap. Rather than one large flood incising the Big Sand Gap from 1310 meters to 1280 meters, multiple shorelines between these elevations suggest more than one downcutting event may have released several smaller floods into Coyote basin. Multiple floods could result in erosion (and downcutting) at different sills at different times in Coyote basin. Temporary equilibration of water levels in the Alvord and Coyote basins may be recorded in the apparently-concordant elevations of some shorelines (1290 m to 1295 m) observed in both basins. A representational profile view of the elevations of several of the more prominent lakeshores, sills and playas in Alvord Valley, plus the elevations of inferred sills of the Coyote basin (Lindberg, 1999 in prep.) is presented in Figure 1.

* David N. Lindberg, RG 5581, CEG 1895 (CA), EG E1627 (OR), Vice President, LACO ASSOCIATES – Consulting Engineers, 21 West Fourth Street, Eureka California 95501, (707) 443-5054, 443-0553 (fax) <laco@northcoast.com>, Humboldt State University MS student.

East of Alvord Desert, surficial deposits consist of late Pleistocene lake sediments and Holocene eolian material and Pleistocene to Holocene alluvium from the range front. Lake sediments include wave-rounded gravel in near shore deposits, which make up the prominent shoreline bars, and fine grained sand and silt which was deposited in deeper water and now underlies the abundant dunes east of the playa and makes up the surface of the playa itself. Paleo shorelines constructed by pluvial Lake Alvord were examined in detail at three locations; Little Sand Gap, Mickey Springs and White Sage Flat, where prominent flights of shoreline terraces are preserved along the range front north of the Tule Springs Rims. Shoreline elevations from various locations in Alvord and Coyote basins are presented in Table 1.

A simple model of the pluvial history of the Alvord Valley suggests that at the onset of pluviation, the Alvord Valley filled first to about 1230 to 1240 meters, creating a lake up to 20 meters deep which would then spill northeast, toward Mickey basin. Mickey Basin, when filled, would merge with Lake Alvord near Mickey Springs (at the 1230 to 1240 m elevation). A continued additional water level rise of 60 meters would flood the Mann Lake Valley at or above elevation 1290 m. Pluvial Lake Alvord then filled to 1310′ meters (Hemphill-Haley, 1987) and spilled east through Big Sand Gap to Coyote Valley.

Reheis (1999) proposed that Coyote Valley may have filled to 1290 meters or more, and spilled to Owyhee River tributaries, the same drainage route proposed by Lindberg and Hemphill Haley (1988). Pluvial Lake Coyote overflowed to the east or north (or both) through the Grassy Ridge Well area (Map 1), or through a prominent notch in the east rim of the Coyote basin, the east Coyote gap (Map 2). Accurate mapping of Coyote shorelines will be necessary to confirm if one lake joined both the Alvord and Coyote basins at some point. Lake Alvord at least, persisted at or above 1290 meters (1290 – 1295 m) for a time sufficient to construct a shoreline before receding to an elevation of 1287 meters (1287 – 1288 m) or greater. Big Sand Gap, at 1280 meters (1280 – 1283 m), is associated with the most prominent shorelines, and seems to have been constructed by the most persistent late Pleistocene lake stand in Alvord Valley.

Coyote basin gaps are now 2 meters or more below the Big Sand Gap, which thus has eroded as much as 20 to 30 meters, while the gaps in Coyote Valley have lowered 12 to 14 meters, or more. Shorelines higher than Big Sand Gap could have been constructed by the lake when constrained by a less-eroded, higher elevation Big Sand Gap, or by earlier higher gaps in Coyote Valley. How the apparent intervals of lake persistence, seemingly punctuated by downcutting and lake recession relate to the current and implicit former sills in the two valleys is not clear. Levees, notable on the 1:24k topographic quad map (Figure 2-9, this volume), were constructed east of Big Sand Gap, and lie at 1280 meters or higher, suggesting pluvial Lake Coyote existed at or below that elevation while significant discharge flowed from Lake Alvord.

Engineering level survey data from prominent shoreline features at Miranda Flat Bar and Mickey Springs were modeled as first order trend surfaces to investigate the possibility that they may have been tilted since their formation. A first order trend surface of the

crest of Miranda Flat Bar suggests it tilts south, toward Alvord Desert, striking N79W and dipping (or tilting) southeast at 3.5 m/km. It is stressed that this is preliminary level survey data and not a closed-loop survey, although it is tied to the nearby USGS 4155-foot benchmark.

Near Mickey Springs a flight of three cuspate shorelines were surveyed by the same methods. First order trend surfaces suggest these shorelines are also tilted. The upper shore of the surveyed suite of shorelines appears to tilt NW 14.2 m/km and to strike about N28E. The second (next) shoreline down appears to strike east - west and tilt north. A third (next lower) shoreline bar, cut by a north - south Holocene normal fault was modeled with two first order trend surfaces. The upthrown block appears to strike approximately north - south, and tilt east at 8.2 m/km. On the downthrown, east side of the fault, the shoreline trend surface suggests that the bar surface tilts north at 2.4 m/km and strikes east – west. Table 2 summarizes these data.

Shoreline suites, like those at White Sage Flat, Mickey Springs and Little Sand Gap imply that at least three persistent stands of pluvial Lake Alvord occupied the Alvord basin in late Pleistocene time. At 1302 to 1310 meters, the highest and oldest of these lake stands was proposed (Hemphill-Haley, 1987) to have initiated the downcutting at Big Sand Gap. Coyote basin then filled to an elevation at or above 1290 meters (Reheis, 1999). A persistent lake cut shorelines in Alvord basin, at an elevation between 1290 and 1295 meters; preliminary data suggest Coyote basin may have contained a lake at or near these elevations also (Reheis, 1999). Lake Alvord above 1290 meters would inundate the Mann Lake basin north of Miranda Flat. Lake Alvord receding below that elevation (1290 m) might hydrologically-isolate the Mann Lake (sub)basin.

Another persistent stand of Lake Alvord constructed shorelines at or above 1287 to 1288 meters before receding and stabilizing again at or near 1280 meters, constructing the most-prominent shorelines preserved in Alvord Valley today. This lake recession may have isolated trout in Mann Lake from their Owyhee River relatives. Lake Alvord at 1280 meters is considered the most persistent late Pleistocene lake stand and was apparently in equilibrium with the sill at Big Sand Gap, and potentially with the Coyote sills, although data from the Coyote basin, it must be stressed, is very preliminary. When Lake Alvord receded from its high stand at 1280 meters and abandoned its outflow at Big Sand Gap, however, Coyote basin appears to have been constrained at elevations 2 to 5 meters lower (Table 3).

Shorelines below the 1290 meter lake stand are interpreted to have been constructed since the last late Pleistocene pluvial maximum. At least one late Pleistocene or Holocene lake below the elevation of Big Sand Gap sill persisted long enough to construct relatively prominent 1244 meters or higher shorelines at Bone Creek and Mickey Springs.

Several shorelines, notably near Mickey Springs, Alvord Point, White Sage Flat and Wildhorse Valley have been offset by normal faults of late Pleistocene to Holocene age. Holocene fault scarps near Alvord Hot Springs and Mickey Springs are likely coincident

in age and displacement, and may be a right step in the Steens Mountain fault zone similar to that described by Hemphill-Haley (1987) south of Alvord point.

Down-to-the-west fault scarps are preserved in the alluvial fans south and east of Mickey Springs. South of Mickey Springs, east of northern Alvord Desert, down-to-the-west normal faulting along the range front appears to swing away from the main trend of the Valley to trend east-northeast into the tertiary volcanic rock. Faults trending south, along the Tule Springs Rims range front from the base of the butte (elevation 5834 ft) southeast of Mickey Springs, pass through alluvial fans where they are expressed as incised scarps up to three meters in height. South along strike, the tertiary volcanic rocks of the Tule Springs Rims range front are dropped down-to-the-east on steep normal faults. The bedrock normal faults project into the alluvial valley fill a few kilometers to the south. South of the point where the faults enter the valley fill, no obvious fault scarps were observed in the dune fields and loess sheets between the playa and the range front.

Holocene faulting is presumed to continue south along the Tule Springs Rims range front east of Alvord Desert. Active eolian processes overlie fine-grained deep-water lake deposits in the area with dune fields and loess sheets making location of fault scarps difficult. Detailed mapping of contacts between the dunes and lake sediments was not attempted along the Tule Springs Rims range front east of Alvord Desert, but offset lake sediments might be exposed among the dunes on the east side of the playa. Possibly other Quaternary fault scarps may exist south of Little Sand Gap on the eastern side of Pueblo Valley. Cleary et al. (1981 a, b) reported large cracks and dismembered greasewood mounds east of Alvord Desert in the area of a gravity gradient he interpreted as a large normal fault; these features have not been located but could be youthful fault scarps.

The prominent fault scarp west of Mickey Springs (T33S, R35E, sec 15) was profiled for degradation modeling (Lindberg, 1999 in prep.) following the methods outlined in Nash (1986 & 1987). Five profiles from alluvial fan surfaces above the 1280 meter lake stand were recorded (Figure 2). Degradation-model ages of about two ka or younger support the field observation of a youthful scarp. A summary of data from analysis of the profiles is presented in Table 4.

The Mickey Springs fault scarp can be followed across the alluvial fans along the southeast face of Mickey Butte for approximately 5.5 km (3.4 mi) from the dune fields at the south end of the butte to the range front north of the hot springs. Beyond Mickey Springs, the Mickey Basin has been mapped by aerial photo reconnaissance with limited field verification. Offset shorelines are observable in the range front northeast of Mickey Springs, as are youthful fault scarps in alluvial fans. In White Sage Flat, a pluvial shoreline is offset two meters, south side down, by a subtle fault in a minor drainage that was evident only by a total station theodolite survey.

The abundance of fault scarps and offset shorelines in the Alvord Valley and Mickey Basin provides an explanation for the variability of shoreline elevations in the area. About two meters of Holocene, down-to-the-east displacement is documented along the

Steens Mountain range front and along the southeast facing escarpment of Mickey Butte. About three meters of Quaternary down-to-the west displacement is apparent southeast of Mickey Springs along the northern Tule Springs Rims range front. Between the range fronts in the Mickey Springs area, a youthful scarp with another two meters of down-to-the-east displacement offsets the late Pleistocene pluvial shoreline associated with the 1280 meter lake stand constrained by Big Sand Gap. Offset shorelines and scarps in alluvial materials also occur north and east of Mickey Springs, and a 2-meter offset was measured on a shoreline in White Sage Flat. In the Wildhorse Valley southwest of Alvord Desert, offset shorelines were documented by Hemphill-Haley et al. (1989).

Tectonic deformation since establishment of Pleistocene and Holocene shoreline features appears to be adequate to account for the disparities in modern elevations of the Alvord Valley shoreline features. The variability of shoreline spacing suggests that fault offsets occurred in different parts of the valley at different times. The blocks on which the shoreline are constructed appear to have moved independently at various times before and after the occupation of the valley by pluvial Lake Alvord.

List of Tables:

Figures:

Maps:

References cited:

Cleary, J., I. M. Lange, A. I Qamar, and H. R. Krouse, 1981 a, Gravity, isotope, and geochemical study of the Alvord Valley Geothermal area, Oregon: Summary; Geologic Society of American Bulletin, Part I, v. 92, p. 319-322.

Cleary, J., I. M. Lange, A. I Qamar, and H. R. Krouse, 1981 b, Gravity, isotope, and geochemical study of the Alvord Valley Geothermal area, Oregon: Geologic Society of American Bulletin, Part II, v. 92, p. 934-982.

Hemphill-Haley, M. A., 1987, Quaternary stratigraphy and late Holocene tectonics along the eastern escarpment of Steens Mountain, southeastern Oregon: Unpublished Masters Thesis, Humboldt State University, Arcata, California, 87 p.

Hemphill-Haley, M. A., W. D. Page, R. M. Burke, and G. A. Carver, 1989, Holocene activity of the Alvord fault, Steens Mountain, southern Oregon: Final report to the U. S. Geological Survey, Grant No. 14-08-0001-G1333, Woodward-Clyde Consultants, Oakland, California.

Lindberg, D. N., 1999 in prep., Quaternary stratigraphy and tectonics of the eastern Alvord Desert, Harney County, Oregon: Unpublished Masters Thesis, Humboldt State University, Arcata, California.

Lindberg, D. N and Hemphill-Haley, M. A.., 1988, Late-Pleistocene pluvial history of the Alvord Basin, Harney County, Oregon: [Abstract] Northwest Science, v. 62, no. 2, p. 81

Nash, D. B., 1986, Morphologic dating and modeling degradation of fault scarps: *in* Studies in Geophysics, Active Tectonics, National Academy Press, Washington D. C., p. 181-194.

Nash, D. B., 1987, Slopeage computer program, v. 2.1; Fenneman-Rich Geomorphic Laboratories: Cincinnati, Ohio, University of Cincinnati, Department of Geology.

Reheis, M. A., 1999, Extent of Pleistocene lakes in the western Great Basin: U. S. Geological Survey Miscellaneous Field Studies Map MF 2323.

Russell, 1884, A geologic reconnaissance in southern Oregon: U. S. Geological Survey Annual Report 4, p. 431-464.

Table 1

WSF[1]	MFB[1]	MS[1]	SM[2]	BSG[1,2]	AP[2,3]	BC[3]	LSG[1]	CB[4]
			1310 m		1304 m		1302 m	
1290 m		1291 m			1295 m		1294 m	1295 m
	1288 m	1287 m					1287 m	
1283 m	1283 m		1280 m	1283 m	1280 m	1280 m		
		1279/1276* m					1278 m	1278 m
1274/1272* m								
							1269 m	
1260 m								
		1247 m				1244 m		

Table 1. Shoreline elevations around the Alvord Desert, and Mickey and Coyote basins. WSF; White Sage Flat surveyed by total station, MFB; Miranda Flat Bar surveyed by engineering level. MS; Mickey Springs (engineering level), SM; Steens Mountain (topo interp. and field verification), BSG; Big Sand Gap (topo interp. and field verification), AP; Alvord Point Saddle (topo interp. and field verification), BC; Bone Creek (topo interp. and field verification), LSG; Little Sand Gap (engineering level and altimeter), CB; Coyote Basin. * Shoreline offset by faulting. References: 1 Lindberg (1999, in prep.), 2 Hemphill-Haley (1987), 3 this report, 4 Reheis (1999).

Table 2

Feature:	Strike Direction	Tilt m/km	Dip Direction	Correlation Coefficient	Standard Deviation	Sample Size
Miranda Flat bar	N79W	3.5	South	0.75	0.2 m	n = 40
Mickey bars:						
Upper	N28E	14.2	NW	0.71	0.7 m	14
Second	E – W	8.9	N	0.93	0.3 m	8
Third (downthrown)	N – S	8.2	E	0.88	0.2 m	10
Third (upthrown)	E – W	2.4	N	0.64	1.0 m	35

Table 2. Summary of apparent tilts of several shoreline features in Miranda Flat and near Mickey Springs.

Table 3

Location:	Elevation Meters (feet)	Measurement method	Sample size	Standard Deviation
White Sage flat:		Total Station		
Upper shoreline	1290 (4233)		13	2.45
Second shoreline	1283 (4210)		41	3.65
Third shoreline (UT)	1274 (4180)		40	3.68
Third shoreline (DT)	1272 (4132)		13	3.04
Fourth shoreline	1260 (4132)		5	2.61
Mickey bars:		Engineering Level		
Upper shore bar	1291 (4236)		14	5.22
Second shore bar	1287 (4222)		8	2.38
Third shore bar (UT)	1279 (4195)		10	1.18
Third shore bar (DT)	1276 (4188)		35	4.12
Fourth shore bar	1247 (4090)		23	8.07
Miranda Flat bar	1283 (4209)	Engineering Level	40	0.92
Little Sand Gap:				
Upper shoreline	1302 (4272)	Altimeter		
Second shoreline	1294 (4245)	Engineering Level	5	0.70
Third shoreline	1287 (4222)		3	3.98
Fourth shoreline	1278 (4193)		3	8.56
Fifth shoreline	1296 (4162)		9	5.74
Big Sand Gap	1283 (4210)	Topo Map, 20' CI.		
Grassy Ridge Well sill (?)	1276 (4185)	Topo Map, 10' CI.		
East Coyote Gap	1278 (4192)	Topo Map, 10' CI.		
Alvord to Mickey Springs sill	1237 (4058)	Topo Map, 20' CI.		
Mickey Springs to Mickey Basin sill	1230 (4036)	Topo Map, 20' CI.		
Alvord Desert playa	1219 (4000)	Topo Map, 20' CI.		
Mickey Springs playette	1229 (4033)	Topo Map, 20' CI.		
Mickey Basin playa	1192 (3910)	Topo Map, 20' CI.		

Table 3. Elevations of features around the north and east Alvord Valley, as measured in the field or interpolated from topographic map contours.

Table 4

Scarp Profile	Offset (meters)	Scarp Face Angle	Correlation (r^2)	Inferred Age (years)
1	1.6	25.2°	0.98	864
2	2.1	23.3°	0.99	2100
3	1.8	21.1°	0.97	1945
3	2.3	24.0°	0.99	1718
5	1.6	19.0°	0.97	1300
Mean	1.9	22.5°		
Std.dev.	0.3	2.5°		

Table 4. Slopeage data for five profiles across the Mickey Springs fault scarp. Fault offset and scarp face angle are also shown. A diffusion constant of 1.1 m^2/ka was assumed for this modeling.

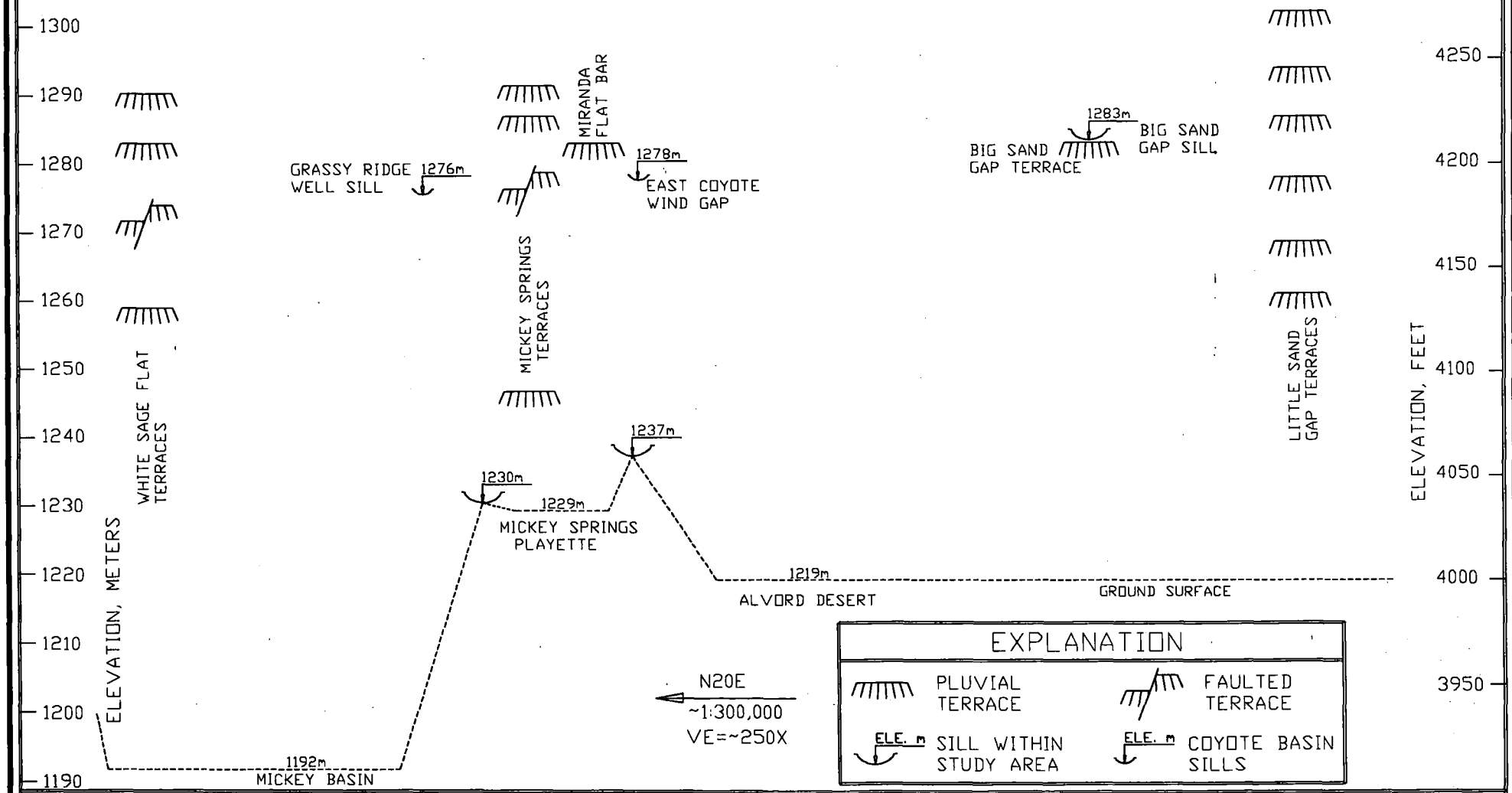

Figure 1. Representational profile showing shorelines, sills and playas in and around the study area. Sills draining the Coyote Lake basin are shown slightly smaller than sills within the study area. Routes of drainage, deformation of shoreline features and correlation of shoreline features from different parts of the study area are discussed in the text. Refer to Table 3 for more detailed information regarding terrace elevations, measurement methods, sample sizes and standard deviations. Offsets shown here on faulted terraces are representational only.

page __

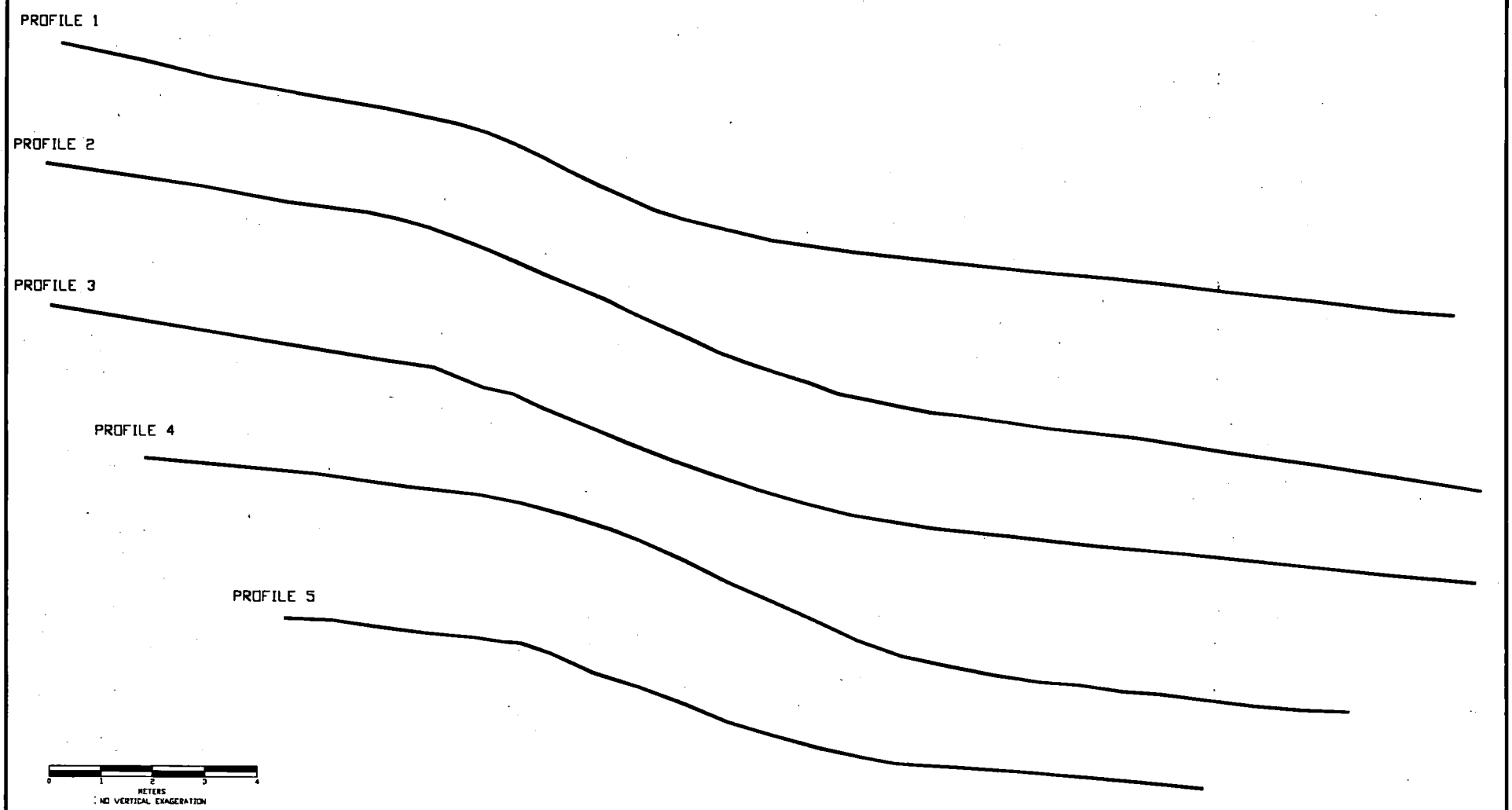

Figure 2. Plots of the five scarp profiles (in alluvial materials) along the Mickey Springs fault. Profiles were measured west and southwest of Mickey Springs. Mean offset is 1.9 meters and mean scarp-face angle is 22.5 degrees. This portion of the fault trends approximately north south, with the downthrown side to the east. Refer to the text for further discussion of the Mickey Springs fault scarp.

page __

Map A3-1.
Area Map of the East Coyote Gap

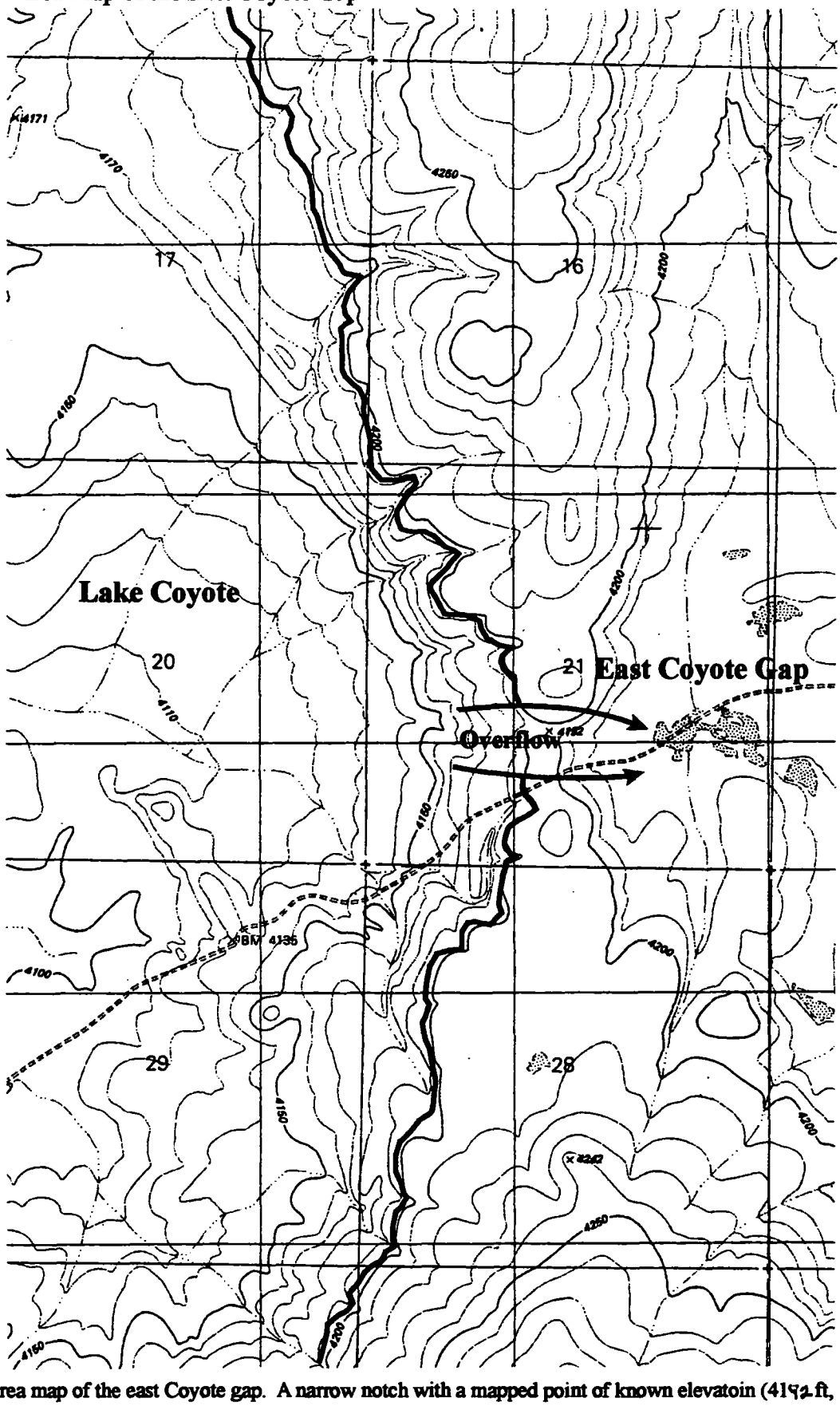

Map A3-1. Area map of the east Coyote gap. A narrow notch with a mapped point of known elevatoin (4192 ft, 1278 m) appears to have been cut into a much broader gap at or below about 1280 m. The heavy line follows the 4200 ft contour to show approximately where the Lake Coyote shoreline would lie with a lake of that elevation in the basin. Contour interval is 10 feet. Map from Coyote Lake East, Oregon Quad, T43, R3E, sec 21.

Map A3-2 Area map of the Grassy Ridge Sill.

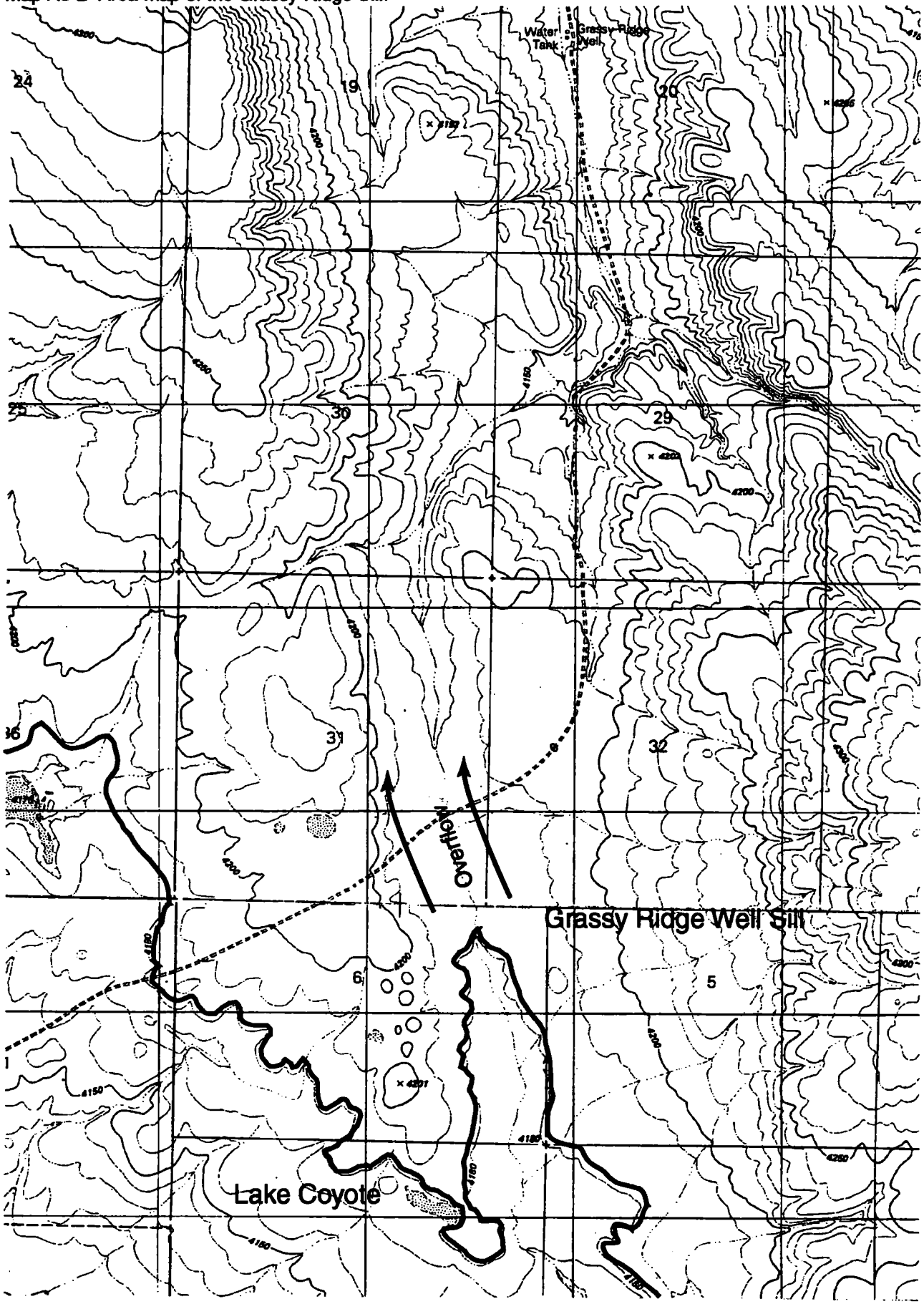

Map A3-2. Area map of the possible overflow route on the north side of the Coyote Lake basin. This possible overflow sill appears to be at about 1276 m, assuming the contour map is correct. Based on the limiting contours, the sill elevation is really between 1274 m (4180 ft) and 1277 m (4190 ft). The heavy line follows the 4180 contour to show approximately where Lake Coyote shore would be with a lake at that elevation in the basin. Contour interval is 10 feet. Map from Grassy Ridge Well quad, T33S, R38E, sec. 31.

Appendix 4

Contemporary Deformation of the Pacific Northwest: Regional Kinematics

Mark A. Hemphill-Haley URS Greiner Woodward-Clyde and University of Oregon
Gene Humphreys University of Oregon

[excerpted from Hemphill-Haley, M. A., 1999, Multi-scaled Analyses of Contemporary Crustal Deformation of North America [Ph.D. thesis]: University of Oregon, 253 p.]

INTRODUCTION

Deformation within the Pacific Northwest consists of three poorly understood, interacting areas with different tectonic styles: 1) the Cascadia subduction zone (CSZ) where the Juan de Fuca plate (JDF) and associated fragments are being thrust obliquely beneath the Coast Ranges; 2) Basin and Range-style faults in the arc and back-arc region that may be driving the fore-arc over the subduction zone and 3) crustal faults distributed across much of northern California, northern Nevada, Oregon, and Washington that may accommodate up to 20% of Pacific-North America plate dextral shear extending northwestward from eastern California and western Nevada along the Eastern California Shear Zone (ECSZ) (Pezzopane and Weldon, 1993). These components are individually clearer elsewhere (i.e., subduction to the north, dextral shear to the south and extension to the east) and provide strong constraint toward their complex interaction in the Pacific Northwest.

The objective of this research is to characterize Pacific Northwest deformation resulting both from the accumulation of interseismic strain along the CSZ and from other sources of strain not directly attributable to subduction-zone interaction. It consists of integrating geologic, geodetic and geodynamic data to provide a kinematic description of the contemporary strain in the region.

I have developed finite element models to describe the complex deformation within the interior of the western United States and its relationship to the CSZ. Penetrative dextral shear combined with gravitational-collapse-driven extension are the primary forces causing this deformation. The transform margin impedes the west-directed extension but induces shear. The CSZ serves as the outlet for both sources of deformation.

I use kinematic modeling to attempt to resolve several outstanding issues regarding Pacific Northwest tectonics and seismic hazards. First, I provide a kinematic assessment of the distribution of strain that accommodates the northern extension of the ECSZ within northern California, Nevada, Oregon and Washington. Second, I estimate the relative convergence velocities between oceanic plates and North America across the CSZ, as represented by the velocity of the Coast Ranges block with respect to the oceanic plate. I compare scenarios where western North America is attached rigidly to the stable interior

of North America (plate-rate model) and where western North America deforms above the subduction zone (my preferred model). Third, I provide a kinematic map depicting deformation within the interior of the western U.S. which may influence deformation along the subduction zone. Fourth, I provide a map that depicts strain within the western U.S., specifically within areas where little contemporary deformation information is currently available.

PROBLEMS WITH MODELING A SIMPLE TECTONIC MARGIN

Based solely on local geologic data there is considerable reason to doubt the existence of 10-15 mm/y of deformation distributed across Oregon and Washington (Pezzopane, 1993; Pezzopane and Weldon, 1993). However, the following simple and persuasive argument supports the contention that this much deformation may exist in the region. North-northwest motion of the Sierra Nevada block at 10-12 mm/y (with respect to North America) is accommodated by deformation concentrated in the ECSZ, which trends through the Walker Lane Belt east of the Sierra Nevada. This rate has been verified by velocities of well-constrained VLBI and GPS sites located nearly on the Sierra Nevada. It also has been largely accounted for geologically south of the latitude of San Francisco (Argus and Gordon, 1991; Dixon et al., 1995; Hearn and Humphreys, 1998). The reportedly intact nature of the Sierra Nevada block requires deformation in the PNW to occur east of this block, whereas the nearly stationary VLBI sites at Vernal (Utah) and Penticton (British Columbia) with respect to North America require that this deformation is confined across the PNW. The nature and distribution of this strain is not well understood. However, constraints may be obtained by applying kinematic modeling that simultaneously includes all pertinent information and includes explicit use of known boundary velocities, faulting style and distribution, and enforces kinematic consistency, followed by comparison of modeling results with independent observations.

MODELING A COMPLEX TECTONIC MARGIN

One aspect of western U.S. deformation that bears on the PNW is that earlier estimates of convergence between Juan de Fuca and North America have not considered that "stable" North America is not located along the western North America margin. In fact, a large portion of the western interior of North America is actively deforming. Fault-slip data and seismic-moment tensors suggest that southcentral and southeastern Oregon are moving to the northwest at about 6 mm/y (Pezzopane, 1993; Pezzopane and Weldon, 1993). This estimate accounts for only 40-50% of the dextral shear associated with the northern part of the ECSZ. VLBI estimates at Ely, NV (Dixon et al., 1993; Dixon et al., 1995) and slip-rate and GPS data along the Wasatch fault (Martinez et al., 1998; Smith and Braile, 1993) indicate that the eastern part of Basin and Range province is extending to the WSW at about 4 mm/y, away from eastern portions of North America. This direction is almost perpendicular to Pacific-North America transform motion

MODELING APPROACH

The project consists of integrating geologic and geodetic data to provide kinematic (and locally dynamic) descriptions of contemporary strain, including both the (variably straining) CSZ and the back-arc region. I use a 2-D finite element code to construct kinematically-consistent map-view models of the Pacific Northwest. Because the quantity and quality of data are always improving, my model is designed to incorporate future changes to the data set.

All modeling is motivated by a desire to include information that is often ignored, and to handle information correctly (i.e., satisfying the relevant equations). One often-ignored constraint that I include here is that of the "compatibility condition". In particular it is geometrically required that the integrated strain along any path connecting two points (and therefore on any surface, such as the Earth's) yields the relative velocity of the end-point with respect to the start-point (as discussed by Minster and Jordan (1987). It is not possible, for instance, to have thrust faulting at depth without having an identical accounting of this deformation at the Earth's surface. Nor is it possible to have the ECSZ accommodate 10 mm/y and eastern Oregon accommodates only 5 mm/y, without having some physical means for accommodating this difference.

KINEMATIC AND DYNAMIC SETTING OF WESTERN NORTH AMERICA

TWO DEFORMATION FIELDS AND AN OUTLET

Western North America can be described as the superposition of two deformation fields. The first process, transform-related shear, is related to plate processes and is controlled by the motion of the large tectonic plates that form the margin. The second deformation field results from gravity and involves the collapse of high-standing material, analogous to a landslide or earthflow. This process can not be directly related to plate tectonics, although, it owes its high potential energy to prior subduction-related tectonics.

Transform-Related Shear and Shear Penetration

The modern plate margin of western North America is dominated by the approximately 5400-km-long Pacific-North American transform plate boundary that extends from the Gulf of Alaska to south of the Baja Peninsula (Figure 1). The margin is composed of two large transform faults, the Queen Charlotte Fault (approximately 1200 km long) to the north and the San Andreas Fault system (approximately 2800 km long, including the spreading Gulf of California) to the south. Dextral shear along the transform faults juxtaposes the oceanic Pacific plate against the continental North American plate. A releasing right-step between the two faults coincides with the CSZ where the waning remnants of the Juan de Fuca plate and lessor Gorda and Explorer plates are thrust obliquely beneath North America. In comparison to the overall length of the transform

margin, the subduction zone is relatively small (Figure 1). Although the plate boundary is relatively simple, the western margin of North America is tectonically complex. Not only is there broadly distributed strain associated with the transform and subduction zone, but the interior of the continent is also collapsing gravitationally.

The tectonic configuration of the northern transform margin along the Queen Charlotte Fault has remained relatively stable for at least the past 30 Ma (Atwater, 1989). Conversely, the southern transform margin has undergone substantial modification in the past 30 Ma, changing from a subduction-bounded margin to strike-slip-bounded margin through a series of Farallon to Pacific-micro-plate transfers (Atwater, 1970; Atwater, 1989; Atwater and Stock, 1998; Severinghaus and Atwater, 1990). The contemporary southern transform margin extends from Rivera to Mendocino and continues to migrate northward, led by the Mendocino Triple Junction.

Gravitational Collapse of High Potential Energy Interior

The continental lithosphere of western North America is inherently weak relative to the strong oceanic lithosphere of the Pacific plate. This has resulted in large amounts of diverse deformation such as Eocene contraction (for example, Laramide deformation within the entire North American Cordillera (e.g., Dumitru et al., 1991; Hamilton, 1988; Humphreys, 1995; Livaccari, 1991)), late Cenozoic extension (for example the contemporary Basin and Range province), and establishment of inland shear zones associated with plate-margin tectonics (for example, ECSZ). Thus, although the Pacific plate is moving in a direction of about N45° to 38°W at a rate of almost 4.8 cm/yr relative to North America, only about two-thirds of that motion can be attributed to the San Andreas fault (Humphreys and Weldon, 1994; Minster and Jordan, 1987; Pezzopane and Weldon, 1993). The rest of the shear deformation has been transferred east of the Sierra Nevada (Humphreys and Weldon, 1994; Pezzopane and Weldon, 1993).

Interior deformation is probably dominated by the post-Laramide collapse of the high-standing, thickened crust (Hamilton, 1988; Humphreys, 1995; Jones et al., 1996). The Laramide Orogeny occurred during the late Cretaceous to early Paleocene when young, buoyant oceanic lithosphere of the Farallon plate was subducted rapidly beneath North America. The rapid introduction of a more buoyant slab resulted in a shallower subduction angle. Contraction occurred far inboard of the subduction zone with the majority of deformation located in the northern and central Rocky Mountains (Hamilton, 1988). Horizontal compressional stresses were sufficient to cause thickening of the lithosphere and resulted in a region of high potential energy. Once a steeper subduction angle was re-established along a new plate margin to the west, and traction between the sub-horizontal slab and the North American lithosphere diminished, the high-standing interior began to collapse. The direction of collapse was toward the poorly-coupled subduction margin free-face.

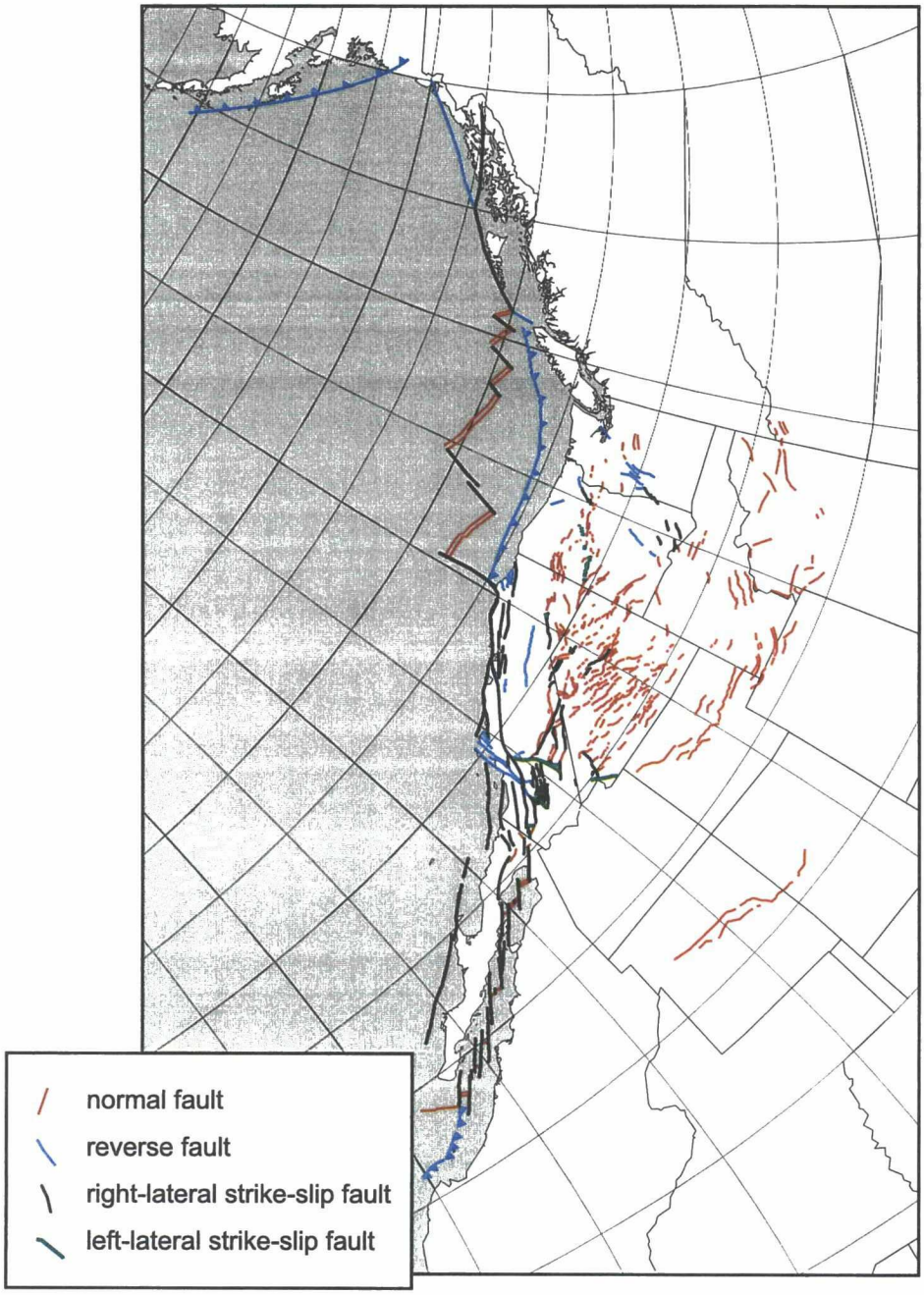

Figure 1 - Map of Late Cenozoic faults within the western United States and adjacent oceanic plates. Oblique Mercator projection about the Pacific-North America Euler pole. Note that the majority of the faults are located within the North America plate which is weak relative to the Pacific Plate.

Subduction Zone Window

Contemporary deformation within the continental lithosphere of western North America is the result of an interplay between the stresses and strengths associated with the expanding transform and diminishing subduction margins, and the ongoing "gravitational collapse" of the interior. For simplicity and to address the two styles of deformation, I consider two orientations of deformation within the continent, one that parallels the margin and one that is directed normal to the margin. I also consider the two types of tectonic margins that are present, the relatively long transform and the smaller subduction zone. Along the transform, margin-parallel deformation is dominated by dextral shear driven by Pacific/North American plate motion. Margin-normal motion, driven by westward collapse of the high standing continental interior, is impeded along the transform by its nearly vertical interface and the unyielding Pacific plate (Figure 2). Along the subduction zone within the United States, margin-parallel deformation occurs as a result of the oblique convergence of the Juan de Fuca plate relative to North America and due to the dextral shear imposed across the step-over by the transform margin. Within Canada, where the convergence direction is nearly normal to the margin, the margin-parallel motion is due solely to the regional transform interactions. Margin-normal motion of western North America is greater near the subduction zone than along the transform because the subduction fault is at a low-angle and is weakly coupled (Wang et al., 1995). This is where North America deformation, which is pervasive in the interior of the western U.S., is accommodated. Thus, the subduction zone allows the North American plate to move westward over the Pacific plate, both as a result of subduction of the sinking oceanic slab and, of the westward collapse of North America. A further consideration is that deformation in the region around the subduction zone is influenced by the presence of a right-step in the transform margin. The dextral plate motion and geometry of the right-step add a component of dilation in the region of the subduction zone in spite of shortening that is occurring at the subduction zone.

MODELING RESULTS FOR THE PACIFIC NORTHWEST

I have defined a rectangular region between 38°N –50°N, and108°W - 129°W as the Pacific Northwest region of the model. It spans an area from central Wyoming and Montana to west of Oregon and Washington and from southern Canada to northern Nevada, Utah, and California. I chose these boundaries for this region to allow a focus on the interaction between the Cascadia subduction zone and the continental interior. In particular I can look at 1) the deformation of the Oregon and Washington Coast Ranges; 2) Klamath Mountains and Modoc Plateau of northern California; 3) northern Basin and Range province of southern Oregon, northern Nevada, and Utah; and 4) the Yellowstone Hot Spot and associated structures, such as the Snake River Plain and northeast Basin and Range province of Idaho. I can also model the interaction between the Snake River Plain and eastern Basin and Range province.

The PNW region is significant for several reasons. First, it contains the transition between subduction-related contraction to the west and back-arc extension associated with the

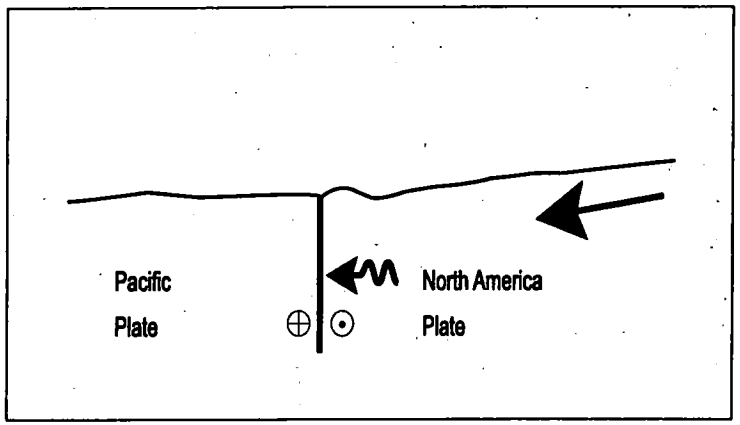

a) Transform margin

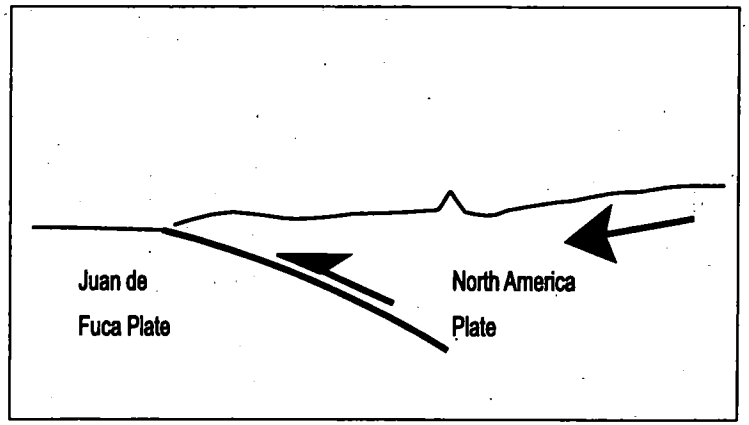

b) Subduction margin

Figure 2 Schematic diagrams showing the different roles that transform and subduction margins may play in the expansion of the continental interior. The transform margin, is a high-angle interface. The rigid Pacific plate to the west does not move to accomodate the expanding North America plate. The low-angle, relatively-poorly-coupled megathrust of the Cascadia subduction zone allows North America to ride over the Juan de Fuca plate. The expansion of North America is due to gravitational collapse of the post-Laramide thickened crust and to shear traction imposed along the transform fault.

Basin and Range province. Second, it is the location where previously unaccounted for significant dextral shear, possibly in excess of 1 cm/y, is proposed to be located within the interior of North America (Pezzopane, 1993; Pezzopane and Weldon, 1993). Third, it is the location where the northern Basin and Range province terminates and gives way to dominant contraction to the north. Fourth, it encompasses the entire path of the northeast migrating Yellowstone Hot Spot (Anders et al., 1989; Pierce and Morgan, 1990; Smith and Braile, 1993).

Constraints on deformation within the PNW region are limited. Permanent geodetic arrays have been deployed across a large portion of the region only within the last seven years (e.g. Pacific Northwest Geodetic Array (PANGA), Canadian Geodetic Survey array (Dragert and Hyndman, 1995; Dragert et al., 1994) and Northern Basin and Range array (Thatcher et al., 1999)). Prior to the installation of these large GPS arrays, deformation was estimated by sporadic level line surveys (e.g., Mitchell et al., 1994), local trilateration networks (e.g., Savage and Lisowski, 1991), incomplete or reconnaissance-level mapping of Holocene faults and folds (Geomatrix Consultants, 1995; Pezzopane, 1993; Pezzopane and Weldon, 1993) and infrequent, heterogeneously distributed historic earthquakes. Seismicity has been located primarily within the Puget Sound, Yellowstone Plateau, and northwest California (Pezzopane, 1993; Pezzopane and Weldon, 1993). There have only been a few moderate earthquakes within Oregon, including the 1962 M_L 5.5 Portland, 1993 M_L 5.6 Scotts Mills earthquakes (Bott and Wong, 1993), and 1993 M 6.0 Klamath Falls events (Wiley et al., 1993).

Through numerous iterations I have defined a preferred model for the region. This model accommodates motions of major blocks along the major deformation zones and satisfies the strain and deformation field to the best of my understanding.

PNW Model Velocities

Regionally, the preferred model shows a relatively simple velocity field (Figure 3). An undulating, roughly northwest-trending northern margin separates the more rapidly deforming part of the continent from nearly stable crust. Through Washington and western Idaho the margin coincides approximately with the location of the cratonic suture (Hooper and Conrey, 1989a). The eastern part of the Great Basin is delineated by the north-northeast–trending cratonic hingeline that traverses Utah (Sloss, 1988). The track of the Yellowstone hotspot obscures the juncture of these two margins by forming a northeast-trending "tongue" of deformation.

In general, velocities are smaller to the east and increase toward the west (Figure 3). Moving from east to west, vector azimuths, originally southwest- and west-directed become directed toward the northwest, a direction that is both subparallel to the Sierra Nevada block vector and toward the subduction zone. In the southeastern part of the region, velocity azimuths trend approximately west near the Wasatch Fault but turn toward the northwest within several hundred kilometers of the Great Basin margin .

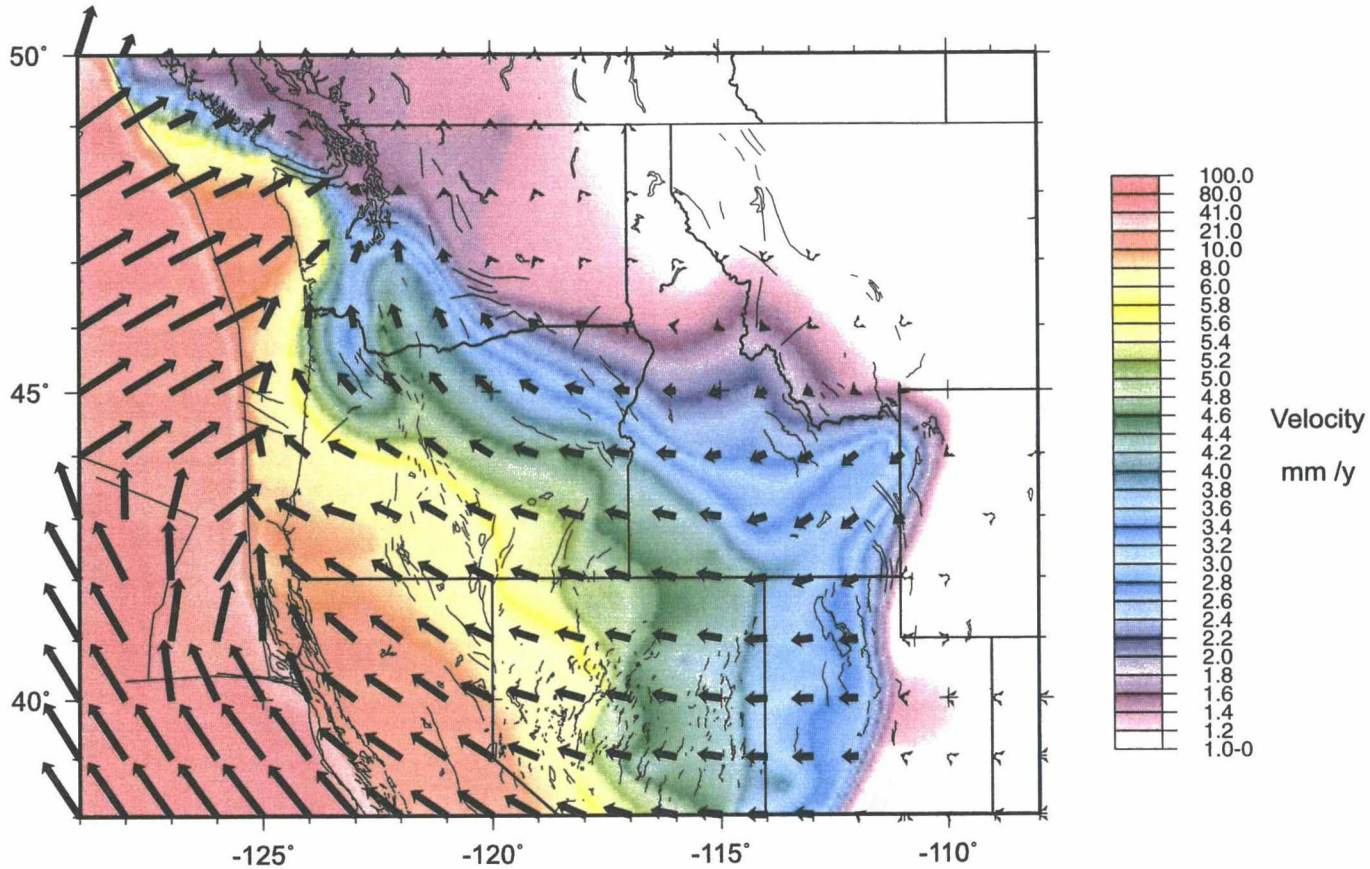

Figure 3 Modeled velocity map for Region 3, Pacific Northwest. Log-scaled vector arrows are calculated by interpolating nodal velocities within 1° grid spacing. Colored contours are calculated from smoothed nodal velocities at the same spacing.

In the northwest quadrant of the model velocities become more north-directed and converge toward the more stable portion of the continent in northeast Washington. Near the southern Puget Sound, the secular motion appears to be to the north-northeast, away from the subduction zone.

The western part of the model is strongly influenced by the clockwise rotation of the Coast Range block toward the subduction zone. The applied velocity of the Coast Range block is similar to that described by Wells *et al.* (1988; 1998) and Magill *et al.* (1982). The southern portion of the block is moving westerly at about 7 mm/y while the northern end of the block is moving north-northwest at about 3 mm/y. This block motion, in conjunction with northwest-trending back-arc motion, enhances the northward movement of the crust toward the Puget Sound (Figure 3).

The Olympic Peninsula, located along the northwest Washington coast, is the locus of velocity convergence from two directions. Northward migration of the Coast Range block (Wang et al., 1997; Wang et al., 1995; Wells et al., 1998) and northeast convergence of the Juan de Fuca plate focus velocities in a confined bend that is buttressed by stable North America (Figure 3).

Differential nodal velocities also provide information about the deformation field (Figure 4). About 7.5 mm/yr of northwest-directed extension occurs between the Oregon and Washington Coast Ranges and the stable craton of western Wyoming. The Basin and Range of Oregon is undergoing about 3.8 mm/y of extension with an azimuth that is slightly more north-directed than the summed extension across the entire province. The Steens Mountain fault zone, forming one of the most prominent Basin and Range escarpments in the region, has a horizontal extension rate of about 0.3 mm/y. The SRP moves to the southwest at about 2.5 mm/y. Extension rates along faults adjacent to the plain (for example the Lost River and Lemhi faults to the north and Swan Valley and Teton faults to the south) are only slightly lower and appear to diminish away from the SRP axis. The Wasatch frontal fault has a horizontal extension rate that increases from 1.9 to 2.3 mm/y from south to north and is directed slightly south of west. Discrete deformation zones within the Basin and Range province of Nevada have higher extension rates than their counterparts in Oregon. The Central Nevada Seismic Zone (historically, the most seismically active portion of the Basin and Range) and eastern Nevada seismic zone have rates of 1.5 and 0.7 mm/y, respectively.

In Washington, the Yakima fold belt is undergoing dominantly dextral, transpression at about 1.7 mm/y with vergence toward the southeast. The differential velocity across the Olympic Peninsula is about 3.2 mm/y directed toward the southwest.

An additional way to view the velocity field is to construct velocity profiles across the model. One transect from the model, east to west-trending transect C-C', runs from stable Wyoming to the Oregon coast and traverses the southern Basin and Range of Oregon (Figure 5). South of Yellowstone, the faults flanking the southern margin of the SRP are moving at about 2 mm/y toward 230°. The western SRP gradually increases in velocity toward the west and rotates toward the northwest. About 3.4 mm/y of 290 to

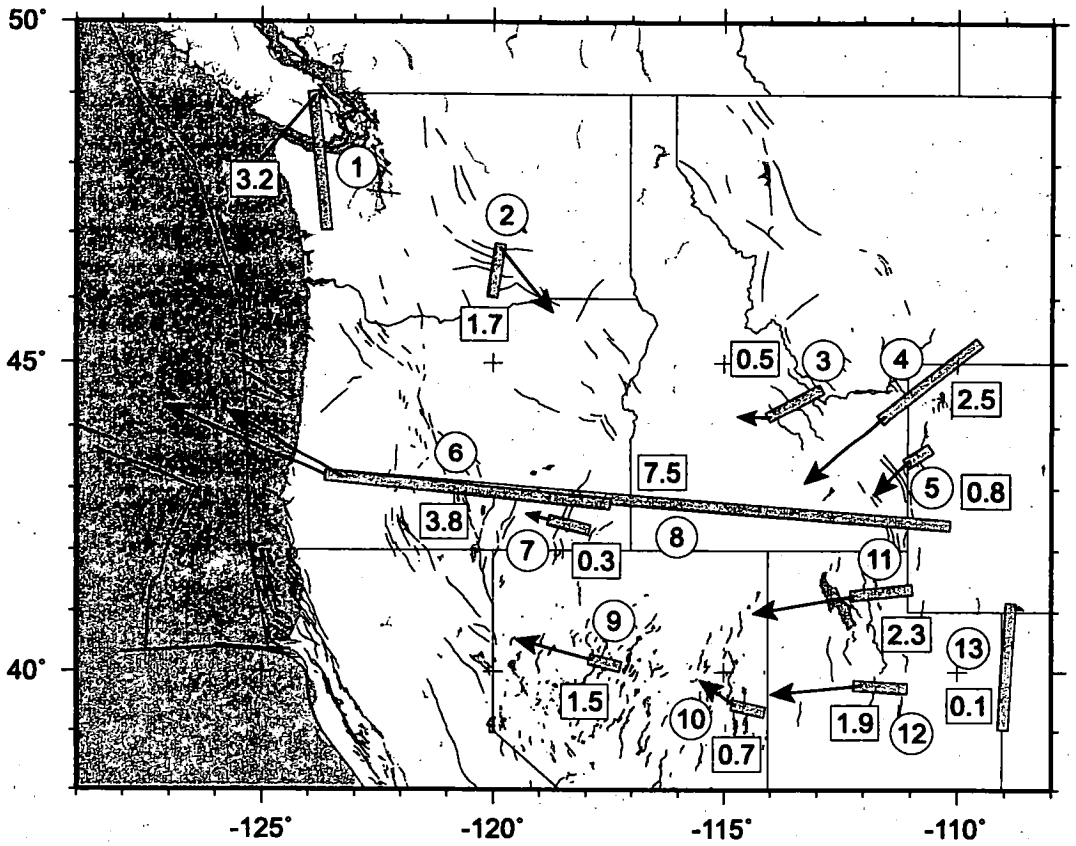

Figure 4 - Differential nodal velocities for the preferred model for selected faults and zones within Region 3, Pacific Northwest. Gray bars represent the width of the zone observed. Bar ends are located on the measured nodes. Arrows depict the motion of one end of the bar with respect to the other end. Values in boxes represent horizontal rate in mm/y. Circled numbers identify measured features: 1) Olympic Mtns., 2) Yakima Fold Belt, 3) Basin and Range North of SRP, 4) Yellowstone Plateau, 5) Teton fault, 6) Oregon Basin and Range, 7) Steens fault zone, 8) northern Basin and Range, 9) Central Nevada Seismic Zone, 10) eastern Nevada zone, 11) northern Wasatch fault, 12) southern Wasatch fault, 13) Uinta Mtns.

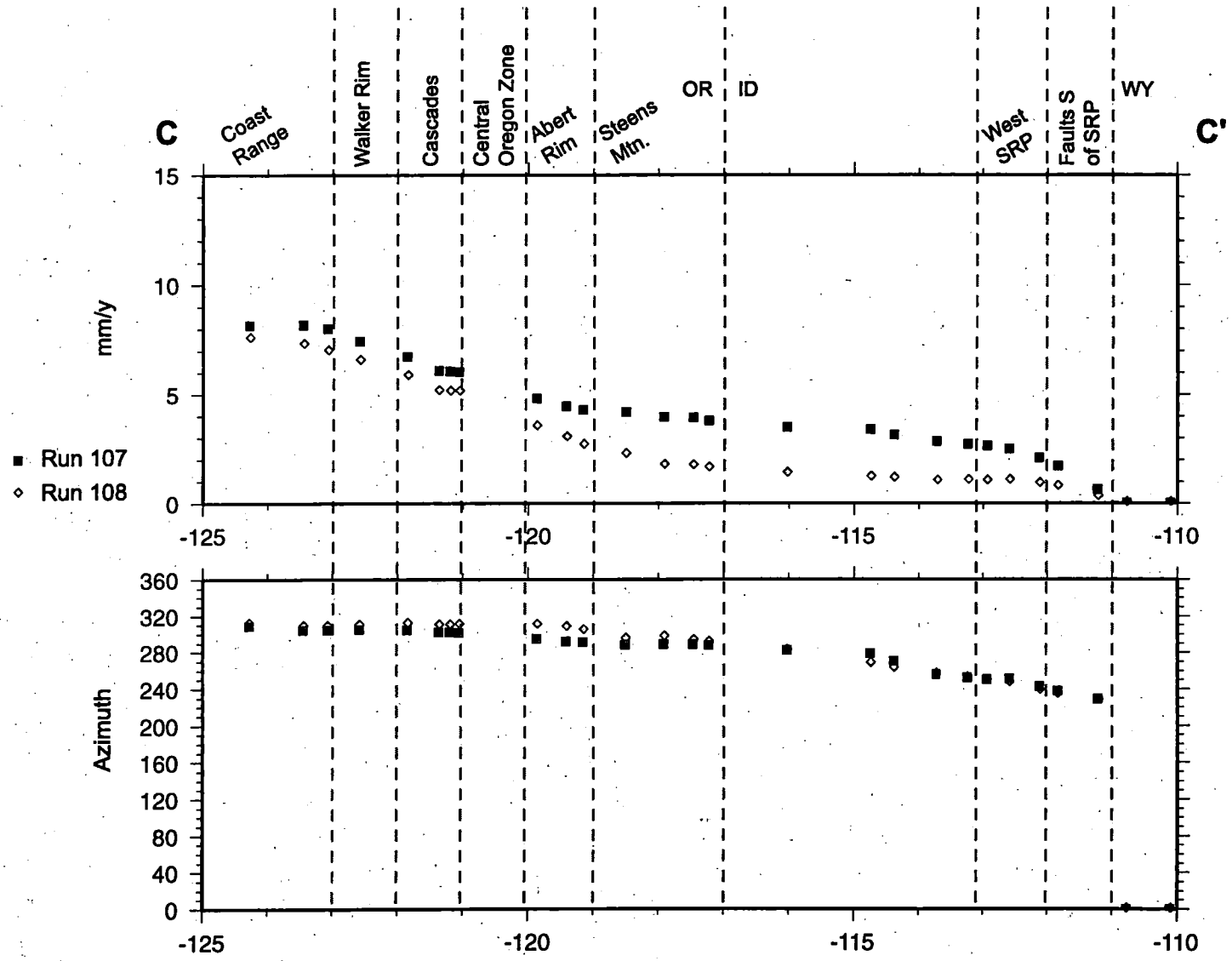

Figure 5 Nodal velocity Transect C-C'. Red points are for the preferred model.

305° directed extension occurs across the Oregon Basin and Range and Cascades back arc. This is in agreement with extension estimates reported as 4±2 mm/y directed toward 300°±30° (Pezzopane and Weldon, 1993).

The total extension across this portion of the Basin and Range, measured from stable Wyoming to the Oregon Coast Range, is 7.5 - 8 mm/y. Discrete steps in velocity mark locations of major faults, such as at Steens Mountain and Abert Rim; otherwise much of the increase is nearly linear. The differential horizontal velocity across the Steens fault zone is about 0.3 mm/y. Previously, I calculated a vertical, long-term slip rate of 0.33 mm/y across the range-front fault based on a maximum vertical separation of the Steens Basalt of about 3000 m (Hemphill-Haley, 1987). Assuming a fault dip of 50°, the horizontal rate is 0.3 mm/y which is in agreement with the model rate. The extension rate across this fault accounts for less than 10% of the extension rate for the region. Three prominent zones of faulting have been identified through the region east of the Coast Ranges, including the eastern Oregon zone containing the Steens Mountain fault (Pezzopane and Weldon, 1993). Perhaps an additional 0.1 mm/y of extension can be attributed to unmapped faults in the eastern Oregon zone. If the other zones have equivalent activity to the eastern zone then up to 45% of the extension can be accounted for. This means that more than 50% of the extension may be taken up as interfault diffuse deformation.

PNW Model Strain

A more intuitive portrayal of the deformation field developed from the preferred model for the region is provided by the isotropic strain map (Figure 6). One of the most striking features of the map is that dilatational strain is concentrated in narrow, generally north-trending zones. Contractional strain within the continent is located near the margin and is associated with broader belts that are oblique to the north-trending grain.

The map shows large contractional strain rates (>130%/m.y.) along the Cascadia Subduction Zone (CSZ). Two prominent areas of contractional strain are located at the southern and northern ends of the CSZ where they protrude into the North American plate. The southern zone (-0.5 to -1.3%/m.y.) coincides with the Klamath Mountains province and may mark the location where inboard dextral strain of the northern extent of the ECSZ makes a restraining step back to the margin. To the north, a large zone of contraction (-0.08 to –1.3%/m.y.) is centered on the Olympic Mountains with its northern margin across southwest Vancouver Island. An arm of the eastern part of the contractional zone extends southeastward and bifurcates at the Cascades volcanic arc. A southern branch (-0.9 to –1.0 %/m.y.) extends along the axis of the Northern Cascades arc and terminates in southern Washington. This coincides with previously identified contraction in the Northern Cascades (Wells et al., 1998). An eastern branch with lower contraction rates (-0.3 to –0.5 %/m.y.) along the Olympic Wallowa Lineament (OWL) contains elements of the Yakima Fold Belt (Hooper and Conrey, 1989b; Mann and Meyer, 1993).

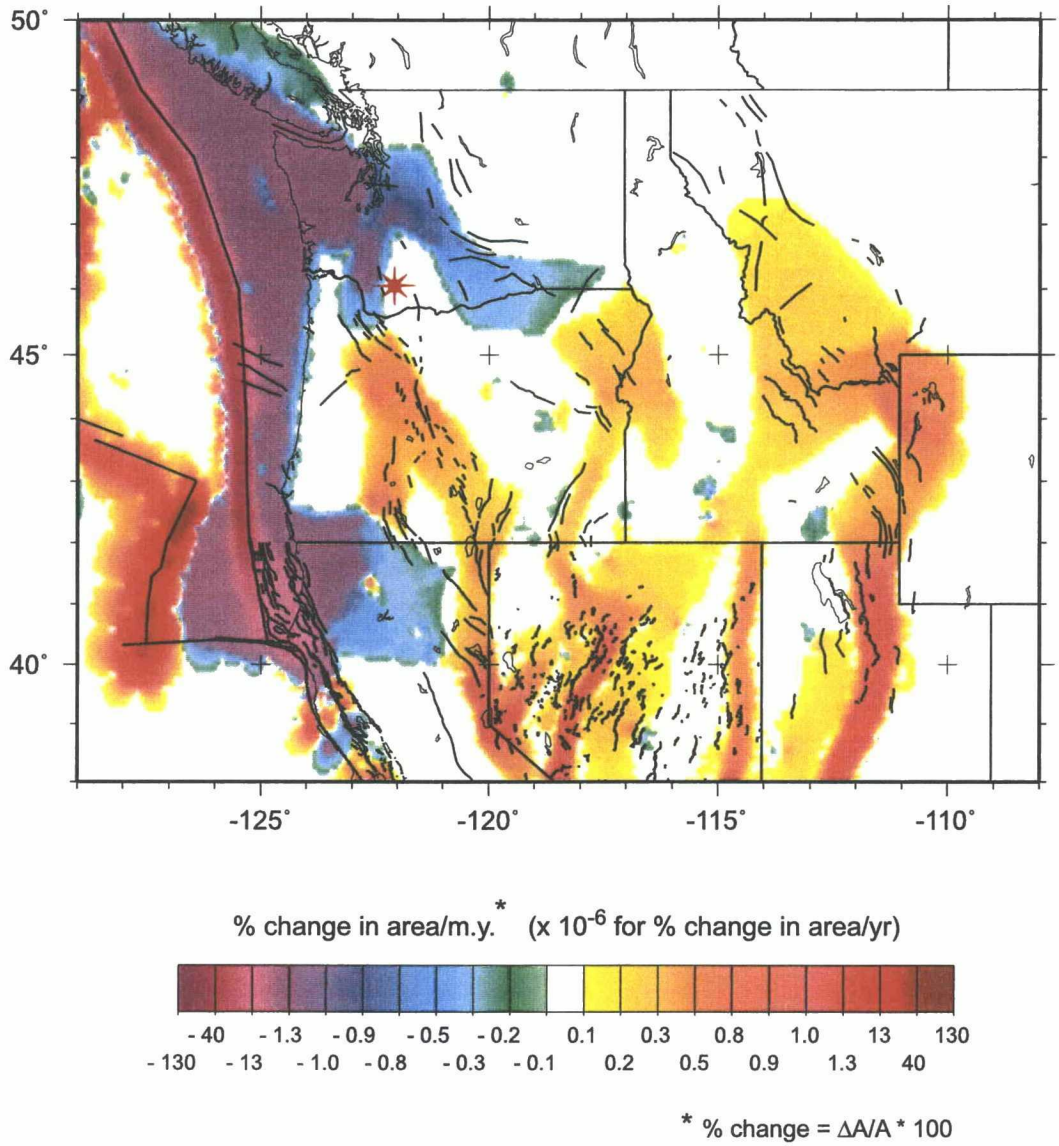

Figure 6 Isotropic strain map for the preferred model for Region 3, Pacific Northwest. Warm colors (red) indicate a gain in area (dilatation). Cool colors (purple) represent a loss of area (contraction). Strain values are log scaled. Largest values are along the Cascadia subduction zone, Gorda ridge, Klamath Mtns. and Olympic Mtns. Red star is the preferred Euler vector location for the Coast Range rotation.

Relatively large dilatational strains (up to 1%/m.y.) occur along the eastern margin of the northern Great Basin where deforming crust is moving away from the stable continental. In particular, these strains occur along the northern Wasatch front, the area immediately adjacent to the Yellowstone Plateau and area surrounding the SRP

The interior of the Great Basin primarily extends along relatively narrow, north-northeast-trending bands (Figure 6). The bands are separated by broad, crustal blocks that exhibit diffuse dilatation. The deformation zones span the Great Basin. The highest dilatational strain rates, located at the margins of the province, are the Wasatch front and Yellowstone Plateau to the east and the ECSZ and Modoc Plateau to the west. With the interior of the Great Basin deformation zones with lower rates include the CNSZ, Black Rock-Carson Sink zone and a zone of Holocene deformation in eastern Nevada that I will informally refer to as the Eastern Nevada deformation zone. Farther to the north, the central Oregon Cascades, back-arc and northern Basin and Range of eastern Oregon and western Idaho are actively extending but at lower strain rates (<0.2%/m.y) than observed to the south. The pattern of deformation is similar to that postulated by Pezzopane and Weldon (1993).

DISCUSSION

The Pacific Northwest region is an area of complex interaction between the transform margin shear, collapse-driven extension and subduction zone contraction. The transition from contraction- to dilatation-dominated domains can be abrupt (for example, in Figure 6 there is a rapid transition from extension in the Modoc Plateau, contraction in the Klamath Mountains and extension again in the southern Cascade region). Crustal motion in the region is strongly influenced by deformation in adjacent regions because flow tends to be directed toward the Pacific Northwest from elsewhere. In addition, the rates of deformation are largely variable, subduction zone-related strains may be four orders of magnitude greater than in the interior, and velocities may differ by more than two orders of magnitude.

REFERENCES

Anders, M. H., Geissman, J. W., Piety, L. A., and Sullivan, J. T., 1989, Parabolic distribution of curcumeastern Snake River Plain seismicity and latest Quaternary faulting: migratory pattern and association with the Yellowstone Hotspot: Journal of Geophysical Research, v. 94, no. b2, p. 1589-1621.

Argus, D. F., and Gordon, R. G., 1991, No-net-rotation model of current plate velocities incorporating plate motion model Nuvel-1: Geophysical Research Letters, v. 18, no. 11, p. 2039-2042.

Atwater, T., 1970, Implications of plate tectonics for the Cenozoic tectonic evolution of western North America: Geological Society of America Bulletin, v. 81, p. 3513-3536.

Atwater, T., 1989, Plate tectonic history of the northeast Pacific and western North America, *in* Winterer, E. L., Hussong, D. M., and Decker, R. W., eds., The Eastern Pacific Ocean and Hawaii: Boulder, Geological Society of America, p. 21-72.

Atwater, T., and Stock, J., 1998, Pacific-North America plate tectonics of the Neogene southwestern United States - an update, *in* Ernst, W. G., and Nelson, C. A., eds., Integrated Earth and Environmental Evolution of teh Southewestern United States: the Clarence A. Hall volume: Columbia, MD, Bellwether Publishers, p. 502.

Bott, J. D. J., and Wong, I. G., 1993, Historical earthquakes in and around Portland, Oregon: Oregon Geology, v. 55, no. 5, p. 116-122.

Dixon, T. H., Bursik, M., Kornreich Wolf, S., Heflin, M., Webb, F., Farina, F., and Robaudo, S., 1993, Constraints of deformation of the resurgent dome, Long Valley Caldera, California from space geodesy, *in* Smith, D. E., and Turcotte, D. L., eds., Contributions of Space Geodesy to Geodynamics: Crustal Dynamics: Washington, D.C., American Geophysical Union, p. 429.

Dixon, T. H., Robaudo, S., Lee, J., and Reheis, M. C., 1995, Constraints on present day Basin and Range deformation from space geodesy: Tectonics, v. 14, no. 4, p. 755-772.

Dragert, H., and Hyndman, R. D., 1995, Continuous GPS monitoring of elastic strain in the northern Cascadia subduction zone: Geophysical Research Letters, v. 22, no. 7, p. 755-758.

Dragert, H., Hyndman, R. D., Rogers, G. C., and Wang, K., 1994, Current deformation and width of the seismogenic zone of the northern Cascadia subduction zone: Journal of Geophysical Research, v. 99, p. 653-668.

Dumitru, T. A., Gans, P. B., Foster, D. A., and Miller, E. L., 1991, Refrigeration of the western Cordilleran lithosphere during Laramide shallow-angle subduction: Geology, v. 19, p. 1145-1148.

Geomatrix Consultants, 1995, Seismic Design Mapping, State of Oregon: for Oregon Department of Transportation, Proj. No. 2442.

Hamilton, W. B., 1988, Laramide crustal shortening, Geological Society of America, p. 27-39.

Hearn, E. H., and Humphreys, E. D., 1998, Kinematics of the southern Walker Lane Belt and motion of the Sierra Nevada block, California: Journal of Geophysical Research, v. 103, no. B11, p. 27,033-27,049.

Hooper, P. R., and Conrey, R. M., 1989a, A model for the tectonic setting of the Columbia River basalt eruptions, *in* Reidel, S. P., and Hooper, P. R., eds., Volcanism and tectonism in the Columbia River flood-basalt province: Boulder, Colorado, Geological Society of America.

Hooper, P. R., and Conrey, R. M., 1989b, The Olympic-Wallowa-lineament (OWL) as a Basin and Range-related megashear, and its control of magmatism during the eruption of the Columbia River basalts: Geological Society of America, Abstracts with Programs, v. 21, no. 5, p. 94.

Humphreys, E. D., 1995, Post-Laramide removal of the Farallon slab, western United States: Geology, v. 23, no. 11, p. 987-990.

Humphreys, E. D., and Weldon, R. J., II, 1994, Deformation across the western United States: A local estimate of Pacific-North America transform deformation: Journal of Geophysical Research, v. 99, no. B10, p. 19,975-20,010.

Jones, C., Unruh, J. R., and Sonder, L. J., 1996, The role of gravitational potential energy in active deformation in the southwestern United States: Nature, v. 381, p. 37-41.

Livaccari, R. F., 1991, Role of crustal thickening and extensional collapse in the tectonic evolution of the Sevier-Laramide orogeny, western United States: Geology, v. 19, p. 1104-1107.

Magill, J. R., Wells, R. E., Simpson, R. W., and Cox, A. V., 1982, Post 12 m.y. rotation of southwest Washington: Journal of Geophysical Research, v. 87, p. 3761-3776.

Mann, G. M., and Meyer, C. E., 1993, Late Cenozoic structure and correlations to seismicity along the Olympic-Wallowa lineament, northwest United States: Geological Society of America Bulletin, v. 105, p. 853-871.

Martinez, L. J., Meertens, C. M., and Smith, R. B., 1998, Rapid deformation rates along the Wasatch fault zone, Utah, from first GPS measurements with implications for earthquake hazard: Geophysical Research Letters, v. 25, no. 4, p. 567-570.

Minster, J. B., and Jordan, T. H., 1987, Vector constraints on the western U.S. deformation from space based geodesy, neotectonics, and plate motions: Journal of Geophysical Research, v. 92, p. 4798-4808.

Mitchell, C., Vincent, P., Weldon, R. J., II, and Richards, M. A., 1994, Present-day vertical deformation of the Cascadia margin, Pacific Northwest, United States: Journal of Geophysical Research, v. 99, no. B6, p. 12,257-12,277.

Pezzopane, S. K., 1993, Active Faults and Earthquake Ground Motions in Oregon [Ph.D. thesis]: University of Oregon, 208 p.

Pezzopane, S. K., and Weldon, R. J., II, 1993, Tectonic role of active faulting in central Oregon: Tectonics, v. 12, no. 5, p. 1140-1169.

Pierce, K. L., and Morgan, L. A., 1990, The track of the Yellowstone Hotspot: Volcanism, Faulting, and Uplift: U.S. Geological Survey Open-File Report, v. 90-415.

Savage, J. C., and Lisowski, M., 1991, Strain measurements and the potential for a great subduction earthquake off the coast of Washington: Science, v. 252, p. 101-103.

Severinghaus, J., and Atwater, T., 1990, Cenozoic geometry and thermal state of the subducting slabs beneath western North America, *in* Wernicke, B. P., ed., Basin and Range Extensional Tectonics Near the Latitude of Las Vegas, Nevada: Boulder, Colorado, p. 1-22.

Sloss, L. L., 1988, Tectonic evolution of the craton in Phanerozoic time, *in* Sloss, L. L., ed., Sedimentary Cover - North American Craton: Boulder, Colorado, Geological Society of America, p. 25-51.

Smith, R. B., and Braile, L. W., 1993, Topographic signature, space-time evolution, and physical properties of the Yellowstone-Snake River Plain volcanic system: the Yellowstone hotspot, *in* Snoke, A. W., Steidtmann, J. R., and Roberts, S. M., eds., Geology of Wyoming, Geological Survey of Wyoming, p. 694-754.

Thatcher, W., Foulger, G. R., Julian, B. R., Svarc, J., Quilty, E., and Bawden, G. W., 1999, Present day deformation across the Basin and Range province, western United States: Science, v. 283, p. 1714-1718.

Wang, K., He, J., and Davis, E. E., 1997, Transform push, oblique subduction resistance, and intraplate stress of the Juan de Fuca plate: Journal of Geophysical Research, v. 102, no. B1, p. 661-674.

Wang, K., Mulder, T., Rogers, G. C., and Hyndman, R. D., 1995, Case for very low

coupling stress on the Cascadia subduction fault: Journal of Geophysical Research, v. 100, p. 12,907-12,918.

Wells, R. E., and Heller, P. L., 1988, The relative contribution of accretion, shear, and extension to Cenozoic tectonic rotation in the Pacific Northwest: Geological Society of America Bulletin, v. 100, p. 325-338.

Wells, R. E., Weaver, C. S., and Blakely, R. J., 1998, Fore-arc migration in Cascadia and its neotectonic significance: Geology, v. 26, no. 8, p. 759-762.

Wiley, T. J., Sherrod, D. R., Keefer, D. K., Qamar, A., Schuster, R. L., Dewey, J. W., Mabey, M. A., Black, G. L., and Wells, R. E., 1993, Klamath Falls earthquakes, September 20, 1993,-including the strongest quake ever measured in Oregon: Oregon Geology, v. 55, no. 127-134.

Appendix 5

Late Quaternary Stratigraphy and Holocene Faulting Along the Eastern Margin of Steens Mountain, Southeastern Oregon

Mark A. Hemphill-Haley, URS Greiner Woodward-Clyde and University of Oregon, Eugene, Oregon
Gary A. Carver, Humboldt State University, Ret., Carver Geologic, Kodiac, Alaska
Bud Burke, Humboldt State University, Arcata, California

INTRODUCTION

Steens Mountain is an isolated, north-northeasterly trending mountain range, located in remote southeastern Oregon (Figure 1). It is 84.5 km (52 mi) south of the town of Burns and 31.5 km (19.5 mi) north of Denio Junction at the Nevada-Oregon border. It is an asymmetric, tilt-block with a gentle west slope and a steep eastern escarpment. The mountain has three geomorphic sections: the central or "High" Steens which reach an elevation of 2967m (9634 ft) flanked by the "Northern" Steens and the "Southern" Steens which reach elevations of only 2400 m (7792 ft). The escarpment adjacent to the High Steens is 1748 m (5733 ft) high. The Alvord Valley, lies to the east of Steens Mountain. The Pueblo Mountains continue south of the Southern Steens to just beyond the Oregon-Nevada border.

Steens Mountain and the Alvord Valley are in the northwestern-most part of the Basin and Range tectonic province. The 100-km-long Steens fault zone is comprised of a series of north- to northeast-trending normal faults that bound the eastern front of Steens Mountain and separates it from the Alvord Valley. Holocene faulting has occurred along much of the base of the High Steens.

Early research in the Steens Mountain-Alvord Valley area was reconnaissance in nature. I. C. Russell (1884, 1903), Davis (1905), Waring (1908), R. J. Russell (1928) Smith (1927) and Walker and Repenning (1965) provided generalized descriptions of the area. Fuller (1931), Wilkerson (1958), Fryeberger (1959), Gunn and Watkins (1970), and Minor et al. (1987 a, b) described the volcanic stratigraphy of Steens Mountain. Donath (1962) and Lawrence (1976) discussed the regional structure. Cleary et al. (1981 a, b) conducted gravity surveys in the Alvord Valley and discussed the geochemical properties of thermal springs located near the mountain range. Hemphill-Haley (1987) investigated the late Quaternary stratigraphy and active tectonic elements along the High Steens. David Lindberg (1999) mapped Quaternary stratigraphy and faulting on the east side of the Alvord Valley along the Tule Springs Rim and Mickey Basin as part of his Master's thesis at Humboldt State University.

A NERHP-funded investigation of the Alvord fault, the Holocene portion of the Steens fault zone that bounds the High Steens, included excavation of two trenches across the fault with

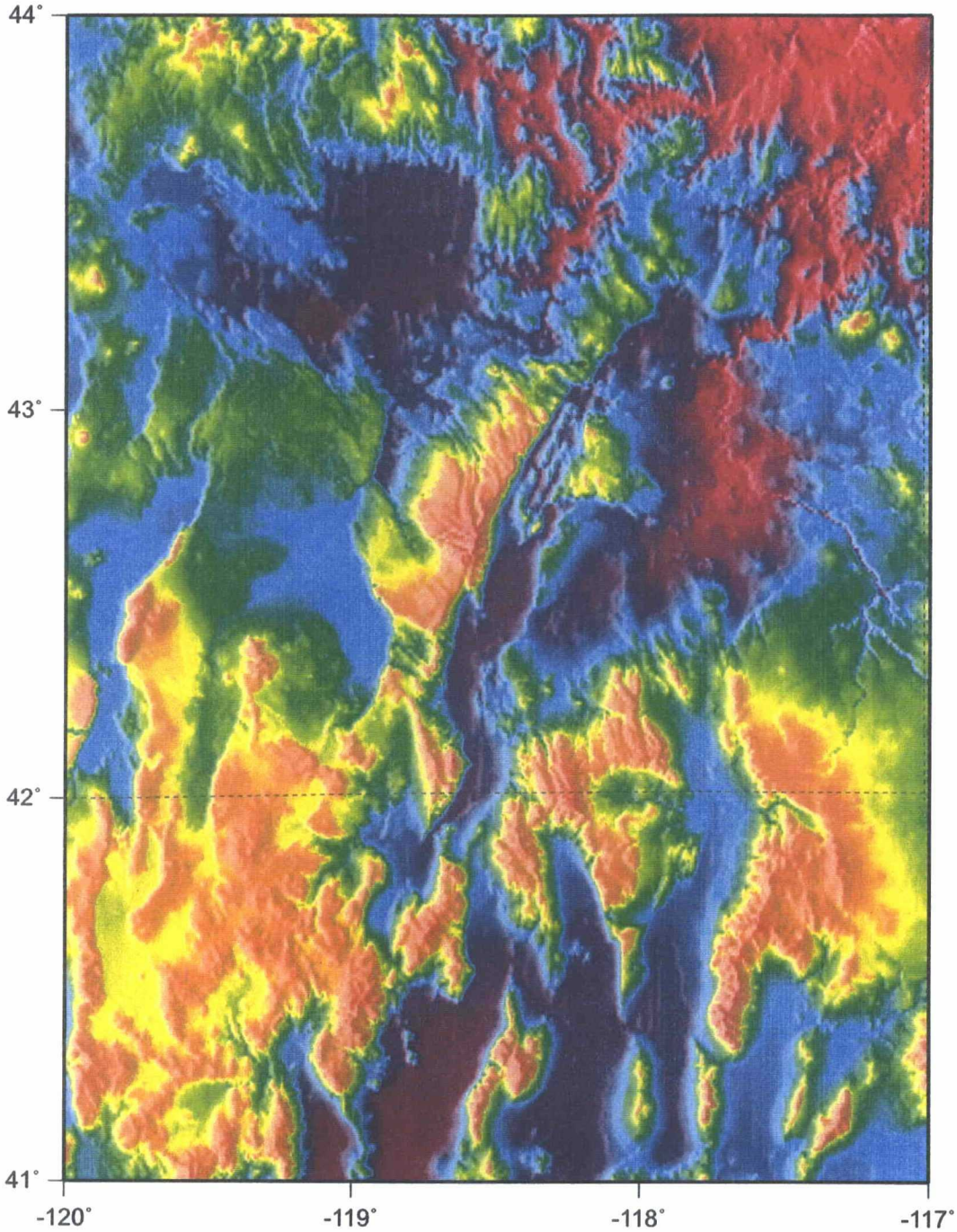

Figure 1 - Color shaded-relief map of southeastern Oregon and northern Nevada. The map is centered on the north-northeast-trending Alvord Valley and Steens Mountain.

the objective of collecting temporal and behavioral information. Additionally, low-sun-angle aerial photographs were flown along the length of the Steens and Pueblo Mountains and the eastern margin of the Alvord Valley along the Tule Springs Rims. The aerial photographs were used for geologic mapping and to site the exploratory trenches.

STRATIGRAPHY

TERTIARY ROCKS:

Steens Mountain is composed of a thick sequence of late Oligocene (?) and Miocene basaltic lava flows, pyroclastic deposits and sedimentary rocks (Minor et al., 1987 a, b, Davis, 1905). The summary description of the units along the eastern escarpment of Steens Mountain and presented below is taken primarily from Minor et al. (1987a, b).

The units exposed comprise several formations. The oldest is the late-Oligocene-(?) to early-Miocene-aged Alvord Creek Formation. It crops out along the lower slope of the escarpment north of the Alvord Ranch, and consists of easily erodable tuffaceous rock, opaline chert and conglomerate. It attains a maximum thickness of 300 m (984 ft). It is overlain by the early Miocene Pike Creek Formation which consists of rhyolitic to acidic flows, minor tuff, and tuffaceous sedimentary rock. The Pike Creek Formation is 600 m (1969 ft) thick several kilometers south of the Alvord Ranch and pinches out north of Little Alvord Creek. The middle-Miocene Steens Mountain volcanic sequence overlies the Pike Creek Formation and consists of andesitic flows, flow breccias and pyroclastic rocks. It attains its maximum thickness of 1350 m (4430 ft) north of Big Alvord Creek.

These rocks are unconformably overlain by late-Miocene-aged Steens Basalts. The Steens Basalts are a 1300-m-thick (4265 ft) series of olivine basalt flows with minor interbeds of tuff (Cleary et al., 1981 a, b). An upper flow of the Steens Basalts has a K-Ar age estimate of 15.5 Ma and a lower flow has an age estimate of 21.9 Ma (Gunn and Watkins, 1970).

The Steens Basalts underlie and form the gently westerly inclined dip-slope of Steens Mountain. The same basalts form the upper, precipitous crest of the eastern escarpment. They also are believed to underlie the Alvord Valley some 305 m (1000 ft) below the valley floor (Cleary et al., 1981 a, b).

The late-Miocene-aged Devine Canyon Tuff, a member of the Danforth Formation, overlies the Steens Basalts with a minor unconformity. They crop out as erosional remnants along the lower and middle parts of the western dip-slope of Steens Mountain (Bentley, 1970). The Devine Canyon ash flow tuff member of the Danforth Formation has a K-Ar age of 9.3 Ma.

QUATERNARY DEPOSITS

Steens Mountain has been subjected to at least two periods of glaciation that are late Quaternary (probably Wisconsin) in age. Deep glacial valleys are found along the north, south and western slopes, while small cirques are situated on the eastern side of the mountain crest (Lund and Bentley, 1976, Bentley, 1970). Small remnants of glacial deposits occur near the mountain crest and on the western slopes of Steens Mountain.

The Alvord Valley, a 13-km-wide (8 mi-wide) graben, is filled with alluvial and lacustrine sediments. Lake shorelines and lacustrine deposits at the surface attest to the presence of at least two late Pleistocene pluvial lakes in the valley that were up to 100 m (325 ft) deep. These lakes drained east into Coyote Lake Valley through the Tule Springs Rims at Big Sand Gap (Figure 2 (see Figure 2-10 from Road Log)). The outlet formed when the rising waters in Lake Alvord overtopped a gentle "sag" in the rim. Down-cutting by the waters that rapidly drained the upper part of the lake carved Big Sand Gap. The "top" of the eroded gap would be at an elevation of approximately 1310 m (4298 ft) and is correlated with the elevation of the highest shoreline on the west side of the Alvord Valley. The base of the gap, at an elevation of about 1280 m (4200 ft), lies approximately 55 m (180 ft) above the present valley floor and is correlated with the intermediate-aged shoreline. Correlation of elevations across the valley is approximate; it does not account for tectonic deformation or possible post-pluvial rebound.

Along the west side of the Alvord Valley, at least three separate late Quaternary-aged lacustrine and alluvial sequences are exposed. The older two are deposits of two late Pleistocene-aged pluvial lakes; younger deposits are latest Holocene. The summary description of these deposits presented below is modified from Hemphill-Haley (1987).

Older Lacustrine Deposits:

The oldest lacustrine deposits in the area are exposed south of Indian Creek along the lower flank of Steens Mountain between 1310 m (4298 ft) and 1280 m (4200 ft) (Figure 3 (see Figure 2-7A from Road Log)). They consist of well-developed beds of silty-sand and medium to coarse-grained sand and gravel. Individual beds are nearly horizontal in most locations, up to 4 cm (1.5 in) thick, and commonly exhibit cross-bedding. An associated, poorly preserved shoreline occurs at 1310 m (4298 ft).

A degraded, arcuate barrier bar, situated about 4.5 km (2.8 mi) south of the mouth of Wildhorse Canyon, is associated with these deposits (Figure 3 (see Figure 2-7A from Road Log)). The bar is 0.7 to 1.0 km (0.4 to 0.6 mi) wide at an elevation just slightly above 1280 m (4200 ft), and is about 14 m (46 ft) above the surrounding lake deposits. The deposits in the bar consist of moderately- to well-stratified, poorly- to moderately-sorted alternating light gray sand, silt and reddish-yellow gravel. Bedding dips to a maximum of 30° to the northeast. Gravel and coarse sand beds are moderately-to well-cemented by calcium carbonate while finer-grained sand and silt beds are poorly-indurated. This barrier bar has relatively low relief, rounded crests, and slope angles of less than 5°. Wildhorse Creek has

cut a broad channel 300 m (984 ft) wide and 9 m (30 ft) deep through the bar. The channel banks have slopes of less than 5°.

The older lake stand, associated with the older lake deposits, is marked by a poorly-defined wave-cut bench. The bench cross-cuts bedding in the Steens Basalts south of Tuffy Creek and along Alvord Point at an elevation of about 1310 m (4298 ft). This approximately corresponds to the elevation of the top of the incised part of Big Sand Gap. Faint recessional shorelines occur down to 1280 m (4200 ft).

Older Alluvial Fan Deposits:

Older alluvial fan remnants occur as the topographically highest fan deposits along the eastern margin of the range-front immediately north of Indian Creek and south of Pike Creek (Figure 3 (see Figure 2-7A from Road Log)). These fan deposits are poorly-sorted, moderately-stratified, and matrix-supported. The materials are angular to sub-angular volcanic sand and gravel. Clasts range up to 2 m (6.5 ft) in diameter. They are moderately-cemented by calcium carbonate and illuvial clays. The fan surfaces are subdued and rounded. Landslide deposits overlie the fans near Pike Creek. The distal portion of the fan at Indian Creek (Figure 3 (see Figure 2-7A from Road Log)) has been modified by wave erosion and is overlain up to an elevation of 1280 m (4200 ft) by intermediate-aged lake deposits.

Intermediate-aged Lacustrine Deposits

Intermediate-aged lake deposits are exposed south of Tuffy Creek below a prominent shoreline cut into the older lacustrine deposits at about 1280 m (4200 ft). They consist of medium- to light-brownish-gray silt to medium- and coarse-grained sand and gravel, grading to fine sand, silt and clay away from the range-front. Bedding is well-developed and beds dip up to 4°; beds thin toward the interior of the basin ranging from 10 cm (4 inches) to less than 1 cm (0.4 in) thick.

Barrier bars associated with intermediate-aged lake deposits are elongate, arcuate or straight mounds, up to 500 m (1640 ft) wide and 3 km (1.9 mi) long. They occur near the mouths of major creeks, such as Big Alvord, Cottonwood, and Pike Creeks, and in the narrows of the northern Alvord Valley. Deposits in the bars are well-stratified, moderately-sorted, light- to medium-gray sand, silt and gravel. Cross bedding dips 40° to 54°, generally to the northwest. Coarse-grained beds are slightly-cemented by calcium carbonate while finer-grained sand beds are poorly-indurated. Maximum heights of the bars relative to adjacent lake deposits vary from 3 m (10 ft) near the range-front in the northern part of the valley to 18 m (59 ft) at locations away from the range-front. The tops of these bars form roughly continuous, nearly planar surfaces at an elevation of 1280 m (4200 ft). The flanks of the bars slope toward the Alvord Valley up to 18°. Where they have been incised by streams, the channels have slopes up to 20°.

Intermediate-aged Alluvial Fans Deposits

Intermediate-aged alluvial fans occur along the eastern escarpment of Steens Mountain (Figure 3 (see Figure 2-7A from Road Log)). From Alvord Point to Tuffy Creek the fans are small. However, northward along the base of the High Steens, the fans are larger and extend farther from the range-front. The deposits consist of light yellowish-red to yellowish-gray poorly-sorted sand and gravel. Sub-angular to sub-rounded clasts range up to boulders that are 5 m (16 ft) diameter and litter the fan surface. A silty-sand matrix-supported texture predominates near fan apexes; a clast-supported texture is more common in the distal portions of the fans.

The fans are moderately dissected. North of Pike Creek the intermediate-aged alluvial fans overlap and partially bury intermediate-aged barrier bar and lake deposits (Figure 3 (see Figure 2-7A from Road Log)).

Younger Alluvial Deposits

Younger alluvial fan and channel deposits are found as active channels and fan lobes. They consist of yellowish-gray to gray, poorly-sorted sand and gravel. Sub-angular to sub-rounded clasts range up to small boulders in size. A clast-supported matrix is characteristic of these deposits which are generally unweathered and non-indurated.

Younger Lacustrine Deposits

Recent, unconsolidated sediments consisting of light-gray coarse sand and gravel have been deposited along the beaches associated with the "present", very low lake levels. Sediments from the playa are light-brown to light-gray, fine silt and clay.

Dune Deposits

Sand dune fields covering areas up to 6 km^2 (2.3 mi^2) occur along the southern margin of the present Alvord dry lake; large individual concentric dunes are also found in the eastern part of the valley. The dunes consist of coarse- to medium-grained light-brown unconsolidated sand that generally overlie the intermediate-aged lake deposits.

Dunes also occur in the Catlow Valley on the western side of Steens Mountain. Mehringer and Wigand (1986) evaluated Indian artifacts associated with the dunes. Radiocarbon ages from the dunes indicate that they stabilized at about 7200 ka.. Assuming similar climatic and physical conditions have occurred in the nearby Alvord Valley, the dunes there probably stabilized at the same time.

PLUVIAL CHRONOLOGY

No radiocarbon or other absolute age dates have been obtained from pluvial Lake Alvord or alluvial fan deposits in the Alvord Valley. Age estimates of the lake deposits are based on our analysis of the stratigraphic and geomorphic relationships within the Alvord Valley and

assumed correlations to other pluvial lakes in the Great Basin where dates have been obtained.

Benson (1981, 1978), Scott (1983), and Thompson et al. (1986) present evidence that, within the Great Basin, levels of the two largest pluvial lakes, Lake Lahontan in western Nevada and Lake Bonneville in western Utah, rose and fell in a generally synchronous manner [*I realize that these do not represent the most recent research on these lakes and look forward to getting updated*]. This indicates that climatic and hydrologic regimes have been generally similar across the width of the Great Basin. The physical characteristics of individual basins, however, have controlled the magnitude of lake levels.

We make the assumption that the chronology of the rising and falling of pluvial Lake Alvord is similar to that of the other pluvial lakes (Figure 4 (see Figure 2-6 from Road Log)). Moreover, because one of pluvial Lake Lahontan's northernmost arms lay about 25 km (15 mi) south of pluvial Lake Alvord in the Denio area (Figure 1), the behavior of pluvial Lake Alvord is correlated to the documented late Pleistocene pluvial history of Lake Lahontan.

Benson (1981, 1978), Davis (1983), and Thompson et al. (1986) report that Lake Lahontan was at an intermediate and probably rising stage of pluviation between about 24 to 16 ka based on tephrochronology and radiocarbon dates. During this period, pluvial Lake Alvord was probably also rising.

The age of the spillover event of Lake Alvord into the Coyote Lake basin through Big Sand Gap is equivocal. It may have happened in the latter part of the most recent major pluviation. Conversely, carbonate development in soils formed on gravel bar surfaces above 1280 m (4200 ft) may indicate an older period of time (early Pinedale?) for formation and stabilization of gravel bars at about 1310 m (4280 ft). The down-cutting event may have occurred at that time and subsequent pluvial stands were pinned to the lower elevation.

Following spillover, the lake probably declined rapidly almost 30 m (100 ft) to about 1280 m (4200 ft) elevation. This is analogous to the rapid decline of pluvial Lake Bonneville following the catastrophic overflow at Red Rock Pass, which prevented development of recessional shorelines between the high Bonneville and lower Provo shorelines (Scott et al., 1983). Similarly, only very faint recessional beach features occur in the Alvord Valley between the 1310 m (4298 ft) and 1280 m (4200 ft) shorelines.

In the Lahontan basin, the period from 16 to 12 ka is associated with the highest stand of the lake (Thompson et al., 1986). Although climatic conditions necessary for a high lake stand would also have presumably existed in the Alvord Basin, the outlet through Big Sand Gap prevented a further rise in lake level. Continuing the correlation with Lake Lahontan, Lake Alvord, which had been maintained at 1280 m (4200 ft) for some time, began to recede rapidly as climatic conditions changed, starting at about 12.5 ka; the lake probably almost completely disappeared by 10 ka.

The Alvord Desert (dry lake) has been partially inundated by water during historic times. A lake formed in 1982; by 1985 the lake was about 1 m (3.3 ft) deep and covered 337 square

km (130 square mi) of the valley floor. Several long-time valley residents reported the 1985 stand as the highest level of the lake in 90 years. This increase in lake level since 1982 coincided with similar high-stands of other lakes in the Basin and Range Province including the Great Salt Lake, Mono Lake, and Warner Lakes. By 1987 the Alvord lake had again dried up.

Interestingly, during wet winters, a small lake commonly will form within a small portion of the playa. Local ranchers tell that during windy spells (they are common here), especially when the wind shifts, the small lake has been known to migrate across the playa. I would love to see this happen.

LATE QUATERNARY TECTONICS

REGIONAL SETTING

Although Wallace (1984) showed that the northwest portion of the Basin and Range province, including southeastern Oregon, had surface faulting within the last 500,000 yrs, it had been regarded as an area of tectonic quiescence during late Quaternary time (Wilkerson, 1958; Thenhaus and Wentworth, 1982). The research of Hemphill-Haley (1987) and Hemphill-Haley et al. (1989) provided the first substantial evidence for Holocene faulting in Oregon. Since that time numerous active faults have been documented locally (e.g., Lindberg, 1999) and elsewhere in the state (Pezzopane, 1994).

The SFZ is located in the northernmost Basin and Range province in a region of transition toward the relatively unfaulted Columbia River plateau to the north and west. Two primary fault trends are found in the northern Basin and Range of Oregon: northwest-trending relatively discontinuous faults and north-northeast-trending faults that form the largest range-bounding structures. Several northwest-trending regional zones of diffuse faulting are also found that traverse Oregon (Lawrence, 1976). Lawerence (1976) proposed that these structures may be dominantly right-slip structures resulting from diminished extension associated with the northern termination of the Basin and Range. One of these structures, the Brothers fault zone (Figure 5), extends from near Newberry Volcano on the east side of the Oregon Cascades and appears to terminate at or near Steens Mountain (Lawerence, 1976). The Brothers Fault zone also lies within the Newberry volcanic trend, a zone of northwest-progressing acidic volcanism that closely mirrors the Yellowstone trend of volcanism.

The Brothers fault zone may actually coincide with the location of transition between the High Steens from the Southern Steens As mapped by Hemphill-Haley (1987) faults that may be associated with the Brothers fault zone show no indication of lateral displacement and do not extend east of the SFZ into the Alvord Valley. A complex zone of faults of various orientations, including nortwest-trends, occurs at the right-step in the Steens Mountain range-front at the transition from the High Steens to Southern Steens (Figure 3 (see Figure 2-6 from Road Log)). This location also coincides with mapped projection of the Brothers fault zone.

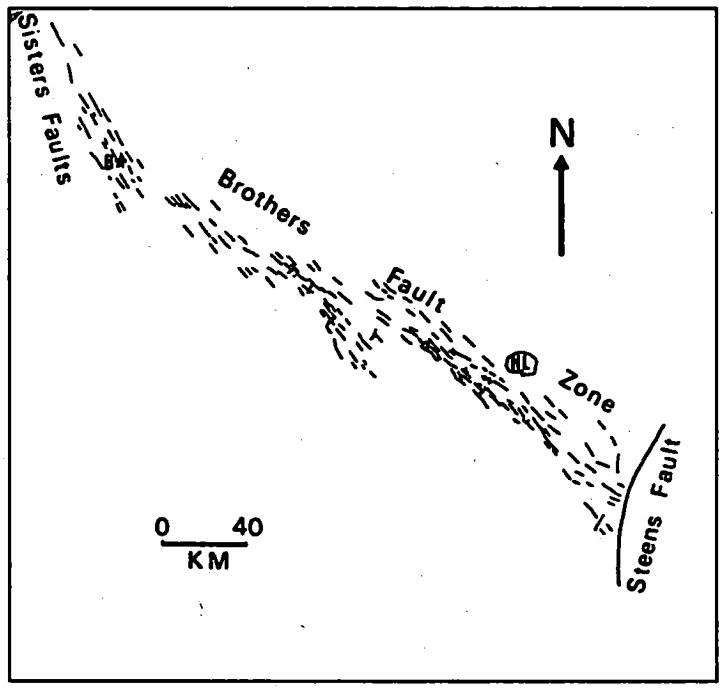

Figure 5 The Brothers fault zone (BFZ) from Lawerence (1976). The fault zone consists of numerous discontinuous tonal lineaments and faults that extend from about Newberry Volcano on the eastern side of the Oregon Cascades to Steens Mountain in southeastern Oregon. Sense of displacement along the BFZ has been speculated to be dextral-normal. This has not been confirmed on the ground.

Pezzopane (1994) and Pezzopane and Weldon (1994) include the Steens fault zone in the eastern Oregon fault zone. They included the zone as a possible branch of the northward extension of the Eastern California shear zone. This is not in conflict with ideas proposed by Wallace (1984) that describes separate extensional tectonic regions in the Basin and Range separated by the Central Nevada seismic zone. Steens Mountain is located near the Black Rock-Carson Sink (BRCS) zone of extension of northwestern Nevada. The BRCS zone terminates to the northeast at the Oregon-Nevada lineament and to the southwest at the Walker Lane. Wallace (1984) shows the northwestern boundary as a finger-shaped zone of denser faulting and also describes faults within the BCSZ that have had Holocene surface rupture. Holocene faulting with the Steens fault zone may be linked to the northwestern boundary of the BRCS zone.

Regional, kinematic, finite element modeling suggests that the northern Basin and Range consists of large, blocks separated by relatively narrow but continuous zones of extension that also accommodate rotation (Hemphill-Haley, 1999). The Steens fault zone is likely linked with the BRCS zone. The Steens Mountain and Pueblo Mountain block may be rotating clockwise at about 0.5°/my (Hemphill-Haley, 1999). The northern end of the block is "pinned" against the accreted terrain of the Blue Mountains while the southern end rotates. Kinematically this satisfies the decreased amount of extension that we observe toward the northern part of the fault zone.

SEISMICITY

Seismic activity in Steens Mountain and the Alvord Valley has been historically low. No instrumentally-located epicenters have been reported. However, Alvord Valley residents near Borax Springs reported a small swarm of tremors in 1918, but shaking was not felt in Fields, 11 km (6.9 mi) to the south; a significant increase in discharge was reported to have occurred at Borax Springs at that time (Cleary et al., 1981 a, b). As in other areas of the Basin and Range, lack of seismicity does not preclude fault activity. Instead, long recurrence intervals on the order of 10^3 to 10^4 years is most likely (Wallace, 1984). It is interesting to note that even the typical "back-ground" seismicity of small < M2 events characteristic of much of the central Basin and Range is largely absent in the Oregon Basin and Range (Figure 6).

The nearest significant historic seismic activity to Steens Mountain was an earthquake swarm in the Warner Valley, 135 km (84 mi) to the west in 1968 (Couch and Johnson, 1969). The largest event (M 5.1) was followed by twelve smaller earthquakes (M> 4.0) within four days. First motions on eight of the events were west-side-down along a north-south trending normal fault, and two events were strike-slip with a preferred northwest-trending nodal plane (Couch and Johnson, 1969).

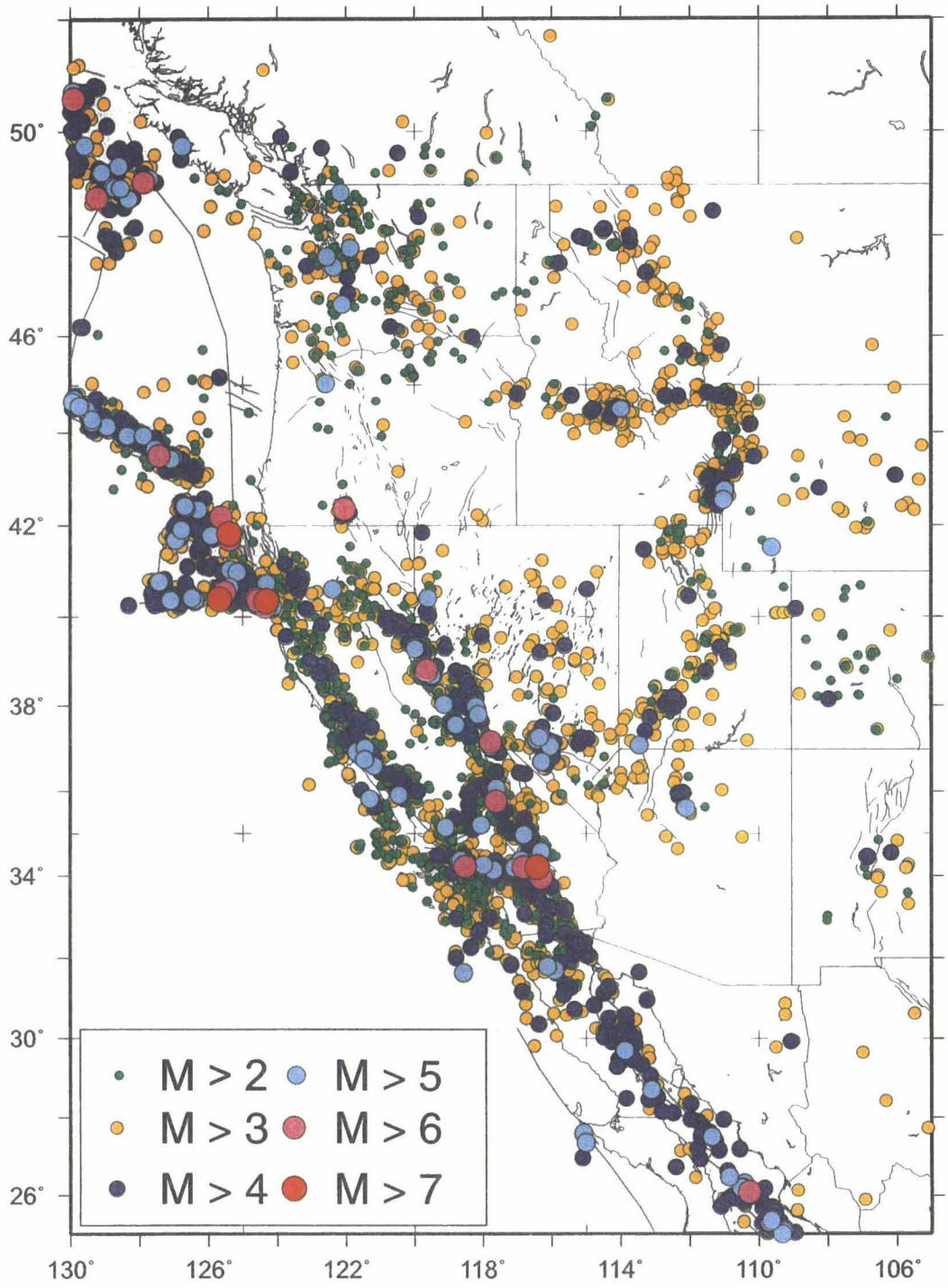

Figure 6 Earthquakes in western North America 1989-1998, M2 to M7. Epicentral data from Iris Data Management Center. Note the paucity of events in southeastern Oregon and northern Nevada.

STEENS FAULT ZONE

The eastern front of Steens Mountain is a rugged, steep escarpment that rises 1748 m (5735 ft) above the Alvord Valley over a horizontal distance of 8 km (5 mi). Erosion by small east-flowing creeks has formed precipitous canyons along the escarpment. Stream gradients are steep with numerous waterfalls and boulder runs resulting from differential erosion. Along the lower elevations of the escarpment, particularly north of Tuffy Creek, numerous large landslides ranging up to 2 km (1.2 mi) long and 0.5 km (0.3 mi) wide, originate in the tuffaceous sediments of the Alvord Creek Formation. No work has been done to see if coseismic shaking has induced any of the landsliding along the escarpment.

The presence of a significant tectonic structure was described by Cleary et al. (1981a, b) in a report of the geothermal characteristics of several of the local hot springs. Cleary et al. (1981a, b) attributed a large, linear gravity low near Alvord Hot Springs to a major fault along the eastern range-front. The geochemistry of the geothermal water suggests meteoric waters percolate through the volcanic rocks of Steens Mountain, are heated at depth by an elevated geothermal gradient and then are recirculated along the fault zone (Cleary et al., 1981a, b).

Long Term Slip Rate

Gravity measurements by Cleary et al. (1981 a, b) indicate that the Steens Basalts lie at a depth of about 1000 m (3281 ft) below the playa surface in the western Alvord Valley adjacent to the High Steens. Hence, about 1000 m (3280 ft) of late Cenozoic volcanic, alluvial and lake sediments fill the western Alvord basin. When this amount of valley fill is added to the 1748 m (5735 ft) elevation difference between mountain crest and valley floor, a total of 2750 m (9022 ft) of apparent vertical displacement has occurred. If uplift initiated near the time of deposition of the Devine Canyon tuff (9.3 Ma), then the minimum long-term, average vertical rate has been approximately 0.3 mm/yr, the horizontal rate is 0.2 mm/yr and slip rate on the fault is about 0.35 mm/yr. If the erosion surface on the western slope of the Steens Basalts is projected eastward to intersect with the projection of an approximately 60° dipping fault, the actual displacement may be about 3150 m (10,335 ft) and the vertical rate may increase to a maximum of about 0.33 mm/yr and the slip rate on the fault may increase to 0.4 mm/yr. This is about average for Basin and Range faults.

Segmentation

One objective of this study was to characterize the physical nature of the Steens fault zone, primarily by interpretation of low-sun-angle aerial photographs flown along the 100 km (60 mile) length of zone. The presence or absence of surface scarps and their morphological differences were noted as a qualitative method of assessing relative age. This analysis indicates that the Steens fault zone may be comprised of rupture segments that different Quaternary displacement. As a result of this reconnaissance-level evaluation, we divide the SFZ into 5 segments based on both structural and apparent temporal differences (Figure 7). Please be aware that very little field-truthing of these photo interpretations has been conducted. From north to south the segments are:

1) Mann Lake segment, ~ 32 km long (20 mi),
2) Alvord segment, ~ 27 km long (17 mi),
3) Fields segment, ~ 22 km long (14 mi),
4) Tumtum segment, ~ 10 km long (6 mi), and
5) Denio segment, longer than 19 km (12 mi) .

The Mann Lake segment forms the range-front escarpment along the Northern Steens. We have not found a late Quaternary fault scarp along the range-front. However, late Quaternary scarps may be present along the eastern side of the narrow valley. The southern end of the segment approximately coincides with an apparent right-step of Holocene faulting toward the eastern side of Mickey Butte (Lindberg, 1999). The Mann Lake segment (also referred to as Crowley segment by Pezzopane (1994)) can be traced from north of Big Alvord Creek to the northern closure of the Alvord basin.

The Alvord segment extends from Big Alvord Creek south for a distance of almost 27 km (17 mi) along the base of the High Steens. It continues southward where it crosses the Alvord Desert and eventually "dies out" within the playa. This segment contains the youngest appearing fault scarps within the SFZ. The northern 16 km (10 mi) of this segment is generally a single trace. The southern portion of the segment, however, branches into several splays that bound the salients of Serrano and Alvord Points. Between Alvord Point and Wildhorse Canyon other smaller faults of similar age to the Alvord fault occur; many of these trend north-south, but several others trend either northwest or northeast. The geomorphic expression of the most recent scarps is similar, suggesting that the entire length of the segment ruptured at or nearly at the same time. This segment was trenched and results are discussed under the section on the Alvord fault.

The Fields segment is located west of and overlaps the southern Alvord segment. It is located along the eastern escarpment of the Southern Steens. It begins at the mouth of Wildhorse Valley at a right-step in the range-front and continues south for a distance of about 22 km (13.7 mi). It "dies out" in the Alvord Desert playa just east of the settlement of Fields. The segment appears to have an older, eroded range-bounding scarp and a youthful appearing fault scarp within the alluvial and playa sediments to the east of the range-front. The northern end of the younger scarp is about 10 km (6 mi) south of the northern end of the older scarp which is in the Wildhorse Valley. The younger scarp diverges from the range-front and trends south-southwest into the Alvord Desert. The older, range-front escarpment is morphologically similar to the scarp of the Mann Lake segment and probably represents an equivalent long period of quiescence. The younger, eastern splay appears to be morphologically only slightly older than the scarps of the Alvord segment.

The Tumtum segment begins directly south of Fields and extends for about 10 km (6 mi) along the range-front west of Tumtum Lake, southeastward to the promontory of Pueblo Mountain. An older, nearly continuous, moderately-eroded scarp lies along the range-front almost continuously for the length of the segment. A younger, discontinuous, slightly eroded scarp, lies slightly east of the range-front. The older scarp does not appear to displace recent alluvial fans but is morphologically younger appearing than the scarps of the northern Fields

Figure 7 Preliminary map of possible rupture segments of the Steens fault zone. Segments are based on apparent differences in scarp morphology from low-sun-angle aerial photography analysis.

and the Mann Lake segments. The younger scarp displaces younger alluvial fans and intermediate (?) aged lacustrine beach bars. Geomorphically it appears to be slightly older than the younger fault of the Fields segment. The northern part of the Tumtum segment overlaps the northern Fields segment for a short distance along a right-step.

The Denio segment lies to the south of the Tumtum segment. The northern portion of the segment appears somewhat older than the youngest scarp of the Tumtum segment. It probably runs along the length of the southern Pueblo Mountains for a distance of at least 19 km (11.8 mi). The relative age of this segment was not assessed based on the lack of data.

The geomorphic expression of the five segments identified during this study (Figure 7) indicate that the SFZ has had several faulting events in late Quaternary time:

- The Alvord segment appears to have ruptured most recently (it also coincides with the highest portion of Steens Mountain).

- The Fields segment contains scarps that are of a similar but possibly slightly older age than those of the Alvord segment. The presence of relatively old scarps that lie directly adjacent to the range-front, but that are to the west and northwest of the younger scarps suggests that more recent surface ruptures have been occurring valley-ward of the range-front and appear to be cutting off the large embayment in the Steens Mountain at Wildhorse Valley.

- The northernmost portion of the Fields segment is overlapped by the recent Alvord fault to the east suggesting a migration of surface rupture toward the east.

- The Tumtum segment represents a zone of rupture that s apparently older than the Alvord and Fields segments.

- The Mann Lake segment and northernmost Fields segments appear to be relatively old and may not have ruptured in late Quaternary time.

Alvord Fault

Our field investigations of the Alvord fault focused on estimating the ages of the most recent faulting on this segment of the SFZ because it has the youngest appearing fault scarps. The Alvord fault parallels the eastern range-front of Steens Mountain. The trend varies from N18°W to N12°E; the average is N01°W. It is expressed on the surface as an east-facing scarp with a maximum height of 2.5 m (8.2 ft).

The southern end of the fault lies in the Alvord playa where it branches and forms a fault zone up to 700 m (2297 ft) wide. In the playa the fault displaces intermediate-aged lacustrine and eolian deposits (Figure 3 (see Figure 2-7A from Road Log)). Along the valley floor, crests of the scarp are sharp and show no sign of wave modification. Thus, the scarp post-dates the most recent high stand of Lake Alvord (ca. 16-12 ka; lake dry at ca. 10 ka). Numerous springs occur along the base of the scarp.

Farther north, the Alvord fault displaces intermediate-aged lake deposits and the shoreline associated with these deposits at 1280 m (4200 ft) elevation (Figure 8 (see Figure 2-14 from Road Log)). West of the fault Tertiary volcanic rocks have been uplifted and back-tilted to the west, forming a prominent spur, informally called Black Dog Spur.

Northward for a distance of about 7 km (4.3 mi) along the eastern flank of Alvord Point the fault displaces intermediate-aged lacustrine and alluvial fan deposits (Figure 3 (see Figure 2-7A from Road Log)). Geomorphic evidence of vertical offset of the fan deposits includes: 1) channel incision above the fault resulting in abandonment of the older fan surface; 2) perched stream terraces above the scarp; and 3) deposition of alluvial fan cones below the scarp. Locally along this section springs characteristically form marshy, thickly vegetated areas along the base of the scarp.

The northern part of the Alvord fault bounds the base of the highest portion of Steens Mountain, the High Steens. In this section, the fault displaces large alluvial fans at the base of the mountain. Immediately north of Tuffy Creek, the Alvord Hot Springs flow from the base of the fault onto the playa (Figure 3 (see Figure 2-7A from Road Log)).

Approximately 400 m (1312 ft) north of the Alvord Hot Springs, the Alvord fault forms two splays: on the east a low, barely perceptible scarp trends northeast into the valley and becomes concealed in the grass covered, marshy distal fan and lake deposits; on the west a distinct east-facing scarp trends northwest toward the range-front. Along the western splay, approximately 600 m (1968 ft) north of the hot springs, the fault displaces the older alluvial fan sediments of Indian Creek. A well-preserved graben exists along the length of the fault within this unit. Preservation of this feature provides evidence for the recency of faulting; coseismic graben are generally filled by sedimentation and masked from the surface in less than a few thousand years elsewhere in the Great Basin. The persistence of the graben at this location is probably due to differences in erodibility of the faulted materials; moderately to well-indurated coarse sands and gravels of the older alluvial fan deposits are more resistant to erosion than are the non-indurated silts, clays and sands of the lacustrine deposits where little or no graben exists. This western splay of the fault begins to form the bedrock colluvial/alluvial contact immediately north of Pike Creek (Figure 3 (see Figure 2-7A from Road Log)). The fault can be traced north of Big Alvord Creek. North of the creek the fault moves into bedrock and landslide deposits.

TRENCH INVESTIGATIONS OF THE ALVORD FAULT

Two trenches, the "Bath House" trench and the "Dust Bowl" trench (Figure 9 (see Figure 2-3 from Road Log)), were excavated across the Alvord fault to expose faulted Quaternary deposits and to assess the character of the fault. Information gathered from these exposures was then used to further describe temporal and behavioral characteristics of the fault.

BATH HOUSE TRENCH

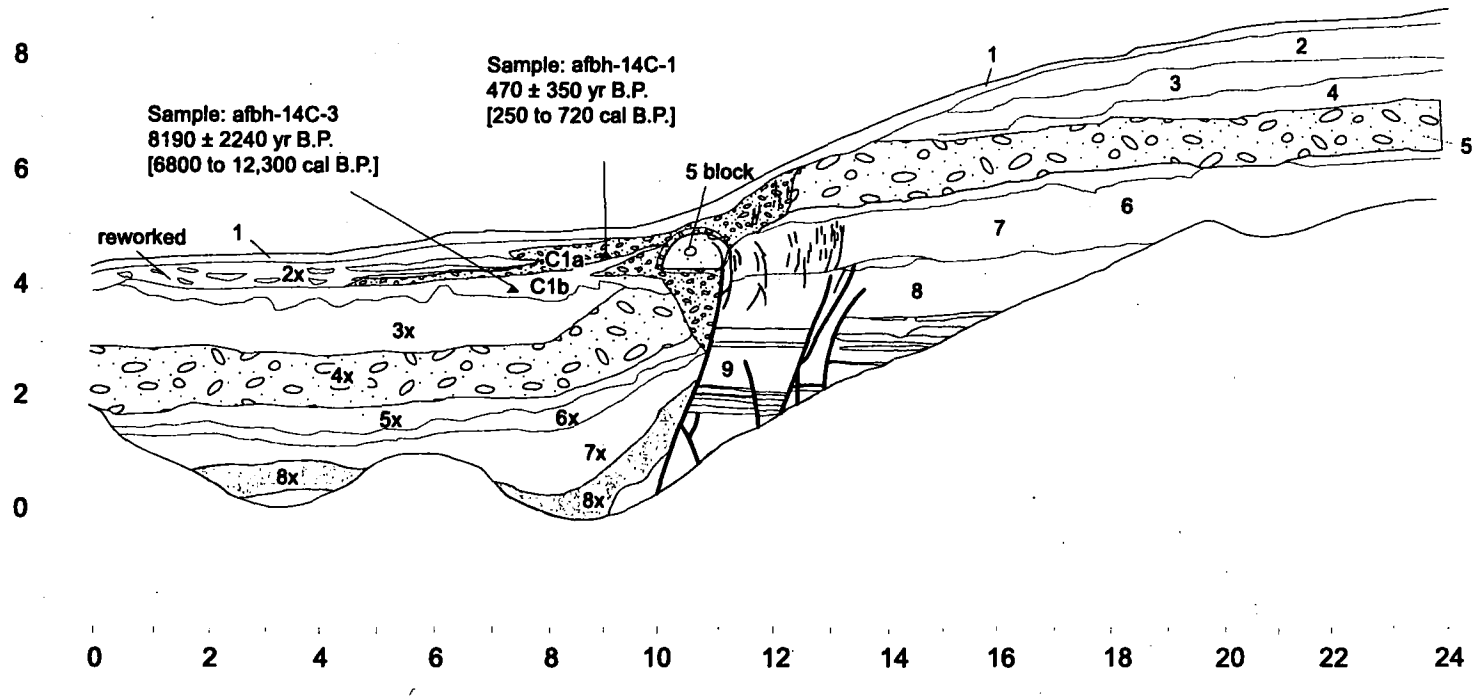

LEGEND

C1	Most recent faulting event colluvia	1	Surface colluvium		Contact
	Distinctive debris flow (units 5 and 4x)	2-9	Footwall units		Fracture
9	Lacustrine deposits (9)	2x-8x	Hangingwall units		Fault
				▲	Location of charcoal sample

Figure 10 Log of the Bath House trench.

BATH HOUSE TRENCH

The northernmost trench, referred to as the Bath House trench because of its proximity to Alvord Hot Springs, was excavated in displaced intermediate-aged lacustrine and intermediate-aged alluvial deposits (Figure 9 (see Figure 2-3 from Road Log)).

Stratigraphy

The trench exposes faulted alluvial and lacustrine deposits (Figure 10). Up to 2 m (6.5 ft) of interbedded lake deposits consisting of sand, silt, clay and thin diatomite beds occur near the bottom of the trench (unit 9). These sediments are overlain by more than 4 m (13 ft) of coarse-grained debris flow deposits (units 2-8). Within this series of debris flow deposits a particularly distinctive debris flow (unit 5) is exposed in the footwall at a depth of about 1 m (3 ft). This coarse-grained debris flow is supported by a sandy clay matrix that contains sufficient amount of pedogenic $CaCO_3$ to give the unit a distinctive whitish cast and to make it relatively resistant. The debris flow deposits are overlain by a 0.5m (1.6 ft) thick loess and colluvium deposit (unit 1).

Materials on the eastern, hanging-wall, side of the fault, consist chiefly of debris flow deposits, fine-grained lacustrine (?) sediments and scarp-derived tectonic colluvium. Unit 4x clearly correlates to the distinctive whitish-colored debris flow (unit 5) across the fault and provides an excellent marker for estimating amount of offset.

The upper 1 m (3 ft) of the eastern portion of the trench is comprised of inter-tonguing alluvial, lacustrine and colluvial sediments that were deposited at the base of the fault scarp. Unit C1 is a scarp-derived colluvium. It has a wedge-shaped morphology that thickens toward the fault. Most of unit C1 is a relatively coarse-grained, proximal facies wedge. Much of the distal facies of the wedge (unit C1a) appears to be inter-bedded with lacustrine sand and silt. The lower part of the colluvium (C1b) consists of silty pebbly colluvium that is 25 cm (10 in) thick. Analysis of a small piece of charcoal collected from near the base of this deposit provides a C_{14} age of 8,190 ± 2,240 years B.P. (6,800 to 12,300 cal B.P. using CALIB from Stuiver and Reimer, 1993) The upper part of the colluvial deposit (unit C1a) consists of inter-bedded, thin lacustrine and colluvial sediments 65 cm (2 ft) thick. Analysis of a small piece of charcoal collected from near the middle of these deposits provides a C_{14} age of 470 ± 350 years B.P. (250 to 720 cal B.P.).

These ages may provide some insight into the age of faulting. The approximately 7 to 12 ka cal B.P. age for the basal colluvium may be an approximate age for the most recent event (MRE). However, caution must be exercised when using what is most likely detrital charcoal as it is a maximum limiting age for the event. Scarp morphology and degradation analysis (later section) suggest that this event is likely considerably younger than the apparent charcoal age. Likewise, the considerably younger age (250 - 720 cal B.P.) in the upper, reworked part of the unit is a minimum limiting age for the event. The charcoal could have been deposited well after the scarp was formed. Additionally, both charcoal samples were extremely small and difficult to analyze.

Soils developed on the scarp and nearby alluvial deposits were described in detail and evaluated to help estimate the age of the the most recent faulting at the trench. Results suggest that the soils in the scarp are younger than late Pleistocene.

Faulting Events

The fault, in the trench, is a high-angle normal fault that dips ~72° to the east. It consists of several strands in a zone about 2 m (6.5 ft) wide and occurs near the base of the prominent surface scarp. The measured height of the surface scarp is 2.5 m (8 ft).

A single, unequivocal surface rupture event is interpreted from the trench exposure. Using units 5 and 4x to measure offset, a total apparent vertical displacement of 2 m (6.6 ft) and associated warping of 1.5 m (5 ft) accounts for a total apparent overall vertical displacement of 3.5 m (11.5 ft). Fissure fill sediments were deposited in an opening in the upper part of the fault during or immediately after the event. Shortly after the earthquake, the fault scarp began to collapse and erode. A large block (marked 5 block) of unit 5 fell upon the infilling colluvium. Pedogenic structures within the block indicate rotation of about 90°. The space vacated by the block was filled by colluvium. Eventually the colluvium buried the block.

An additional, equivocal faulting event may be interpreted from the trench. At the base of the hanging-wall exposure, an undulatory debris flow deposit (unit 9x) is exposed. The deposit is folded against the fault at a higher angle than the distinctive debris flow unit. In addition, the folding of the unit predates the deposition of overlying deposits. Also, where the fault displaces older alluvial fan deposits (map unit Qaf_1) a few hundred meters to the north of the trench, a slightly bevelled low-angle upper scarp slope is evident above the steep lower scarp. This low-angle scarp may have formed as the result of the previous faulting event and was subsequently extensively eroded..

DUST BOWL TRENCH

The southernmost trench (Figure 9 (see Figure 2-3 from Road Log)) was located in the relatively flat sand dune and playa complex about 3.2 km (2 mi) south of Alvord Point At this location, the Alvord fault displaces unconsolidated sand dune and intermediate-aged lake deposits (Qsd and Qld_2 respectively). The Dust Bowl trench (Figure 11) was 18 m (59 ft) long and 2 m (6.6 ft) deep, the depth to groundwater.

Stratigraphy

The deposits exposed in the trench consist chiefly of lacustrine silt, sand and clay beds with lesser dune sand. None of these deposits could be correlated across the fault. On the west side of the fault lacustrine deposits, units3 - 14, are the oldest deposits exposed. Unit 2 unconformably overlies these lower deposits.

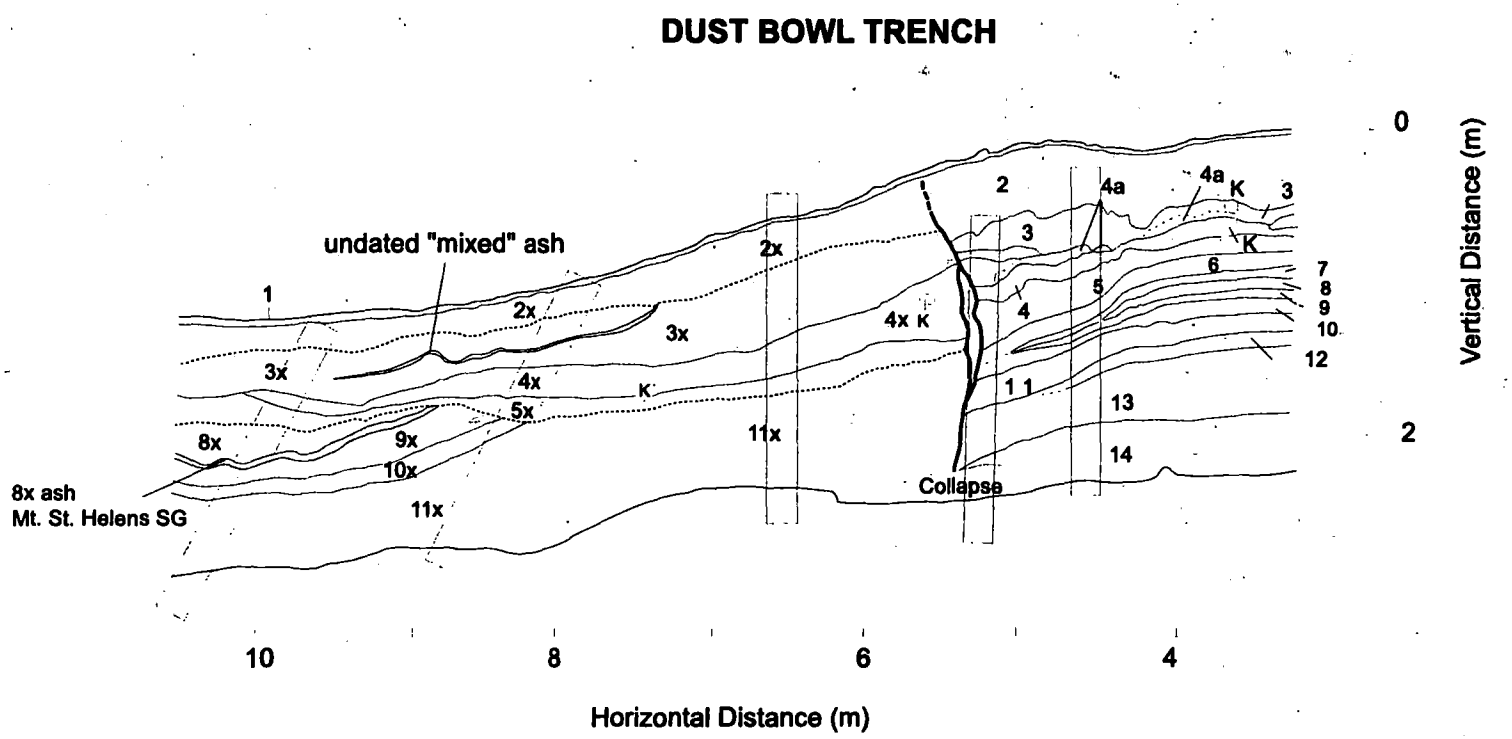

LEGEND

2-14	Units logged on the west side of the fault		Contact
2x - 11 x	Units logged on the east side of the fault		Fault
	There was no correlation of units across the fault		Tectonic ? Unconformity
	Unit 8x ash is Mt. St. Helens SG ash		Tephra
	(11,900 ± 300 yr B.P. - 13,100 ± 350 yr B.P.)		

Figure 11 - log of a portion of the Dust Bowl trench

On the east side of the fault three lacustrine "packages" are separated by two unconformities. The oldest lacustrine units (6x (off log) to 10x) contain a tephra deposit that is several centimeters thick (Ash 8x). Analysis of this tephra (SMP-WC-E8) by Andre Sarna-Wojcicki, of the U.S. Geological Survey, indicates that it is Mt. St. Helens ash SG. Radiocarbon ages established for this ash range between 13,100 ± 350 to 11,900 ± 300 years B.P. These older lacustrine deposits are folded in an open syncline. Lacustrine deposits, units 3x - 5x unconformably overly this lower group of sediments and truncate Ash 8x. Unit 3x contains a tephra (Ash 3x) that is a mixture of several ashes. This tephra unit (SMP-WC-E3) could not be correlated with any documented ashes. Units 3x - 5x are also gently folded and are, in turn, unconformably overlain by lacustrine unit 2x. Soil development on the surface of this deposits is poor indicating a relatively young age, clearly Holocene, for this scarp.

Faulting Events

The Alvord fault in the Dust Bowl trench is a nearly vertical single fault that forms a narrow zone of deformation less than 0.5 m (2 ft) wide. The sense of displacement on the fault is not readily discernable. The surface scarp suggests a significant component of down-to-the-east displacement. However, thickness changes across the fault, the nearly vertical fault dip, and lack of clearly definable scarp-derived colluvia prevent us from dismissing a lateral component of slip.

We interpret three faulting events from the Dust Bowl trench exposure. Two deformation events are evident within the deposits on the eastern side of the fault where two unconformities clearly truncate deformed lake beds and tephras (Figure 11). Individual displacement events are separated by periods of erosion causing truncation of beds and folds. The MRE is represented by the fault which nearly reaches the surface and the surface scarp. Displacement values could not be estimated because of erosion and the inability to correlate units across the fault.

The Mount St. Helens SG tephra (ash 8x) was faulted and folded during the oldest exposed event. Thus, the event occurred less than 11,900 to 13,000 years B.P. This event was followed by a period of erosion, probably during a stand of Lake Alvord, that truncated units 6x through 10x, and then deposited lacustrine units 3x - 5x.

During the penultimate event, lacustrine deposits up to 3x were faulted and folded. Erosion then truncated a portion of unit 3x and unit 2x was deposited.

The MRE formed the surface scarp. Vertical displacement of at least 1.1 m (3.6 ft) occurred during this rupture as measured from the scarp height. Of this amount warped sediments account for about 70 cm (2.3 ft) of deformation, and faulting accounts for about 40 cm (1.3 ft).

The Dust Bowl trench records more events and apparently less displacement per event on the southern part of the Alvord fault than is evident in the Bath House trench, about 11 km (7 mi) to the north. The reduced amount of displacement may be due to diminished displacement along the southern end of the Alvord fault as it dies out in the Alvord Desert. The multiple

exposed events may reflect an older stratigraphic sequence preserved in the Dust Bowl trench. This may be due, in part, to lower sedimentation rates in the playa than at the range-front. Additionally, the additional events may also reflect a more complex faulting history on this part of the Alvord fault due to the proximity to and overlap with the nearby Fields segment to the east.

SCARP DEGRADATION ANALYSIS

Geomorphic analysis of the eroded scarp of the Alvord fault provides additional evidence of the fault's recent history and an approximation of the age of the MRE. Twenty five profiles of the central and northern parts of Alvord fault were measured following the procedures outlined by Wallace (1977), Bucknam and Anderson (1979) and Hanks et al. (1984). Representative scarp profiles are shown in Figure12. Table 1 provides results from a recent re-analysis of degradation of the scarp using the highly illuminating paper by Hanks (1998). In that analysis we evaluated 7 "bagged" scarps. Younger scarp ages (0.75 – 2.3 ka) are estimated for the lowest elevation scarps (near the Bath House trench site). The higher elevation scarps (also located within the older, more consolidated fan deposits) have ages ranging from 3.7 to 6.8 ka. We suspect that some post-seismic reworking of the lower elevation scarps may be largely responsible for this difference.

Additionally, as stated earlier, the scarp appears to be the result of two faulting events. The penultimate event may be represented by a faint bevel Nonetheless it appears that the scarp data and trench-derived ages are consistent and allude to at least one Holocene event on this part of the Steens fault zone.

The lack of a substantially larger, compound scarp in the older fan deposits than in the younger fan and lacustrine deposits less than 1 km (0.6 mi) away suggests that the recurrence time for faulting events may be on the order of tens of thousands of years; an estimate not unlike elsewhere in the Basin and Range.

ACKNOWLEDGEMENTS

Hemphill-Haley's M.S. thesis research was funded, in part, with generous grants from The Mazamas, Sigma-Xi,, The Northwest Scientific Association and Woodward-Clyde Consultants. A later program of investigation was funded by a U.S. Geological Survey National-Earthquake-Hazard-Reduction-Program grant (Number 14-08-0001-G1333).
We are grateful to the residents of the Alvord Valley who allowed us to work on the Mann Lake, Wildhorse, and Serrano Point Ranches. Much of this research was conducted on the Alvord Ranch. Without the generosity of Ed and Loni Davis, and their sons Paul, Mike and Frank, little of the work reported here would have been accomplished.

We also thank several researchers from the U. S. Geological Survey who helped the project: Robert Wallace and David Schwartz for their review, comments and ideas. Hemphill-Haley specifically thanks Tom Hanks for advice regarding scarp degradation analysis and for always reminding me about "the paper". Andre Sarna-Wojcicki identified tephras found in trenches. We were assisted in the mapping of the trenches and measuring the scarp profiles by David Lindberg, Gary Simpson, Gilbert Craven, all of whom were students at Humboldt State University and Jim Hengesh of Idaho State University.

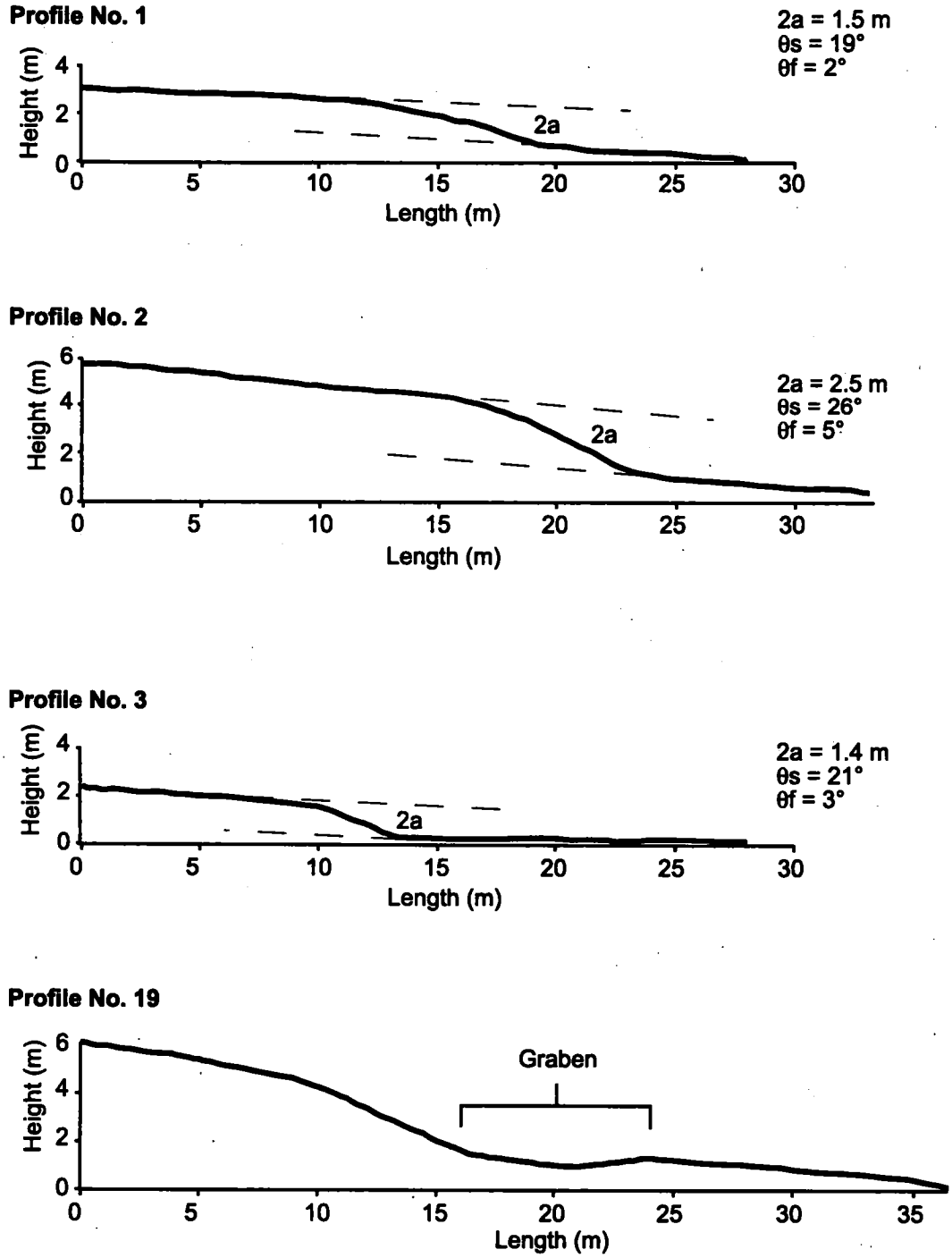

Figure 12 Representative scarp profiles along the Alvord fault (from Hemphill-Haley, 1987). In all, 25 profiles were measured of fault and shoreline scarps. The first three profiles shown here were measured near the location of the Bath House trench. The final profile (No. 19) was measured ~ 800 m north of the trench site. The presence of a graben, while attesting to the young age of the scarp, prohibits degradation analysis.

Profile #	2a (m)	θs	θf	θr (assumed)	tan θs	tan θf	Reduced Scarp (tan θs - tan θf)	α-b	t'	κ (m^2/ka)	a (m)	t (yrs)
1	1.5	19	2	35	0.344	0.035	0.309	0.665	2.9	1.1	0.75	1500
2	2.5	26	5	35	0.488	0.087	0.401	0.613	1.6	1.1	1.25	2300
3	1.4	21	3	35	0.384	0.05	0.334	0.65	1.7	1.1	0.7	750
10	2.5	21	8	35	0.384	0.141	0.243	0.559	4.8	1.1	1.25	6800
11	2.2	20	7	35	0.364	0.123	0.241	0.577	4.9	1.1	1.1	5400
13	1.8	17	7	35	0.306	0.123	0.183	0.577	9.5	1.1	0.9	6800
16	1.7	18	5	35	0.325	0.087	0.238	0.613	5.6	1.1	0.85	3700

Appendix 5 - Table1: Results of degradational analyses following methods in Hanks (1998).

REFERENCES

Benson, L. V., 1978, Fluctuation in the level of pluvial lake Lahontan during the last 40,000 years: Quaternary Research, v. 9, 300-318.

Benson, L. V., 1981, Paleoclimatic significance of lake-level fluctuations in the Lahontan Basin: Quaternary Research, v. 16, p. 390-403.

Bentley, E. B., 1970, The glacial geomorphology of Steens Mountains, Oregon: unpublished Masters thesis, University of Oregon, 98 p.

Bucknam, R. C. and Anderson, R. E. 1979, Estimation of fault scarp ages from a scarp-height slope-angle relationship: Geology, v. 7, p. 11-14.

Cleary, J., Lange, I. M., Qamar, I. A., and Krouse, H. R., 1981a, Gravity isotope and geochemical study of the Alvord Valley geothermal area, Oregon: Summary, Geological Society of America Bulletin, Part 1, v. 92, p. 322-329.

Cleary, J., Lange, I. M., Qamar, A. I., and Krouse, H. R., 1981b, Gravity, isotope, and geochmical study of the Alvord Valley geothermal area, Oregon: Geological Society of America Bulletin, Part II, v. 92, p. 934-962.

Couch, R., and Johnson, S., 1968, The Warner Valley earthquake sequence; May and June, 1968: The Ore Bin, v. 30, no. 10, p. 191-204.

Davis, J. O., 1983, Level of Lake Lahontan during deposition of the Trego Hot Springs tephra about 23,400 years ago: Quaternary Research, v. 19, p. 312-324.

Davis, W., 1905, The mountain ranges of the Great Basin: Bulletin of the Campus Museum, 7001, Harvard, v. XLII, p. 164-172.

Donath, F. A., 1962, Analysis of Basin-Range structure, south-central Oregon: Geological Society of America Bulletin, v. 73, p. 1-16.

Fryeberger, J. S., 1959, The geology of Steens Mountain, Oregon: unpublished Masters thesis, University of Oregon, 65 p.

Fuller, R. E., 1931, The geomorphology and volcanic sequence of Steens Mountain in southeastern Oregon: University of Washington Publications in Geology, v. 3, no. 1, 130 p.

Gunn, B. M. and Watkins, N. D., 1970, Geochemistry of the Steens Mountain basalts, Oregon: Geological Society of America Bulletin, v. 81, p. 1497-1516.

Hanks, T. C., 1998, The age of scarplike landforms from diffusion-equation analysis, *in* Sowers, J. M., Noller, J.S., Lettis, W.R., ed., Dating and Earthquakes: Review of Quaternary Geochronology and Its Application to Paleoseismology, Nucliear Regulatory Commission, p. 497-535.

Hanks, T. C., Bucknam, R. C., Lajoie, K. R., and Wallace, R. E., 1984, Modification of wave-cut and faulting-controlled landforms: Journal of Geophysical Research, v. 89, no. 137, p. 5771-5790.

Hemphill-Haley, M. A., 1999, Multi-scaled Analyses of Contemporary Crustal Deformation of North America [Ph.D. thesis]: University of Oregon.

Hemphill-Haley, M. A., 1987, Quaternary stratigraphy and late Holocene faulting along the base of the eastern escarpment of Steens Mountain, southeastern Oregon: Master's thesis, Humboldt State University, 87 p.

Hemphill-Haley, M. A., Page, W. D., Burke, R., and Carver, G. A., 1989, Holocene Activity of the Alvord Fault, Steens Mountain, Southeastern Oregon: Woodward-Clyde Consultants,, U.S. Geological Survey Grant No. 14-08-0001-G1333.

Lawrence, R. D., 1976, Strike-slip faulting terminates the Basin and Range province in Oregon: Geological Society of America Bulletin, v. 87, p. 846-850.

Lindberg, D. N., 1999, Quaternary stratigraphy and tectonics of the eastern Alvord Desert, Harney County Oregon. Masters thesis, Humboldt State University, Arcata.

Lund, E. H. and Bentley, E., 1976, Steens Mountain, Oregon: The Ore Bin, v. 38, No. 4, p. 51-66.

Mehringer, Jr. P. J., and Wigand, P.E., 1986, Holocene history of Skull Creek dunes, Catlow Valley, Oregon, U.S.A.: Journal of Arid Environments, v. 11, no.2, p. 117-138.

Minor, S. A., J. J. Rytuba, C. A. Goeldner, and K. J. Tegtmeyer, 1987a, Geologic map of the Alvord Hot Springs quadrangle, Harney County, Oregon: U.S. Geological Survey, Washington, D.C.

Minor, S. A., Rytuba, J. J., van der Meulen, D. B., Grubensky, M. J., and Tegtmeyer, K. J., 1987b, Geologic map of the Wildhorse Lake quadrangle, Harney County, Oregon: U.S. Geological Survey, Washington, D.C.

Nash, D. B., 1980, Morphologic dating of degraded normal fault scarps: Journal of Geology, v. 88, p. 353-360.

Pezzopane, S. K., 1993, Active Faults and Earthquake Ground Motions in Oregon [Ph.D. thesis]: University of Oregon, 208 p.

Pezzopane, S. K., and Weldon, R. J., II, 1993, Tectonic role of active faulting in central Oregon: Tectonics, v. 12, no. 5, p. 1140-1169.

Russell, I. C., 1884, A geological reconnaissance in southern Oregon: U.S. Geological Survey, Fourth Annual Report, no. 435-465.

Russell, I. C., 1903, Notes on the geology of southwestern Idaho and southeastern Oregon: U.S. Geological Survey Bulletin, no. 217, 83 p.

Russell, R. J., 1928, Basin Range structure and stratigraphy of the Warner Range northwestern California: University of California Publications, Bulletin of the Department of Science, v. XVII, p. 427.

Scott, W. E., McCoy, W. D., Shroba P. R., and Rubin, M., 1983, Reinterpretation of the exposed record of the last two cycles of Lake Bonneville, western United States: Quaternary Research v. 20, p. 261-285.

Smith, W. D., 1927, Contribution to the geology of southeastern Oregon (Steens and Pueblo Mountains): Journal of Geology, v. 35, p. 421-440.

Stuiver, M., and Reimer, P. J., 1993, Extended ^{14}C database and revised CALIB radiocarbon calibration program: Radiocarbon, v. 35, p. 215-230.

Thenhaus, P. C. and Wentworth, C. M., 1982, Map showing zones of similar ages of surface faulting and estimated maximum earthquake size in the Basin and Range province and selected adjacent areas: U.S. Geological Survey Open-File Report, no. 82-742.

Thompson, R. S., Benson, L. V., and Hattori, E. M., 1986, a revised chronology for the last Pleistocene lake cycle in the central Lahontan Basin: Quaternary Research, v. 25, p. 1-9.

Walker, G. W. and Repenning, C. A., 1965, Reconnaissance geologic map of the Adel quadrangle, Lake, Harney and Malheur Counties, Oregon: U.S. Geological Survey Miscellaneous Geologic Investigations Map I-446.

Wallace, R. E., 1977, Profiles and ages of young fault scarps, north-central Nevada: Geological Society of America Bulletin, v. 88, p. 1267-1281.

Wallace, R. E., 1984, Patterns and timing late Quaternary faulting in the Great Basin province and relation to some regional tectonic features: Journal of Geophysical Research, v. 89, p. 5763-5769.

Waring, G. A., 1908, Geology and water resources of a portion of southeastern Oregon: U. S. Geological Survey Water-Supply Paper, no. 220, 86 p.

Wilkerson, W. L., 1958, The geology of a portion of the southern Steens and Pueblo mountains, southeastern Oregon: U.S. Geological Survey Bulletin, no. 995-B, p. 19-77.

APPENDIX 6

FRIENDS OF THE PLEISTOCENE 1999 FIELDTRIP-- REGIONAL TECTONIC SETTING AND FAULT STUDIES IN QUINN RIVER VALLEY AND SURROUNDING REGIONS, OREGON AND NEVADA

Silvio Pezzopane*

Lakewood Colorado

FOP'99 Very Regional Tectonic Setting

Early kinematicians [e.g., Wise, 1963; Hamilton and Myers, 1966; Atwater, 1970] recognized that motion between the Pacific and North American plates in the western United States is broadly distributed across a diffuse zone between the western continental shelf and the eastern front of the Basin and Range Province (Figure A6-1). Geologic and geodetic studies later revealed that 3 to 4 centimeters per year (cm/yr), of the overall 5 cm/yr of relative motion between these plates, was accommodated as slip along the San Andreas fault system; most of the remainder of the motion was distributed inboard of the San Andreas along the western edge of the Basin and Range Province, in the Mojave Desert, and east of the Sierra Nevada [e.g., Weldon and Humphreys, 1986; Minster and Jordan, 1987; DeMets et al., 1987; Argus and Gordon, 1991; Richard, 1992]. Early studies of fault slip in the Basin and Range Province recognized these regional zones of right-lateral and extensional faulting in California and Nevada [e.g., Wise, 1963; Shawe, 1965; Stewart et al., 1968], yet the kinematic connection to plate boundary slip was not clear. Numerous surface-rupturing earthquakes within the past 125 years have rejuvenated many of the normal and strike-slip fault scarps along this zone [e.g., Wallace, 1984], marking a northward trend that projects into southern Oregon.

In 1988, I began a comprehensive compilation of published studies about earthquakes and faulting in Oregon and surrounding areas as part of my doctoral dissertation with Dr. Ray Weldon at the University of Oregon. Published geologic maps [e.g., Walker, 1977; Tolan and Reidel, 1989; Walker and MacLeod, 1991] showed few young faults in Oregon, so I used available mapping with aerial photography of various scales to identify faults that appear to offset or deform young geological deposits. Geological field investigations mainly in southern and central Oregon revealed numerous faults that commonly displace late Pleistocene and Holocene lacustrine, alluvial, and colluvial deposits and locally cut late Pleistocene volcanic and pyroclastic units [Pezzopane, 1993].

*also employed at the US Geological Survey, Denver.

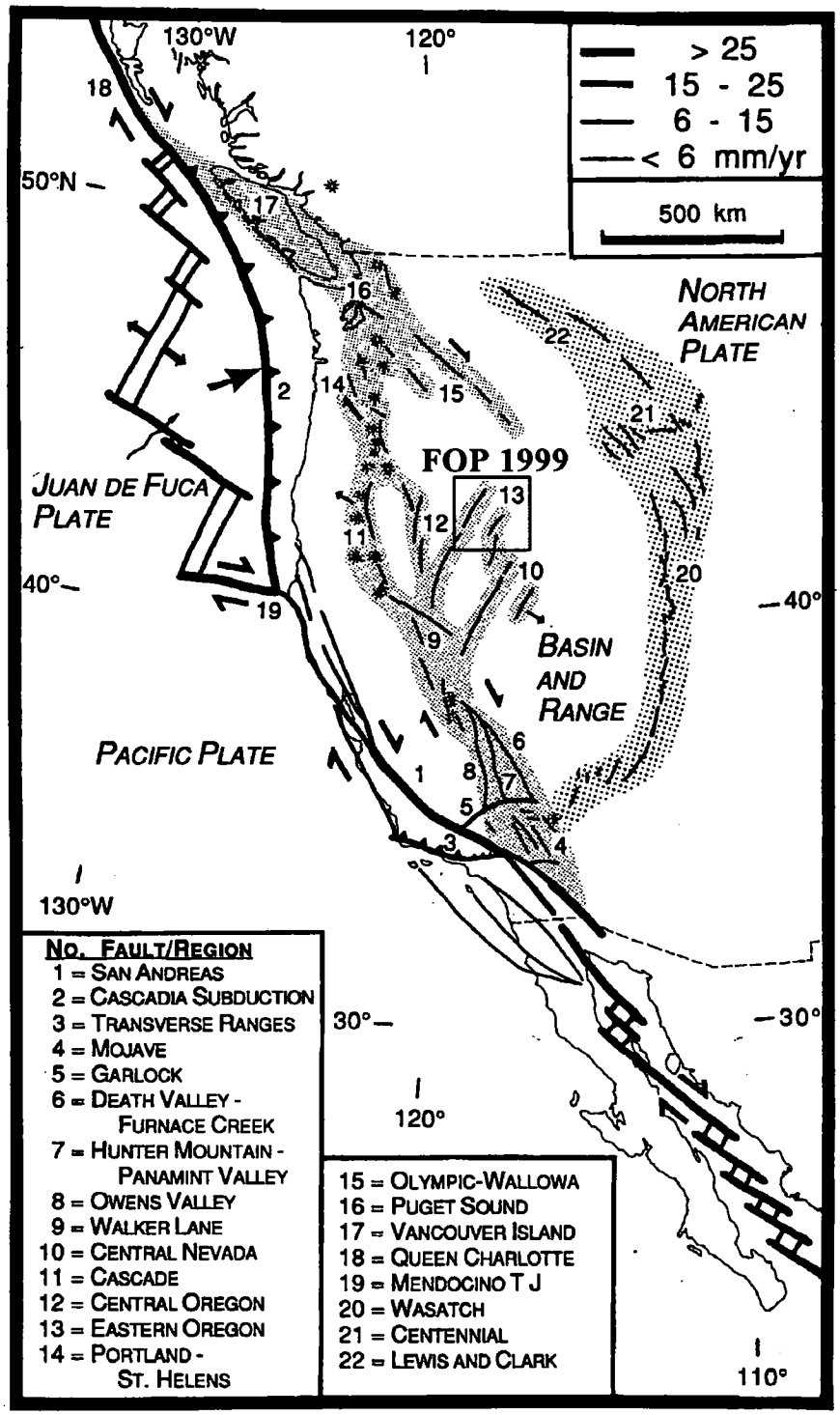

FIGURE A6-1. Map of Pacific, North America, and Juan de Fuca plate boundaries, and recognized active fault zones idealized with line thickness proportional to fault zone slip rate in millimeters per year. The FOP 1999 Fieldtrip area is outlined. Fault activity (labeled by number and stippled) is compiled from sources described in Pezzopane [1993; and Weldon, 1993]. Dense stipple indicates the "eastern shear zone" continuing northward across Oregon. Vent pattern shows Cascade volcanoes.

In addition, several Humboldt State University students had worked, or were currently working, on mapping and neotectonic studies in southern Oregon. Dr. Carver and Dr. Burke and many HSU students have been working in southern Oregon for several years, both independently, and as part of class projects; several HSU Master's theses have involved neotectonic and Pleistocene geomorphology and stratigraphy studies [e.g., Hemphill-Haley, 1987; Hemphill-Haley et al., 1989; Lindberg, 1989; Simpson, 1990; Craven, 1991]. A common theme in these neotectonic studies in Oregon is to map the Late Quaternary geology and fault-related geomorphology along the zones, trench the young scarps if possible, profile the scarp topography as well as examine the pluvial lake shoreline elevations, and use the pluvial and tephra stratigraphy to determine the ages and styles of deformation. These techniques were used in central Oregon to evaluate the amounts of displacement and styles of faulting. Fault slip rates were estimated from offsets measured in fault scarp profiles and pluvial lake shoreline elevations, together with estimated or, in some cases, absolute ages of fault-related deposits.

The fault and seismicity compilation [Pezzopane, 1993] indicated that young faulting (late Pleistocene to historic) is concentrated mainly in north-trending zones that traverse northward from active faults in eastern California and western Nevada, across the northwestern Basin and Range Province into central and eastern Oregon, and into the Cascade volcanic arc, ultimately merging northward with transpressional fault and historic earthquake zones that cross southern and central Washington (Figures A6-2). The intraarc and backarc fault zones serve to separate crustal blocks of Western Oregon from "stable" North America. In a plate tectonic context, relative to fixed North America, pieces of Western Oregon are moving northwestward and rotating, probably in a similar manner as they have done for millions of years [Magill et al., 1982; Wells and Heller, 1989].

Regional geodetic measurements (VLBI), historic earthquake moment tensors (Figure A6-3), and the orientations and slip rates of late Quaternary faults (Figure A6-2) that cross Oregon, are the basis for constructing a kinematic model of this zone [Pezzopane, 1993; Pezzopane and Weldon, 1993]. The model indicates that active faults in Oregon accommodate overall motion in a direction ~N60°W ± 25° at a rate between ~2 and 12 mm/yr, depending on location and other assumptions. Crustal intraarc and backarc faults in Oregon and Washington can account for as much as 10% to 20% of the total Pacific-North American transform motion and almost all of the lateral component of Juan de Fuca plate motion relative to the North American plate. Wells et. al. [1999] recently published a refined kinematic model of microplate motions in the Pacific Northwest.

Regional Geologic Setting

The FOP'99 fieldtrip traverses a series of alternating structural blocks with alluvial basins of low relief and bedrock mountain ranges of moderate to high relief. Santa Rosa Peak is slightly higher in elevation than Steens Mountain; yet they have remarkably similar maximum elevations of 9773 feet and 9781 feet, respectively (US Geological Survey, 1:100k-scale topographic maps). The valleys that flank their range fronts have similar minimum elevations of approximately 4200 feet, and are long, narrow graben blocks that structurally separate the intervening ranges. The Alvord Desert playa lies in Pueblo Valley beneath the Steens Mountains whereas the Quinn River Valley flows southward along the

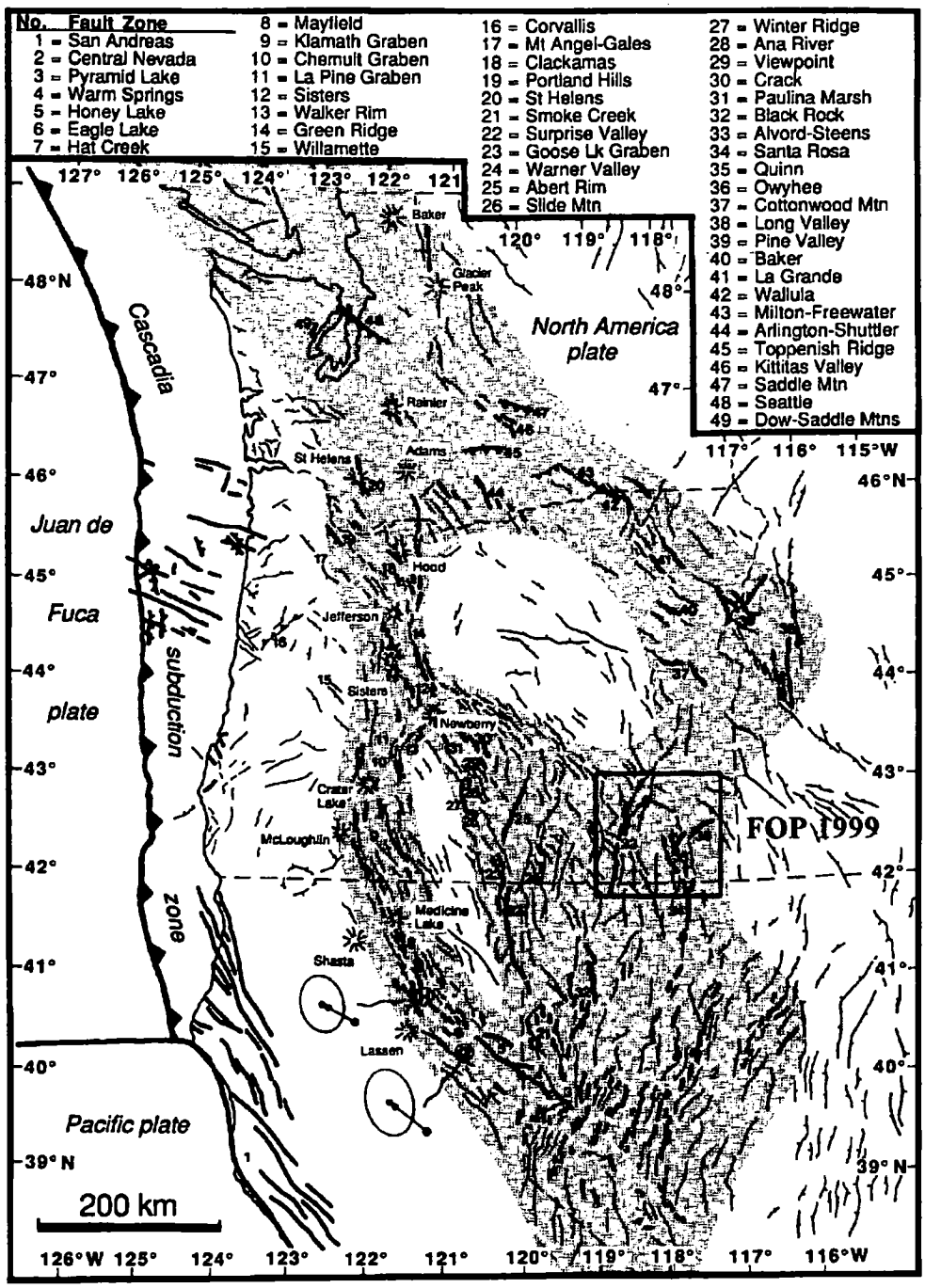

FIGURE A6-2. Map of middle Tertiary and younger fault activity in Oregon. Late Quaternary and Holocene fault activity (bold lines) indicates active backarc and intraarc fault zones that stretch from northern California to southern Canada. The FOP 1999 Fieldtrip area is outlined. Throughgoing zones of deformation are stippled; individual fault zones are numbered. Vent pattern shows Cascade volcanoes. The vector velocities at VLBI stations HATC (9.4 ± 2.6 mm/yr, N62°W ± 8°) and QUIN (12.0 ± 3.1 mm/yr, N52°W ± 9°) are relative to "fixed" North America, which includes a station at Ely, Nevada, and indicate that as much as 1 cm/yr of crustal strain is concentrated along this zone at the south. Base map from Walker [1977; and MacLeod, 1991] and further discussion and complete references cited in Pezzopane [1993; and Weldon, 1993].

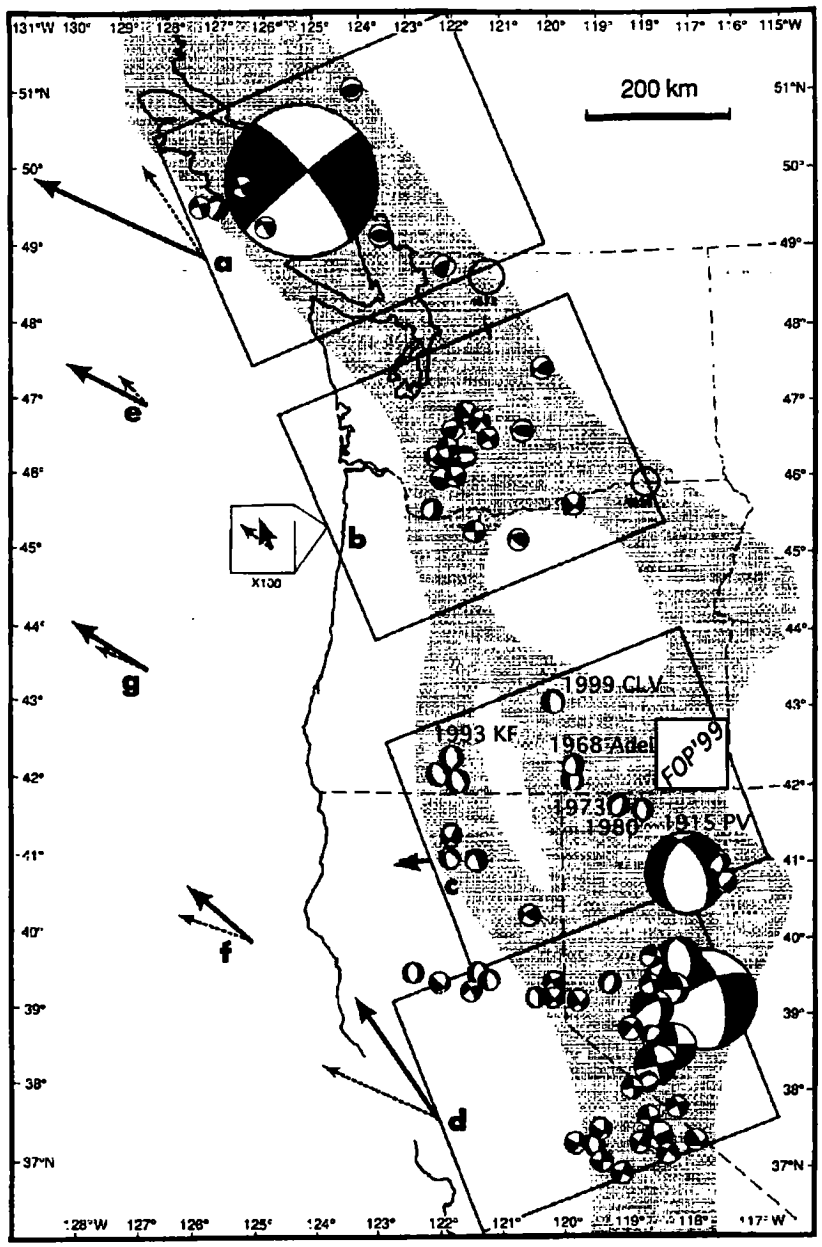

FIGURE A6-3. Map of lower hemisphere focal mechanisms of crustal earthquakes (positioned above their epicenters) near Oregon occurring between 1872 and 1999. Velocities across the deforming zones (solid vectors) are shown for earthquakes in (a) Vancouver Island; (b) Central Washington; (c), Southern Oregon and Northern Nevada; and (d) Central Nevada and Walker Lane; (e) the sum of the two northernmost volumes; (f) the sum of the two southernmost volumes; and g) the combination of all earthquakes along the entire zone. Focal mechanisms are plotted with their area proportional to their seismic moment, except for events smaller than about magnitude 6, which are plotted as symbols of constant size. The seismic moment tensors from historical earthquakes in each volume are rotated to a reference frame with axes parallel to the edges of the volume and summed. Overall directions of motions across the zones (vectors) range from E-W to about N20°W. Rates of motion across the zone range from less than 1 mm/yr to as much as 7 mm/yr, although a reasonable average is ~3 ± 1 mm/yr. See Pezzopane [1993; and Weldon, 1993] for explanation. KF is Klamath Falls. CLV is Christmas Lake Valley. PV is Pleasant Valley. The FOP 1999 Fieldtrip area is outlined.

western Santa Rosa range front and ultimately west-southwestward into the Black Rock Desert playa.

The Quinn River graben separates the Santa Rosa Range from the Salient Peak - Hoppins Peak Range to the west; with maximum elevations of approximately 6200 feet, together these ranges form the western flank of the McDermitt caldera complex. Northward into Oregon, the Santa Rosa Range lowers gradually into diffuse hills of the southern Owyhee Plateau including Horse Hills and Battle Mountain with maximum elevations of nearly 6500 feet. Several structural blocks with maximum elevations over 7200 feet form upland pass areas that mark the divides between the Quinn River Valley, the Coyote Lake Valley, and the Alvord Desert playa in Pueblo Valley to the northwest. These structural blocks include (from east to west) the Blue Mountains, Oregon Canyon Mountains, and Trout Creek Mountains and consist primarily of late Miocene extrusive volcanics [Walker and McCleod, 1991] (Figure A6-4) uplifted along sets of northeast-striking high-angle normal faults, some of which alternate dip thus forming gentle ramp and relay structures. Latest Pleistocene and younger faulting is concentrated mainly along the north to northeast striking range fronts whereas northwest and rare east-west striking young faults are present locally [Donath, 1962; Pezzopane, 1993; Narwold and Pezzopane, 1997].

FIGURE A6-4. FOP'99 fieldtrip portion of Geologic Map of Oregon from Walker and McCleod [1991].

The FOP'99 fieldtrip examines scarps along the Steens fault zones and what I called the Santa Rosa-Quinn River-Owyhee River fault zone [Pezzopane, 1993] (Figure A6-2). The fieldtrip area is approximately 150 km north of surface ruptures associated with the moment magnitude (Mw) 6.9 Pleasant Valley earthquake in 1915 [Wallace, 1977,1984; Doser, 1988] (Figure A6-3). Roughly 150 km west of the fieldtrip area was an earthquake swarm in 1968 near Adel, Oregon, consisting of several magnitude 4+ events, and one or two small magnitude 5 earthquakes [Schaff, 1976; Patton, 1985]. Two earthquakes occurred at the southern end of the Pueblo Mountains in 1973 (Mw 4.6) and 1980 (Mw 4.1) [Patton and Zhandt, 1991]. Historical seismicity in the region commonly occurs as earthquake swarms and sequences of two or more, shallow (< 10-15 km) moderate magnitude (< Mw 6) events [Couch and Lowell, 1971; Doser, 1988]. Focal mechanisms in the region indicate mostly pure normal faulting along north-south to northeast striking faults -- and here, like throughout the northwestern Basin and Range Province, the relative tensional stress axes of earthquake mechanisms are commonly near horizontal and oriented towards the Mendocino Triple Junction [Patton and Zhandt, 1991].

Santa Rosa-Quinn River-Owyhee Fault Studies

In 1990-1991, Professor Takashi Nakata, from Hiroshima University, Japan, was in Oregon as a visiting scientist with Dr. R. Yeats at Oregon State University. During a portion of this time Nakata visited the University of Oregon, became interested in the active faults of Oregon, and examined nearly 9000 aerial photographs from the comprehensive Photography Library at the University of Oregon, which was also one of the primary resources for my dissertation. Working both independently and together at various times, Nakata and I examined many of the same photographs, mostly of ~1:24k-scale vertical aerial photographs, and recognized many similar fault-related geomorphic features, especially along faults in south-central Oregon where I had concentrated the most effort.

From aerial photos, Nakata initially interpreted young faulting in the Quinn River Valley of southeastern Oregon and north-central Nevada [Nakata et al., 1992], but was hindered because aerial photo coverage stretched only a few frames southward into Nevada. (However 3 years later I learned that ~1:12k- to 1:20k-scale low-sun aerial photos of the entire Santa Rosa-Quinn River zone were in the Mackay School of Mines Library from the collection of D.B. Slemmons at the University of Nevada Reno, who appears to have examined this zone of faulting over a decade earlier.)

In the winter of 1992, I made a reconnaisance investigation of faults in the Quinn River Valley and confirmed that young scarps were located on both southern flanks of the Blue Mountains, that scarps crossed Holocene(?) stream terraces along the east flank of Oregon Canyon Mountains; scarps crossed the valley axis north of McDermitt and continued southward along both valley sides into Nevada. The fang-toothed young fault scarps along the western flank of Santa Rosa Peak, due east of Orovada, Nevada, were impressive. Yet, I could not map these faults accurately because of lack of photo coverage and time was running out on my graduate career. Faults as young as Late Pleistocene (10-130 ka) in age were mapped along both sides of the Quinn River graben in Nevada [Dohrenwend and Moring, 1991]. Later, the Santa Rosa fault zone was examined, and evidence of Holocene activity was reported [Michetti and Wesnousky, 1993]. Most recently, C. Narwold (this volume) of Humboldt State University has been studying the northernmost third of this

active fault zone [Narwold and Pezzopane, 1997] that stretches north-south for approximately 100 km or more (perhaps capable of a small to moderate Mw 7 earthquake assuming the entire length of the zone ruptured in a maximum earthquake).

In April, 1997, C. Narwold and I investigated what I called the Owyhee zone (Figure A6-3), the northernmost northeast striking zone of normal faults that curve eastward from the Bowden Hills to the south flank of Grassy Mountain, a broad Pliocene and Miocene shield volcano of diktytaxitic olivine basalt and mafic vent rocks [Walker and McCleod, 1991] (Figure A6-4) situated approx. 10 km west of the Owyhee River Canyon. The faults form broad, flat-floored grabens and half-grabens in flat to gently dipping Miocene basalts of the Owyhee plateau, and Jackies Butte is a Pleistocene and Pliocene shield volcano of diktytaxitic olivine basalt situated within a northeast trending graben. Aerial photographs of this zone showed many sharp and prominent fault scarps, and my fault activity map compilation indicated Late Quaternary to possible Holocene fault activity on some of the most prominent faults in this zone on the basis of aerial photo interpretations without field reconnaisance. Older(?) Pleistocene alluvial fan deposits of Rattlesnake and Battle Creeks have been offset along the westernmost reach of the fault (Narwold, this volume).

Reconnaisance to Grassy Mountain revealed scarps that are 100s of feet in height having broad gentle slopes. In places, the basalt bedrock forms platforms and risers that appear similar to terraces (Figure A6-5A). Scarp slopes appear rough and corrugated in profile, and the lower scarp slopes are smoother and gentler than the upper scarp. The uppermost "riser" is steep to near-vertical, a few meters or more in height, and appears as the tallest and freshest "scarp". Bedrock and bouldery colluvium appear to form successively lower and smaller risers, which are likely weathered out of bedrock and buried increasingly deeper downslope across the scarp face. The scarp toes are, in places, scalloped by ephemeral slope and stream wash in the broad flat floor of the graben (Figure A6-5B). Terraces of unknown age are preserved along the easternmost reach of the fault zone where it crosses the Owyhee River Canyon (Figure A6-5C). Reconnaisance evidence indicates a lack of young fault activity along the Owyhee zone near Grassy Mountain, yet relatively young stratigraphy with which to record faulting is lacking.

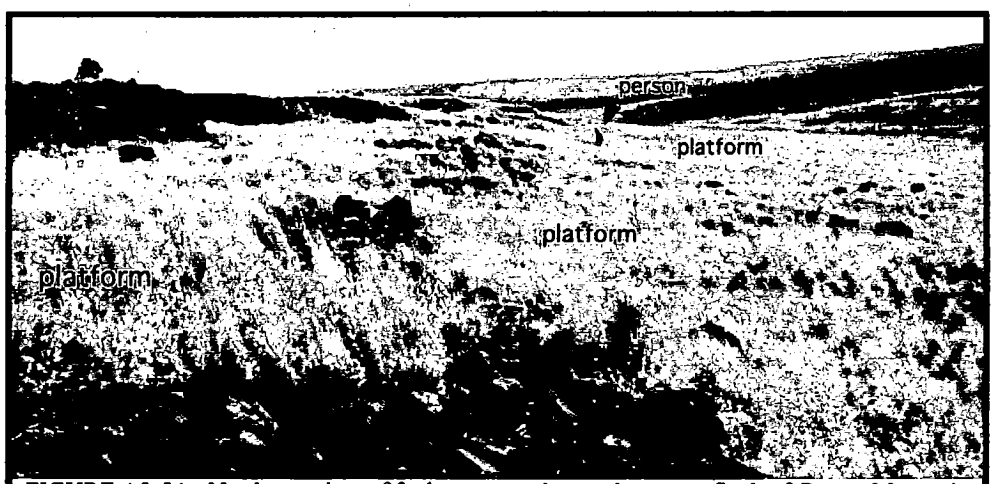

FIGURE A9-5A. Northeast view of fault scarp on the southwestern flank of Grassy Mountain in the northern Owyhee zone. Person is standing on riser between the second and third platform below the scarp crest. Bouldery colluvium is weathering from the basalt bedrock scarp. Scarp crest is marked by rock cairn.

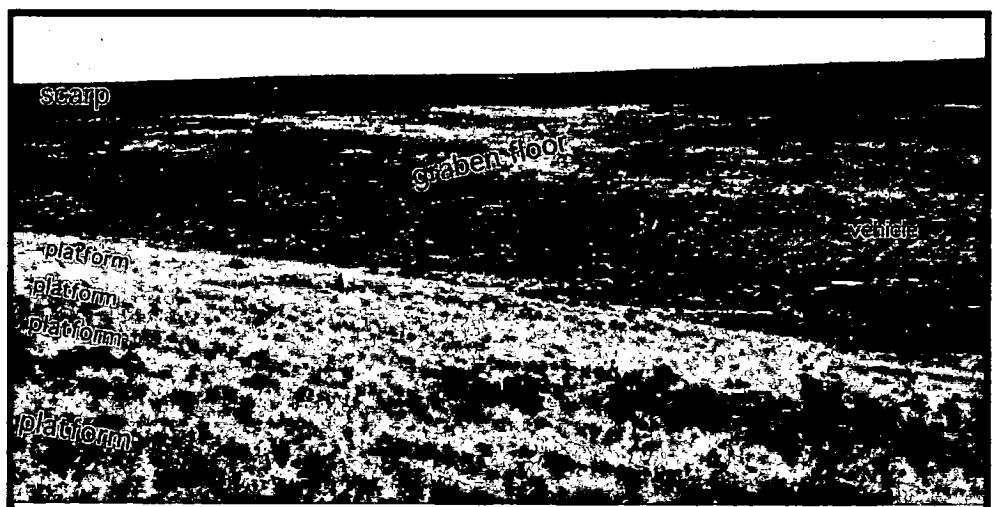

FIGURE A9-5B. East-southeast view of graben structure and fault scarps southwest of Grassy Mountain in the northern Owyhee zone. Bedrock(?) platforms or terraces(?) occur on the lower fault scarp slope which is scalloped and enhanced by slope and ephemeral stream wash on the flat floor of the graben. Northwest facing fault scarp in distance.

FIGURE A9-5C. Southeast view of fault and terraces in the Owyhee River Canyon east of Grassy Mountain, southeast Oregon.

REFERENCES CITED

Argus, D. F., and R. G. Gordon, Current Sierra Nevada-North America motion from very long baseline interferometry: Implications for the kinematics of the western United States, Geology, 19, 1085-1088, 1991.

Atwater, T., Implication of plate tectonics for Cenozoic tectonic evolution for Western North America, Geol. Soc. Am. Bull., 81, 3513-3536, 1970.

Couch, R. W., and R. P. Lowell, Earthquakes and seismic energy release in Oregon, Ore Bin, 33, 61-84, 1971.

Craven, G. F., The tectonic development and late Quaternary deformation of Warner Valley south of Hart Mountain, Oregon, M.S. thesis, 94 pp., Humboldt State University of California, Arcata, Oct. 1991.

DeMets, C., R. G. Gordon, S. Stein, and D. F. Argus, A revised estimate of Pacific-North America motion and implications for Western North America plate boundary zone tectonics, Geophys. Res. Lett., 14, 911-914, 1987.

Dohrenwend, J.C., and B.C. Moring, Reconnaissance photogeologic map of young faults in the McDermitt 1° by 2° quadrangle, Nevada, Oregon, and Idaho, scale 1:250,000, U.S. Geol. Surv. Map MF-2177, 1991.

Donath, R., Analysis of basin-range structure, south-central Oregon, Geol. Soc. Am. Bull., 73, 1-16, 1962.

Doser, D. I., Source parameters of earthquakes in the Nevada Seismic Zone, 1915-1943, J. Geophys. Res., 93, 15,001-15,015, 1988.

Hamilton, W., and W. B. Myers, Cenozoic tectonics of the Western United States, Rev. Geophys., 4, 509-536, 1966.

Hemphill-Haley, M. A., Quaternary stratigraphy and late Holocene faulting along the base of the eastern escarpment of Steens Mountain, southeastern Oregon, M.A. thesis, 87 pp., Humboldt State Univ., Arcata, Calif., 1987.

Hemphill-Haley, M. A., W. D. Page, R. Burke, and G. A. Carver, Holocene activity of the Alvord Fault, Steens Mountain, southeastern Oregon (report), 38 pp., Woodward-Clyde Consultants, Oakland, Calif., 1989.

Lindberg, D. N., Extending the zone of recognized late-Holocene faulting in the Basin and Range of southeastern Oregon (abstract), Geol. Soc. Am. Abstr. Programs, 21, 106, 1989.

Magill, J. R., R. E. Wells, R. W. Simpson, and A. V. Cox, Post 12 m.y. rotation of southwest Washington, J. Geophys. Res., 87, 3761-3776, 1982.

Minster, J. B., and T. H. Jordan, Vector constraints on western U.S. deformation from space geodesy, neotectonics, and plate motions, J. Geophys. Res., 92, 2798-4804, 1987.

Michetti, A.M., and S.G. Wesnousky, Holocene surface faulting along the west flank of the Santa Rosa Range (Nevada-Oregon) and the possible northern extension of the Central Nevada Seismic Belt, Geol. Soc. Am. Abstr. Programs, 25, 120-121, 1993.

Nakata, T, R. J. Weldon, S. K. Pezzopane, C. Rosenfeld, and R. S. Yeats, Preliminary aerial photo-interpretation of active faults in Oregon, Geol. Soc. Am. Abstr. Programs, 24, 72, 1992.

Narwold, C. F., and S. K. Pezzopane, Preliminary analysis of Late Quaternary faulting along the Quinn River fault zone, Northern Nevada–Southeastern Oregon, Geol. Soc. Am. Abstr. Programs, 29, A-232, 1997.

Patton, H. J., P-wave fault-plane solutions and the generation of surface waves by earthquakes in the western United States, Geophys. Res. Lett., 12, 518-521, 1985.

Patton, H. J., and G. Zandt, Seismic moment tensors of Western U.S. earthquakes and implications for the tectonic stress field, J. Geophys. Res., 96, 18,245-18,259, 1991.

Pease, R. W., Normal faulting and lateral shear in northeastern California, Geol. Soc. Am. Bull., 80, 715-720, 1969.

Pezzopane, S. K., Active faults and earthquake ground motions in Oregon, Ph.D. dissertation, 208 pp., University of Oregon, Eugene, 1993.

Pezzopane, S. K., and R. J. Weldon, (1993), Tectonic role of active faulting in Central Oregon, Tectonics, v. 12, p. 1140 – 1169, 1993.

Richard, S. M., (ed.), Deformation associated with the Neogene Eastern California Shear Zone, southeastern California and southwestern Arizona,in: Proceedings of the workshop on the Eastern California Shear Zone, 78 pp., San Bernardino County Museums Spec. Pub. 92-1, Redlands, California, 1992.

Sauber, J., Geodetic measurement of deformation in California, NASA Tech. Mem. 100732, 211 pp., 1990.

Schaff, S., The 1968 Adel, Oregon, earthquake swarm, M.S. thesis, Univ. of Nevada at Reno, 1976.

Shawe, D. R., Strike-slip control of Basin-Range structure indicated by historical faults in western Nevada, Geol. Soc. Am. Bull., 76, 1361-1378, 1965.

Simpson, G. D., Late Quaternary tectonic development of the northwestern part of the Summer Lake basin, south-central Oregon, M.S. thesis, Humboldt State Univ. of Calif., Arcata, May 1990.

Stewart, J. H., J. P. Albers, and F. G. Poole, Summary of regional evidence for right-lateral displacement in the western Great Basin, Geol. Soc. Am. Bull., 79, 1407-1414, 1968.

Tolan, T. L., and S. P. Reidel, Structure map of a portion of the Columbia River flood-basalt Province, in: Volcanism and Tectonism in the Columbia River Flood-Basalt Province, Geol. Soc. Am. Spec. Pap. 239, edited by S. P. Reidel, and P. R. Hooper, 386 pp., 1989.

Walker, G. W., Geologic map of Oregon east of the 121st meridian, scale 1:500,000, U.S. Geol. Surv. Map I-902, 1977.

Walker G W., and N. S. MacLeod, Geologic map of Oregon, 2 sheets, scale 1:500,000, U.S. Geol. Survey, Washington, D. C., 1991.

Wallace, R. E., Profiles and ages of young fault scarps, north-central Nevada, Geol. Soc. Am. Bull, 88, 1267-1281, 1977.

Wallace, R. E., Patterns and timing of Late Quaternary faulting in the Great Basin Province and relation to some regional tectonic features, J. Geophys. Res., 89, 5763-5769, 1984.

Weldon, R., and E. Humphreys, A kinematic model of Southern California, Tectonics, 5, 33-48, 1986, .

Wells, R. E., and P. L. Heller, The relative contribution of accretion, shear, and extension to Cenozoic tectonic rotation in the Pacific Northwest, Geol. Soc. Am. Bull., 100, 325-338, 1989.

Wells, R.E., C.S. Weaver, and R.J. Blakely, Fore-arc migration in Cascadia and its neotectonic significance, Geology, 26, 759-762, 1999.

Wise, D. U., An outrageous hypothesis for the tectonic pattern of the North American Cordillera, Geol. Soc. Am. Bull., 74, 357-362, 1963.

TEMPORAL AND SPATIAL PATTERNS OF QUATERNARY FAULT ACTIVITY IN NORTHWESTERN NEVADA

Thomas L. Sawyer[1] and Kenneth D. Adams[1&2]

[1] Piedmont Geosciences, Inc., 10235 Blackhawk Drive, Reno, NV, 89506, Ph.: 775-972-3234, E-mail: piedmont@reno.quik.com

[2] Desert Research Institute, 2215 Raggio Parkway, Reno, NV, 89512, Ph. 775-673-7345 E-mail kadams@dri.edu

We recently compiled Quaternary fault maps and a relational database for much of the State of Nevada, including northwestern Nevada, based on available information. With the exception of a few detailed studies (e.g., Dodge, 1982; Michetti and Wesnousky, 1993; Narwold, in prep.), regional reconnaissance mapping based on interpretation of aerial photographs with little or no field support (e.g., Slemmons, ca 1966a, 1966b; Dohrenwend and Morning, 1991a, 1991b) is the primary source of information.

The distribution and activity of Quaternary faults in northwestern Nevada reflects patterns of late Cenozoic deformation of the region. As might be expected the most active faults, in terms of recency of movement (e.g., Dohrenwend and Morning, 1991a, 1991b) and preliminary slip rate estimates (e.g., dePolo, 1998), coincide with regions of greatest structural relief. Specifically, latest Quaternary faults (<15 ka) with relatively high slip rates (0.2 to 1.0 mm/yr) typically bound prominent north-trending ranges and (or) traverse broad, deep structural basins (graben). These faults form a north-trending zone that is approximately 120 km wide at 41 N. Lat. and narrows to approximately 80 km in width at the Nevada-Oregon border (i.e., 42 N. Lat.). The principal structures in this zone include the Black Rock fault zone, the Pueblo Mountains fault zone, the Jackson Mountains fault zone, the eastern Bilk Creek Mountains fault zone, the Montana Mountains-Desert Valley fault zone, and the Santa Rosa Range fault zone (Quinn River fault zone of Narwold and Pezzopane, 1997), from southwest to northeast. This well-defined structural zone of classic Basin and Range topography is surrounded by regions to the east and west that have much lower structural relief and fewer active faults with lower slip rates.

Only the Pueblo Mountains and Santa Rosa Range fault zones appear to extend northward into Oregon. The Pueblo Mountains fault zone apparently comprises the southern part of a system of Quaternary faults that includes the Steens Mountains fault in southeastern Oregon. Michetti and Wesnousky (1993) concluded that the main neotectonic and geomorphic features along the Santa Rosa Range fault zone are similar to faults in the central Nevada seismic belt located to the south. Therefore, large earthquakes in the near future would not be a surprise along this fault zone (Michetti and Wesnousky, 1993).

Late Quaternary faults (<130 ka) throughout the region tend to occur in distributed clusters, where they commonly bound low hills or cross piedmont slopes and alluviated basins, and all are assigned to the lowest of four slip rate categories (i.e., <0.2 mm/yr) used in the compilation.

Scattered clusters of predominantly northeast-striking late Quaternary faults have been mapped from the east flank of the southern Santa Rosa Range eastward to the Midas Trough. Although, the largest cluster is at the north end of the Black Rock Desert between and bounding the Pine Forest Range and Bilk Creek Mountains. Within this cluster, faults strike from northwest to northeast and one fault at the north end of the Pine Forest Range has an unusual semi-circular trace. A short section of the west front of the Montana Mountains is also bounded by late Quaternary faults.

Older Quaternary faults (>130 ka) and suspected Quaternary faults bound generally dissected range fronts and are widely distributed across elevated volcanic plateaus (e.g., Owyhee Desert) where they are commonly expressed as low topographic escarpments. With few exceptions these faults also are assigned to the lowest slip rate category.

Additional studies of Quaternary faults are needed to improve our understanding of regional neotectonic activity and to assess whether short term, geodetic rates of movement (Bennett et al., 1998) are reflected in long term slip rates. In particular, information on the little studied Pueblo Mountains, eastern Bilk Creek Mountains, and Montana Mountain-Desert Valley fault zones undoubtedly would significantly contribute to characterizing the neotectonic setting and may be timely in light of historical faulting in the central Nevada seismic belt.

References

Bennett, R.A., Wernicke, B.P., and Davis, J.L., 1998, Continuous GPS measurements of contemporary deformation across the northern Basin and Range province: Geophysical Research Letters, v. 25, no. 4, p. 563-566.

dePolo, C.M., 1998, A reconnaissance technique for estimating the slip rates of normal-slip faults in the Great Basin, and application to faults in Nevada, U.S.A.: University of Nevada Ph.D. Dissertation, 199 p.

Dodge, R.L., 1982, Seismic and geomorphic history of the Black Rock fault zone, northwestern Nevada: Colorado School of Mines, Golden Colorado, unpublished Ph.D. dissertation, T-2593, 271 p., 1:24,000 scale.

Dohrenwend, J.C., and Moring, B.C., 1991a, Reconnaissance photogeologic map of young faults in the McDermitt 1° by 2° quadrangle, Nevada, Oregon, and Idaho: U.S. Geological Survey, Miscellaneous Field Studies Map MF-2177, 1:250,000 scale.

Michetti, A.M., and Wesnousky, S.G., 1993, Holocene surface faulting along the west flank of the Santa Rosa Range (Nevada-Oregon) and the possible northern extension of the Central Nevada Seismic Belt: GSA abstracts with Programs, v. 25, no. 5, p. 120-121, (faults compiled from unpublished 1:100,000 scale maps that accompanied presentation).

Narwold, C.F., in prep., Late Quaternary faulting along the Quinn River fault zone, northern Nevada-southeastern Oregon: unpublished Master's Thesis, Humboldt State University, Arcata, California.

Narwold, C.F., and Pezzopane, S.K., 1997, Preliminary analysis of late Quaternary faulting along the Quinn River fault zone, northern Nevada-southeastern Oregon: GSA Abstracts with Programs, v. 29, no. 6, p. A-323.

Slemmons, D.B., ca. 1966a, Quaternary fault map of the McDermitt 1°X2° sheet: unpublished map compiled for Figures 3, 4, 5, 6, and 8 in Slemmons (1967), 1:250,000 scale map.

Slemmons, D.B., ca. 1966b, Quaternary fault map of the Vya 1°X2° sheet: unpublished map compiled for Figures 3, 4, 5, 6, and 8 in Slemmons (1967), 1:250,000 scale.

The Rush Peak Fault Zone, Cuddy Mountains, Western Idaho: Evidence for sinistral-oblique Late-Quaternary movement and analysis of longitudinal stream profiles crossing an active range front.

Sara C. Smith: ssmith@trex.boisestate.edu, Department of Geosciences, Boise State University

Introduction

The southern range-front of the Cuddy Mountains in western Idaho is bounded by the Rush Peak Fault Zone (RPFZ), a generally N70E striking, 12 km long fault that juxtaposes Mesozoic granitic basement on the north against Miocene volcanic rocks of the Columbia River Basalt Group (CRBG) on the south (Figure 1). Vertical displacement across the RPFZ exceeds 700 m in the vicinity of Rush Peak, near Cambridge. In Rush Creek canyon, two parallel fault scarps separated by approximately 50 m displaced Quaternary alluvium and are coincident with the trace of the RPFZ. The largest of the scarps is approximately 10-15 meters high. The second scarp segment is 4-7 meters high and left-laterally displaces a boulder levee 5.5-6.5 meters. Four scarp profiles were surveyed and mid-slope angle of 17° was calculated, substantiating the 16° mid-slope scarp angle measured by Zollweg and Wood (1993). Using the method of Bucknam and Anderson (1979), this mid-slope angle, and 5-7 m scarp height, indicates a scarp age of 10 to 100 ka. Soil developed on the offset boulder levee has a color B horizon (7.5 YR 3/2) to 0.32 m and (7.5 YR 4/3) to 0.75 m and contains aphanitic Imnaha basalt cobbles that have weathering rinds with thickness of 0.2 mm (Smith et. al., 1999). Personius (1998) correlated soil-profile development of a faulted fan surface to last-glacial Pilgrim Cove (Pinedale-equivalent) in Long Valley, 50 km to the east, at a similar elevation (approximately 4,500 feet). Type Pinedale has been dated by cosmogenic isotopes at 23-16 ka (Phillips et.al., 1997). Collectively, these data suggest age of last offset could be less than 20 ka as suggested by Personious (1998).

The absolute length of Quaternary activity along the RPFZ has not been constrained, in part because conventional methods including fault-scarp morphologies, alluvial-channel geometries and mountain-front geometries can only be applied to a few select areas. An alternative method for assessing recent tectonic activity of a range-front area is to examine the longitudinal profile of the entire main-trunk streams using stream-gradient (SL) index developed by Hack (1973).

Hack's Semi-log Equilibrium Long Profile

The equilibrium long profile of a stream flowing across rocks of uniform resistance to erosion describes a negative logarithmic function (Goldrick and Bishop,1995; Hack,1973). The equation for a stream profile for a straight segment on such a plot is $H = C - k \ln L$, where C is a constant and k is the slope of the line (Hack, 1973). Actual stream slope, S, is the derivative of this equation with respect to L, or:

$$S = dH / dL = d(k \ln L) / dL = k / L$$

"The slope of a straight segment on the semi-logarithmic plot is k, which is equal to the product SL" (Merritts and Vincent, 1989). "For a graded stream flowing across lithologies of uniform erosional resistance, a plot of elevation versus the natural logarithm of downstream distance describes a straight line, the slope of which Hack (1973) defined as the stream-gradient index. The average value of the SL index for any reach, between b and c, is constant for lithologies of uniform erosional resistance".

The formula for stream-gradient index (SL) is:

$$SL = \frac{h_b - h_c}{\ln d_c - \ln d_b} = \frac{\Delta H * L}{\Delta L} \quad \text{because } \Delta(\ln L) = \frac{\Delta L}{L}$$

where h_b and h_c are the elevations and d_b and d_c are the downstream distances of b and c. The quantity L is the stream length measured from the drainage divide at the source of the longest stream in the drainage basin above a locality on a reach. ΔH is the difference in elevation between the ends of the reach, and ΔL is the length of the reach (Figure 2) (Hack, 1973). ΔL must be a smaller value than L.

Applying Hack's (1973) methods to the evolution of bedrock stream profiles can help interpret the relative uplift and/or the lithological resistance in an area that causes longitudinal profile steepening. Steepening longitudinal profiles are based on the change in altitude at a rate equal to the rate of uplift minus the rate of incision as a stream incises bedrock (Merritts and Vincent, 1989). Such steepening is important in interpreting landscape history and neotectonism (Goldrick and Bishop, 1995). Longitudinal profiles may reach equilibrium, or maintain a steady shape, in two ways. A stream not subjected to base-level change may reach a stable longitudinal form reflecting no net erosion or deposition and stay "at grade" (Mackin, 1948 as cited by Merritts and Vincent, 1989). A stream reach subjected to base-level drop can also maintain a steady longitudinal form by uniform incision (Merritts and Vincent, 1989). This stable longitudinal form occurs only when the rate of incision is equal to the rate of uplift.

Merritts and Vincent (1989) discuss several aspects of base-level change due to tectonic uplift and their effects on longitudinal profiles. Longitudinal profiles that steepen as a result of disequilibrium effects, such as relative change of base-level or uplift on a graded stream with uniform lithology, is the result of the upstream migration of a knickpoint formed in response to base-level drop (Figure 3) (Goldrick and Bishop, 1995). Furthermore, relative base-level drop at a specific area in a drainage basin creates an elevation potential, which locally increases stream gradient, and therefore increases the stream's ability to erode. The effect of base-level lowering propagates and diffuses upstream. For example, a large stream may have sufficient discharge to incise uniformly with the rate of uplift, and thus all of the base-level fall would be transmitted upstream. "The first reach upstream that has insufficient stream power to incise at the same rate as base-level fall will increase in gradient". The stream-gradient at any point along the stream channel and it tributaries records the total height of the knickpoints that have migrated upstream past the area of an over-steepened reach (but have not migrated completely to the head of the stream) (Merritts and Vincent, 1989; Goldrick and Bishop, 1995). In addition, Goldrick and Bishop, 1995, found that knickpoints decline in height or flatten as they migrate upstream due to the decline in the projected degree of base level lowering upstream (Figure 3). It is logical that high SL values would be upstream of the location of the uplifting fault scarp(s) if the climatic conditions and rock resistances are fairly consistent (Goldrick and Bishop, 1995). Areas with uniform rock resistances that produce anomalously high SL values should reflect tectonic activity (Keller, 1977 as cited by Merritts and Vincent, 1989).

Rush Peak Fault Zone

In this study, second and third order streams that interacted with the RPFZ in the Goodrich, Rush Peak and Advent 7.5 quadrangles were measured following Hack's (1973) and Merritts and Vincent (1989) parameters, systematically calculating the SL values at regular intervals. Inasmuch the $L/\Delta L$ is a dimensionless ratio, the measurements of horizontal distance were calculated in inches and vertical distance ΔH was determined from 40 foot contours intervals on a 1:24,000 scale map (Hack, 1973). "The gradient index is the product of a ratio and a distance, so it is conveniently expressed as *gradient-feet*" (Hack, 1973). In areas close to the stream origin, SL values were calculated at 1 or 2 inch intervals (2,000 – 4,000 feet) depending on topography. As the intervals came closer to the RPFZ, SL values were calculated at ½ inch (1,000 feet) intervals so that critical high SL value areas were not unnoticed. If high SL values were calculated using the ½ inch intervals, then intervals of ¼ inch (500 feet) were measured in the area to aid in narrowing location of the highest SL value.

I devised a method of analyzing and contouring SL values that attempts to normalize differences in stream power of large and small streams (i.e. streams of different order) (Figure 4). Rather than contour SL values directly, I categorized SL index values differently depending on stream order. First, I assigned a rank of low, medium and high to the reaches of the streams. For example, on second order streams a low magnitude ranking SL value would be 100-1000; medium (1000-2000), and high (2000-3000). Third order streams were divided into magnitudes; low (100-3000), medium (3000-6000), and high (6000-9500) . The four different magnitudes of SL values from the second and third level order streams were contoured according to rank rather than numerical value. Low SL values of second order streams (100-1000) were weighted equally with the low SL values of third order streams (100-3000) respectively. This method departs from (Hack, 1973 and others) by ranking SL index rather than

contouring the numerical values themselves. Ranking in this way resolves the problem of comparing SL index of streams of different order.

Conclusions

Contouring SL values of main-channel streams crossing the RPFZ displays a correlation between high SL values and the location of the fault scarps (Figure 4). As seen in the contour map, segments of the RPFZ trend south of the High SL value contour zones on Beaver, Rush, Grizzly, and Cow Creeks. Zollweg and Wood (1992) and Personius (1998) suggest that the east segment of the RPFZ appears to curve sharply to the north-northeast. Though it is unlikely that this continuation is part of the same fault segment, looking at the contour map, there appears to be an uplift that trends in the north-northeast direction supporting their observations. The above authors also mention another possibility of the RPFZ's continuation that has been identified as the east-striking Goodrich Creek fault. The medium and high contour zones suggest a fault matching their description of Goodrich Creek trending approximately 2 miles south of the RPFZ. Zollweg and Wood (1992) mention that the locality of Goodrich Creek fault is obscure due to growth of dense brush and lack of large surface rupture. Provided high gradients are not influenced by resistant rock, analyzing the area using SL values allows for an independent assessment of the zone of uplift and location of the active fault segment.

It was found that second order streams do not show profound effects of uplift in longitudinal profiles. Profiles of the lower reaches in third order streams, near the RPFZ and possible continuing segments, exhibited change in gradient values as seen by the upward migration of knickpoints formed in response to base-level lowering. These effects can be seen specifically above the RPFZ in the lower reaches of Rush Creek (Figure 5). Other possible knickpoint migrations include both medium ranked areas on Goodrich Creek and the medium ranked area in the lowest reach of Johnson Creek (Figure 4). In all cases, knickpoints have migrated about 0-5 km from the range-front. From this analysis, I conclude that the longitudinal profiles and knickpoints in this area preserve a record of Quarternary uplift.

High values of gradient-index on third order streams in this area appear to be good indicators of either erosion of resistant rock or zones of uplift. Despite this ambiguity, an analysis of stream-gradient index can be a useful aid in geologic mapping. Availability of digital elevation models (DEMs) and GIS systems should allow rapid analysis of regions and serve as a useful tool, provided stream order is taken into account. It is especially helpful, as suggested in this study, in focusing the location of active faults that create base-level lowering. Active faults might not be detected by conventional methods, particularly in areas without substantial accumulations of Quaternary deposits deposited across the fault trace.

References

Bucknam, R.C. and Anderson, R.E., Estimation of fault-scarp ages from a scarp-height-slope angle relationship. Geology, v. 7, p. 11-14.

Goldrick, G. and Bishop, P., 1995, Differentiating the roles of lithology and uplift in the steepening of Bedrock River long profiles: An example from southeastern Australia. The Journal of Geology, v. 103, p. 227-231.

Hack, J.T., 1973, Stream-profile analysis and stream gradient index. Journal of Research U.S. Geological Survey, v. 1, no. 4, p. 421-429.

Keller, E.A., 1977, Adjustment of drainage to bedrock in regions of contrasting tectonic framework. Geological Society of America Abstracts with Programs, v. 9, no.7, p. 1046.

Mackin, J.H., 1948, Concept of the graded stream. Geological Society of America Bulletin. V. 59, p. 463-512.

Mann, G. M., and Meyer, C. E., 1993, Late Cenozoic structure and correlations to seismicity along the Olympic-Wallowa Lineament, northwest United States. Geological Society of America Bulletin, v. 105, p. 853-871.

Merritts, D. and Vincent, K.R., 1989, Geomorphic response of coastal streams to low, intermediate, and high rates of uplift, Mendocino triple junction region, northern California. Geological Society of America Bulletin, v. 101, p. 1373-1388.

Personius, S. F., 1998, Surficial geology and neotectonics of selected areas of western Idaho and northeastern Oregon. Open-File Report 98-771, U.S. Geological Survey.

Phillips, F.M., Zreda, M.G., Gosse, J.C., Klein, J., Evenson, E.B., Hall, R.D., Chadwick, O.A. and Sharma, P., 1997, Cosmogenic ^{36}Cl and ^{10}Be ages of Quarternary glacial and fluvial deposits of the Wind River Range, Wyoming. Geologic Society of America Bulletin, v. 109, no. 11, p. 1453-1463.

Smith, S.C., Northrup, C.J. and Wood, S.H., 1999, The Rush Peak Fault Zone, Cuddy Mountains, western Idaho: Evidence for sinsistral-oblique Late Quaternary movement. Geological Society of America Abstracts with Programs, October, 1999, Annual Meeting in Denver.

Zollweg, J. E., and Wood, S. H., 1993, Faulting relationships, seismicity, design arthquakes, and peak ground accelerations at the hydroelectric facilities in Hells Canyon of the Snake River, Idaho-Oregon. Unpublished report prepared for Idaho Power Company.

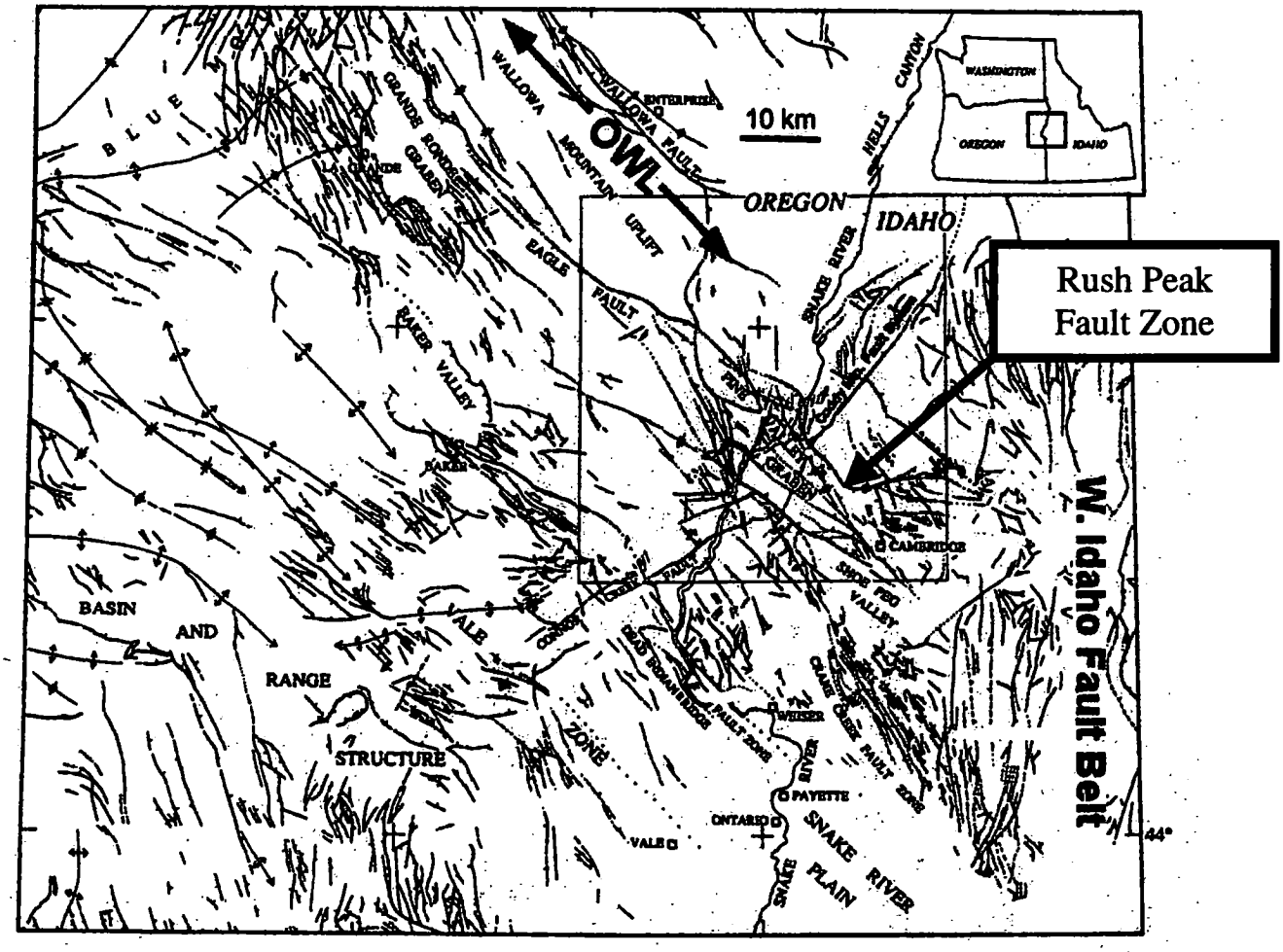

Figure 1. Regional late Cenozoic tectonic map showing the location of the Cuddy Mountain area. Also shown are major regional fault domains, including Rush Peak Fault Zone, the Olympic-Wallowa Lineament (OWL), Western Idaho Fault Belt, and Pine Valley Graben System. (modified from Mann and Meyers, 1993)

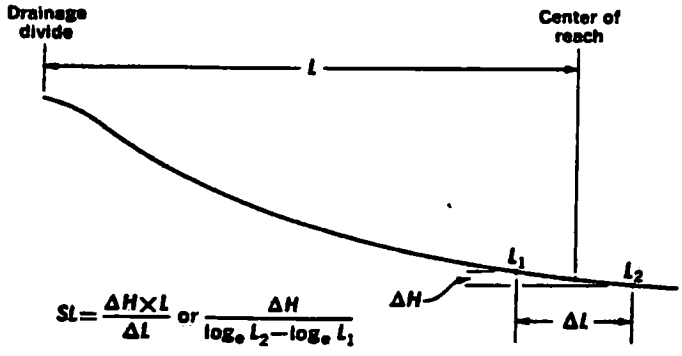

Figure 2. Measured parameters used in calculation of long profile gradient index. Symbols are defined in text. (modified from Hack, 1973)

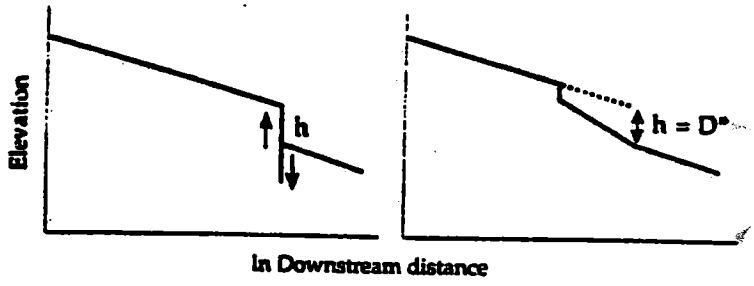

Figure 3. The effect of base-level change on the of a previously graded stream. The value D*at any point along the stream is equal to the total height of knickpoints that have migrated upstream past that point. (modified from Goldrick and Bishop, 1995)

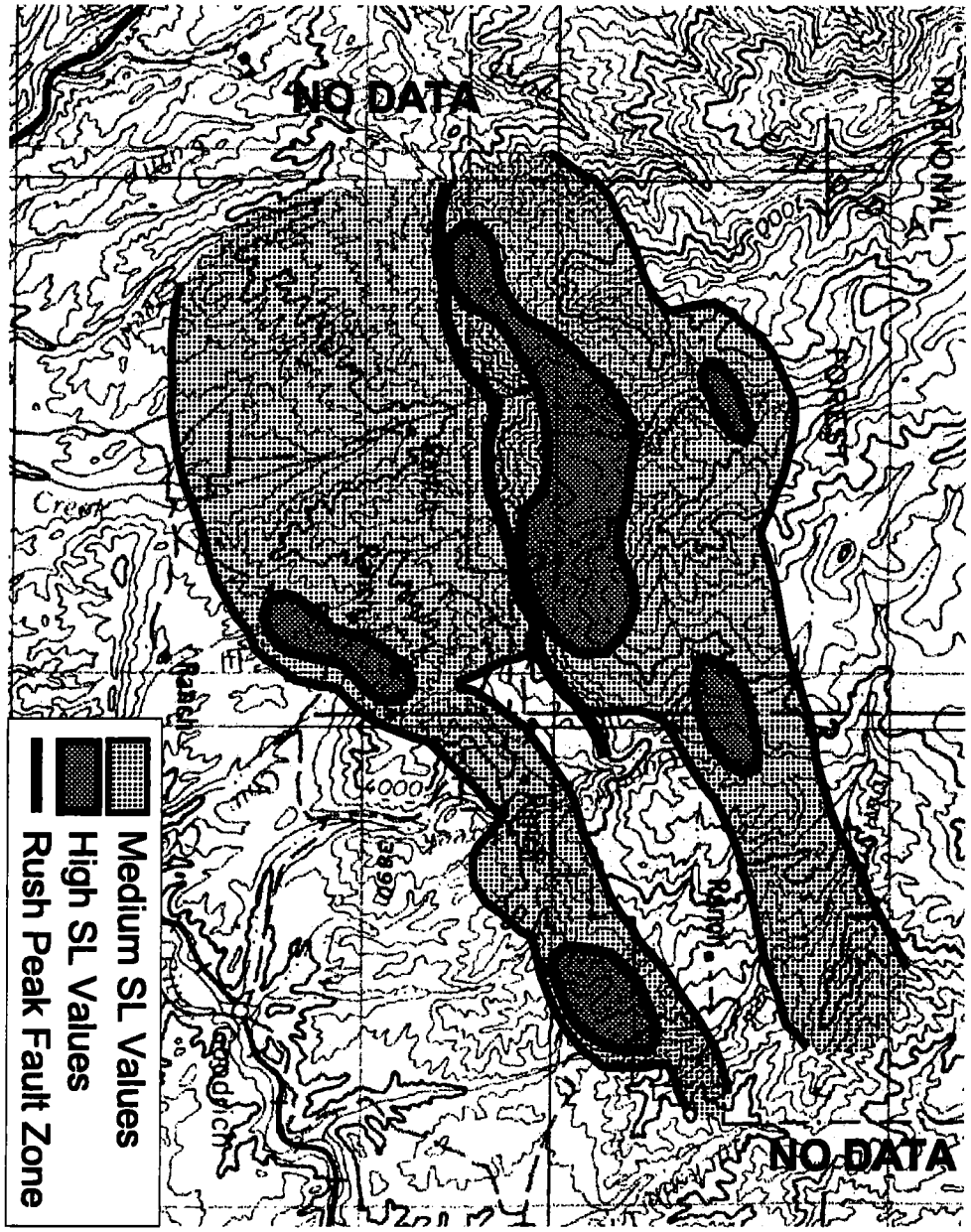

Figure 4b. Figure shows locations of SL Values in relation to Rush Creek Fault Zone. Scale 1:250k.

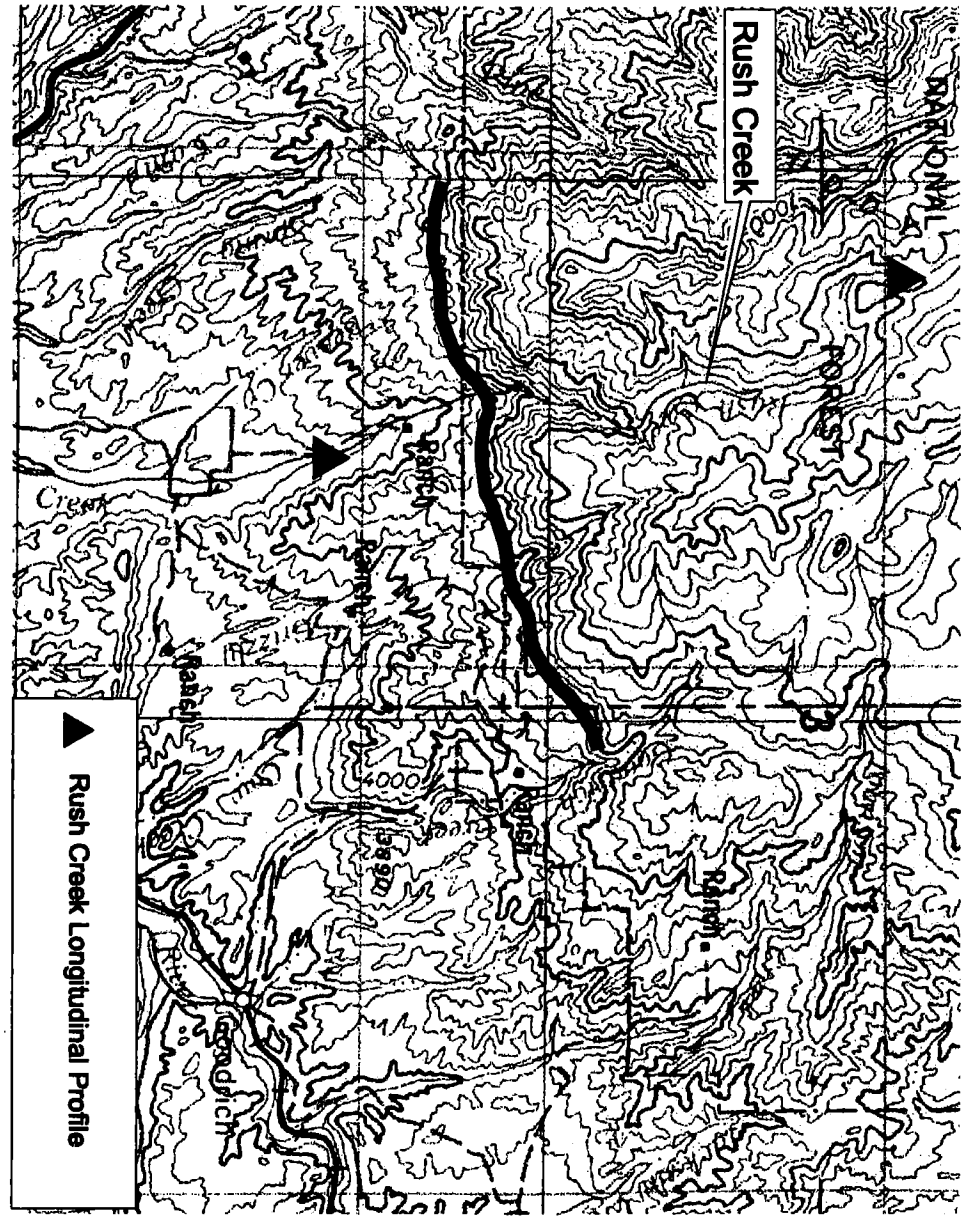

Figure 4a. Rush Creek locations of longitudinal profile and Rush Peak Fault Zone. Scale 1:250k

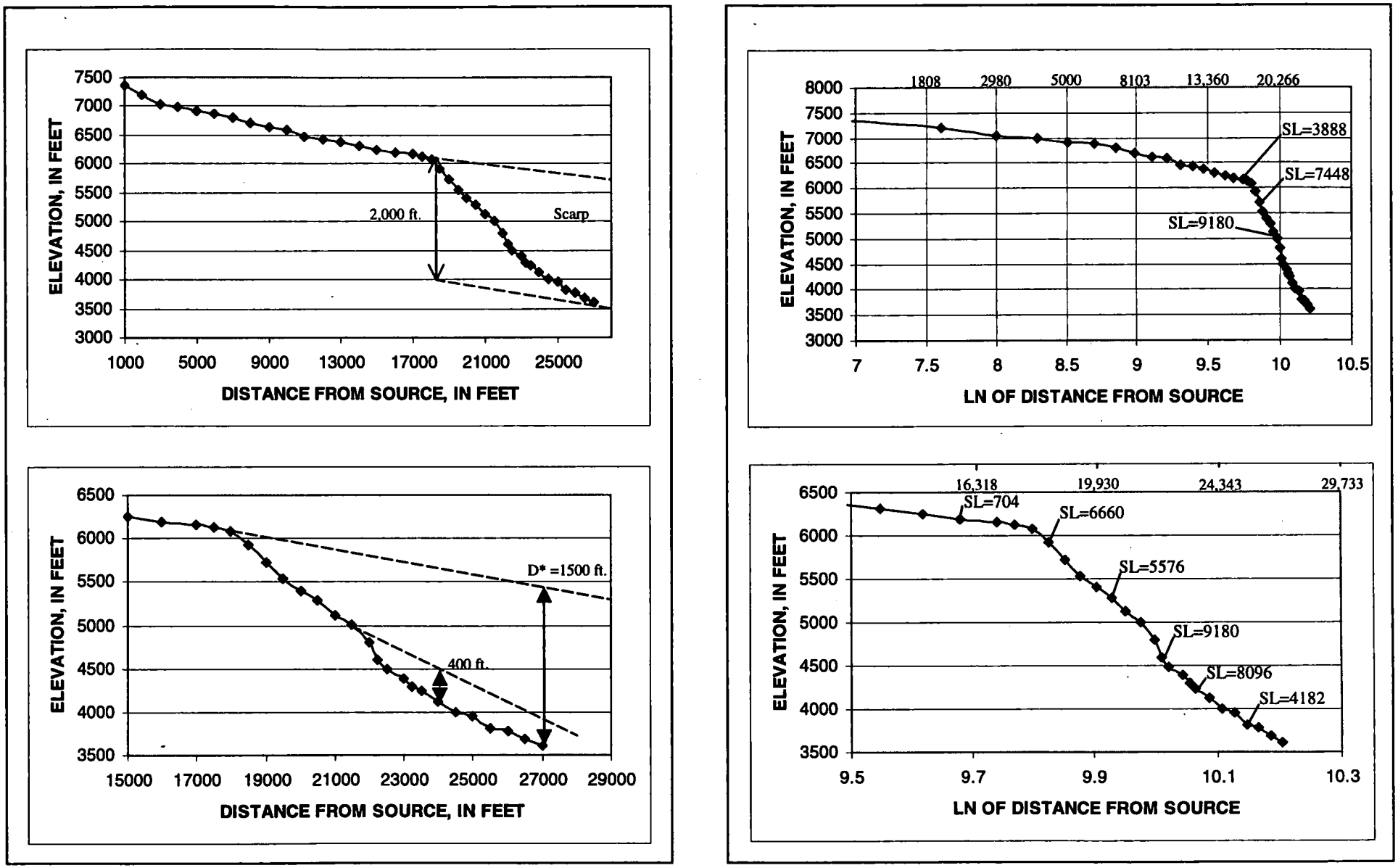

Figure 5. Representative longitudinal profile for Rush Creek. Profile shown in both arithmatic and semi-logarithmic plots. Magnitudes for Stream-gradient index values (SL) for Rush Creek, third order stream, are Low= 100-3,000; Medium= 3,000-6,000; High= 6,000-10,000 gradeint-feet.

Review of Evidence for Late Quaternary Faulting in Southwest Idaho and Adjacent Oregon

Spencer H. Wood
Department of Geosciences,Boise State University
Boise, Idaho 83725 swood@boisestate.edu

The central border region of Oregon and Idaho is one of spectacular relief, much of which owes much of its origin to faulting in the late Cenozoic. The strong lineaments expressed on the physiographic map (Fig. 1) are mostly normally faulted mountain ranges, but many differ in orientation from the strong north-south orientation of the Basin and Range Province of Nevada to the south. Neotectonics of the region is poorly understood, but several localities show clear evidence of late Quaternary faulting. The purpose of this report is to make those localities known and direct the reader to the studies in which that evidence is presented.

Many of these studies are reports for dam-safety concerns and are not published, but are available to the public. I adopt the definition of "active fault" proposed by the U.S. Bureau of Reclamation (1993), because it is based upon recognition of late Quaternary faulting, and not the Holocene definition used for fault-rupture hazard zones by California (Hart, 1980).

> A fault is classified as "active" and is considered to be a potential source of future earthquakes if there is evidence for repeated surface displacement in deposits younger than 130,000 years (late Quaternary), and/or if the fault is associated with a moderate- to large magnitude historical earthquake or a pattern of microearthquakes suggestive of an active fault. A fault is classified as "potentially active" and is considered to be a potential source of future earthquakes if there is evidence suggesting repeated surface displacement during the late Quaternary, but the age of the most recent event is unknown, or if..... A fault is judged "not active" if the preponderance of data indicate that the fault has not experienced surface faulting during the late Quaternary, or if available evidence suggests that return periods of potential large events are greater than 10,000 years for significant hazard dams to 50,000 years for high hazard dams (U.S. Bureau of Reclamation, 1993).

A broad region of seismicity trends east-west across central Idaho which Stickney and Bartholomew (1987) named the Centennial seismic zone. In the region of Figure 1 (the western part of the zone), no historic events of magnitude greater than 7 have occurred; however, a few magnitude 5 events are well documented, and patchy microseismicity occurs over the area.

In Figure 1, I have ***not*** shown fault segments which are considered active based upon microseismicity. These faults are the Pine Valley faults between Halfway, Oregon and Brownlee Dam on the Snake River, and several faults associated with Long Valley near Cascade, Idaho (Knudsen and others, 1996; Zollweg and Wood, 1993; Zollweg and Jacobson, 1986; and Zollweg, 1994 and 1998). Presently, faulted deposits or scarps of late Quaternary age associated with these faults have not been found, but they have not been intensively studied.

One cannot ignore the impressive north escarpment of the Wallowa Mountains along the projected trace of the Olympic-Wallowa lineament. I am unaware of recent or detailed studies of the Wallowa fault, but previous workers examining air photos of prominent Bull Lake age moraines have not detected surface faulting (Simpson and others, 1993). Zollweg and Wood (1993) estimate 2.2 km of offset of the 14 Ma Columbia River basalt along this fault. That offset indicates an average vertical slip rate of 0.16 mm/yr since the Miocene. Presumably the slip occurred much more recently than the Miocene, which would suggest a high rate of activity at

one time. One cannot help but suspect fault movement in the Quaternary, and it is puzzling that no one has found offset glacial deposits.

The following discussion reviews the evidence for late Quaternary faulting. Location of the faults is shown on Figure 1. Most of these fault systems were reviewed in comprehensive reports by Knudsen and others (1995) and Knudsen and others (1996)

Cottonwood Mountain Fault: Youthful scarps and offset Pleistocene alluvium are on the east side of Cottonwood Mountain, and young offset is documented along parts of the 36-km long fault (Knudsen and others, 1995). Scarp profiles show a 13 m scarp with a 29° maximum slope angle on the South Fork of Little Willow Creek, and one to two meter scarps with maxiumum angles in the range 11 to 16° on Mud Creek and Turner Creek. These indicated to Knudsen and others (1995) that the last surface faulting event occurred in middle to late Holocene and produced an average vertical surface separation of 0.75 ± 0.25 m. The higher scarps indicate repeated late Quaternary movement. Knudsen (1995) estimated a vertical slip rate on the order of 0.03 to 0.15 mm/yr. His study is the most complete available. The fault has not been trenched, but he did describe faulted Quaternary alluvium and colluvium in a gully wall on the north side of Morrison Reservoir.

Juniper Mountain Fault: Knudsen (1995) made an aerial reconnaissance and prepared a 1:24,000 photogeologic map of the faulted Quaternary deposits along the 15 km trace of the fault. The fault trends east-west with the north side down. Scarps across late Pleistocene and possible Holocene surfaces, and the relatively larger scarps in older deposits suggest multiple surface faulting events. Simpson and others (1993) conducted limited ground reconnaissance of selected sites along the fault, but it has not been intensively studied.

King Mountain fault: The fault has prominent geomorphic expression directly north of Unity Reservoir (Simpson, 1993; Knudsen, 1995). A well-defined west-facing scarp can be traced for 2.5 km, and is associated with a 2000-ft long broad, discontinuous graben with low northeast-facing antithetic scarps. They describe a 2-3 m scarp, but the nature of the material in which the scarp occurs is not described. They state that older deposits are faulted, and that no scarps or other fault related features cross the young (late Pleistocene) or Holocene alluvial and debris flow deposits. Knudsen (1995) classified this fault as potentially active.

The Steens Mountain fault zone: The active faults associated with this spectacular range with a 1,750 m southeast facing escarpment formed by faulting is discussed extensively in this guidebook.

Grande Ronde graben: The system of active faults bounding the Grande Ronde graben has been most recently studied by Simpson and others (1993) and Personius (1998). On the west side of the valley, Personius found an eastern splay of the main fault with a 1.5-km-long fault scarp, few hundred meters east of the main trace of the La Grande segment northwest of the city of LaGrande. He obtained two scarp profiles across faulted older landslide deposits with 7-8 m of surface offset and maximum scarp-slope angles of 24 to 27°, suggesting to him that one or more surface-faulting events had occurred in the last 15,000 years. On the east side of the graben he obtained profiles on steeper deposits that also suggest a very late Pleistocene age for surface faulting.

West Baker Valley faults: The Washington Gulch segment of the West Baker fault offsets several late Quaternary fan surfaces and scarps in older deposits are larger than those in younger deposits (Simpson and others, 1993). These scarps have not been studied in detail to my knowledge. Other late Quaternary features are discussed in the report by Geomatrix Consultants (1989), but neither of the investigations found clear evidence of Holocene displacement.

Rush Peak fault: The Rush Peak fault along the south side of the Cuddy Mountains has an unusual northeast trend. Zollweg and Wood (1993) discovered a late Quaternary scarp in alluvial deposits on Rush Creek. A scarp profile yielded a maximum scarp angle of 16° on a 7 m scarp indicating a late Pleistocene age. This age is also confirmed with slope profiles by Personius (1998). Smith (this guidbook) and Smith and others (1999) found a late Pleistocene debris-flow levee associated with this scarp that shows a left-lateral component to the offset, and horizontal slickensides on bed rock. Left-lateral movement on the fault was hypothesized by Mann and Meyer (1993), but they did not publish supporting field evidence. Smith (this guidebook) has found a second 10-m high scarp along Rush Creek, which is being evaluated.

Mud Creek fault within Long Valley: Knudsen and others (1996) found subdued lineaments and scarps defining a graben form (over a distance of 1.5 km) in Pinedale age deposits out in Long Valley, on the hanging wall of the Long Valley fault system The east boundary of the graben is a dissected, approximately 1-m-high scarp. The scarp and lineaments have partially directed drainage channels. Surface deformation is estimated to be late Pleistocene or early Holocene.

The north-south-trending Long Valley fault system has an impressive east-facing escarpment, and possibly offsets the Miocene Columbia River basalt as much as 6 km (Knudsen and others, 1996). However, faulted late Quaternary deposits have not been reported in the abundant glacial deposits that cross the fault (Personius, 1998; Knudsen and others, 1995; Wood, 1990).

Squaw Creek fault: The east side of Squaw Butte is an escarpment formed by down-to-east faulting along the Squaw Creek fault. Gilbert and others (1983) trenched a 2.4-m-high scarp in fan deposits, along this fault, south of Sucker Creek on the west margin of Ola Valley. They found features interpreted as a colluvial wedge and a faulted unit containing the 6,850 year old Mazama ash.

Shirt Creek fault zone: North of the Squaw Creek fault system, Knudsen and others (1996) found scarps in late Pleistocene alluvial fan deposits. The scarp is 3.9 m high in older deposits, and 1 meter high in nearby younger Pleistocene fan deposit. They interpreted this relationship to indicate two or more late Pleistocene surface-faulting events on this fault.

Big Flat-Jakes Creek fault system: Gilbert and others (1983) described scarps up to 10 m high that cross colluvial deposits along this fault system. Trench studies at Jakes Creek showed faulted colluvium which they interpreted as late Pleistocene to Holocene based on soil development and comparison with soils in the trench at Squaw Creek developed on deposits containing Mazama ash.

Halfway Gulch - Water Tank fault system: In a geotechnical study for the Mountain Home Air Force Base, the U.S. Army Corps of Engineers (1983) noted fault offset of fan surfaces along the southwest margin of the western Snake River Plain. That system of faults was studied in detail by Beukelman and others (1996) and Beukelman (1997). The main scarp averages 8 m in height with a maximum height of 11 m. Identifiable late Quaternary scarps can only be traced

for a length of 5.3 km. Maximum scarp slope angles range from 23 to 30°, and suggest a mid-Holocene to late Pleistocene age. The scarp lies in a proposed wilderness area and trenching was not permitted by the BLM, so Beukelman (1997) excavated another fault of the system, 8 km northeast of the main scarp. This scarp is about 2.5 km long with a 3 to 4 m offset, and a maximum slope angle of about 17°, which suggests an age of 6 - 23 ka. Soil and colluvial-wedge stratigraphy of the faulted deposits indicate 5 discrete events during the last 26 ± 8 ka.

CONCLUSION

No clear pattern of regional late Quaternary surface faulting is shown by this compilation. It is likely that other localities on other fault zones will turn up in future investigations. In eastern Oregon and on the southeast side of the western Snake River Plain, northwest-trending systems show late Quaternary activity. In west-central Idaho, there are a number of active faults with other orientations, in an area generally between the western plain and the Olympic-Wallowa lineament. The identified traces of active faults are scattered over an area of 200 km by 200 km, and generally spaced about 40 km.

REFERENCES

Beukelman, G.S., Waag, C.J., and Zollweg, J.E., 1996, Paleoseismic evidence for active faulting along the southwestern margin of the western Snake River Plain, Idaho: Geological Society of America Abstracts with Programs, v. 28, no. 7, p. 55

Beukelman, G.S., 1997, Evidence of active faulting in the Halfway Gulch-Little Jacks Creek area of the western Snake River Plain, Idaho: Boise, Boise State Univerity M.S. thesis, 170 p. and 4 plates.

Geomatrix Consultants, 1989, Seismotectonic evaluation, Mann Creek and Mason Dam Sites, Oregon: unpublished report prepared for the U.S. Bureau of Reclamation, 118 p. and appendix.

Gilbert, J.D., Piety, L., and Laforge, R.C., 1983, Seismotectonic study, Black Canyon diversion Dam and Reservoir, Boise Project, Idaho: Seismotectonic Report 83-7, U. S. Bureau of Reclamation, 75 p., 4 appendices, and 8 plates..

Hart, E.W., 1980, Fault-rupture hazard zones on California: Alquist-Priola Special Studies Zone Act of 1972 with index to Special Studies Zones Maps: California Division of Mines and Geology Special Publication 42, 25 p.

Knudsen, K.L, Wong, I.G., Bott, J.D.J., Weber, G.E., Silva, W.J., and Lettis, W.R., 1995, Seismotectonic evaluation , Agency Valley and Bully Creek Dams, Vale Project, east-central Oregon: Report prepared by William Lettis and Associates and Woodward-Clyde Federal Services for the U. S. Department of Interior, Bureau of Reclamation, 181 p. and 3 plates.

Knudsen, K.L, Wong, I.G., Sawyer, T.L., Bott, , Silva, W.J., and Lettis, W.R., 1996, Seismotectonic evaluation, Cascade Dam, Boise Project, west-central Idaho: unpublished report prepared for the U.S. Bureau of Reclamation by William Lettis and Associates, Walnut Creek California and Woodward-Clyde Federal Services, Oakland California, 183 p. 2 appendices, and 3 plates.

Mann, G.M., and Meyer, C.E., 1993, Late Cenozoic structure and correlations to seismicity along the Oympic-Wallowa lineament, northwest United States: Geological Society of America Bulletin, v. 105, p. 853-871.

Personius, S.F., 1998, Surficial geology and neotectonics of selected areas of western Idaho and northeastern Oregon: U. S. Geological Survey Open-File Report 98-771, 26 p.

Smith, S.C., 1999, The Rush Peak fault zone, Cuddy Mountains, western Idaho: Evidence for sinistral-oblique late Quaternary movement and analysis of longitudinal stream profiles crossing an active range front (this guidebook)

Smith, S.C., Northrup, C.J., and Wood, S.H., 1999, The Rush Peak fault zone, Cuddy Mountains, western Idaho: Evidence for sinistral-oblique late Quaternary movement (abs.) Geological Society of America annual meeting, Denver, October, 1999.

Stickney, M.C., and Bartholomew, M.J., 1987, Seismicity and late Quaternary faulting on the northern Basin and Range Province, Montana and Idaho: Bulletin of the Seismological Society of America, v. 77, p. 1602-1625.

U.S. Army Corps of Engineers, 1983, Seismic geotechnical report, Composite Medical Facility, Mountain Home Air Force Base, Mountain Home, Idaho: Seattle District, U. S. Army Corps of Engineers.

U. S. Bureau of Reclamation, 1993, Development of seismotectonic and ground motion parameters: Working draft, ACET Technical Memorandum no. 20, 24 p. plus appendices.

Wood, S.H., 1990, Evaluation of potential geologic hazards, proposed Valbois Destination Resort, Valley County, Idaho: Report prepared for Valbois, Inc. and released in Environmental Impact Statement to the U.S. Forest Service, 36 p.

Zollweg, J.E., and Jacobson, R.S., 1986, A seismic zone on the Oregon-Idaho border: The Powder River earthquakes of 1984: Bulletin of the Seismological Society of American, v. 76, p. 985-999.

Zollweg, J.E., and Wood, S.H., 1993, Faulting relationships, seismicity, design earthquakes, and peak ground accelerationss at hydroelectric facilities in Hells Canyon of the Snake river, Idaho-Oregon: Unpublished report prepared by Boise State University Geosciences Department for Idaho Power Company, 158 p. , 3 plates.

Zollweg, J.E.,1994, Microseismicity of the Cascade, Idaho Region - A preliminary report: Department of Geosciences, Boise State University, 11 p.

Zollweg, J.E., 1998, Hells Canyon regional seismicity - 1998: Boise State University, 14 p.

FIGURE CAPTIONS

Figure 1. Map showing traces of active faults (late Quaternary movement) that have been identified in the southwestern Idaho and adjacent eastern Oregon. The map shows only those faults for which studies have documented the paleoseismicity. Faults considered active due to a pattern of microseismicity are ***not*** shown. OWL is the Olympic-Wallowa lineament. Sources of information are discussed in this report.

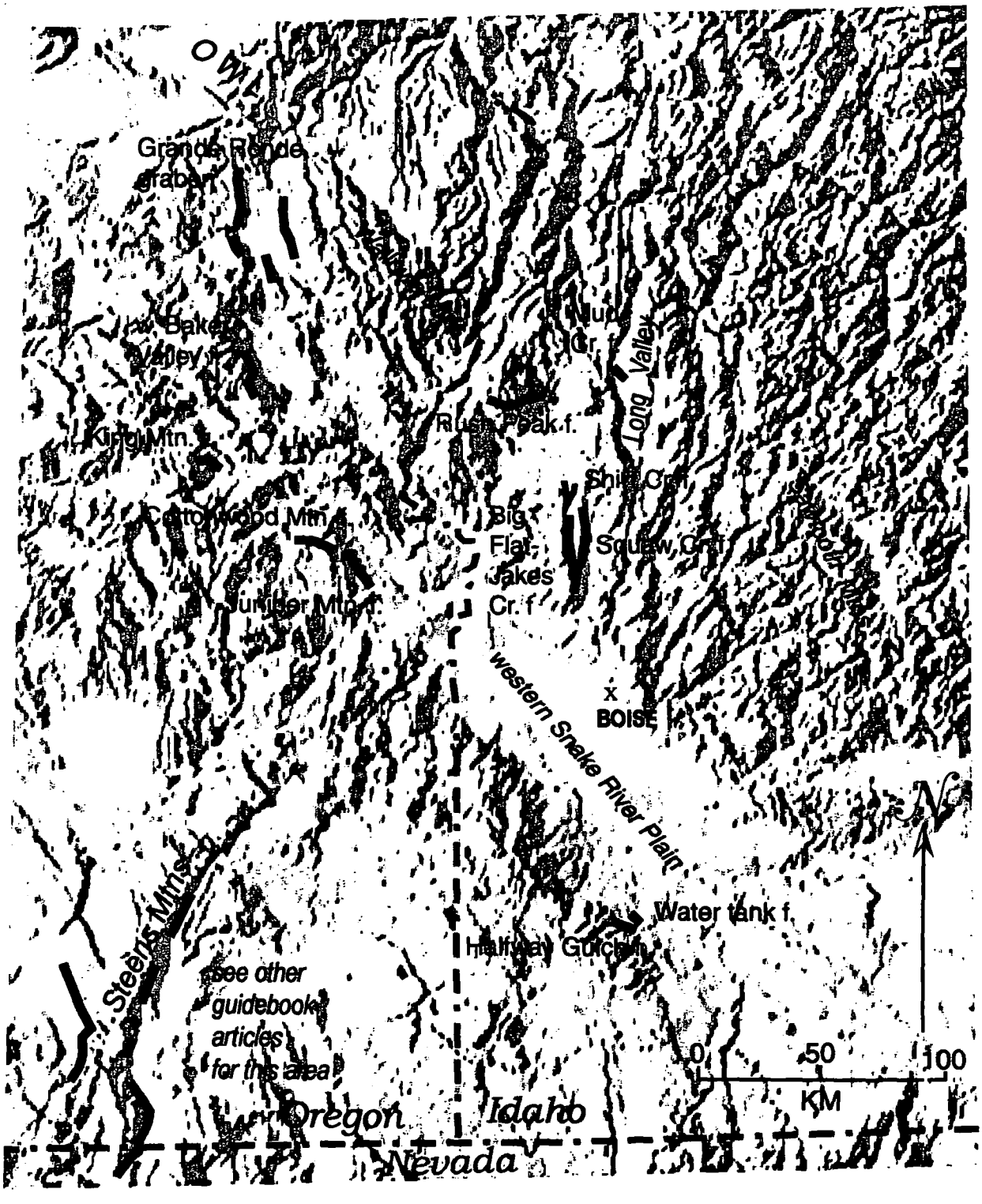

Figure 1. Map showing traces of active faults (late Quaternary movement) that have been identified in the southwestern Idaho and adjacent eastern Oregon. The map shows only those faults for which studies have documented the paleoseismicity. Faults considered active due to a pattern of microseismicity are *not* shown. OWL is the Olympic-Wallowa lineament. Sources of information are discussed in this report.

A Brief History of Glaciation at Steens Mountain, Southeast Oregon

Kenneth A. Bevis

Steens Mountain is the spectacularly uplifted fault-block mountain range to the west of the Alvord Valley (Fig. 1). Although the eastern side of the Steens Mountain block is bounded by a steep, 1700m escarpment that extends northeast-southwest for nearly 100 kilometers, the western side dips much more gently, forming a large area of broadly undulating high elevation plateau. This plateau can generally be divided into the South Steens and the High Steens by a northwest trending fault scarp about 600 m high. The High Steens is dissected by several immense glacial troughs and is covered in a thick blanket of drift which may represent several periods of glaciation during which an ice cap developed on Steens Mountain and glacial ice coalesced to flow down major stream valleys draining the plateau.

The glacial record of several stream valleys flowing from the High Steens was studied intensely during field investigations in 1990 and 1996. These are the westward sloping drainages of Fish Creek, Blitzen Creek, and Big and Little Indian Creeks; McCoy Creek which drains to the northwest; and northeast sloping stream valleys of the plateau area to the northeast of Kiger Creek (Fig. 1). All of the watersheds expose thick flows of Steens Basalt which dip toward the northwest; basalts and andesites of this unit comprise the dominant source material for surficial deposits.

I initially identified four sets of moraines in the watersheds draining the west and northwest slopes of the High Steens (Fig. 1). The youngest set is composed of one or more moraine crests that are entirely confined to north- and northeast-facing cirque basins, especially along the main eastern escarpment and along the upper west side of Kiger Creek's canyon. They extend downvalley to an average elevation of 2203 m (8420 ft) and to an average distance of about 0.3 km from cirque headwalls. These are well preserved, bouldery moraines, with sharp crests and steep slopes that show no sign of gullying or axial stream dissection. Several small lakes are impounded by these moraines.

The next older set of moraines is apparently only preserved in the watersheds draining the northwestern portion of Steens Mountain (McCoy Creek and Fish Creek) (Fig. 1). They occur at an average elevation of about 1952 m (7460 ft) and at an average distance of 2.8 km from cirque headwalls. This set of moraines is well preserved with sharp crests and steep slopes only slightly modified by gullying. Axial stream dissection is limited to a few meters. The third set of moraines occurs much farther downvalley, often at the mouths of canyons draining Steens Mountain, at an average elevation of 1612 m (6120 ft) and at an average distance of 7.2 km from cirque headwalls. The terminal moraines are generally well preserved, although crests are often more rounded and slopes exhibit more gullying. Axial stream dissection is

more pronounced and may occur to depths exceeding 20 m. Lateral moraines are not preserved on the steep, unstable slopes within the canyons draining Steens Mountain.

The oldest moraines often occur slightly beyond the third moraine set at an average elevation of about 1516 m (5792 ft) and at an average distance of 8.8 km from cirque headwalls. These moraines have well rounded crests and gentle slopes. Gullying is extensive and axial stream dissection cuts entirely through moraines and into several meters of bedrock below. Lateral moraines are nonexistent and small terminal moraine remnants are preserved in the watersheds of Blitzen Creek, Big and Little Indian Creeks, and McCoy Creek.

An excellent sequence of moraines exhibiting a similar age trend in morphologic features, although more limited in aerial extent, occurs in stream valleys draining a smaller, isolated high plateau area to the northeast of Kiger Creek (Fig 1). Moraines in this area are exceptionally well preserved, showing lateral continuity even among the oldest moraines. The watersheds head in northeast-facing cirques with the youngest and oldest moraines reaching about 0.3 km and 4.8 km downvalley, and occupying positions at an average elevation of 2520m (8267 ft) and 2070m (6792 ft), respectively. An intermediate complex of several nested and overlapping moraine crests occurs between 1.6 and 2.5 km downvalley from cirque headwalls at elevations ranging from 2329 m (7640 ft) and 2201 m (7220 ft) and may represent a telescoped version of the more widely spaced intermediate moraines observed in the westward sloping valleys.

I collected relative dating (RD) parameter data at 29 moraine crest locations showing minimal post-depositional alteration (Fig. 1). Soil profile descriptions, particle-size distributions, and surficial boulder weathering data are available upon request from the author. Table 1 presents a summary of the RD weathering criteria used to estimate morainal ages.

An initial comparison of mean RD values suggests that there are only three distinct groups for most of the weathering parameters, with the exception of the MPD, %O, and %S data, which indicate relatively indistinct changes between the first three moraine sets downvalley. The differences in weathering between RD groups are best expressed by changes in mean profile development indices (4.5, 9.8, and 25.9), the percentage of fresh surface boulders (33.7, 16.2, and 6.9), and surface boulder frequency (438, 186, and 113). For a comparison of individual sites, examine the downvalley sequence of RD sites 28, 23, 24, and 27 from the northeastern plateau area. All of the RD data indicates that the youngest and oldest moraines are significantly different in age (for example, compare RD sites 28 and 29 from the northeastern plateau area). However, weathering on the two intermediate sets of moraines appears to be nearly indistinguishable (for example, compare RD sites 19 and 20 from McCoy Creek), and their RD data has been grouped together in Table 1. RD parameter development on the youngest moraines is not much less than the inner (upvalley) intermediate moraines,

especially MPD, %O, and %S, which suggests they may be separated by a relatively short weathering interval.

Each grouping of RD data is interpreted to represent weathering of a distinct drift unit (III, II, and I from youngest to oldest), suggesting a three-fold sequence of glaciation on Steens Mountain. The relative differences in the degree of RD parameter development (Table 1) suggest that drift unit I is significantly older than drift units II and III, and that these latter two units are separated by a much shorter weathering interval. The high content of fines present in the A horizons of soils from RDS 14 and 15 of drift unit III may represent incorporated distal Mazama ash. This feature, combined with the extremely high surface SBF and poorly developed soils, suggests that this drift unit was deposited during a neoglacial event. Drift unit II probably represents a composite of terminal and recessional moraines deposited during the same glaciation. The relatively weak soil development and surface boulder weathering on moraines of drift unit II (compared with drift unit I) suggests that this unit was deposited during a recent glacial period, probably the late Pleistocene glaciation maximum (oxygen-isotope stage 2). The high degree of weathering exhibited by drift unit I indicates a much older glacial period, probably correlative with oxygen-isotope stage 6. However, the soil development and clay accumulation at RD sites 18, 27, and 29 is much greater than at other sites in drift unit I and these moraines may actually indicate deposition during an even older glaciation.

TABLE 1

Values of Surface and Subsurface Weathering Criteria at Steens Mountain, Oregon

Drift Unit	RD Site	RD Parameters PDI	WR (mm)	% P	MPD (cm)	% O	% S	% F	SBF
III	RDS 14	5.7	0.27+/-0.16	50.0	3.8+/-1.2	37.0	10.0	30.0	447
	RDS 15	3.7	0.26+/-0.15	43.0	3.6+/-2.1	50.0	10.0	37.0	468
	RDS 28	4.1	0.22+/-0.13	40.0	3.4+/-1.9	40.0	7.0	34.0	398
	Mean	**4.5**	**0.25**	**44.3**	**3.6**	**42.3**	**9.0**	**33.7**	**438**
	Std. Dev.	**1.1**	**0.15**	**5.1**	**1.7**	**6.8**	**1.7**	**3.5**	**36**
II	RDS 3	10.8	0.40+/-0.21	67.0	4.0+/-1.9	53.0	10.0	17.0	188
	RDS 4	14.4	0.50+/-0.21	67.0	3.7+/-1.9	43.0	13.0	20.0	191
	RDS 6	14.6	0.42+/-0.21	70.0	3.5+/-1.7	47.0	7.0	13.0	252
	RDS 13	9.4	0.37+/-0.25	63.0	3.6+/-1.5	50.0	13.0	23.0	182
	RDS 16	8.3	0.40+/-0.37	57.0	3.3+/-2.2	30.0	10.0	30.0	207
	RDS 17	9.9	0.27+/-0.21	70.0	3.6+/-1.6	50.0	10.0	13.0	223
	RDS 19	6.1	0.31+/-0.23	67.0	3.6+/-1.8	47.0	3.0	17.0	155
	RDS 20	4.5	0.36+/-0.26	67.0	3.5+/-1.8	43.0	7.0	20.0	144
	RDS 22	14.4	0.35+/-0.27	77.0	3.9+/-1.9	63.0	7.0	10.0	159
	RDS 23	10.0	0.69+/-0.47	63.0	3.6+/-3.3	37.0	27.0	7.0	237
	RDS 24	10.5	0.52+/-0.38	67.0	4.6+/-3.1	50.0	13.0	13.0	162
	RDS 25	7.1	0.53+/-0.29	80.0	3.9+/-1.7	50.0	13.0	7.0	146
	RDS 26	7.5	0.43+/-0.23	77.0	3.7+/-1.7	53.0	13.0	20.0	174
	Mean	**9.8**	**0.43**	**68.6**	**3.7**	**47.4**	**11.2**	**16.2**	**186**
	Std. Dev.	**3.2**	**0.28**	**6.6**	**2.0**	**8.3**	**5.9**	**6.9**	**36**
I	RDS 1	26.4	0.43+/-0.24	67.0	6.0+/-4.9	53.0	20.0	17.0	87
	RDS 2	27.3	0.39+/-0.19	80.0	5.6+/-4.3	70.0	23.0	7.0	122
	RDS 5	20.2	0.42+/-0.28	70.0	3.9+/-2.0	60.0	23.0	13.0	179
	RDS 7	22.1	0.58+/-0.53	70.0	5.6+/-2.5	63.0	30.0	7.0	116
	RDS 8	20.1	0.42+/-0.28	90.0	5.3+/-4.2	70.0	20.0	3.0	89
	RDS 9	17.6	0.46+/-0.45	80.0	5.7+/-3.1	70.0	20.0	7.0	39
	RDS 10	21.0	0.51+/-0.37	87.0	5.8+/-3.6	70.0	27.0	10.0	103
	RDS 11	20.1	0.46+/-0.24	83.0	6.2+/-4.1	63.0	30.0	10.0	155
	RDS 12	22.7	0.56+/-0.44	83.0	6.4+/-4.0	70.0	20.0	7.0	103
	RDS 18	39.0	0.41+/-0.28	87.0	5.5+/-3.1	60.0	17.0	3.0	144
	RDS 21	18.7	0.53+/-0.40	83.0	5.3+/-4.4	63.0	20.0	3.0	73
	RDS 27	39.1	0.74+/-0.52	87.0	5.5+/-2.6	77.0	17.0	0.0	113
	RDS 29	41.8	0.81+/-0.57	83.0	6.3+/-4.7	77.0	17.0	3.0	152
	Mean	**25.9**	**0.52**	**80.8**	**5.6**	**66.6**	**21.8**	**6.9**	**113**
	Std. Dev.	**8.5**	**0.37**	**6.3**	**3.7**	**5.9**	**4.7**	**3.8**	**39**

Explanation: PDI - Profile Development Index, WR - Weathering Rinds, %P - % of Pitted Boulders, MPD - Mean Pit Depth, - %O of Oxidized Boulders, %S - % of Split Boulders, %F - % of Fresh Boulders, and SBF - Surface Boulder Frequency

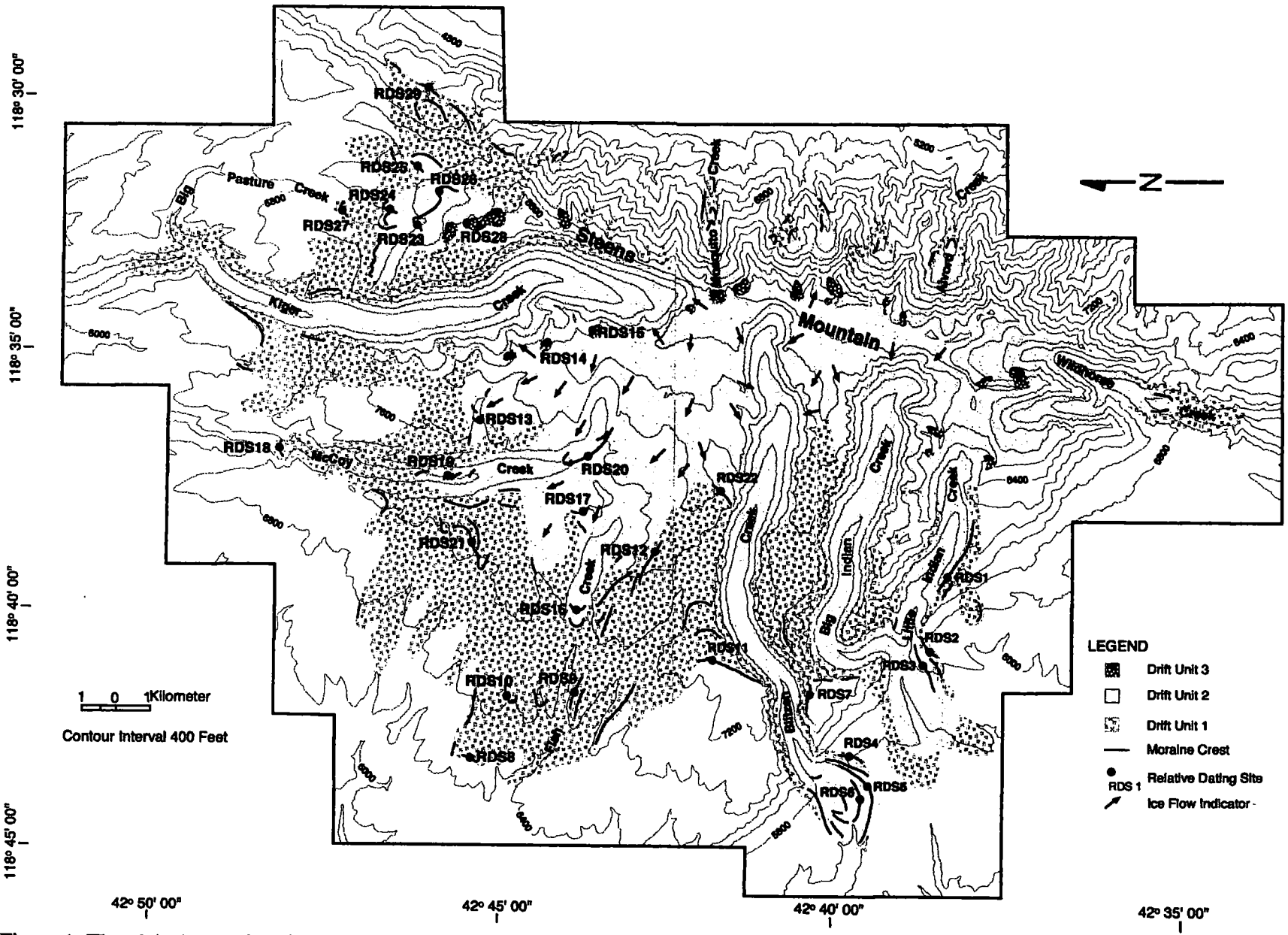

Figure 1. The glaical deposits of Steens Mountain. Moraine crests, ice flowdirections and RD parameter collection sites are indicated.

HOLOCENE DEFORMATION OF SHORELINES IN WARNER VALLEY CORRELATED WITH 1968 EARTHQUAKE SWARM EPICENTERS AND MIOCENE STRUCTURAL CONTROL

Gilbert Craven

Background

Two interpretations of the locations and mechanisms of foci associated with the 1968 Warner Valley earthquake swarm were advanced by Couch and Johnson (1968) and Schaff (1976). Couch and Johnson's explanation has been fairly widely cited because it is consistent with the standard Basin-Range mechanism of rangefront normal faulting. Schaff's interpretations of earthquake foci concentrated beneath the rangefront block west of Warner Valley (Figure 1), and a reverse mechanism for one event along a fault plane dipping 80 degrees east, are difficult to understand in the context of generally understood Basin-Range tectonics. The data on late Pleistocene shoreline elevations presented in this paper, however, show that the locations of the earthquake foci interpreted by Schaff correspond to a zone of Holocene subsidence, and the focal mechanism interpreted by Shaff is consistent with the pattern of subsidence. Additionally, Couch and Johnson's interpretation of the 1968 earthquake swarm is not supported by any field evidence, and Schaff's interpretation of earthquake foci is based on data collected from a temporary seismic net that constrained the focal locations more tightly than the data used by Couch and Johnson.

The faults along the eastern escarpment of Hart Mountain and the western escarpment of Warner Valley south of Crump Lake (Figure 1) are part of a lineament that extends on LANDSAT imagery to the vicinity of Surprise Valley in northeastern California (Craven, 1991). The Tertiary stratigraphy of the Hart Mountain block and adjacent uplands (Larson, 1965) indicates that the Hart Mountain block was displaced upward along its eastern escarpment during the mid-to-late Miocene. The displacement of the western escarpment of Warner Valley is constrained to the post late Miocene. The lineament that includes these two features is apparently an important structural discontinuity with segments that occasionally become active in varying tectonic regimes.

Shoreline Elevation Data

Shoreline elevations in the study area delineated on Figure 1 were surveyed in a series of nine leveling survey transects. The shoreline elevation data allow a three-dimensional interpretation of Late Quaternary and Holocene deformation within the study area. The surveyed shoreline elevations are the backedge elevations of beaches and of wave-cut inflections on talus slopes. The backedges of the wavecut inflections on the talus slopes frequently show strands of fine sand and silt, equivalent to beach deposits, collected between the talus blocks. The elevations of the shorelines along the eastern and western boundaries of the study area are shown in Figure 2 and Figure 3, respectively.

The east side shorelines are essentially undeformed within the precision of the survey data, and can be correlated into five distinct sets. The highest shoreline is at 1447-1448 meters elevation. The straightedge fit of the shoreline elevations indicates a maximum scatter in measured elevations of +/-1 meter. The top two shorelines, separated by ca. 3 meters, are resolved the precision of the survey data.

The west side shorelines show ca. 12 meters of relative deformation down to the north, constrained to within 11 km by the survey transects. Table 1 shows that the spacing of shorelines B, C, and D below shoreline A in the transects that define their central segments, and consequently the deformation in all four shoreline sets, are reproducible. The reproducible amount of deformation in the four shoreline sets indicates that the deformation initiated after the formation of the most recent shoreline. Table 2 shows that the shoreline spacing is reproducible between the east side and the west side shorelines.

Since the east side shorelines are essentially undeformed, they serve as a reference datum for the elevations of the west side shorelines before deformation. Using the 1447 – 1448 meter elevation of shoreline A on the east side as a reference datum, the 12 meter down-to-the-north relative deformation in the west side shorelines consists of 4 meters uplift on the southern segment and 8 meters subsidence on the northern segment.

The relative amounts of deformation in the northern and southern segments of the west side shorelines serve as a relative age control for the shorelines. A full analysis of the relative deformation and relative ages of the shorelines is presented in Craven (1991). To summarize, shoreline A is the least deformed, and therefore the youngest, shoreline and the lake level curve derived from relative shoreline ages is similar in form to the lake level curve derived by Benson and Thompson (1987) for Lake Lahontan. The down-to-the-north warping along the west side of Warner Valley is Holocene.

Conclusions

Figure 4 shows the location of the Holocene deformation derived from analysis of shoreline elevations. The zone of subsidence is correlated with the locations of the 1968 Warner Valley earthquake swarm epicenters (Schaff, 1976) and the location of Crump Lake. The focal mechanism derived by Schaff is consistent with subsidence in the vicinity of the western escarpment of Warner Valley. Warping and subsidence are the most plausible causes for the 1968 earthquake swarm, since their significance as long term processes during the Holocene is demonstrated by the shoreline elevation data. Crump Lake is located within the zone of subsidence, and as such appears tectonically controlled. The 1968 earthquake swarm epicenter zone and Crump Lake are bounded on their eastern sides by the lineament between the eastern escarpment of Hart Mountain and the western escarpment of Warner Valley (Figure 1). The Miocene (or earlier) structure that forms this lineament appears to control an axis of Holocene warping.

References

Benson, L. V., and Thompson, R. S., 1987, Lake-level variation in the Lahontan Basin for the past 50,000 years: Quaternary Research, 28, p. 69 – 85

Couch, R., and Johnson, S., 1968, The Warner Valley earthquake sequence: May and June, 1968: Ore Bin, 30, p. 191 – 204

Craven, G. F., 1991, The Tectonic Development and Late Quaternary Deformation of Warner Valley South of Hart Mountain, Oregon: Unpublished M. S. Thesis, Humboldt State University, 94 p.

Larson, E. E., 1965, The Structure, Stratigraphy, and Paleomagnetics of the Plush Area, Southeastern Lake County, Oregon, Unpublished Ph. D. Dissertation, University of Colorado, 166 p.

Schaff, S. C., 1976, The 1968 Adel, Oregon, earthquake swarm, Unpublished M. S. Thesis, University of Nevada, Reno, 63 p.

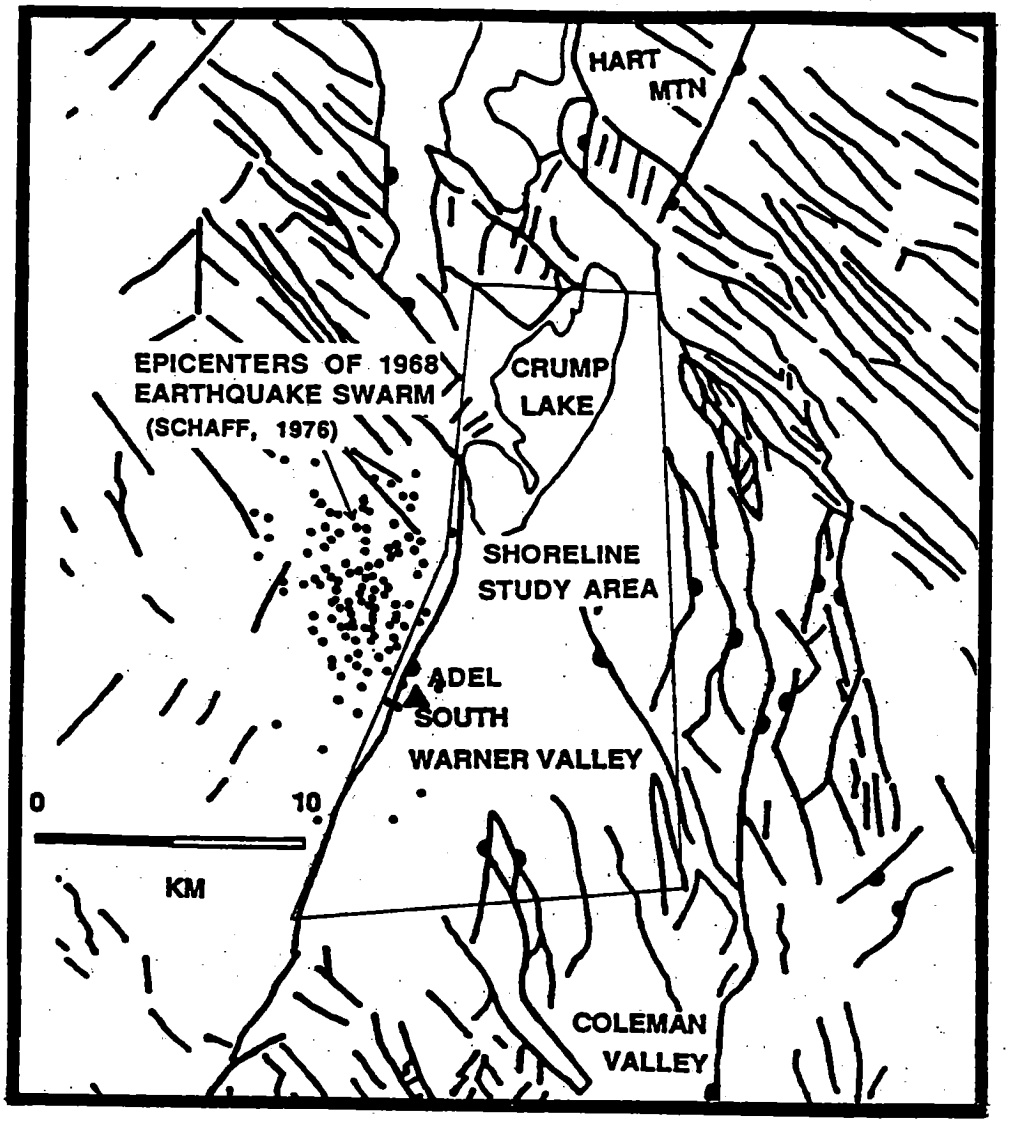

Figure 1. Location of study area.

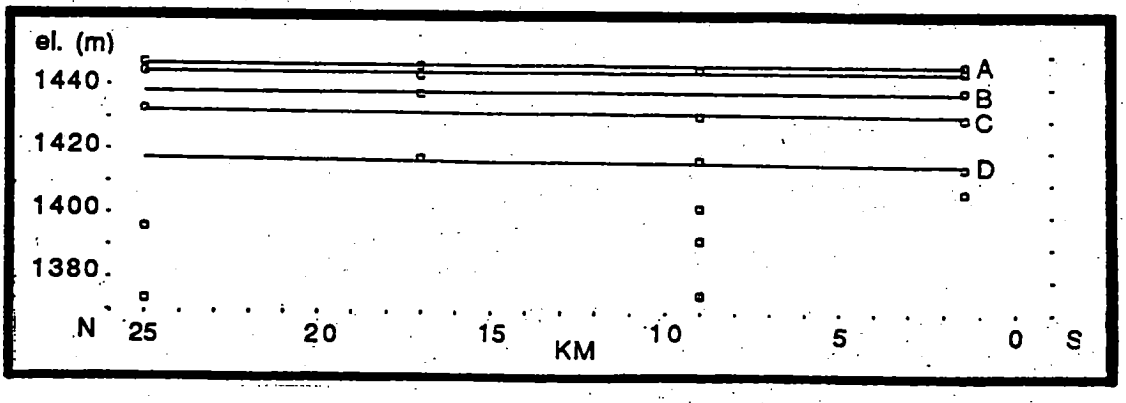

Figure 2. Elevations of east side shorelines.

Table 1. Elevation spacing and correlation of west side shorelines.

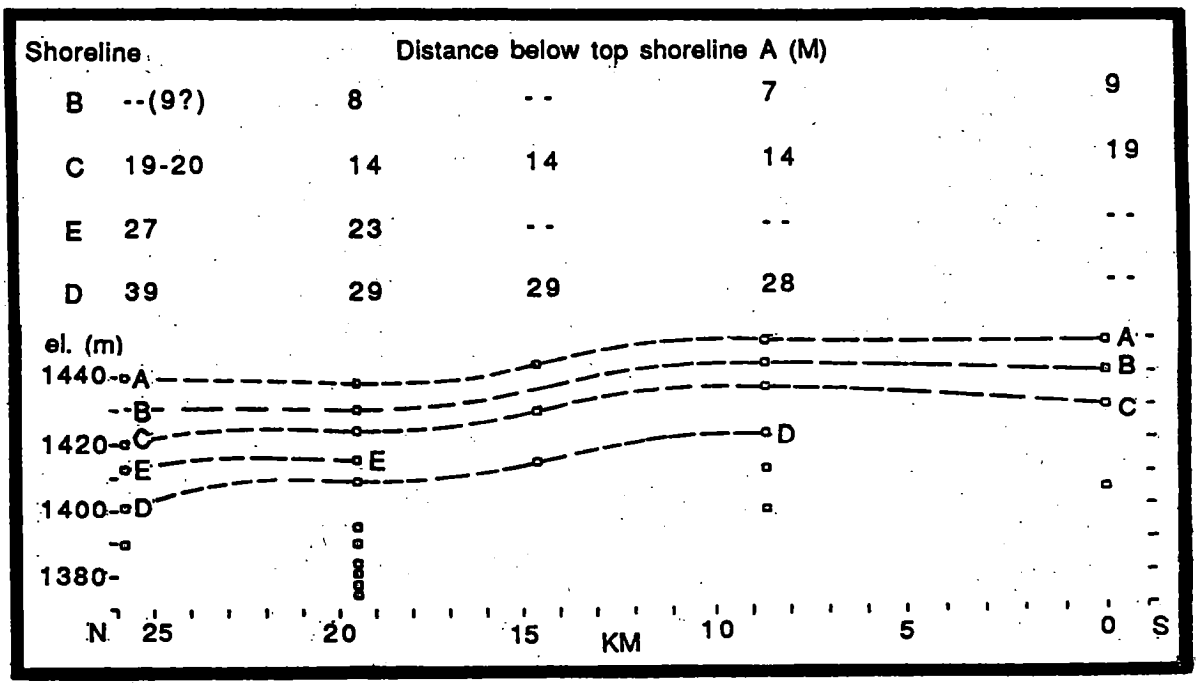

Figure 3. Elevations of west side shorelines.

Table 2. Shoreline spacing and correlation between west and east side shorelines.

Shoreline	Distance below top shoreline A (m)	
	west side (central segment)	east side
B	7-8	8
C	14	15
D	28-29	30

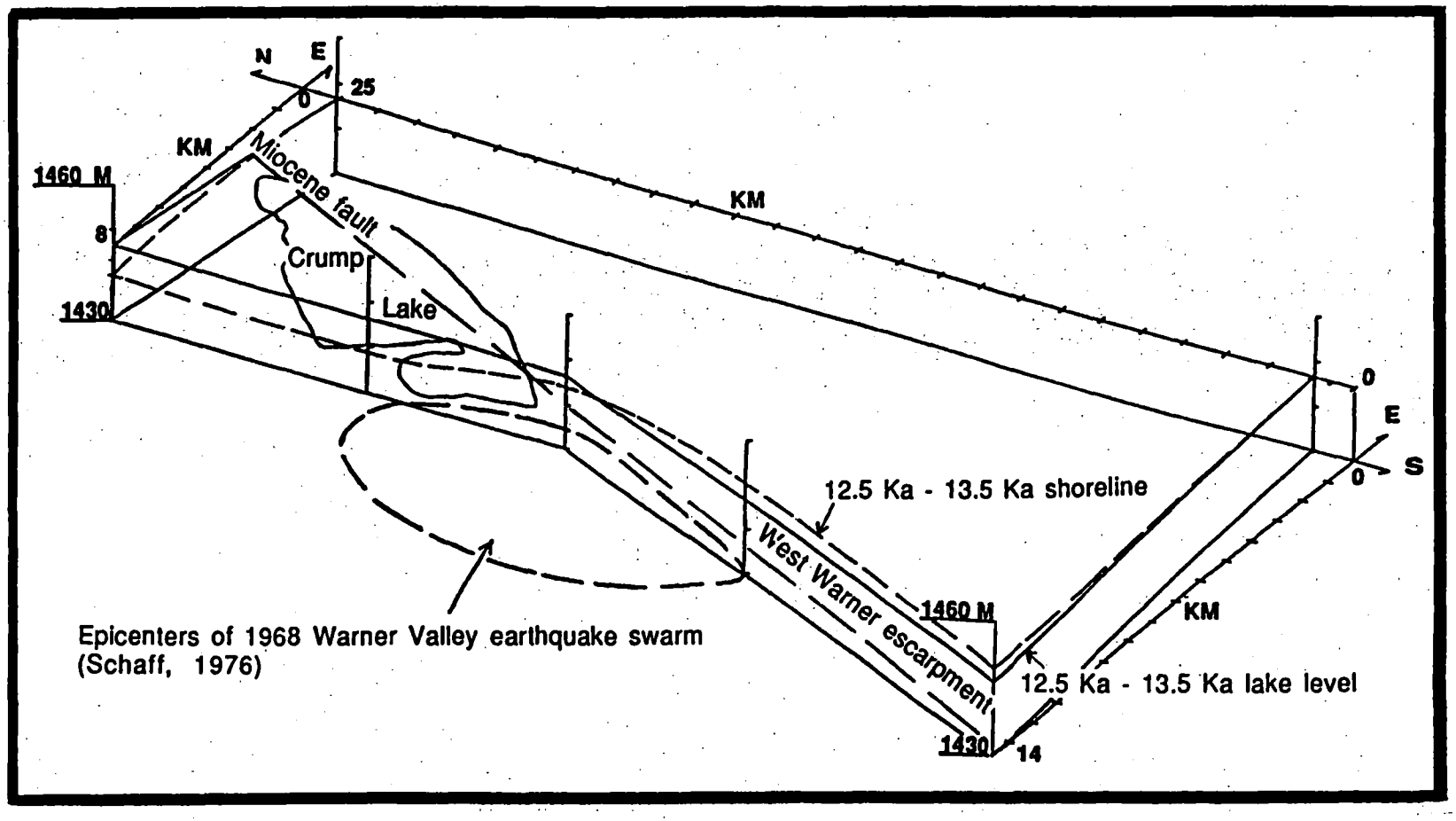

Figure 4. Holocene deformation and correlated features.

Compressional Deformation of Late Pleistocene Pluvial Sediments in the Northwestern Summer Lake Basin, South-Central Oregon

Simpson, Gary D., and Davis, Jonathan O.*

Sediments of south-central Oregon's pluvial Lake Chewaucan exposed in the northwestern Summer Lake basin were compressed between about 19,000 and 12,000 years ago. This affects the stratigraphic column of 55 or more tephra on the Ana River, and poses kinematic questions as well. Deformation consists of thrust features and small to large-scale recumbent folds, and seems to have occurred when the sediments were saturated. The section comprises lacustrine silts and clays interbedded with ash-fall tephra layers of varying thicknesses. These two materials have contrasting strength characteristics and consequently much of the deformation occurs as folding and faulting along bedding planes, sandwiched between apparently undeformed sediments. Deformation is especially intense in the upper sediments, including the Marble Bluff/St. Helens C (35,000 BP), Wono (25,000 BP), Tregon Hot Springs (23,000 BP), and St. Helens Mp (18-20,000 BP) tephra layers. The deformed sediments are truncated by an unconformity which does not bear a soil profile, and are overlain by a few meters of undeformed lacustrine silt and sand which contain no tephra layers.

The age of the deformation is constrained by the following: St. Helens Mp tephra is deformed; the sediments were saturated when deformed; deformation was followed by lacustrine erosion and deposition; and Pluvial Lake Chewaucan probably desiccated about 12,000 years BP. Therefore the compressional structures exposed today were formed between 19,000 (St. Helens M) and 12,000 BP (lake desiccation). Structural fabric forms a radial pattern which suggested to one author (JOD) that compression was due to landsliding from the winter Rim into the pluvial lake, rather than to deep-seated tectonics forces.

*Reprinted from: Geological Society of America, 1989 Abstracts with Programs, v. 21, no. 5, p. 144.